THE UNIVERSITY OF
WARWICK

AUTHOR: **Adam J. H. Newton** DEGREE: **Ph.D.**

TITLE: **Modelling adenosine dynamics in neural tissue**

DATE OF DEPOSIT: .....

I agree that this thesis shall be available in accordance with the regulations governing the University of Warwick theses.
I agree that the summary of this thesis may be submitted for publication.
I **agree** that the thesis may be photocopied (single copies for study purposes only).
Theses with no restriction on photocopying will also be made available to the British Library for microfilming. The British Library may supply copies to individuals or libraries, subject to a statement from them that the copy is supplied for non-publishing purposes. All copies supplied by the British Library will carry the following statement:

> "Attention is drawn to the fact that the copyright of this thesis rests with its author. This copy of the thesis has been supplied on the condition that anyone who consults it is understood to recognise that its copyright rests with its author and that no quotation from the thesis and no information derived from it may be published without the author's written consent."

AUTHOR'S SIGNATURE: .....

USER'S DECLARATION

1. I undertake not to quote or make use of any information from this thesis without making acknowledgement to the author.
2. I further undertake to allow no-one else to use this thesis while it is in my care.

DATE SIGNATURE ADDRESS

.....

.....

.....

.....

.....

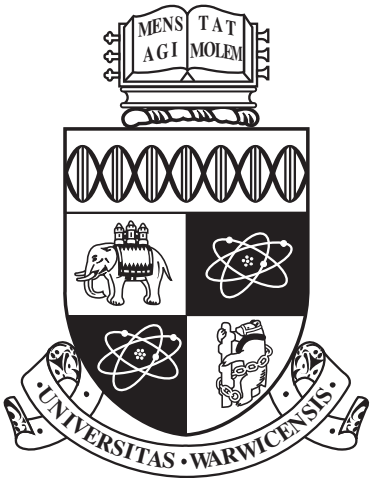

Modelling adenosine dynamics in neural tissue

by

Adam J. H. Newton

Thesis

Submitted to the University of Warwick

for the degree of

Doctor of Philosophy

Complexity Science Doctoral Training Centre

September 2015

THE UNIVERSITY OF
WARWICK

Contents

Acknowledgments

First and foremost I would like to express my gratitude to my supervisor Dr Magnus Richardson for his continuous support and guidance throughout my PhD. I would also like to thank Dr Mark Wall for his advice and insight.

I would also like to thank the Warwick Complexity Science Doctoral Training Centre for the opportunity to undertake this project and the Engineering and Physical Sciences Research Council for providing funding.

Finally I would like to thank my parents, Annette and David, for their patience and support while I have been writing this thesis and throughout my studies.

Declarations

I, Adam Newton, hereby declare that all the work within is my own unless otherwise stated in text or figure legends. None of this work has previously been submitted for a degree at this or any other institution. All sources used in the preparation of my thesis are indicated in the references.

Abstract

The neuromodulator adenosine is involved in both physiological and pathological activity, such as sleep, epilepsy and stroke. However, the complex processes underlying the release, transport and clearance of adenosine from the extracellular space and their interactions are still poorly quantified. In this thesis I develop the first detailed model of the dynamics of adenosine in neural tissue, including intracellular and extracellular metabolism, using parameters taken from an extensive search of the literature. This approach also identifies physiological and metabolic parameters that have yet to be experimentally measured. The model provides estimates of the range of influence of adenosine, the distance where the extracellular concentration is greater than that required for half of the maximum inhibition by the dominant type of adenosine receptors in the cortex, and suggests that under physiological conditions the adenosine signal will be highly localised. The model predicts that adenosine concentration profiles are primarily determined by diffusion and that neuronal transport and metabolism are the dominant clearance mechanisms. The model can be used with either experimental or endogenous sources of adenosine, and I apply it to the bath application of adenosine to a tissue slice, (a method used extensively to study the effect of adenosine on synaptic transmission). The model is used to predict the effective dose response curve of bath applied adenosine and to compare the effects of transporter blockers. I then turn to the modelling of biosensors, which are used extensively to measure the concentration of various analytes in tissue, including adenosine. Biosensors are often calibrated in a flow injection system with a known concentration of the analyte. Mathematical and computational models are used to compare the response characteristics of biosensors in this free environment with the tortuous environment in which they are used. An estimated correction factor is obtained together with the sensitivity of this factor to the characteristics of the biosensor. This work provides a framework to move from qualitative studies of changes of adenosine in the brain to quantitative analysis of the spatio-temporal dynamics of adenosine signalling and its influence on networks of neurons.

Abbreviations

5′N	5′-nucleotidase
5′N II	5′-nucleotidase II
ATP	adenosine triphosphate
ACh	acetylcholine
ADA	adenosine deaminase
ADK	adenosine kinase
ADK	adenosine kinase
AdoHcyase	s-adenosyl-L-homocysteine hydrolase
ADP	adenosine diphosphate
ADSL	adenylosuccinate lyase
ADSS	adenylosuccinate synthetase
AK	adenylate kinase
AMN	adenosine monophosphate nucleosidase
AMP	adenosine monophosphate
APRTase	adenine phosphoribosyltransferase
ATPase	ATP monophosphatase
CLE	chemical Langevin equations
CME	chemical master equation
CNT	concentrative nucleoside transporter
EC50	half maximal effective concentration
ECS	extracellular space
ENT	equilibrative nucleoside transporter
EPSP	excitatory postsynaptic potential

GCPR	G protein-coupled receptors
HGPRT	Hypoxanthine-guanine phosphoribosyltransferase
IC_{50}	half maximal inhibitory concentration
LFP	local field potential
MM	Michaelis-Menten
MSD	mean squared displacement
NT	nucleoside transporter
PNPase	polynucleotide phosphorylase
PNPase	polynucleotide phosphorylase
Q_{10}	change in a reaction rate as a result of a 10°C increase in temperature
QSSA	Quasi steady state approximation
RRE	Reaction rate equations
TTX	tetrodotoxine
VT	Volume transmission
XO	xanthine oxidase

Parameters used for the models of adenosine clearance, (chapter 2) and (chapter 3.)

α		extracellular volume fraction
β		intracellular volume fraction
β_n		neuronal volume fraction
β_g		glial volume fraction
D^*	$\mu m^2/s$	free diffusion coefficient
D	$\mu m^2/s$	tortuous diffusion coefficient
θ		tortuosity
k_B	J/K	Boltzmann's constant
T	K	temperature
η	Pas	dynamic viscosity of adenosine or the break-down products
V_1	$\mu M/s$	maximum velocity of ecto-adenosine deaminase
K_1	μM	Michaelis-Menten constant of ecto-adenosine deaminase

V_2	μM/s	maximum velocity of neuronal adenosine transport
K_2	μM	Michaelis-Menten constant of neuronal adenosine transport
V_3	μM/s	maximum velocity of neuronal break-down product transport
K_3	μM	Michaelis-Menten constant of neuronal break-down product transport
V_4	μM/s	maximum velocity of adenosine deaminase
K_4	μM	Michaelis-Menten constant of adenosine deaminase
V_5	μM/s	maximum velocity of glial adenosine transport
K_5	μM	Michaelis-Menten constant of glial adenosine transport
V_6	μM/s	maximum velocity of glial break-down product transport
K_7	μM	Michaelis-Menten constant of glial break-down product transport
μ_8	s^{-1}	non-saturating rate for glial removal of breakdown products
A_e	μM	extracellular adenosine
P_e	μM	extracellular break-down products
A_n	μM	neuronal adenosine
A_n	μM	neuronal break-down products
A_g	μM	glial adenosine
P_g	μM	glial break-down products
ϕ		proportion of bound A_1R receptors
ϕ_{50}		proportion of bound A_1R required to half an EPSP
λ	μm	characteristic length scale
τ	s	characteristic time scale

Parameters used for the biosensor models, (chapter 4).

r_b	μm	radius of the biosensor core
w	μm	thickness of the enzyme layer
d	μm	thickness of the damaged region
v_b	1/s	biosensor enzyme reaction rate
v_t	1/s	clearance rate of the analyte in tissue
D_b	$\mu m^2/s$	diffusion coefficient of the analyte in the enzyme layer
D_f	$\mu m^2/s$	diffusion coefficient of the analyte in the damaged region

D_t	μm^2/s	diffusion coefficient of the analyte in tissue
D_h	μm^2/s	diffusion coefficient of the electroactive product in the enzyme layer
α_t		extracellular volume fraction in tissue
α_b		free volume fraction in the biosensor enzyme layer
A^*	(μM)	steady-state tissue concentration of the analyte
w_2	μm	thickness of the second enzyme layer for a two or three enzyme biosensor
v_{b_2}	1/s	biosensor enzyme reaction rate for the second analyte
v_{t_2}	1/s	clearance rate of the second analyte in tissue
D_{b_2}	μm^2/s	diffusion coefficient of the second analyte in the enzyme layers
D_{f_2}	μm^2/s	diffusion coefficient of the second analyte in the damaged region
D_{t_2}	μm^2/s	diffusion coefficient of the second analyte in tissue
A_2^*	(μM)	steady-state tissue concentration of the second analyte
w_2	μm	thickness of the third enzyme layer for a three enzyme biosensor
v_{b_3}	1/s	biosensor enzyme reaction rate for the third analyte
v_{t_3}	1/s	clearance rate of the third analyte in tissue
D_{b_3}	μm^2/s	diffusion coefficient of the third analyte in the enzyme layers
D_{f_3}	μm^2/s	diffusion coefficient of the third analyte in the damaged region
D_{t_3}	μm^2/s	diffusion coefficient of the third analyte in tissue
A_3^*	(μM)	steady-state tissue concentration of the third analyte
σ		diffusion module
C	(nA/μM)	biosensor calibration for a known concentration
$C_i^{(j)}$	(nA/μM)	a j-layer biosensor calibration for the i^{th} analyte
m		calibration multiplier for a single-layer biosensor
m^b		calibration multiplier for a two-layer biosensor with both analytes
m_i^b		calibration multiplier for a two-layer biosensor with the i^{th} analyte
m^c		calibration multiplier for a three-layer biosensor with three analytes
m_i^c		calibration multiplier for a three-layer biosensor with the i^{th} analyte

Chapter 1

Introduction

Since adenosine was first identified as a neuromodulator (Sattin and Rall 1970), it has been shown to play a prominent role in both physiological and pathological brain function. Recent developments of electrochemical and voltammetric biosensors allow adenosine concentrations to be observed at high spatio-temporal resolutions either *in vivo* or *in vitro* (Llaudet et al. 2003; Swamy and Venton 2007). Adenosine signalling is complex with multiple sources and release sites that vary with brain region and stimulus. Adensoine has different effects on cells depending on the class of receptor and may also interact with the receptors for other neuromodulators. However, there is little work on the diffusion and clearance of adenosine in the brain. Here a detailed model of adenosine transport in neural tissue is constructed, based on an extensive search of the literature and includes approximations of extracellular and intracellular metabolism. A mathematical description of biosensors themselves is then developed to estimate the concentration necessary to produce the observed response, so that the predictions of the model could be better compared and validated against experimental work.

1.1 Neurotransmitters and neuromodulators

The brain is principally composed of two cell classes; neurons which communicate with one another forming networks capable of processing information, and glia which are traditionally viewed as having a supportive role, providing electrical insulation and metabolic support, but have also been shown to play a role in signalling (Araque et al. 1999). The membrane potential of

neurons is able to change rapidly, due to voltage-gated ion channels. Given enough stimulation the membrane will rapidly depolarise in an action potential or spike. This can be communicated to other neurons via electrical or chemical synapses. In general a neuron is formed of three distinct parts; dendrites, a branching structure that receives input from other cells, the cell body, and an axon which communicates the signal to other cells and can be insulated by myelin, produced by glia, to speed up conduction. The membrane potential of the giant axon of a squid was first described mathematically by the Hodgkin-Huxley model (Hodgkin and Huxley 1952), which has been widely applied to many neurons in many species (Pospischil et al. 2008). The state variables are the membrane potential together with gating variables for the potassium and sodium ion channels. At the resting potential (~ -70mV) both the sodium and potassium channels are closed. As the membrane potential is increased the sodium channels open causing the membrane to rapidly depolarise producing an action potential. This causes the sodium channels to close and opens the potassium channels ($\sim$40mV), which polarises the neuron. The potassium channels start to close, but are relatively slow, so the neuron may become hyper-polarised after the spike.

The action potential is a signal that is communicated to other neurons via synapses. A chemical synapse is formed by two growths (bouton) that leave a small gap or synaptic cleft ($\sim$10nm) between the axon of the presynaptic neuron and the dendrite or cell body of the postsynaptic neuron. The action potential causes some vesicles in the presynaptic terminal to fuse with the membrane, releasing neurotransmitter into the synaptic cleft. The neurotransmitters rapidly diffuse across the synaptic cleft and activate corresponding receptors. The effect this has on the membrane potential of the postsynaptic neuron depends on the neurotransmitter. In general synapses can be inhibitory *e.g.* $\gamma-$aminobutyric acid (GABA) or excitatory *e.g.* glutamate. The effect also depends on the current membrane potential and the reversal potential.The membrane potential, where the neurotransmitter causes no net flow of ions *e.g.* in the mature rat brain GABA has a reversal potential of ~ -70mV so is inhibitory, whereas in the immature brain it is ~ -40mV so is excitatory (Ben-Ari et al. 2012).

Glia can also be involved in synaptic transmission, particularly a star shaped

class of glia, astrocytes. These can encase synaptic connections and respond to activity over multiple synapses, elevating intracellular Ca^{2+} and causing the release of gliotransmitters, such as ATP, which can directly influence both the presynaptic and postsynaptic neuron, (Araque et al. 1999) as well as being metabolised extracellularly to produce adenosine. Astrocytes also shuttle lactate to neurons as a source of energy (Chih and Roberts 2003). Astrocytes communicate with one another via gap junctions, which allow both chemical and electrical signals to pass between them (Nagy et al. 2004).

Direct communication between neurons is also supplemented through broadcast communication by neuromodulators. Several neuromodulators have been identified; dopamine, acetylcholine, adenosine, noradrenaline, and serotonin (Rang et al. 2003). Neuromodulators are distinct from neurotransmitters in that they influence a relatively large volume of brain tissue, although there are chemicals that serve as both neurotransmitters and neuromodulators, such as acetylcholine. Neurotransmitters are rapidly cleared from the synaptic cleft, preventing them from influencing other cells, however they can spill over *e.g.* by blocking glutamate transporters (Diamond 2001). Neuromodulators must diffuse through the extracellular space (ECS) to influence a volume of tissue. To quantify the spatio-temporal dynamics of adenosine it is essential to account for the effect of the tissue's geometry. Brain tissue essentially resembles a foam, with the cells representing the bubbles and the ECS the water (Kuffler and Potter 1964). As neuromodulators like adenosine cannot easily cross the cell membranes their diffusion is impeded by the tortuosity of the ECS. Tortuosity is a multiplicative factor of the path length for diffusing particles, due to the geometry of its environment. It is empirically defined as the square root of the ratio of the free to tortuous diffusion coefficients and has been experimentally determined for many brain regions, with a range of $1.2 - 1.8$ (Nicholson 2001). Action potentials are not modelled in this work, but are considered as a way of characterising the range of influence of adenosine.

1.2 Adenosine as a neuromodulator

Adenosine was first implicated in extracellular signalling through investigations into cardiac function in 1929 by Drury and Szent-Gyorgyi, but it was not until the 1970s that it was shown to act as a neuromodulator, initially by the observation of adenosine-mediated changes in cyclic-AMP in guinea pig cortical slices (Sattin and Rall 1970). Adenosine influences cell surface G-protein coupled receptors (GPCR), also called serpentine receptors or heptahelical receptors, because they weave through the cell membrane seven times. They are metabotropic as opposed to ionotropic receptors as they are indirectly linked with ion channels. Initially two classes of GPCRs were identified for purines, P_1R (for adenosine) and P_2R (for ATP/ADP) (Burnstock 1978), the P_1R was later subdivided into four types of adenosine receptor A_1R, $A_{2A}R$, $A_{2B}R$ and A_3R (Calker et al. 1979; Van Calker et al. 1978; Bruns et al. 1986; Ribeiro and Sebastiao 1986). Broadly A_1R mediates a decrease in cyclic AMP levels. It activates several types of K^+ channels and inactivates other channels including Ca^{2+} (Fredholm et al. 2001a). $A_{2A}R$ and $A_{2B}R$ mediate an increase in cyclic AMP levels, they have high and low binding affinities respectively and A_3R mediates a reduction in calcium currents (Chin 1989). It also seems to play a role in many conditions, *e.g.* It has been shown to have both a protective and degenerative role during ischemia, a restriction in blood supply (Gessi et al. 2008).

In the cortex adenosine acts to reduce neuronal activity via A_1Rs. Pyramidal neurons form excitatory glutamatergic synapses. When an action potential reaches such a synapse it can result in a small voltage change in the postsynaptic neuron, called an excitatory postsynaptic potential (EPSP). Such EPSPs can be observed directly via intracellular recording, where a sharp glass micropipette filled with a conductive ionic solution is inserted into the cell body or the dendrites, and the voltage is recorded. The characteristic shape of an EPSP is a rapid rise followed by slow exponential decay (Figure 1.1). Adenosine is able to reduce the amplitude of the EPSP by activating the A_1R which opens several types of potassium channels while closing some types of calcium channels. (Fredholm et al. 2001b). Extracellular recordings involve a microelectrode being inserted into the extracellular space to record the local field potential (LFP). When several neurons spike at the same time

a population spike can be observed followed by a field EPSP (fEPSP), which is also used to study the influence of adenosine (Dunwiddie and Diao 1994).

There is usually some adenosine in the extracellular space. This concentration is called the adenosine tone or endogenous tone and has been observed *in vivo* and *in vitro* either directly via microdialysis (Sharma et al. 2014), and biosensor recordings (Wall et al. 2007; Sims et al. 2013) or indirectly by observing the changed EPSPs (Figure 1.1), inhibitory postsynaptic potentials and fEPSPs (Kerr et al. 2013; Zhang et al. 2015; Dunwiddie and Diao 1994; Clasadonte et al. 2014). The endogenous tone observed varies with brain region, species and methodology, but is usually between 200nM and 1μM (Dunwiddie and Masino 2001). It is known to increase during wakefulness and reduce during sleep (Sims et al. 2013) and has been shown to increase during development (Kerr et al. 2013).

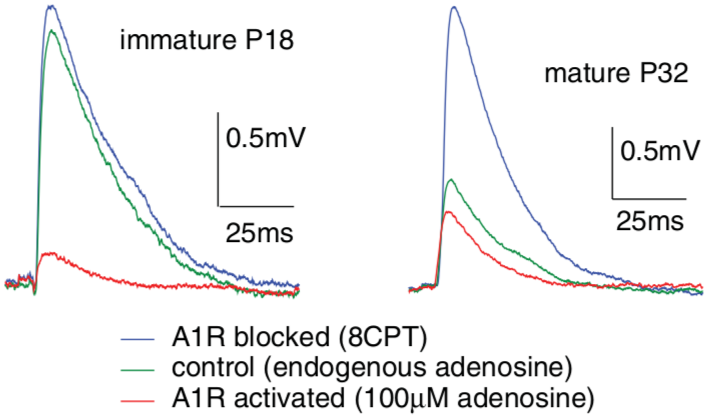

Figure 1.1: **An endogenous tone of adenosine is present in the cortex and additional adenosine further reduces excitation.** Paired intracellular recordings of two connected rat neocortical layer 5 pyramidal cells, where a presynaptic neuron is stimulated to produce an action potential, producing an EPSP recording in the postsynaptic neurons. This shows an endogenous tone of adenosine in the mature and immature rat cortex, revealed by A_1R antagonist 8-cyclopentyltheophylline (8CPT), but the tone is far greater in the mature rat cortex. Additional bath applied adenosine in still able to reduce the amplitude of the EPSP. Extracted from figure 1F (Kerr et al. 2013).

Adenosine has been implicated in many psychological disorders, as in the adenosine hypothesis of schizophrenia (Fuxe et al. 2009; Boison et al. 2011) and in degenerative diseases through the use of $A_{2A}R$ agonists. In Alzheimer's disease the agonists have been shown to improve cognitive func-

tion (Rahman 2009) and in Parkinson's Disease to reduce the characteristic motor deficits (Schwarzschild et al. 2006). Adenosine receptors are expressed ubiquitously throughout the brain, and adenosine has been implicated in a multitude of different functions. In the cortex and hippocampus, adenosine is thought to be important for working memory (Singer et al. 2012), through the balance of A_1R and $A_{2A}R$ activation. Adenosine is able to shape striatal function though receptor heterodimers, where the adenosine GPCR is linked with another *e.g.* $A_{2A}R$ and dopamine D_2R. In addition adenosine can effect glutamate signalling, *e.g.* alcohol drinking increases in mice with impaired adenosine clearance (Lee et al. 2012). In the cerebellum adenosine has been shown to modulate ethanol and cannabinoid induced ataxia (Dar and Mustafa 2002). Subsequently adenosine has become a promising target for pharmacological treatments for a wide array of cognitive, mood and degenerative disorders (Chen et al. 2013). However the key areas of adenosine study are sleep, epilepsy and hypoxia.

1.2.1 Sleep cycles

Caffeine, the worlds most popular recreational drug, is an adenosine receptor antagonist and promotes wakefulness, whilst adenosine is thought to promote sleep, the concentration of extracellular adenosine increases during wakefulness and decreases during sleep. For example microdialysis showed an increase in adenosine tone ∼30% in the basal forebrain during the dark cycle (Murillo-Rodriguez et al. 2004), similarly biosensor measurements in mouse hippocampal slices showed a ∼70% decrease in adenosine tone between the light and dark cycle (Schmitt et al. 2012).

Conversely, interfering with adenosine concentration influences the duration of sleep and wakefulness, *e.g.* direct intracerebroventricular infusion of adenosine in rats reduced the time spent awake by ∼30% (Virus et al. 1983) and ethanol leads to increases in extracellular adenosine in the perifornical hypothalamus, due to the effect of ethanol on adenosine clearance. This increase in extracellular adenosine acts on the A_1R of orexin neurons, a class of neurons which produce orexin, a neuropeptide involved in wakefulness and appetite. This inhibition reduces stimulation of wake-active neurons and increases sleep (Sharma et al. 2014). In addition to changes in the concentration of adenosine during the sleep wake cycles, changes have also

been observed in the enzymes involved in metabolising adenosine. For example, higher enzyme activity was observed in brain homogenates from the rat cortex taken at night (Kovács et al. 2011).

Adenosine fulfils many of the requirements of a sleep regulatory substance and may be a molecular marker of sleep drive; infusion of adenosine promotes sleep, concentration increases with sleep deprivation and disruption of receptors or metabolism alters sleep. However, the rapid clearance of extracellular adenosine makes it unlikely that it is involved in long term sleep maintenance, instead influencing sleep transitions and intensity (Holst and Landolt 2015; Krueger et al. 2013). This work quantifies how rapidly adenosine is cleared from the ECS and the influence sleep-wake changes in metabolism have on this clearance rate.

1.2.2 Epilepsy and seizures

Epilepsy is a condition where the subject is prone to seizures, characterised by hypersynchronous discharge of a population of neurons. The excessive neuronal activity can cause damage to the tissue and cell death. Adenosine is released during seizures (Figure 1.2) and is involved in seizure termination, primarily via the A_1R. The application of adenosine receptor antagonists have a proconvulsant effect, whilst agonists reduce the length of seizures (Dunwiddie and Masino 2001). Endogenous adenosine builds up during seizures, *e.g.* measurements made by fast-scan cyclic voltommetry (FCSV) found a 260% increase in extracellular adenosine prior to seizure termination (Van Gompel et al. 2014), while biosensor measurements found an increase of 3.2μM' of adenosine and its breakdown products (Etherington et al. 2009).

Adenosine regulation may also cause epilepsy. Adenosine kinase (ADK) is an enzyme that catalyses the transfer of a phosphate from adenosine triphosphate (ATP) to adenosine, resulting in adenosine diphosphate (ADP) and adenosine monophosphate (AMP). The ADK hypothesis of epileptogenesis suggests ADK as a diagnostic marker of epilepsy, with overexpression of ADK in mice reducing adenosine tone and increasing sezure activity, with increased sensitivity to brain injury from seizure (Boison 2008).

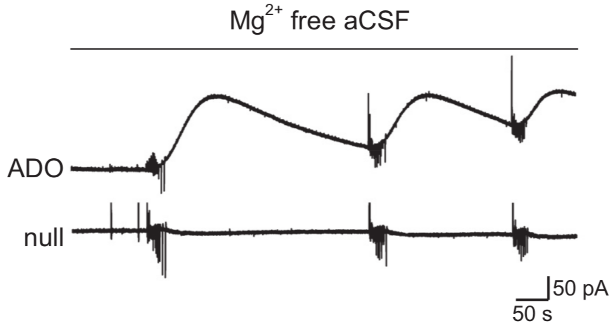

Figure 1.2: **Adenosine biosensor signal rises in response to pathological network activity.** Seizures induced in slices of the rat somatosensory neocortex with magnesium free solution, produce a large increase in the adenosine (ADO) biosensor signal but not the null sensor. The ADO biosensor is sensitive to adenosine, inosine and hypoxanthine. So the rise must be due to an increase in extracellular adenosine, or its breakdown products inosine and hypoxanthine. Extracted from figure 5A (Wall and Richardson 2014).

1.2.3 Hypoxia-ischemia

A lack of oxygen (hypoxia) or an inadequate blood supply (ischemia) to brain tissue results in a rapid increase in extracellular adenosine (Dale and Frenguelli 2009). Adenosine released during hypoxia can have a neuroprotective effect by reducing electrical activity, conserving energy and causing vasodilation, attempting to increase the supply of blood and oxygen. Hypoxic adenosine release is dependent on prior exposure to hypoxia and can be displaced *e.g.* Within 5 minutes of hypoxia adenosine increased by 3.0μM' in rat hippocampal slices, but this was reduced by ~45% in a second hypoxic insult 28 minutes later (Frenguelli et al. 2003).

1.2.4 Adenosine sources

Adenosine can form in the extracellular space by metabolism of ATP, which is released at synapses as a co-transmitter or from hemichannels in astrocytes. Adenosine could also be released directly by transporters or by exocytosis (Figure 1.3). There is evidence for multiple release pathways depending on brain region and the nature of the stimulus. Adenosine released spontaneously due to endogenous activity (Nguyen et al. 2014) or experimentally by stimulating cells is termed activity-dependent release (Wall

and Dale 2007; Wall and Dale 2013; Pajski and Venton 2010; Klyuch et al. 2011; Swamy and Venton 2007). Adenosine may be neuroprotective, and is released as a result of insults, such as hypoxia, ischemia, oxygen glucose deprivation, mechanical stimulation (Frenguelli et al. 2003; Frenguelli et al. 2007).

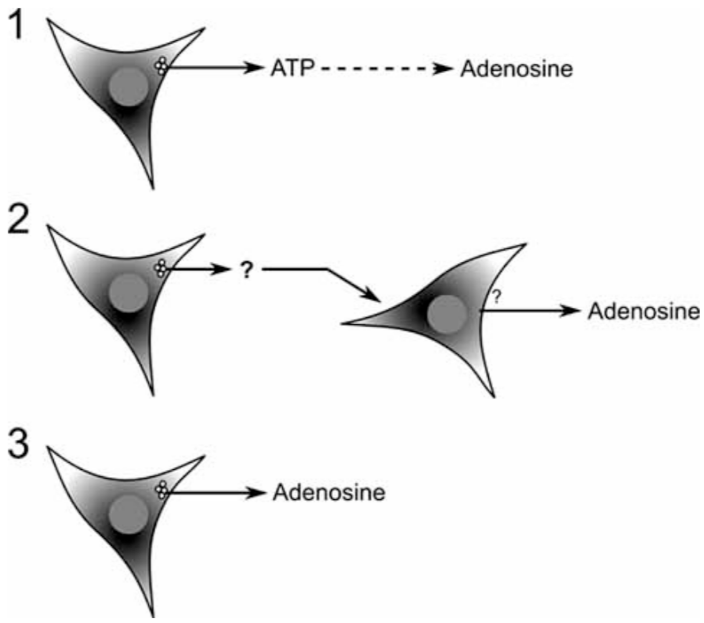

Figure 1.3: **Possible mechanisms for adenosine release**. **1)** ATP can be released into the extracellular space as a co-transmitter at synapses from hemichannels in astrocytes, which can then be metabolised resulting in adenosine. **2)** Indirect adenosine release can occur when another signalling molecule such as glutamate provokes adenosine release from a downstream cell. **3)** Adenosine can be released directly either by exocytosis or via transporters. Figure 1 from (Wall and Dale 2008).

Activity-dependent release in the striatum following low frequency stimulus was greatly diminished ($\sim$60%) by chemically inhibiting extracellular degradation of ATP, but release following a high frequency stimulus was unaffected. Furthermore neither were affected by inhibiting cellular transport and the release was dependent on both calcium and glutamate receptors, suggesting the stimulated neurons signalled other cells which then released adenosine by exocytosis (Pajski and Venton 2010). With focal stimulation in the mouse hippocampus $\sim$60% of the rise in extracellular adenosine is due to extracellular metabolism of ATP (uncovered using CD73 knockout mice) with $\sim$40% of adenosine release due to transporters (Wall and Dale

2013). In the cerebellum half of activity-dependent adenosine release is due to metabolism of ATP release by exocytosis from parallel fibers. There are multiple source of adenosine, this work estimates their duration and range of influence, which is essential to quantify their impact on network dynamics.

1.3 Volume transmission

Volume transmission (VT) in the brain refers to all the possible mechanisms that cells could utilise for communication without the need for a connection, such as a synapse or a gap-junction. These mechanisms have been divided into physical and chemical signals. The physical signals could comprise of pressure waves, temperature values and electrical currents (local field potentials). The chemical signals are where a cell releases some substance, (neuromodulator, growth factor, etc.) into the ECS, which then diffuses along concentration, electrical, temperature and pressure gradients to other cells. The chemical signals can be further classified by whether they are: 'Safe', reach the destination unaltered, (*e.g.* microvesicles, exosomes) or 'Unsafe', (*e.g.* neuromodulators, neurotransmitters). 'Reserved', only received by cells with specialised mechanisms for decoding the signal (*e.g.* adenosine require GCPR) or 'Broadcast' (*e.g.* carbon dioxide). Lipophilic, able to pass through the cell membrane (*e.g.* carbon dioxide) or Hydrophilic (*e.g.* neuromodulators). Focusing on neuromodulators in general and specifically adenosine, it is an unsafe reserved hydrophilic chemical signal. (Agnati et al. 2010).

Reaction-diffusion dynamics in tissue have been studied at different levels of description, particularly focused on the non-linear Michaelis-Menten kinetics, which characterises many enzyme reactions and active transport mechanisms (section B.1). Assuming a well-mixed system, the state can be described by a vector where each element represents the number of molecules of a chemical species. Representing reactions as transition probabilities between states gives rise to the chemical master equation, (CME) a Markov process that provides a full stochastic description of the system. In a well mixed system at thermal equilibrium (so the probability of a collision between chemical species is the same throughout the system), in the gas-phase

(so from collision theory the reaction rate will follow a Maxwell-Boltzmann distribution) the CME can be derived from a microphysical description of the system (Gillespie 1992).

The chemical Langevin equations (CLE) is a continuous approximation of the CME (which is valid when the system is sufficiently large), dealing with the concentration of each substance (Gillespie 2000). So instead of a vector representing the number of each chemical species, there is a vector representing the concentration of each chemical species and the transitions follow a Gaussian distribution. Reaction rate equations (RRE) are deterministic approximations of the CLE, *i.e.* the mean of the CLE and are valid when the system is large enough that the fluctuations are relatively small. This can be further reduced using a Quasi-steady-state approximation (QSSA) to give a one-dimensional ODE (discussed in section B.1).

In order to allow for spatial non-uniformity in the distribution of substances that occur in tissue, general purpose computational tools have been developed *e.g.* MesoRD (Hattne et al. 2005) and Smoldyn (Andrews and Bray 2004), which have been applied to specific problems in systems biology, including general problems such as simulating diffusion in various tortuous topologies (Tao and Nicholson 2004) and specific problems such as determining the roles of different NMDAR subtypes (Farzan 2010). Here a macroscopic model of tissue is developed, it could be extended to included microscopic features of tissue, but little is known about the distribution of the model components at a subcellular scale.

1.3.1 Volume fraction

Activity of signalling molecules in the ECS interacting with receptors, enzymes and transporters depends on their concentration. The concentration can be defined in two ways; the total concentration, ratio of the amount of substance with the volume of tissue, or the relative concentration, the ratio of the amount of substance with the volume of the ECS. The two concentrations are related by the free volume fraction, the volume of the ECS divided by the volume of the tissue α which is around 20% in neural tissue, but can fall to $\sim$5% in pathological conditions (Syková et al. 1994). It is

the relative concentration which is relevant when considering the influence and clearance of adenosine, however many experimental results are given in terms of the total concentration.

1.3.2 Cellular transport

Adenosine is a nucleoside, a subunit of nucleic acid adenine, and can be transported across cell membranes by nucleoside transporters (NT). The NT are divided into two solute carrier families, SLC28 the concentrative NT (CNT) and SLC29 the equilibrative NT (ENT), ENTs are further subdivided into four classes ENT1 transport is inhibited by nitrobenzylthioinosine (NBMPR) whereas ENT2 is insensitive to NBMPR. The other two classes ENT3 and ENT4 are less well characterised and are thought to be primarily involved with transport within cells (Baldwin et al. 2004). ENT1 is ubiquitously expressed, they have been 'ultralocalised' to subcellular structures in the rat spinal cord and are found on the soma of neurons, myelinated and unmyelinated axons, glial and oligodendrocytes. They are expressed both presynaptically and postsynaptically. However there is some evidence that they are more densely concentrated in the region around the soma (Governo et al. 2005). The role of ENTs have also been explored using transgenic mice which lack ENT1 (Choi et al. 2004). The CNTs are sodium/nucleoside co-transporters and have been divided into three subtypes, CNT1, CNT2, and CNT3. CNT1 and CNT2 are found in the rat brain (Anderson et al. 1996), with CNT2 having a greater affinity for adenosine. However research has focused on the role of ENTs as there are currently no good inhibitors for CNTs. Within cells diffusion is far slower, $\sim 5 - 20$ times than free diffusion. This is primarily due to macromolecular crowding (Schnell and Turner 2004), so is less relevant to the range of adenosine signalling that extracellular diffusion. In addition purines are transported between the cytosol and the nucleus and mitochondria, but this is unlikely to play a substantial role in adenosine clearance.

1.4 Purine metabolism

Purines consist of two rings, and form many biologically significant compounds including two of the nucleotide bases adenine and guanine. The purine metabolism is a group of 27 enzymes catalysing reactions for synthesis, recycling, conversion and disposal of the various purines. Adenosine triphosphate (ATP) is known as the molecular unit of currency, as it is used ubiquitously for energy storage and transfer. The evolution of purines for signalling may be as a result of the ever-present nature of ATP.

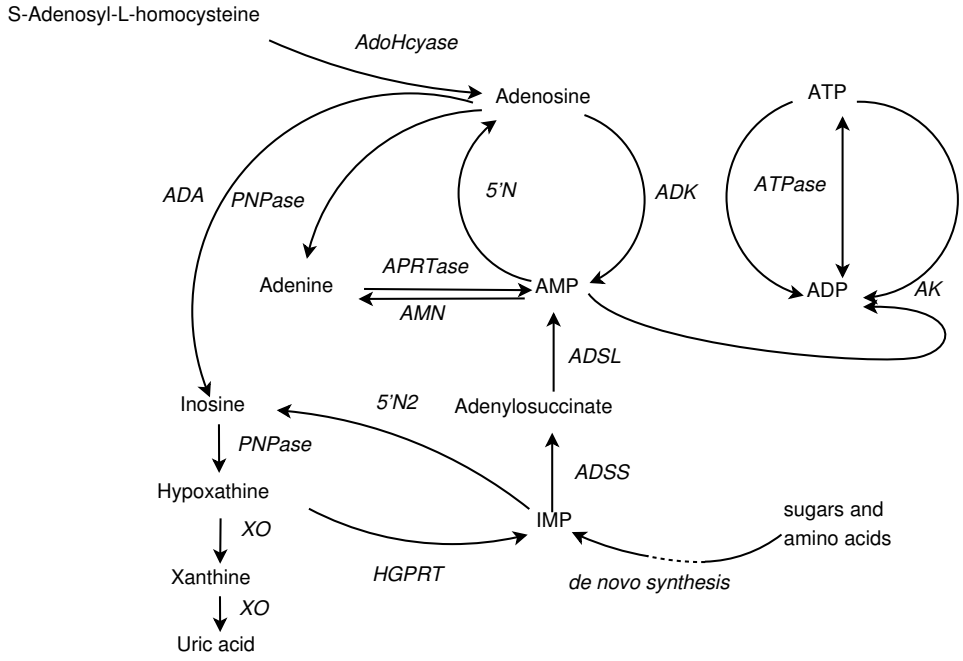

Figure 1.4: **The purine metabolism responsible for synthesis, salvage and removal of adenosine.** The enzymes shown are; s-adenosyl-L-homocysteine hydrolase (AdoHcyase), polynucleotide phosphorylase (PNPase), adenine phosphoribosyltransferase (APRTase), adenosine monophosphate nucleosidase (AMN), adenosine deaminase (ADA), 5′-nucleotidase (5′N), adenosine deaminase (ADA), adenosine kinase (ADK), ATP monophosphatase (ATPase), adenylate kinase(AK), adenylosuccinate lyase (ADSL), adenylosuccinate synthetase (ADSS), Hypoxanthine-guanine phosphoribosyltransferase (HGPRT), 5′-nucleotidase II (5′N II), polynucleotide phosphorylase (PNPase) and xanthine oxidase (XO). This is only a part of the full purine metabolism and many of the enzymes are involved in additional reactions not depicted here. *E.g.* ADK transfers a phosphate from ATP to adenosine resulting in an ADP and AMP molecule.

There are two sources of AMP, *de novo* synthesis or building it from the com-

ponent parts (sugar and amino acids) and the salvage pathway, where the by-products of consuming ATP are recycled (Berg et al. 2002). The *de novo* pathway first involves 10 reactions to create inosine monophosphate (IMP), the salvage pathway can convert products such as ADP, AMP, adenosine, inosine, IMP or hypoxanthine to ATP (Figure 1.4). Under resting conditions there is considerable activity through the futile cycle between adenosine and AMP (Dunwiddie and Masino 2001).

Immunohistochemistry is used to locate specific enzymes (Nagy et al. 1985) or transporters (Guillén-Gómez et al. 2004) within the brain. This information is useful in deciding which processes may be relevant for adenosine clearance and for comparing brain regions. Quantitative information for the enzymes of purine metabolism have been determined in either the whole rat brain or the rat cortex, principally by dissecting the brain and homogenising it in a centrifuge. Then different concentrations of the substrate are added to the homogenate to measure the initial rate at which the reaction products are formed, which provides an estimate of the enzyme kinetics. The transporters require the cells to remain intact, so while they can be located immunohistochemically, the kinetics can be quantified using radio or florescent labelled purines, and cell cultures rather than brain tissue. However there is little work on the diffusion and clearance of adenosine in the brain, with the kinetics of only a few of the enzymes in the purine metabolism and some of the aspects of transport available. The complex and multifaceted role of adenosine in both physiological and pathological tissue is further masked by multiple release and removal mechanisms.

1.5 Measuring extracellular adenosine concentration

Early methods of measuring adenosine concentrations include direct measurement of the CSF via dialysis or microdialysis, which has good chemical resolution but poor temporal resolution (typically around 10 minutes) and due to the large probe size ($> 200\mu$m) is likely to cause significant tissue damage, effecting tissue up to 1mm from the site (Robinson et al. 2008). Destructive techniques, such as rapid freezing and homogenisation of brain tis-

sue have also been used (Winn et al. 1979), however it is not clear how much the methodology will distort these measurements. Indirect measurements provide a qualitative estimate of the amount of adenosine by measuring its effect on cells via electrophysiology (Dunwiddie and Diao 1994), however it is difficult to infer the concentration of adenosine as the effect of additional adenosine depends on the amount present, described by the dose response curve of the receptor. More recently positron emission tomography has been used, which requires the use of labelled receptor agonist/antagonists that are subsequently displaced by endogenous adenosine (Paul et al. 2011). Recent developments in microelectrode biosensors (Frenguelli et al. 2003) and fast-scan cyclic voltammetry (Swamy and Venton 2007) allow adenosine concentration in tissue to be measured directly at high spatio-temporal resolution. However FSCV and biosensors remove the adenosine they detect, potentially resulting in a significantly lower concentration near the biosensor surface, this work estimates the extent of this effect has on a biosensor signal.

1.6 Outline

Here two problems are addressed, the first relating to adenosine clearance in the brain. Information about the various clearance process is taken from an extensive literature review and used to; construct the first detailed model of adenosine clearance, estimate both the range of influence and the duration of an adenosine signal, and identify aspects of adenosine cleanse that have yet to been quantified. The second is to evaluate the efficacy of biosensors, which are extensively used to measure the concentration of neuroactive substances, (including adenosine) in neural tissue. To achieve this a mathematical model is constructed for a tortuous tissue environment and compared with a model for the free-flow calibration environment.

In chapter 2 a hierarchy of adenosine transport models are constructed to evaluate the relative significance of the different clearance mechanisms. Several abstractions necessary to create a parsimonious description of adenosine dynamics are explained, such as not including ATP concentrations and limiting the intracellular space to two cell classes; neurons and glia. Details of the parameter estimates are given, together with how they are inferred

from the information obtained from an extensive literature search. Chapter 3 outlines the model prediction and the limits where the model can be solved analytically and via numerical solutions. These indicate a dominant role for diffusion and neuronal clearance, as well as the influence of endogenous tone on clearance mechanisms. In chapter 4 the biosensors used to monitor adenosine activity in brain slices are modelled at microscopic and macroscopic levels. Particle simulations, analytic and numeric solutions are obtained in 2D and 3D, showing that a correction is required when biosensors are calibrated in a free environment, but used in a tortuous one. Finally the conclusion and discussion of the findings and limitations are given in chapter 5.

Chapter 2

Models and parameters available in the literature

2.1 Introduction

This chapter describes the first detailed model of adenosine transport in neural tissue, including an approximation of extracellular and intracellular metabolism. Adenosine is involved in physiological and pathological brain function, so it would be beneficial to be able to predict the duration and range of influence of endogenous adenosine. Adenosine is removed from tissue by various clearance mechanisms, which may be be pharmacologically blocked (Dunwiddie and Diao 1994) or genetically removed (Choi et al. 2004). To quantify the relative importance of the clearance mechanisms a hierarchy of models is constructed. The structure of the models is general and can be adapted to different tissue, however as an example, rat cortical tissue is modelled, using parameters obtained by an extensive literature search. Due to the current ambiguity in adenosine release pathways (Wall and Dale 2008; Dale and Frenguelli 2009; Nguyen et al. 2014), four abstract endogenous sources are considered: A constant uniform and a constant point source, appropriate for modelling the basal tone of adenosine, a brief uniform source and a brief point source, corresponding to activity-dependent and spontaneous release events. The models are applicable to experimental setups, and bath application of adenosine for tissue slices is considered so as to inform experimental work.

The process of release and clearance of extracellular adenosine and the appropriate scale at which to model these processes in tissue is discussed. This allows the development of a hierarchy of models and consideration of how reasonable parameters can be inferred from the available literature. The analytic and numerical solution for the models is described, with discussion of how it can be applied or compared with experimental work, and the limitations of the approach adopted.

2.2 Model components

A number of physiological processes, and a hierarchy of models is considered. Removal of adenosine from the extracellular space depends on cellular uptake and the purine metabolism. Enzymes of the purine metabolism can either build on the adenosine molecule, creating AMP then ADP and ATP or breakdown the adenosine molecule giving rise to inosine then hypoxanthine. A macroscopic model is developed, so appropriate scales are micrometres, seconds and micro molars, therefore amounts are stated in zeptomols, because 1zmol in $1\mu\text{m}^3$ is $1\mu\text{M}$.

2.2.1 Adenosine source

A number of spatiotemporal patterns for adenosine sources are considered. There is uncertainty regarding the mechanisms for endogenous adenosine release, with evidence for multiple release pathways depending on the brain region and the nature of the stimulus (Swamy and Venton 2007; Wall and Dale 2008; Cechova et al. 2010; Klyuch et al. 2012a; Nguyen et al. 2014). With little known about the amount of adenosine released, a range for the source function $S(t, x)$ has to be inferred. Adenosine could enter the extracellular space as a result of metabolic break down of ATP, so the metabolic cost of activity suggests the relevant order of magnitude. Many activities metabolise ATP such as; vesicle release 300zmols, mini-EPSP, $1,000$zmols, action potential $640,000$zmol and a neuron $570,000$zmol/s or glia $170,000$zmol/s at rest (Attwell and Laughlin 2001; Silver et al. 2003). These estimates of ATP consumption suggest a reverent scale, not a specific source intensity, as it is not clear how much of the ATP consumption would ultimately be

converted to adenosine or how much of the adenosine created though energy consumption would be released into the extracellular space.

The source term $S(t, x)$ in equations (2.17), (2.20), (2.22), (2.28) and (2.34), for a constant uniform source is $S(t, x) = C$ [μM/s], whereas a brief uniform source $S(t, x) = C_0\delta(t)$ [μM]. For a constant point source $S(x) = \delta(x)F$ [zmol/s] and a brief point source $S(t, x) = \delta(x)\delta(t)F_0$ [zmol]. To inform experimental work, bath applied adenosine is considered, where the bath-applied concentration provides the surface boundary condition with a fixed concentration at the top and bottom of the slice.

2.2.2 Deamination in the extracellular space and within neurons

Adenosine deaminase (ADA), irreversibly deaminates adenosine to inosine. This is modelled in the QSSA of MM kinetics (Eq. 2.6), although product inhibition, where large amounts of inosine inhibits ADA, have been ignored, (which is justified as the effect requires relatively high concentrations, $K_i = 143\mu$M) (Saboury et al. 2002). ADA is part of both the extracellular metabolism (ecto-ADA) and the neuronal metabolism for a subset of neurons, including those in restricted areas of the cortex and striatum (Yamamoto et al. 1987). Immunohistochemistry suggests ADA is either absent in glia or present in such low concentration as to be undetectable (Nagy et al. 1984; Yamamoto et al. 1990). Cultures show activity for both neurons and glia, which may be due to membrane bound ecto-ADA. In these models ADA is limited to the extracellular and neuronal metabolism.

2.2.3 Phosphorylation within glia

The purine metabolic pathway contains several cycles, the most important for controlling basal levels of adenosine is the cycle of AMP to adenosine via 5′-nucleotidase (5′N) and adenosine back to AMP via adenosine kinase (ADK) or to ADP via adenylate kinase (AK). AK catalyses the reaction $AMP + ATP \leftrightarrow 2ADP$ and is in part responsible for amplifying small changes in ATP concentration to large (20 fold) changes in AMP. Currently

six isoforms of AK have been identified, AK1, AK4 and AK5 have been localised to brain tissue (Noma et al. 2005), with AK1 limited to neurons in the rat and mouse brain (Janssen et al. 2004). AK5 is cytosolic and shows strong staining for neurons and moderate for glia in humans (Kampf et al. 2009), whereas AK4 is confined to mitochondrial matrix. Unfortunately the kinetics of AK4 and AK5 are currently unavailable for the rat. The MM constants of AMP $K_m = 172\mu$M for AK5 humans (Solaroli et al. 2009), compared to $K_m = 250\mu$M for 5′N, suggest AMP will preferably bind to AK5 in glia for low intracellular concentrations of AMP, so most AMP will be phosphorylated to ADP. Here AMP, together with ADP and ATP are not explicitly included in the model, but implicitly through the source term, as they interact with so many other pathways, so would greatly increase the model's complexity. This may exaggerate the role of ADK, with all adenosine that is phosphorylated to AMP being removed from the model.

2.2.4 Clearance and salvage within glia

Adenosine deaminated to inosine by ADA can be metabolised by purine nucleoside phosphorylase (PNPase) to produce hypoxanthine. A series of enzymes can then recover AMP from hypoxanthine via hypoxanthine-guanine phosphoribosyltransferase (HGPRT), or further metabolise it via xanthine oxidase (XO), so it can be removed by erythrocytes through the blood brain barrier (BBB). The BBB is a highly selective permeable membrane separating the blood from the cerebrospinal fluid (CSF) that fills the ECS of the brain. An unsaturating removal rate (μ_8) is used to capture the metabolism of inosine. The removal of inosine is limited to glia, because transport of nucleosides through the BBB is mediated by astrocytes, and some evidence suggests PNPase is restricted to glial metabolism (Castellano et al. 1990), although other work shows activity in both glia and neurons (Zoref-Shani et al. 1995; Parkinson and Xiong 2004). Removal though the BBB is only relevent for applying the model in the *in vivo* case, *in vitro* loss though the surface of the slice will have a substantial effect.

2.3 Diffusion and tortuosity

Macroscopic models of tissue take an average over; spatial structures, sources and sinks, with a smaller diffusion coefficient to account for the tortuosity of the medium. Macroscopic models of brain tissue are considered valid for length scales of order 10μm (Nicholson 2005). The concentration of adenosine and its breakdown products are modelled, so it is necessary to account for the volume fraction of the extracellular and intracellular space, to deal with transport between them and to translate the source term from an amount to a concentration of adenosine. The models described below include diffusion, described by Laplace operator ∇^2 which depends on the coordinate system. For a point source spherical coordinates are used, whereas the bath applied case is solved in one-dimension, the depth into the slice. For a uniform source and the diffusion term can be removed from the models. Diffusion in the intracellular space is omitted from the models, this is necessary for any macroscopic model of tissue. A mesoscopic or microscopic model, with the geometry of cell membranes and distribution of transporters could include intracellular diffusion. However, it would be difficult to constrain the parameters of such a model, given the paucity of information available at this time.

The extracellular space in neural tissue essentially resembles a foam, with the cells representing the bubbles and the ECS the water. This structure is typically described by the volume fraction or permeability (α), the ratio of extracellular volume to the total volume. As well as the tortuosity (θ), the proportional increase in the average path a particle must take to move around obstructions. Early estimates of volume fraction and tortuosity were performed using radio tracers. They would be perfused into the ventricle cavities of the brain of a living animal. The animal was then killed and the brain frozen and sectioned. The radioactivity of sections could be measured together with their distance from the ventricle cavities, allowing the effective diffusion coefficient to be estimated. The tortuosity squared θ^2 is estimated as the ratio of the free to effective diffusion coefficients;

$$\theta^2 = \frac{D^*}{D} \tag{2.1}$$

where D^* is the free diffusion coefficient and D is the effective diffusion coef-

ficient in the torturous medium. Additionally the volume fraction and first order removal kinetics for the blood brain barrier (BBB) can be inferred (Blasberg et al. 1975). This method allowed the properties of tissue for a wide variety of chemicals to be measured. However if the analyte is transported to the intracellular space or lost too rapidly through the BBB it will not provide an accurate measurement.

Real-time iontophoresis (RTI) is used to deliver a constant point source of an ion, *e.g.* Calcium (Ca^{2+}) or Tetramethylammonium$^+$ (TMA^+), which is then measured using an ion-selective microelectrode (ISM) placed at distance R, usually $30-60\mu$m away. Then assuming no entry into cells or loss across the BBB, the solution to the diffusion equation in spherical coordinates provides a function for the concentration $M(t)$ at the ISM, which is proportional to the signal. When there is uptake into the cells, (assuming first order kinetics) the concentration is given by (Eq. 2.3), (Nicholson and Rice 1987).

$$M(t) = \frac{Q\theta^2}{4\pi D^*\alpha R}\text{erfc}\left(\frac{R\theta}{2\sqrt{D^*t}}\right) \tag{2.2}$$

$$\begin{aligned} M(t) = \frac{Q\theta^2}{8\pi D^*\alpha R}\Bigg[&\text{erfc}\left(\frac{R\theta}{2\sqrt{D^*t}} + \sqrt{kt}\right)\exp\left(r\sqrt{\frac{r}{D^*}}\right) \\ &+\text{erfc}\left(\frac{R\theta}{2\sqrt{D^*t}} - \sqrt{kt}\right)\exp\left(-r\sqrt{\frac{r}{D^*}}\right)\Bigg] \end{aligned} \tag{2.3}$$

Where R is the distance between the iontophoresis source and the ISM, D^* is the free diffusion coefficient of the ion used and Q is the source strength. A nonlinear fit of (Eq. 2.2) to the signal obtained from the ISM gives an estimate of α and θ. This method has been extended to include first-order removal kinetics and anisotropy (Syková and Nicholson 2008). It has been used to estimate tissue parameters in many brain regions and species (Syková and Nicholson 2008). Including 1.6 for layers II-III of the rat neocortex (Pérez-Pinzón et al. 1995) with values ranging from 1.5 for layer II and 1.7 for layer VI (Lehmenkühler et al. 1993), the diffusion curves for layer I were not stable possibly due to the small layer width or damage caused by opening the skull.

The obstacles to diffusion may not be spatially uniform and instead prefer-

Parameter	Value	Temperature
D^*	$520\mu m^2 s^{-1}$	Diffusion coefficient of adenosine at 25.5°C (Bowen and Martin 1964) in a free environment
D^*	$690\mu m^2 s^{-1}$	Diffusion coefficient of adenosine at 37°C
D^*	$610\mu m^2 s^{-1}$	Diffusion coefficient of adenosine at 32°C
D	$260\mu m^2 s^{-1}$	Tortuous diffusion coefficient at 37°C with tortuosity of 1.6 for rat cortex (Pérez-Pinzón et al. 1995; Nicholson 2001)
D	$230\mu m^2 s^{-1}$	Tortuous diffusion coefficient at 32°C

Table 2.1: **Free and tortuous diffusion coefficients of adenosine.** The free diffusion coefficient of adenosine was estimated at physiological and experimental temperatures using (Eq. 2.11). The effective diffusion coefficient was estimated from the tortuosity of the rat cortex determined by the diffusion of Tetramethylammonium$^+$ (TMA^+).

entially inhibit diffusion in a specific direction. In this case the tortuosity, θ and α are tensors not a scalar. For example, in the rat auditory cortex the additional distance required to move within a layer are 1.5 and 1.7 whereas to go perpendicularly within a column is 1.8, determined using diffusion-weighted magnetic resonance imaging to monitor the apparent diffusion coefficient of water in each of the directions (Voříšek et al. 2002).

It has been suggested that bulk flow of metabolites is an important clearance mechanism, referred to as the glymphatic pathway (Nedergaard 2013; Iliff et al. 2012). Flow has been observed *in vivo* through a closed cranial window in mice, where CSF passes through the para-arterial space where aquaporin-4 (AQP4) channels on astrocytes facilitated convective flow from the para-arterial space to the ECS, which drives waste products from arteries and toward the veins. However this flow is very sensitive to the pressure gradient, as it is only observed if the cranial window is closed. The flow occurs in perivascular spaces which have a far wider diameter $\sim 5-10\mu$m than the space between cells, the ECS $\sim 40-60$nm where there may be little bulk flow (Wolak and Thorne 2013; Abbott 2004). Hence flow has not been included in the models.

2.4 Volume fractions

The extracellular volume fraction (α) is obtained from the same experiments as tortuosity, by fitting a solution to the diffusion equation (Eq. 2.2) to the ISM signal obtained. The sum of the extracellular and intracellular (β) volume fraction together with the solid volume fractions (γ), accounting for cell membranes, must equal one.

$$1 = \alpha + \beta + \gamma \tag{2.4}$$

Here the intracellular volume fraction is divided between neurons (80%) and glia (20%). Several estimates could be made from the available literature, all of which give a similar ratio. These include, qualitative analysis of the volume composition of the human neocortex (84% to 16%) (Bennett 2011), density and weight ratios from cell isolation (90% to 10%) (Subbalakshmi and Murthy 1985) and the ratio of neuron soma (18%), glia soma (7%) and neuropil (75%) in the rat cortex (Miller and Potempa‘ 1990) together with the division of neuropil between axons, dendrites and glia in the rat hippocamupus (81% to 19%) (Mishchenko et al. 2010). Cell counts combined with estimates of the cell size suggest a ratio of (84% to 13%) (Subbalakshmi and Murthy 1985; Bass et al. 1971; Miller and Potempa‘ 1990). These estimates appear to contradict a study of antioxidants ascorbate and glutathione (Rice and Russo-Menna 1997), which found a 40% neuronal and 60% glial volume fraction to be consistent with the compartmentalisation of both antioxidants. However, this may be due to properties of the antioxidants, as it would violate the 3/5 rule, where, for optimal connections, 3/5 of the neuropil is composed of axons and dendrites (Chklovskii et al. 2002).

There are different estimates available for the number and ratio of glia to neurons in the rat cortex, *e.g.* a cell isolation study suggests 1.8 times as many neurons as astrocytes (Subbalakshmi and Murthy 1985) Staining gives ratios of neurons to glia between 2.1 and 3.5 for different layers of the rat somatosensory cortex, with an estimated $130,000$ neurons to $53,000$ glia in 1mm^3 (Bass et al. 1971). The glia can be further subdivided, cell counts suggests around 56% of glia in the rat cortex (at 0.75 months) are astrocytes, (Ling and Leblond 1973) with a similar proportion of 52% found in adult rat somatosensory cortex (Ren et al. 1992). The gila have a variety

Parameter	Value	Description
α	0.21	Extracellular volume fraction (Rice and Nicholson 1991)
β	0.59	Total intracellular volume fraction based on extracellular and solid volume fraction (Rice and Russo-Menna 1997)
β_n	0.47	Neuron volume fraction 80% of intracellular volume
β_g	0.12	Glial volume fraction 20% of intracellular volume

Table 2.2: **Volume fractions for extracellular, neuronal and glial space in the rat cortex.**

of intricate shapes related to their function, which makes estimating their volume quite challenging. Assuming the intracellular volume of each class of glia is proportional to the volume of its nucleus (estimated from diameter by assuming it is approximately spherical) provides an estimate for the relative cell size for the different types (microglia and oligodendrocytes). Together with the cell counts this suggests that astrocytes account for around 87% of the glia volume fraction (Ling and Leblond 1973). As astrocytes make up the majority of the glia volume fraction, it is assumed that the intracellular metabolism for all glia in the model behave as astrocytes.

2.5 Michaelis-Menten kinetics

The key component of all the models are transporters and enzymes of the purine metabolism. Here a review of the literature on the purine metabolism is presented, together the with the methods required to obtain parameters in a form that can be used in the models. Immunohistochemistry is used to locate specific enzymes (Nagy et al. 1985) or transporters (Guillén-Gómez et al. 2004) within the brain. This information is useful in deciding which processes may be relevant for adenosine clearance and for comparing brain regions. Quantitative information for the enzymes of purine metabolism have been determined in either the whole rat brain or the rat cortex, principally by dissecting the brain and homogenising it in a centrifuge. Then

different concentrations of the substrate are added to the homogenate to measure the initial rate at which the reaction products are formed, which provides an estimate of the enzyme kinetics. The transporters require the cells to remain intact, so while they can be located immunohistochemically, the kinetics can be quantified using radio or florescent labelled purines, and cell cultures rather than brain tissue is used.

The parameters for the enzyme kinetics available in literature are most often available in the form of Michaelis-Menten (MM) kinetics which describe the following reaction;

$$E + S \underset{k_{-1}}{\overset{k_1}{\rightleftharpoons}} ES \overset{k_2}{\rightarrow} E + P \tag{2.5}$$

Where E is the enzyme and S is the substrate. The irreversible product formation $ES \overset{k_2}{\rightarrow} E + P$ assumes that either there is far more substrate than product or that the energy released by the reaction is large. By making the further assumptions that the total enzyme concentration does not change and that the bound complex $[ES]$ does not change with the same timescale as the product formation. It is possible to derive the quasi-steady-state approximation (QSSA);

$$\frac{dP}{dt} = \frac{V_{\max}[S]}{K_m + [S]} \tag{2.6}$$

where

$$K_m = \frac{k_2 + k_{-1}}{k_1} \tag{2.7}$$

$$V_{\max} = k_2 E_0 \tag{2.8}$$

The derivation of the QSSA form (Eq. 2.6) is given in B.1. The enzyme kinetics are typically determined by removing a region of the brain and homogenising it with a centrifuge. A detergent may be used to degrade membranes and the homogenate will be separated into different fractions, *e.g.* cytosol, synamtosomes and nuclear fraction. The enzyme reactions are then determined by adding different concentrations of the substrate (S_0) to the homogenate and terminating the reaction after a fixed time period. The concentration of the product of the reaction is used to determine the

velocity V, which is then fitted to the QSSA of the reaction kinetics (Eq. 2.9). Traditionally the kinetics were determined with a double reciprocal (or Lineweaver-Burk) plot, where the reciprocal of the velocity $\frac{1}{V}$ was plotted against $\frac{1}{S_0}$, then a linear fit is used to determine the gradient $\frac{V_{\max}}{K_m}$ and the y-intercept $\frac{1}{V_{\max}}$. Unfortunately this method magnifies small errors in measurements and depends on extrapolation. An Eadie-Hofstee diagram or Hanes-Woolf plot could also be used, based on a similar rearrangement of the MM dynamics and with the same issues. In more recent work typically software is used to perform non-linear regression (Greco et al. 1982; Perrella 1988).

$$V = \frac{V_{\max} S}{K_m + S} \tag{2.9}$$

Where V is the reaction velocity, $V_{\max}$ the maximum reaction velocity, K_m the MM constant and S is the substrate concentration. The kinetics for ADA in the rat cortex are determined at pH 7.0 30°C with $V_{\max} = 54 \pm 11$ nmol/min/g wet weight and $K_m = 17 \pm 2$ with standard deviation from $n = 6$ (Phillips and Newsholme 1979). ADK kinetics were also determined for the rat cortex with $V_{\max} = 2.0 \pm 0.5$ nmol/min/g wet weight and $K_m = 25 \pm 6$.

Unfortunately, the information available in literature is rarely in an appropriate form for use in the models. The enzyme kinetics have been adjusted using Q_{10} values to a physiological temperature of 37°C, (or 32°C a temperature typically used in experiments to avoid damaging the tissue by overheating it). Similarly the diffusion coefficient was adjusted for the temperature using the Stokes-Einstein equation. The enzyme kinetics were all obtained from studies with similar acidity, with a pH between 7 and 7.5. As tissue was homogenised to measure the enzyme activity, further estimates of the proportion of enzyme in the neuronal, glial or extracellular space were required. The volume fraction of extracellular space (α) and space occupied by membranes are available, the remaining fraction of intracellular space (β) must be divided between neurons and glia. The models do not distinguish between different classes of glia or neurons. Although astrocytes and other types of glia have different roles currently there is insufficient information regarding purine transport and metabolism. So only astrocytes are included in the model. Here all the glia volume fraction is assumed to have the as-

trocytic metabolism (this is likely to be an overestimate of the role of glia), the other extreme would be to assume that glia which are not astrocytes contribute to the solid volume fraction of the cell membranes, (this would be an underestimate of the role of glia).

2.5.1 Temperature correction

The reaction catalysed by an enzyme speeds up as the temperature increases until it reaches an optimal temperature, beyond which the reaction slows again as the enzyme is more likely to degrade. Over a relatively small range of temperatures, it is possible to interpolate to obtain an estimate of the reaction rate for the desired temperature. The Q_{10} temperature coefficient describes the change in a reaction rate as a result of a 10°C increase in temperature;

$$Q_{10} = \left(\frac{R_2}{R_1}\right)^{\frac{10}{T_2 - T_1}} \tag{2.10}$$

where T_1 and T_2 are temperatures which result in reactions occurring at rates R_1 and R_2 respectively. The Q_{10} for ADA is 3.7 as the $V_{\max} \propto k_2$ (Eq. 2.5) is 199s^{-1} at pH 7.5 and 20°C (Kurz et al. 1992) and 385s^{-1} at pH 7.5 and 25C (Wang et al. 2012). Similarly the Q_{10} of ADK is 1.9 estimated based on enzymes obtained from the rat heart (De Jong and Kalkman 1973). These values are used to provide the parameter estimates for reactions at the physiological 37°C given in Table 2.3. Similar estimates were obtained for the experimental temperature of 32°C where necessary.

The free diffusion coefficient of adenosine $D^* = 520 \pm 1.0\mu\text{m}^2/\text{s}$ at 25.5 ± 0.5°C in water pH $6.0 - 7.0$ with and without 1mM $MgCl_2$ buffer (Bowen and Martin 1964), can provide the diffusion coefficient at the required temperature with the Stokes-Einstein equation;

$$D = \frac{k_B T}{6\pi\eta r} \tag{2.11}$$

where k_B is Boltzmann's constant, T is the temperature in kelvin, η is the dynamic viscosity, for water this is 8.8×10^{-4}Pas (pascal seconds) at 25.5°C and 6.9×10^{-4}Pas at 37°C (Haynes 2012) and r is the radius of the spherical

particle 0.98nm for (TMA^+) and 5.5nm for adenosine. So as the diffusion coefficient D_1 and viscosity is known at temperature T_1, then the diffusion coefficient at temperature T_2 is given by;

$$D_2 = \frac{D_1 \eta_1 T_2}{\eta_2 T_1} \tag{2.12}$$

The diffusion coefficient of inosine is similar to that of adenosine, $475 \pm 5\mu m^2/s$ in water and $520 \pm 0\mu m^2/s$ with 1mM $MgCl_2$. Hypoxanthine diffuses faster, with coefficient $720 \pm 1\mu m^2/s$ in water and $680 \pm 2\mu m^2/s$ with $MgCl_2$ (Bowen and Martin 1964), correcting the temperature and accounting for tortuosity gives a diffusion coefficient of $320\mu m^2/s$.

2.5.2 Volume fraction correction

In a small given volume of brain tissue V is the sum of a volume of cell membranes V_m, intracellular volume V_i and extracellular volume V_e. Consider an amount of substance in the extracellular space N_e, then the concentration can be defined in two ways, as the total concentration C_T or the relative concentration C_R;

$$C_T = \frac{N_e}{V} \tag{2.13}$$

$$C_R = \frac{N_e}{V_e} \tag{2.14}$$

They are related by the volume fraction $C_T = \alpha C_R$, similarly for intracellular concentrations. In these models the relative concentrations are used. However enzyme kinetics estimated from brain homogenate are given in terms of activity per wet weight of tissue for amount of protein. In each case it is necessary to estimate the activity per volume of brain tissue. The density of brain tissue is similar to water at $\sim 1.1 g/ml$ and a milligram of protein is obtained from ~1g of tissue (Nicholson 1995). Enzyme activity in the model occurs in sub volumes of the brain tissue (section 2.4) and as relative concentrations are used, it is necessary to scale the maximum velocity and MM constant by the volume of the compartment. In the ECS by $\frac{1}{\alpha}$, in neurons by $\frac{1}{\beta_n}$ and glia by $\frac{1}{\beta_g}$, these apply to the enzymes kinetics but not to the transporter kinetics (Eqs. 2.26, 2.27, 2.32, 2.33) as the change in volume fraction is included in the models (section B.2.1).

2.5.3 Estimation using the steady state

The salvage/removal rate of breakdown products in glia, (μ_8) could not be directly inferred from the literature. It could be calculated from the uniform steady-state concentrations, with the concentrations in the CSF (Phillis et al. 1987) and those obtained from brain homogenates (Winn et al. 1979) providing the extracellular and total concentration. The intracellular concentration is found by subtraction. Then the ratios between neuron and glia cultures allow the intracellular purines to be divided between neurons and glia (Matz and Hertz 1989). This approach would suggest a uniform steady-state concentrations of $A_e = 49.3$nM, $A_n = 27$nM, $A_g = 86$nM, $P_e = 77$nM, $P_n = 99$nM and $P_g = 23$nM, where A is adenosine and P breakdown products, with subscripts indicating; e extracellular, n neuronal or g glial. Such a steady-state could be obtained with $\mu_8 = 4.7 \times 10^{-5}$/s, a relatively slow removal rate. However as it is inferred from estimated steady-state concentrations, intracellular volume fraction and ENT kinetics, it is unlikely to be very reliable. Instead a removal rate μ_8, of 5×10^{-4}/s is considered relatively slow and 5/s is relatively fast compared with the rates of other mechanisms (Table 2.3) and the influence of this parameter is evaluated.

2.6 Transporters

Adenosine is cleared from the extracellular space by nucleoside transporters (NT). Transport is rapid and significantly alters the extracellular concentration of adenosine, with the IC_{50} (the concentration of bath applied adenosine required to half the amplitude of fEPSPs) $\sim$30 fold smaller for adenosine in the presence of uptake inhibitors (Dunwiddie and Diao 1994). However the enzymes can saturate, and the transporters can reverse their direction of flow (Brundege and Dunwiddie 1996). Here uptake parameters are estimated from the kinetics of primary cell cultures of rat neurons or astrocytes. Equilibrative nucleoside transporters (ENTs) transport both adenosine and its breakdown products between the intracellular and extracellular space according to the concentration gradient.

There are two solute carrier (SLC) families relevant to adenosine clearance, these are the equilibrative nucleoside transporter (ENT or SLC28) and the

concentrative nucleoside transporter (CNT or SLC29). Concentrative nucleoside transporters use one sodium ion to transport one nucleoside from the extracellular to the intracellular space and are thought to be the reason for the higher intracellular concentration of nucleosides (Gray et al. 2004). Equilibrative nucleoside transporters do not depend on sodium and attempt to equilibrate nucleoside concentration between the intracellular and extracellular space. ENTs have been subdivided into four classes; ENT1, ENT2, ENT3 and ENT4. ENT1 is sensitive to the inhibitor nitrobenzylmercaptopurine riboside (NBMPR), ENT2 which is insensitive to NBMPR but is inhibited by dipyridamole. ENT3 and ENT4 are less well characterised, but have lower affinity for nucleoside transport than either ENT1 or ENT2 and may be primarily involved in transport within cells (Baldwin et al. 2004).

Early work on transporters used four different experimental procedures for use with erythrocytes (red blood cells) which lack the enzymes to metabolise adenosine (Wu and Phillis 1984). These include: Zero-trans procedures, where the substrate concentration is initially zero inside the cell and the concentration outside the cell is varied. Equilibrium exchange procedure, where the substrate concentration on the two sides of the membrane are held equal. Infinite-trans procedure, where the inside of the cell has a substrate concentration in excess of the MM constant. Infinite-cis procedure, where labelled substrate outside the cell is at concentrations much higher than the MM constant, and the labelled concentration inside the cell is varied. A variation of the infinite-cis procedure, is 'accelerated exchange diffusion', where the labelled concentration inside the cell is varied. This can distinguish between the dynamics of 'loaded' and 'unloaded' transporters. Studies with cultures of neurons or glia have used the infinite-cis procedure for adenosine transport to infer MM kinetics of the transporter.

The kinetics for the specific class of ENT have been obtained by creating chimeras expressing the relevant transporter. Using *Xenopus* oocytes to produce dose-response curves for inhibitor NBMPR (Yao et al. 1997, figure 5) together with the values for the effect of NBMPR on rat cortical neuron and astrocyte transport (Nagai et al. 2005, figure 5), can give an estimate of the relative contribution of ENT1 and ENT2. Equilibrative transport in neurons is approximately 30% ENT1 and 70% ENT2, while in astrocytes

it is 15%, and 85% respectively. Such dose-response curves are useful for altering the parameters of the model to conform to experimental work where specific transport blockers have been applied (section 3.5.2). RNA extraction suggests neurons express more CNT2 than astrocytes which gives rise to the high affinity (ENT2) and low affinity (CNT2) uptake observed in neurons but not astrocytes. Here only the high affinity transport for neuron will be used, as CNT2 is thought to have only a minor effect on uptake with its low-affinity transporter only having a significant impact under pathological conditions. The ENT parameters are inferred from studies of cell cultures by using an estimate of 1.4ng of protein per neuron and glia transport 1.0ng of protein per astrocyte (McKinney et al. 1996).

A further difficulty with modelling the transporters is that the kinetics for the breakdown products inosine and hypoxanthine are currently unknown. So here the ENTs parameters for breakdown products have been set equal to those for adenosine transport. Such parameters can be inferred from the model by comparison with radio labelling studies, but would require the relevant volume fractions for cell cultures.

Obtaining parameter estimates for the transport of adenosine into neurons and astrocytes is problematic because of extracellular breakdown. Uptake kinetics are available for cell cultures (Nagai et al. 2005); however it is difficult to estimate the equivalent values for tissue. The MM constants are assumed to be the same between culture and tissue, while the maximum velocity is based on a cell count estimated from total protein concentration, this is at best only accurate to the nearest thousand cells (Laughton 1984).

As concentrations are being modelled, the transport between the spaces must be scaled by the relevant volume fraction, this leads to a system of four differential equations (2.22-2.25) describing model II where neuronal transport and metabolism is include with the extracellular diffusion and metabolism of model I. The transporters like the enzymes are modelled using the QSSA (Figure 2.1), with parameter values inferred from the literature. The derivation of the QSSA is based on the assumption of a fixed total amount of transporters that the concentrations of the bound transporters changes on a slower timescale and is given in section B.2.

2.7 Range of influence

The principal effect of adenosine in the cortex is to reduce neuronal activity via the A_1R. A dose-response curve for bath applied adenosine is obtained by applying different concentrations of adenosine to a tissue slice and measuring the corresponding reduction in excitatory post synaptic potentials (EPSPs). This curve can be characterised by its IC_{50} value, the concentration of adenosine applied to the tissue to halve the amplitude of the EPSPs. A bath applied IC_{50} of 15μM was found in layer V pyramidal neurons in the rat cortex (Kerr et al. 2013), or 2.7μM (Stutzmann et al. 2001). The lower concentration may be due to using thinner tissue slices. The concentration of adenosine at the synapses is lower than the bath applied concentration due to clearance mechanisms. Using an adenosine agonist, such as N6-Cyclopentyladenosine (CPA), that is not affected by clearance gives a second dose-response curve, with IC_{50} 10nM (Stutzmann et al. 2001). Cell cultures suggest that CPA has approximately 28 times the affinity of adenosine for A_1R, based on equilibrium disassociation constants (K_d) of $58nM$ for CPA and 1630nM for adenosine (Gerwins et al. 1990). Assuming the same efficacy allows a local dose-response curve to be estimated by shifting the CPA curve to match the potency of adenosine, which yields an IC_{50} value of 280nM, this is the response due to a concentration of adenosine at the synapse.

adenosine

$$\begin{array}{c} E + A_e \\ {\scriptstyle k_2}\uparrow\downarrow{\scriptstyle k_1} \\ EA \\ {\scriptstyle k_1}\uparrow\downarrow{\scriptstyle k_2} \\ E + A_i \end{array}$$

breakdown products

$$\begin{array}{c} E + P_e \\ {\scriptstyle k_4}\uparrow\downarrow{\scriptstyle k_3} \\ EP \\ {\scriptstyle k_3}\uparrow\downarrow{\scriptstyle k_4} \\ E + P_i \end{array}$$

(a) **Reaction kinetics for ENTs.** Where A is adenosine, P the breakdown products and E are ENTs, with subscript e indicating extracellular and i intracellular. The forward rate constants k_1, k_3 determine how rapidly the ENTs are loaded, while the reverse rate constants k_2 and k_4 describe how rapidly the loaded ENT reverts to unloaded state.

Quasi steady state approximation

Neuronal ENT

$$K_2 = \frac{2k_2}{k_1} \quad V_2 = k_2 [E]_0 \qquad K_3 = \frac{2k_4}{k_3} \quad V_3 = k_4 [E]_0$$

Glia ENT

$$K_5 = \frac{2k_2}{k_1} \quad V_5 = k_2 [E]_0 \qquad K_6 = \frac{2k_4}{k_3} \quad V_6 = k_4 [E]_0$$

(b) **QSSA for ENTs.** Where $[E]_0$ is the total concentration of transporters, V_2 is the maximum velocity of adenosine transport between neurons and the extracellular space, similarly V_3 for breakdown products, with V_4, V_5 for transport between glia and the extracellular space. K_2 and K_3 describe how adenosine and its breakdown products saturate neuronal transport, similarly K_5 and K_6 for glial transport. Neuronal and glial transports have the same form, but the parameter values are different.

$$J_n^A = \frac{V_2}{K_2\left(1 + \frac{P_e+P_n}{K_3}\right) + A_e + A_n}(A_n - A_e)$$

$$J_n^P = \frac{V_3}{K_3\left(1 + \frac{A_e+A_n}{K_2}\right) + P_e + P_n}(P_n - P_e)$$

$$J_g^A = \frac{V_5}{K_5\left(1 + \frac{P_e+P_g}{K_6}\right) + A_e + A_g}(A_g - A_e)$$

$$J_g^P = \frac{V_6}{K_6\left(1 + \frac{A_e+A_g}{K_5}\right) + P_e + P_g}(P_g - P_e)$$

(c) **Macroscopic form for ENT transport** Where A_e is the extracellular adenosine concentration, P_e is the extracellular concentration of breakdown products, A_n and P_n are the neuronal concentrations, A_g and P_g are the glial concentrations. The transport of adenosine from neurons into the extracellular space J_n^A and the transport of breakdown products from neurons into the extracellular space J_n^P. Similarly the transport from glia are J_g^A for adenosine and J_g^P for breakdown products

Figure 2.1: **Rate equations for the equilibrative nucleoside transporters.** The QSSA for the transport of both adenosine and its breakdown products between the extracellular space and neurons (J_n^A and J_n^P) or glia (J_g^A and J_g^P) are derived (section B.2) from a plausible reaction schematic to give a saturating form similar to MM enzyme kinetics.

The IC_{50} is an equilibrium measurement; when considering a brief source it is necessary to account for the kinetics of the A_1R. The proportion of bound A_1R, ϕ is modelled as single site receptor model, which has the following form;

$$\frac{\partial \phi}{\partial t} = k_1 A_e(1-\phi) - k_{-1}\phi \tag{2.15}$$

where k_1 is the binding rate and k_{-1} is the unbinding rate. Given $K_d = \frac{k_{-1}}{k_1}$ for this single site model, if $A_e = IC_{50}$, then by solving for ϕ_{50} the steady-state proportion of bound receptors necessary to halve and EPSP;

$$\phi_{50} = \frac{IC_{50}}{K_d + IC_{50}} \tag{2.16}$$

With the values given above, $\phi_{50} = 0.15$, so just 15% of the receptors are necessary to halve the amplitude of an EPSPs which corresponds with the observations of spare A_1R (Lohse et al. 1987). Assuming this simple single site receptor model captures the inhibitory process, the range of influence can then be quantified as the maximum distance from the source where the proportion of bound receptors exceeds 15%, in the steady state this is equivalent to the maximum distance where the extracellular concentration exceeds the IC_{50}.

2.7.1 Adenosine receptors

The A_1R has been shown to have a high and low affinity binding state and there are several endogenous proteins that influence agonist binding. These include adenosine deaminase (ADA), heat shock cognate protein 73 (HSC-73), caveolin-1 and protein 4.1G (Ciruela et al. 2010). The A_1R is also involved in several receptor mosaics, including A_1R-A_1R, A_1R-$A_{2A}R$, A_1R-D_1R, A_1R-D_2, A_1R-$mGluR_1$ and A_1R-P_2Y_1R (Fredholm et al. 2011; Franco et al. 2006; Guidolin et al. 2011). The use of a single state receptor model here is due to the difficulty in obtaining estimates for the kinetics for the A_1R, while there are several studies involving radioligand binding of A_1R in membrane extracts for more complex receptor dynamics, *e.g.* 14 parameter two-state model (Waldhoer et al. 1999). These preparations of membrane extracts have been shown to be unphysiological (Lohse et al. 2008).

Recently fluorescence resonance energy transfer (FRET) has been used to study the binding kinetics of GPCR for intact cells, *e.g.* $k_{-1} = 0.03s^{-1}$, $k_1 = 0.4\mu M^{-1}s^{-1}$ for human A_1R and the fluorescent agonist ABA-X-BY630 with $K_d = 80nM$ (May et al. 2010). However the rat A_1R has a higher affinity than the human receptor and adenosine has a lower affinity than ABA-X-BY630. A range of plausible kinetics is obtained by scaling the rate constants independently to obtain the equilibrium dissociation constant $K_d = \frac{k_{-1}}{k_1}$, 1630nM for adenosine binding to the rat A_1R. Taking the midpoint of this range gives $k_{-1} = 0.4s^{-1}$ and $k_1 = 0.2\mu M^{-1}s^{-1}$, which corresponds to a half-life ($t_{1/2}$) of 2s, faster than other values for GPCR obtained from intact cells, as FRET studies tend to use high-affinity agonists. *E.g.* neurokinin A receptor $t_{1/2}$ 3s with agonist K_d of 9.4nM (Palanche et al. 2001) and A_3R $t_{1/2}$ 53s with agonist K_d of 7.2nM (May et al. 2010).

2.8 Models

A hierarchy of models is developed using the literature to define the current best estimates of their parameters. A simple mathematical approximation is deduced and compared to computational results. An endogenous source of adenosine is modelled in two ways; a constant source is used to model the basal tone of adenosine, whereas a brief source is used for activity-dependent or spontaneous release. A uniform source is considered, this is appropriate when adenosine acts as a global modulator of activity, such as sleep or addiction (Dunwiddie and Masino 2001; Nam et al. 2013), or for comparison with measurements made with low spatial resolution, *e.g.* high performance liquid chromatography of the outflow from a tissue slice (Pedata et al. 1993). Due to evidence of heterogeneities in the adenosine signal, (Wall et al. 2007), an isolated point source is also modelled. This allows the range of influence of an adenosine source to be estimated. Finally an experimental setup is considered where adenosine is applied to the surface of a tissue slice, this provides insight into standard experimental setups and could be used to validate the model.

V_{max}	Value (μM/s)	K_m	Value (μM)	Description
V_1	1.42	K_1	80.71	Ecto-ADA for the rat cerebral cortex[1]
V_2	0.29	K_2	4.41	Adenosine transport for neuron in the rat cerebral cortex due to high affinity ENT2[2]
V_3	0.29	K_3	4.41	Inosine uptake for rat cortical neurons[3]
V_4	3.98	K_4	35.79	ADA for the rat cerebral cortex[1] (for the cytoplasm of neuron)
V_5	0.14	K_5	30.50	Adenosine uptake for glia[4]
V_6	0.14	K_6	30.50	Inosine uptake for glia[3]
V_7	6.56	K_7	4.18	ADK from whole rat brain (assumed to be entirely intracellular)[1]
μ_8				Non-saturating rate approximation for inosine clearance via PNPase[6]

Table 2.3: **Values of the Michaelis-Menten parameters for the models.** 1] performed at 30°C, pH 7.5 and based on activity per gram of tissue with 10.6% of activity in membranes 66.9% in cytoplasm and the remainder in vesicles, synaptosomes and mitochondria. (Yamamoto et al. 1987), Q_{10} of 3.7 (Wang et al. 2012) and brain tissue density $\sim 1.1 g/ml$. 2] uptake performed at 37°C in a cell culture (Nagai et al. 2005), assumed an average 2ng protein per neuron to estimate equivalent uptake kinetics in the brain. (Chun and Patterson 1977) 3] ENT velocity and affinity for inosine are assumed to be the same as for adenosine. 4] performed at 37°C in a cell culture (Nagai et al. 2005), using the ratio of astrocytic glutamate uptake in slice and culture to estimate the equivalent uptake kinetics in the brain. (Hertz et al. 1978). 5] performed at 30°C, pH 7.5 (Arch and Newsholme 1978), temperature corrected to 37°C using Q_{10} of 1.9 estimated for ADK in the rat heart (De Jong and Kalkman 1973) 6] two extreme values are considered, slow removal 5×10^{-4}/s and fast removal 5/s of breakdown products.

The simplest model in the hierarchy is the diffusion model, where adenosine just diffuses through the extracellular space with no uptake or breakdown and is described by the following parabolic partial differential equation (PDE);

$$\frac{\partial A_e}{\partial t} = D\nabla^2 A_e + \frac{1}{\alpha} S(t,x) \tag{2.17}$$

where D is the effective diffusion coefficient that takes into account the tortuosity of the extracellular space, α is the extracellular volume fraction or porosity and $S(t,x)$ [μM/s] is a generic source in terms of a total concentration so it is scaled to give the relative concentration (section 2.5.2). Initially the concentration is zero. Endogenous non-uniform sources are solved in spherical coordinates assuming radial symmetry, with the boundary conditions;

$$\lim_{r\to\infty} A_e(t,r) = 0 \tag{2.18}$$

$$\left.\frac{\partial A_e}{\partial r}\right|_{r=0} = 0 \tag{2.19}$$

In models with more state variables, similar initial and boundary conditions are applied. In the bath applied case, the boundary conditions are $A_e(t,\pm\frac{h}{2}) = A_0$, where A_0 is the applied concentration of adenosine and h is the depth of the slice.

2.8.1 Model I

Extracellular breakdown by ADA is added to the diffusion model (Figure 2.2a). It is described by the coupled PDEs;

$$\frac{\partial A_e}{\partial t} = D\nabla^2 A_e - \frac{V_1 A_e}{K_1 + A_e} + \frac{1}{\alpha} S(t,x) \tag{2.20}$$

$$\frac{\partial P_e}{\partial t} = D\nabla^2 P_e + \frac{V_1 A_e}{K_1 + A_e} \tag{2.21}$$

where A_e is the extracellular concentration of adenosine and P_e is the concentration of breakdown products, V_1 is the maximum velocity and K_1 the MM constant for ecto-ADA.

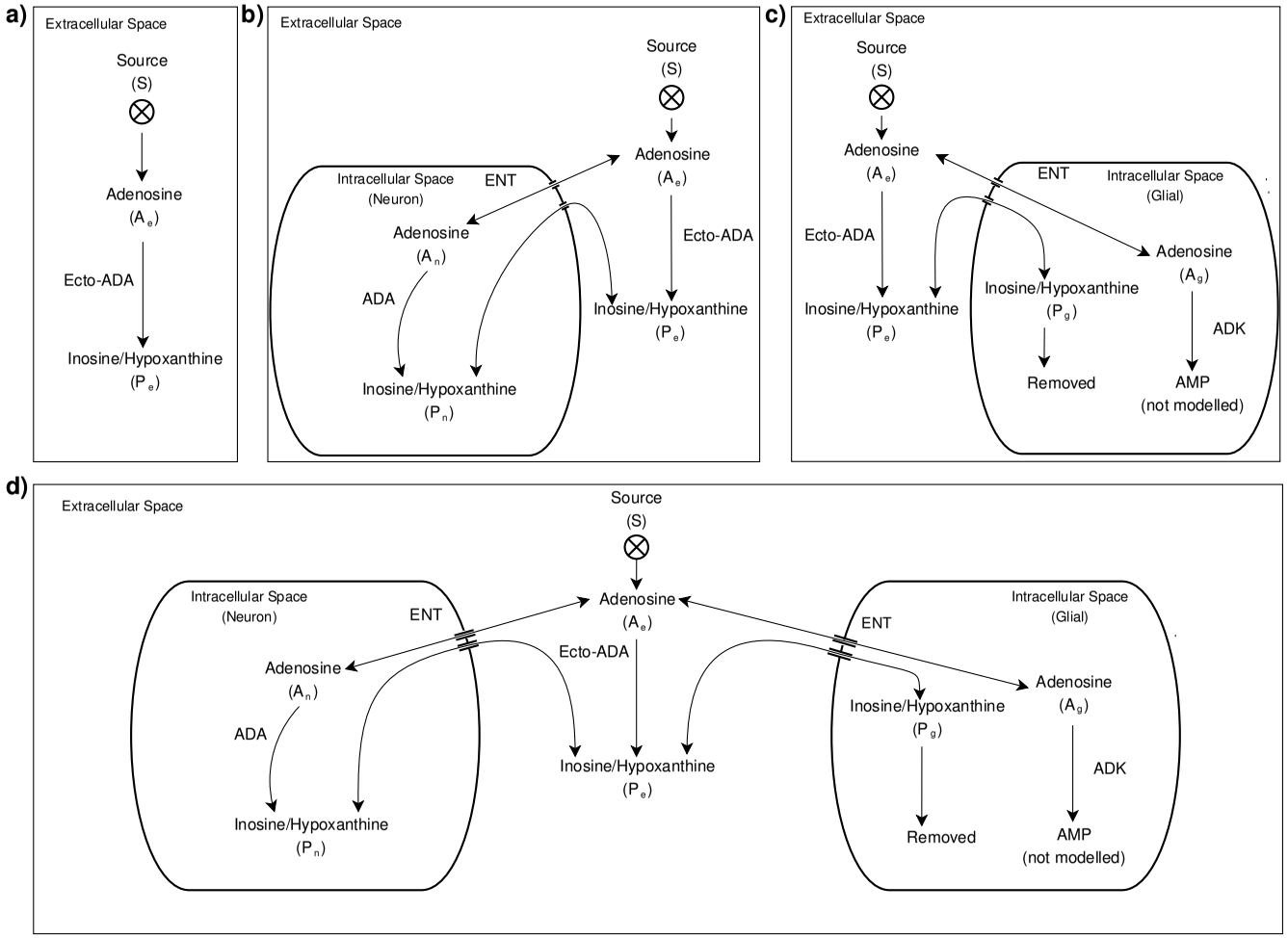

Figure 2.2: **Model hierarchy a)** Model I includes the tortuous diffusion of adenosine in the extracellular space and the breakdown by membrane bound ecto-ADA. **b)** Model II, in addition to extracellular breakdown, purines can also be transported between the extracellular and intracellular space of neurons. In the intracellular neuronal space there is no diffusion but adenosine is converted to inosine by ADA. The breakdown products in turn competitively inhibit the equilibrative transport of adenosine. **c)** Model III includes extracellular breakdown as in model I, with the addition of glia transport. Intracellular adenosine is phosphorylated to AMP by ADK, For simplicity AMP is not modelled, similarly the clearance and salvage pathway has been approximated by an unsaturating rate. Break-down products are transported by ENTs, but are not metabolised by glia; they simply provide competitive inhibition of adenosine transport. **d)** Model IV provides the most realistic model of tissue, including extracellular and intracellular metabolism with transport between the extracellular space and either neurons or glia.

2.8.2 Model II

Model II additionally takes into account removal by neurons, (Figure 2.2b).

$$\frac{\partial A_e}{\partial t} = D\nabla^2 A_e - \frac{V_1 A_e}{K_1 + A_e} + \frac{1}{\alpha} J_n^A + \frac{1}{\alpha} S(t,x) \tag{2.22}$$

$$\frac{\partial P_e}{\partial t} = D\nabla^2 P_e + \frac{V_1 A_e}{K_1 + A_e} + \frac{1}{\alpha} J_n^P \tag{2.23}$$

$$\frac{\partial A_n}{\partial t} = -\frac{1}{\beta_n} J_n^A - \frac{V_4 A_n}{K_4 + A_n} \tag{2.24}$$

$$\frac{\partial P_n}{\partial t} = -\frac{1}{\beta_n} J_n^P + \frac{V_4 A_n}{K_4 + A_n} \tag{2.25}$$

Where β_n the neuronal volume fraction and V_4 and K_4 are the MM parameters for ADA, A_e and P_e are the extracellular concentration of adenosine and its breakdown products, A_n and P_n are the corresponding neuronal concentration. This model includes ENTs, the QSSA (Figure 2.1), which gives the following formula for the transport depending on the intracellular and extracellular concentration of adenosine and its breakdown product;

$$J_n^A = \frac{V_2}{K_2\left(1 + \frac{P_e + P_n}{K_3}\right) + A_e + A_n} (A_n - A_e) \tag{2.26}$$

$$J_n^P = \frac{V_3}{K_3\left(1 + \frac{A_e + A_n}{K_2}\right) + P_e + P_n} (P_n - P_e) \tag{2.27}$$

2.8.3 Model III

Model III includes the extracellular and the glial metabolism but not neuronal uptake, (Figure 2.2c). Transport into the intracellular space has the same form as model II but with different parameters, (Figure 2.1). AMP is not modelled, this simplification avoids the inclusion of ATP which is used ubiquitously in the cell. The clearance/salvage pathway for the breakdown product inosine is modelled as a single unsaturating rate μ_8. The resulting system is as follows;

$$\frac{\partial A_e}{\partial t} = D\nabla^2 A_e - \frac{V_1 A_e}{K_1 + A_e} + \frac{1}{\alpha} J_g^A + \frac{1}{\alpha} S(t,x) \tag{2.28}$$

$$\frac{\partial P_e}{\partial t} = D\nabla^2 P_e + \frac{V_1 A_e}{K_1 + A_e} + \frac{1}{\alpha} J_g^P \tag{2.29}$$

$$\frac{\partial A_g}{\partial t} = -\frac{1}{\beta_g} J_g^A - \frac{V_7 A_g}{K_7 + A_g} \tag{2.30}$$

$$\frac{\partial P_g}{\partial t} = -\frac{1}{\beta_g} J_g^P - \mu_8 P_g \tag{2.31}$$

where β_g is the volume fraction of glia, V_7 and K_7 are the MM parameters for ADK and μ_8 is a first order approximation of the clearance and salvage pathways. The ENTs are modelled using the QSSA (Figure 2.1), which gives the following equations for transport;

$$J_g^A = \frac{V_5}{K_5\left(1 + \frac{P_e + P_g}{K_6}\right) + A_e + A_g}(A_g - A_e) \tag{2.32}$$

$$J_g^P = \frac{V_6}{K_6\left(1 + \frac{A_e + A_g}{K_5}\right) + P_e + P_g}(P_g - P_e) \tag{2.33}$$

Where A_e and P_e are the extracellular concentration of adenosine and its breakdown products, with A_g and P_g the corresponding glial concentrations.

2.8.4 Model IV

The full tissue model combines the extracellular space (ECS), neurons and glia, (Figure 2.2d). Transport between the intracellular and extracellular space, (Figure 2.1c) and the intracellular compartments are modelled as before, (Eq. 2.24, 2.25) and (Eq. 2.30, 2.31). The extracellular concentrations are determined by;

$$\frac{\partial A_e}{\partial t} = D\nabla^2 A_e - \frac{V_1 A_e}{K_1 + A_e} + \frac{1}{\alpha} J_n^A + \frac{1}{\alpha} J_g^A + \frac{1}{\alpha} S(t,x) \tag{2.34}$$

$$\frac{\partial P_e}{\partial t} = D\nabla^2 P_e + \frac{V_1 A_e}{K_1 + A_e} + \frac{1}{\alpha} J_n^P + \frac{1}{\alpha} J_g^P \tag{2.35}$$

2.9 Hippocampus

The models described here can be applied to different species or brain regions by altering the parameter values. In addition to the rat cortex estimates, pa-

rameter estimates for rat hippocampus were obtained (Table 2.4 and Table 2.3), to demonstrate the wider applicability of the models and allow comparison of the effects of ENT inhibitors in different brain regions (section 3.5.2).

Although ENT1 and ENT2 have not been measured in either neurons or glia of the rat hippocampus, the relative amount of isolated mRNA for ENT1 is 1.5, which is 8% higher than the cortex. Similarly for ENT2 is 0.7 which is 52% higher than the cortex. Assuming the same ratio of expression of ENT1 and ENT2 transporters in hippocampal cells as cortical cells, this suggests an increase ∼40% in maximum velocity for neurons and ∼50% for glia (Anderson et al. 1999).

Adenosine deaminase (ADA) measured in homogenised hippocampus at $37°C$, pH 7, has Michaelis-Menten constant $K_m = 40\mu$M and $V_{\max} =$ 36nmol/mg protein/30min (Geiger and Nagy 1986). The homogenate was also shown to have activity 4nmol/mg tissue/30min and was further subdivided into P_1 containing the dense nuclear fraction, P_2 composed of the mitochondria, myelin, microsomes and synaptosomes, which provides a crude estimate for the ecto-ADA activity of 22% and P_3S the soluble fraction corresponding to the cytosolic-ADA 68%. As with the rat cortex, adenosine kinase (ADK) has not been characterised in the rat hippocampus, so the kinetics derived from the whole brain are used.

The hippocampus is formed of the dentate gyrus, an outer layer around the hippocampus proper or four Cornu Ammonis regions (CA1-CA4), the largest of these are CA1 and CA3. The volume fraction for the regio inferior (CA3) is $\alpha = 0.13$ and regio superior (CA1) is $\alpha = 0.20$. The tortuosity for CA1 is 1.5 and CA3 is 1.6 (Pérez-Pinzón et al. 1995). To obtain an estimate for the whole hippocampus (Table 2.4), these values can be averaged over the relative volume of the regions, regio superior 17mm^3 and regio inferior 13mm^3 (West et al. 1978).

The solid volume fraction is $\gamma \approx 0.2$, based on the ratio of the density of neural tissue to water, which implies an intracellular volume fraction $\beta = 1 - \gamma - \alpha = 0.63$, similar to both the cortex $\beta = 0.59$ (Rice and Nicholson 1991) and the striatum $\beta \approx 0.65$ (Nicholson 1995). The neuronal

Parameter	Value	Description
α	0.17	Extracellular volume fraction (Pérez-Pinzón et al. 1995)
β	0.63	Total intracellular volume fraction
β_n	0.50	Neuron volume fraction 80% of intracellular volume
β_g	0.13	Glial volume fraction 20% of intracellular volume
D*	$690\mu m^2 s^{-1}$	Diffusion coefficient of adenosine at 37°C in a free environment(Bowen and Martin 1964)
D	$300\mu m^2 s^{-1}$	Diffusion coefficient given tortuosity of 1.58 for rat hippocampus (Pérez-Pinzón et al. 1995)[b]

Table 2.4: **Volume fractions and diffusion coefficients for the rat hippocampus.** Temperature changed using the Stokes-Einstein equation (Eq. 2.11). Estimates of tortuosity based on the diffusion of Tetramethylammonium$^+$ (TMA$^+$)

volume fractions have been estimated in the rat hippocampal neuropil using electron microscopy reconstruction as ∼90% and glial as ∼8% (Mishchenko et al. 2010). However there is no estimate for the volume fraction which includes the cell bodies, so a similar volume ratio of neuronal (80%) to glial (20%) intracellular space as the cortex is assumed.

V_{max}	Value (μM/s)	K_m	Value (μM)	Description
V_1	2.91	K_1	227	Ecto-ADA for the rat hippocampus
V_2	0.19	K_2	4.41	Adenosine transport for neuron in the rat hippocampus due to high affinity ENT2
V_3	0.19	K_3	4.41	Inosine uptake for rat hippocampal neurons
V_4	3.12	K_4	78.2	ADA for the rat hippocampus (for the cytoplasm of neuron)
V_5	0.31	K_5	30.50	Adenosine uptake for glia
V_6	0.31	K_6	30.50	Inosine uptake for glia
V_7	4.46	K_7	15.23	ADK from whole rat brain (assumed to be entirely intracellular)
μ_8				Non-saturating rate approximation for inosine clearance via PNPase

Table 2.5: **Values of the Michaelis-Menten parameters for the hippocampus.**

Chapter 3

Adenosine sources and range of influence

3.1 Introduction

Extracellular adenosine can increase as a result of normal neuronal activity, (Wall and Dale 2007; Brundege and Dunwiddie 1996; Klyuch et al. 2011; Klyuch et al. 2012a; Klyuch et al. 2012b; Sims and Dale 2014; Cechova et al. 2010; Pajski and Venton 2010; Nguyen et al. 2014), pathological neuronal activity (seizures) (Etherington et al. 2009), hypoxia (Frenguelli et al. 2003; Fujita et al. 2011; Gourine et al. 2005), ischemia (Dale and Frenguelli 2009; Frenguelli et al. 2007) and damage (Ross et al. 2014; Latini and Pedata 2001). Extracellular adenosine also increases during waking and falls during sleep (Clasadonte et al. 2014; Sharma et al. 2014) and is affected by alcohol (Sharma et al. 2014; Clasadonte et al. 2014). There is uncertainty regarding the mechanisms for endogenous increase in extracellular adenosine concentration, with evidence for multiple release pathways depending on brain region and the nature of the stimulus.

For the models a number of idealised endogenous sources are considered: a constant uniform and constant point source, appropriate for modelling the basal tone of adenosine; and a brief uniform and brief point source, corresponding to activity-dependent and spontaneous release events. Here the models are used to estimate the duration of an adenosine signal and its range of influence, as a function of the source intensity. In general the

adenosine signal appears to be relatively short and highly localised *e.g.* the range ($\sim$20μm) and duration ($\sim$7s) for relatively brief point source (Figure 3.9n,o), or the characteristic length scale of a constant point source ($\sim$40μm). The hierarchy of models allows a comparison of the different clearance mechanisms and suggests that neuronal uptake has the greatest effect on extracellular adenosine concentrations. The uniform source is used to determine the endogenous tone that would result from different source intensities. The model of a uniform source suggests changes in adenosine concentration with the sleep/wake cycle are unlikely to be the result of a simple change in source intensity, with more adenosine being produced when awake.

Numerical solutions are obtained using finite differences, forward time center space for a brief point source are obtained using a fourth order Runge-Kutta method for spherical coordinates. Isotropy allows it to be solved in terms of the radius alone (Figure 3.1a). A time-step of 1ms and a uniform grid of 100,000 points between 1μm and 5cm is used. The large upper limit is to ensure boundary has little influence on the solution. The time-step and space-step satisfy the Von Neumann stable condition for the diffusion equation $\frac{D\delta_x^2}{\delta_t} < \frac{1}{2}$ and are validated by reducing the values and demonstrating no substantial effect on the solution. The source is initially distributed in a sphere with volume 1μm^3 of extracellular space. The steady state is found by iterating until the total changes in the state of the system falls below a threshold of 0.1nM/s. Similarly the time dependant solution for the bath applied problem is found via a fourth order Runge-Kutta method, using a uniform grid of one thousand points between a depth of 0 and either 300μm or 400μm (Figure 3.1b).

3.2 Low concentration limit

These nonlinear models cannot be solved analytically, however the models become linear in both the high and low concentration limit. In the high extracellular concentration limit, ecto-ADA kinetics and ingress to the intracellular space are described by zero-order kinetics. The low concentration limit is also linear, with a first-order reaction, where the velocity is given

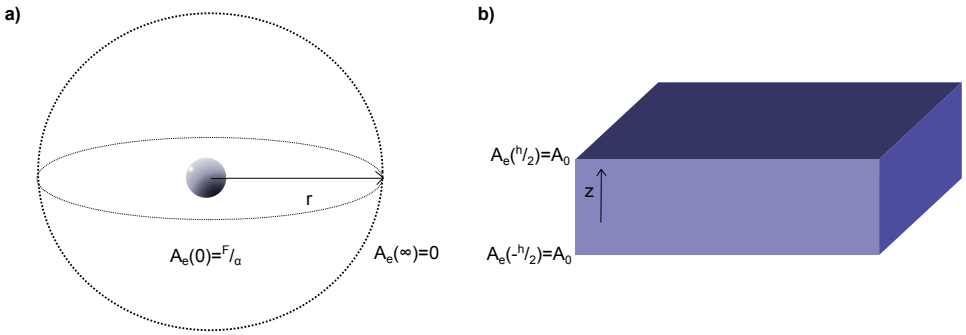

Figure 3.1: **Schematic of the domain and boundary conditions. a)** A constant point source is solved radially, for the steady-state solution the boundary at $r = 0$ is given by $\frac{F}{\alpha}$, whereas for brief source the condition is $\frac{F_0}{\alpha}\delta(t)$. In both cases the concentrations are otherwise initially zero and $\lim_{r\to\infty} A_e(r) = 0$. **b)** For bath applied adenosine the tissue slice is relatively thin, so it is reasonable to solve it for depth alone. The boundary conditions at the surface of the slice $\pm\frac{h}{2}$ (where h is the thickness of the slice) are equal to the applied concentration A_0 [μM] which may be zero (section 3.3.1.1).

by a constant rate multiplied by the adenosine concentration. The steady state for the low extracellular concentration limit can be written in terms of a characteristic length scale λ (Table 3.1), determined by the ratio of diffusion to clearance. The steady-state extracellular adenosine concentration in the low concentration limit is described by;

$$0 = \nabla^2 A_e - \frac{A_e}{\lambda^2} + \frac{S(x)}{D\alpha} \tag{3.1}$$

The length scale for model IV (derived in section B.3) is;

$$\lambda = \sqrt{D\left(\mu_1 + \frac{1}{\alpha}\left(\frac{\beta_n\mu_2\mu_4}{\beta_n\mu_4 + \mu_2} + \frac{\beta_g\mu_5\mu_7}{\beta_g\mu_7 + \mu_5}\right)\right)^{-1}} \tag{3.2}$$

where $\mu_i = \frac{V_i}{K_i}$ is the removal rate of a given mechanism in the low concentration limit, *i.e.* μ_1 ecto-ADA, μ_2 neuronal transport, μ_4 neuronal ADA, μ_5 glial transport and μ_7 ADK. The length scale for other models can be obtained by removing the relevant clearance terms. The extracellular concentration of breakdown production in the low concentration limit is also determined with an additional linear differential equation;

Model	λ (μm)	V_{max} (μM/s)	τ (s)
I) Extracellular only	122.2	1.4	56.8
II) Extracellular & neuronal	41.0	2.8	6.4
III) Extracellular & glial	85.8	2.1	28.1
IV) Extracellular, neuronal & glial	38.7	3.5	5.7

Table 3.1: **Neurons have a substantial impact on the range of influence for a constant point source compared with the effect of glia**. The steady-state solution in the low concentration limit (section 3.2), provides a characteristic spatial scale (λ) and temporal scale ($\tau = \lambda^2/D$). The maximum removal velocity V_{max} is the sum of the relevant maximum velocities for transporters and enzymes in the high concentration limit, these characteristic scales are listed for models I-IV. They show that the clearance mechanisms localise the effect of adenosine.

$$0 = \nabla^2 P_e + \frac{A_e}{\kappa_1^2} - \frac{P_e}{\kappa_2^2} \tag{3.3}$$

Where for model IV;

$$\kappa_1 = \sqrt{D\left(\mu_1 + \frac{1}{\alpha}\frac{\beta_n\mu_3\mu_4}{\beta_n\mu_4 + \mu_2}\right)^{-1}} \tag{3.4}$$

$$\kappa_2 = \sqrt{D\alpha\frac{\beta_g\mu_8 + \mu_6}{\beta_g\mu_6\mu_8}} \tag{3.5}$$

This low concentration limit provides a good approximation of the non-linear solution (Figure B.1c), because diffusion substantially diminishes the concentration with distance from the source (Figure 3.6).

3.3 Constant sources and the adenosine tone

The adenosine tone varies with the sleep/wake cycle (Sims et al. 2013) and with age (Kerr et al. 2013). This tone must result from a balance between a source of adenosine and the clearance mechanism. Here this is described in the models with a constant source. The constant source may give rise to a steady-state concentration, which can be found analytically for models I and II (Eq. 3.6), or numerically for models III and IV.

3.3.1 Uniform sources

The extent to which glia clear adenosine from the extracellular space is influenced by the removal rate of breakdown products μ_8, (representing the action of enzymes PNPase, XO and HGPRT as well as transport through the BBB via erythrocytes). It is clear comparing the fast and slow removal rates that in model III glia can have a substantial impact on the basal tone by clearing adenosine from the ECS, (Figure 3.2), as without sufficiently rapid removal of breakdown products they accumulate and competitively inhibit uptake of adenosine by both neurons and glia. In the presence of neurons, (model IV) removal of breakdown products is the dominant role played by glia. So in model IV neurons act as a source of breakdown products, because ADA is faster then ecto-ADA, while glia act as a sink, salvaging the breakdown products.

Glia are essential for the removal of breakdown products, by both salvage and transport through the BBB via erythrocytes. Subsequently for a uniform source, models I and II do not have a steady state for the breakdown products, they accumulate indefinitely (Figure B.3). However, the steady state can be obtained for extracellular adenosine, by considering a high concentration limit of the breakdown products, in which case model II is the same as model I, which has an analytic solution;

$$A^* = \frac{K_1 C}{\alpha V_1 - C} \tag{3.6}$$

Where C is the source in terms of the total concentration (section 2.5.2), *i.e.* $S(t,r) = C$ [μM/s] in (Eqs. 2.20, 2.22, 2.28, and 2.34). In figures 3.2 and 3.5 the source is given in terms of a relative concentration, *i.e.* $S(t,r) = \alpha C$ [μM/s] in (Eqs. 2.20, 2.22, 2.28, and 2.34). This solution shows that there is a maximum velocity at which adenosine can be removed. This is the case for all the models ($V_{\max}$ in Table 3.1), this maximum velocity assumes that the extracellular adenosine concentration is far greater than that of the breakdown products (section B.4), if this is not the case, saturation of transporters will reduce this maximum velocity towards the value given for model I. If the source of adenosine exceeds this maximum velocity, then the

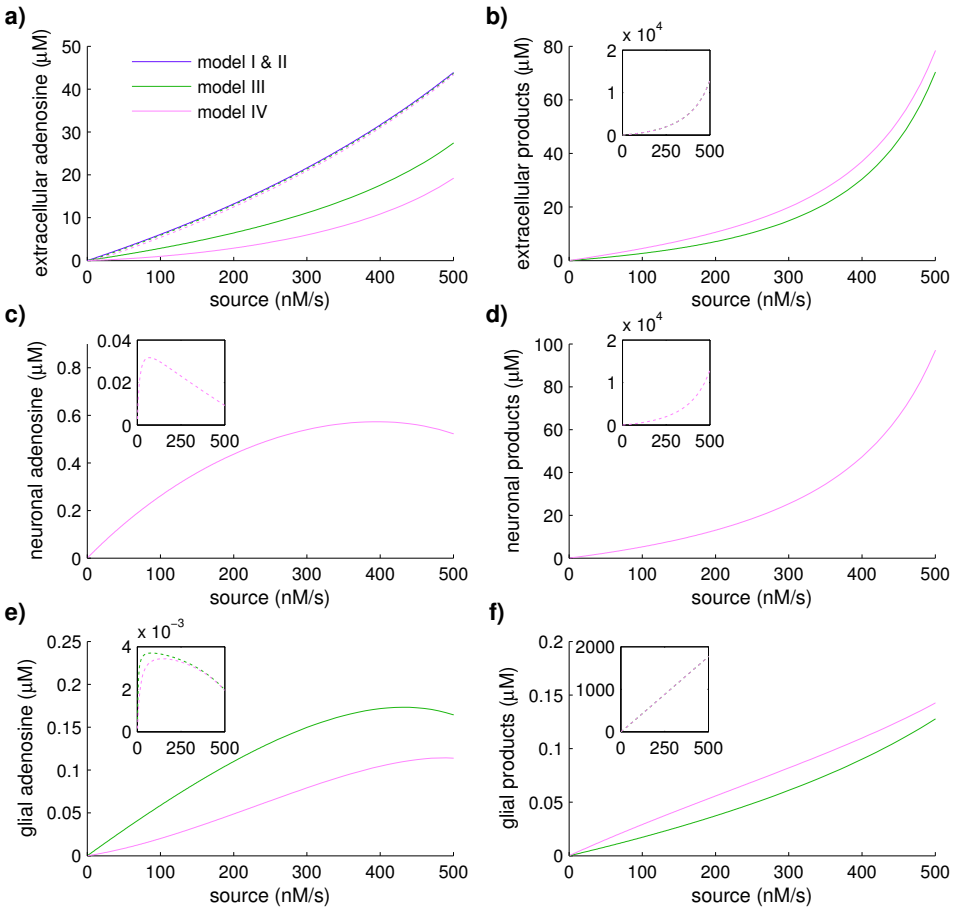

Figure 3.2: **The endogenous tone of adenosine diverges as the source rate approaches the maximum removal rate.** The uniform steady-state concentration of **a)** extracellular adenosine with fast removal of breakdown products in glia $\mu_8 = 5/\text{s}$ (solid) and slow removal $\mu_8 = 5 \times 10^{-4}/\text{s}$ (dashed). With a slow removal rate μ_8, transporters become saturated by breakdown products which rapidly increase in **b)** extracellular space, **d)** neuronal space, and **f)** glia. Hence the addition of glia and neurons in model IV has little effect on the resulting endogenous tone and **a)** the extracellular solutions of models III and IV meet with models I and II. For rapid removal of breakdown products, neurons and glia do have a substantial impact, however for larger sources the transporters ultimately become saturated and the endogenous tone diverges for all models.

concentration will grow indefinitely. This also means that a small change in the source rate could substantially increase the endogenous tone (Figure 3.2).

3.3.1.1 Efflux from a tissue slice

The efflux from a tissue slice may be measured via high performance liquid chromatography (Fowler 1993) or with biosensors (Wall et al. 2007), to infer either the endogenous tone or a release event. Modelling adenosine *in vitro* means the boundary conditions at the edge of the slice may influence the observed signal. Here the low concentration limit (section 3.2) is used to determine the relative effect of clearance mechanisms and boundary conditions on a constant uniform source. This simplified model can be used to determine the efflux from a tissue slice, taking the steady-state low concentration limit and a constant source $S(x,t) = C$ [μM/s], (Eq. 2.17, 2.20, 2.22, 2.28 and 2.34) given the following ODE; ;

$$0 = \nabla^2 A - \frac{A}{\lambda^2} + \frac{C}{D\alpha} \tag{3.7}$$

Where C [μM] is the source intensity, λ is the length scale (Eq. 3.2) (Table 3.1). The steady-state solution for a slice of tissue, thickness h with boundary conditions $A\left(\frac{h}{2}\right) = A\left(-\frac{h}{2}\right) = 0$ is;

$$A(z) = \frac{C\lambda^2}{D\alpha}\left(1 - \frac{\cosh\left(\frac{z}{\lambda}\right)}{\cosh\left(\frac{h}{2\lambda}\right)}\right) \tag{3.8}$$

Then the loss rate due to clearance mechanisms is;

$$L_c = \frac{1}{h}\int_{-\frac{h}{2}}^{\frac{h}{2}} dz \frac{D}{\lambda^2} A(z) \tag{3.9}$$

$$= \frac{C}{\alpha h}\left(h - 2\lambda \tanh\left(\frac{h}{2\lambda}\right)\right) \tag{3.10}$$

The loss rate due to flux at the boundaries of the slice is;

$$L_b = \frac{1}{h}\left(D\frac{dA}{dz}\Big|_{z=\frac{-h}{2}} - D\frac{dA}{dz}\Big|_{z=\frac{h}{2}}\right) \tag{3.11}$$

$$= 2\frac{C\lambda \tanh\left(\frac{h}{2\lambda}\right)}{\alpha h} \tag{3.12}$$

Together with the length scales (Table 3.1) this suggests that clearance mechanisms surpass loss through the slice surface for slices thicker than $\sim$100μm.

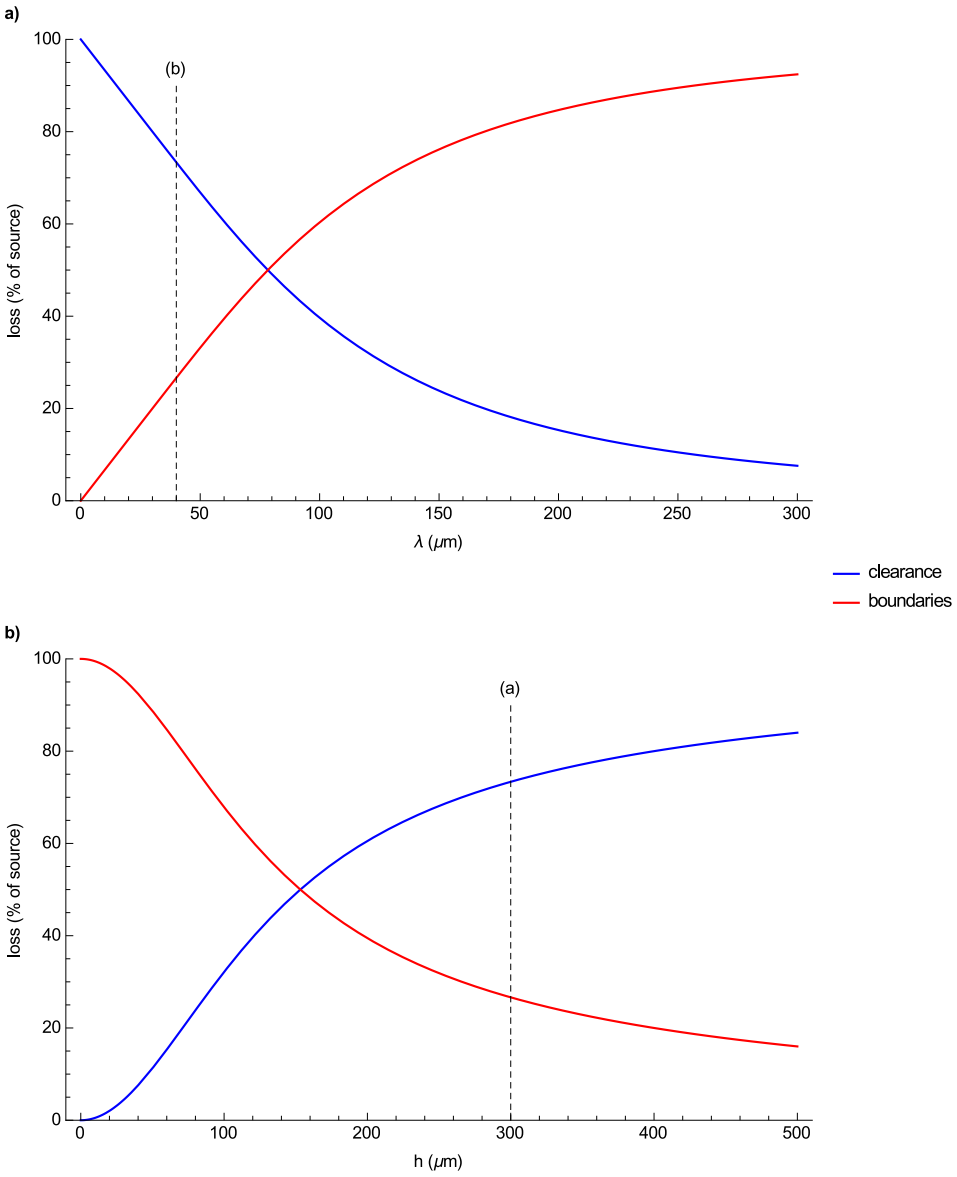

Figure 3.3: **Clearance mechanisms have a greater influence on adenosine concentration than the boundary conditions for slices thicker than** 100μ**m** The percentage of a constant uniform source lost in the steady-state due to clearance mechanisms and diffusion out of the slice. **a)** For a 300μm slice with range clearance length scales λ (Table 3.1) (the average distance adenosine diffuses before being removed by endogenous clearance mechanisms), dashed line at $\lambda = 40\mu$m for comparison with **b)** the effect of influence of slice thickness on loss of adenosine, with $\lambda = 40\mu$m, dashed line at thickness 300μm for comparison with **a)**.

3.3.1.2 Sleep cycles

Extracellular adenosine increases during waking periods and decreases during sleep. Here the simplest way to incorporate aspects of the sleep/wake cycle into a model of adenosine clearance is considered. This is with two constant uniform sources representing extracellular adenosine produced in a waking and a sleeping state. The different rates could result from higher waking brain activity or as a result of circadian clocks regulating astrocytic ATP release (Marpegan et al. 2011). C_w [nM/s] is a source intensity for waking states with a smaller source C_s [nM/s] for sleeping states. The model suggests an initial rapid change in extracellular concentration, followed by a slower change dependent on glial dynamics. With fast removal of breakdown products ($\mu_8 = 5$/s) 95% of the rise from sleeping to waking adenosine concentration occurs within 40s, similarly 95% of the fall from waking to sleeping concentration takes place within 75s. Whereas with slow removal ($\mu_8 = 5 \times 10^{-4}$/s) the same rise takes 80s, and the fall takes 6.7 hours. (Figure 3.4a,b).

Modelling the larger changes in concentration seen in old rats, 97nM to waking concentration 128nM (Murillo-Rodriguez et al. 2004) shows similar dynamics (Figure 3.4c,d), taking 40s to rise and 100s to fall with fast adenosine removal compared to 2.3 hours and 7.7 hours with slow breakdown product removal rate. Monitoring the changes in adenosine concentrations in the rat hippocampus suggests a slow increase during the dark period which returns to baseline within an hour (the next data point) at the onset of the light period (Huston et al. 1996). Whilst the rapid removal of breakdown products is consistent with the model, the temporal resolution is too low to validate the model's predictions. The model suggests the change in extracellular adenosine concentration with sleep/wake cycle is unlikely to be due to a simple increase in adenosine production during waking states. As with such rapid accumulation of adenosine it is unlikely it could serve as a marker for sleep drive (Holst and Landolt 2015).

Evidence suggests that the activity of some enzymes of the purine metabolism are reduced during waking periods. The enzymes relevant for the clearance models are ADA, which is reduced by 43% and ADK which is reduced by 54% of the day time (sleeping) levels (de Sa et al. 1993). Reducing purine

metabolism in the waking state has little effect on the dynamics in either young or old rats (Figure 3.4), but substantially reduces the source intensity required for a given endogenous tone (Figure 3.5)

The model can also be applied to sleep deprivation, It suggests there would be no change in adenosine tone as a result of sleep deprivation because the steady state would be reached in the normal waking hours and persist throughout the sleep deprived state, consistent with some observations *in vitro* (Sims et al. 2013). Extracellular adenosine appears to increase with sleep deprivation in the basal forebrain (BFB) (Kalinchuk et al. 2006), but not the cortex. The adenosine clearance models do not explain the discrepancy, but it may be due to differences in the source. In the BFB the peak adenosine release resulting from α-amino-3-hydroxy-5-methyl-4-isoxazolepropionic acid receptor (AMPAR) stimulation increased with sleep deprivation, while in the cortex it remained the same (Sims et al. 2013). This suggests that the amount of adenosine as a result of neuronal activity during sleep deprivation would increase in the BFB, while remaining unchanged in the cortex.

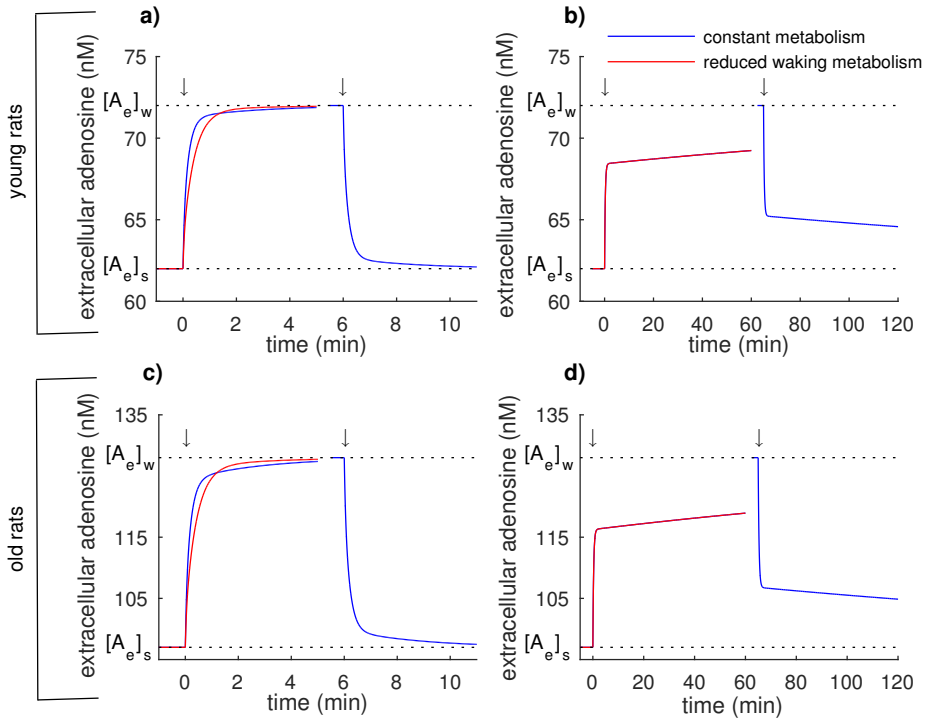

Figure 3.4: **Changing the source intensity corresponding to sleep/wake states of rats rapidly alters the extracellular adenosine concentration but the time required to reach a steady state is dependant on the glia metabolism.** Both plots show the change from the observed sleeping extracellular adenosine concentration $[A_e]_s$ (62nM in young 97nM in old rats) to waking concentration $[A_e]_w$ (72nM in young and 129nM in old rats). **a)** and **c)** Fast removal of breakdown products in glia $\mu_8 = 5$/s. With corresponding source intensities required for the steady-state extracellular adenosine; **a)** waking $C_w = 2.5$nM/s with constant metabolism (blue) or $C_w = 1.5$nM/s with reduced metabolism (red) and sleeping $C_s = 2.1$nM/s. **c)** waking $C_w = 4.2$nM/s with constant metabolism (blue) or $C_w = 2.7$nM/s with reduced metabolism (red) and sleeping $C_s = 3.2$nM/s. **b)** and **d)** Slow removal of breakdown products in glia $\mu_8 = 5 \times 10^{-4}$/s. With corresponding source intensities required for the steady-state extracellular adenosine; **b)** waking $C_w = 0.9$nM/s with constant metabolism (blue) or $C_w = 0.8$nM/s with reduced metabolism (red) and sleeping $C_s = 0.8$nM/s. **d)** waking $C_w = 1.5$nM/s with constant metabolism (blue) or $C_w = 1.1$nM/s with reduced metabolism (red) and sleeping $C_s = 1.3$nM/s. Arrows indicate the time when the source intensity changes *i.e.* the first arrow is at waking while the second is at sleep onset

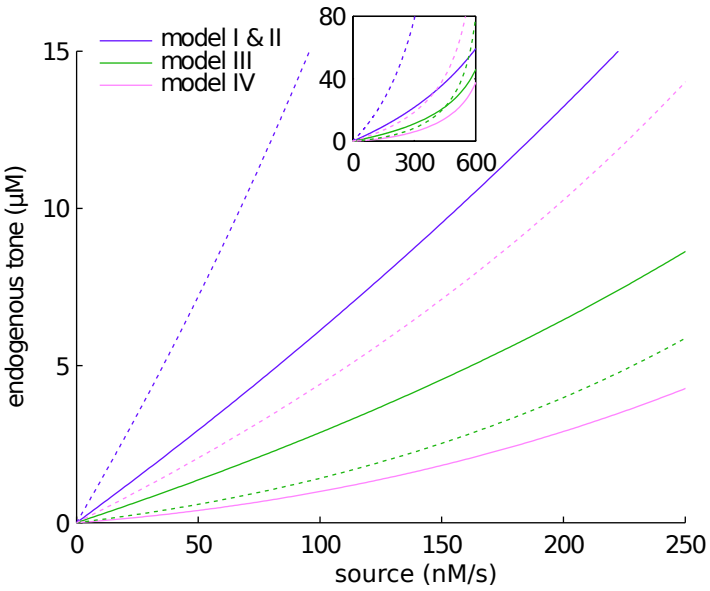

Figure 3.5: **Reduced enzyme activity in awake rats allows a smaller source intensity to produce a substantially greater endogenous tone of extracellular adenosine.** Solid lines show the daytime (sleeping) tone resulting from a constant uniform source, dashed lines show the endogenous tone where the maximum velocity of ADA (V_1 and V_4) are reduced by 43% and ADK V_7 is reduced by 54% of the day time (sleeping) level (de Sa et al. 1993). We assume fast removal of breakdown products in glia $\mu_8 = 5/\text{s}$.

3.3.2 Isolated point source

There is evidence of heterogeneities in the basal tone of adenosine from direct measurements using biosensors and indirectly from the difference in EPSPs when an A_1R agonist or antagonist is applied, (Wall et al. 2007; Kerr et al. 2013), which could arise from spatial variation in the sources. The simplest way to capture such variation in the models is with an isolated point source. Here the low concentration limit (section 3.2) is solved analytically and two numerical solutions are compared. One considers a relatively large source $F = 10,000$zmol/s, $\sim$1.5% of the total ATP required to generate one action potential per second, and the other considers a relatively small source $F = 1,000$zmol/s, corresponding to the ATP required for a single mEPSP or for $\sim$5 vesicles releases per second. The two examples are almost identical, scaled for concentration (Figure 3.6), because rapid diffusion in the ECS ensures that, apart from a small region around the source, the concentration is below the MM constants of both transporters and ecto-ADA, *e.g.* for the large source term, the concentration is 15μM within 1μm but is less than 1μM around 12μm from the source. This means that the clearance mechanisms are well described by the linear low concentration limit.

The range of influence is an important factor to consider when modelling heterogeneities in the basal tone of adenosine. For relatively small sources the range for all models is determined by diffusion with clearance mechanisms having only a minor effect. The range due to diffusion scales linearly with the size of the source (Eq. 3.14) and logarithmically with clearance length scale (Eq. 3.16), as the concentration profiles for the models differ more from diffusion as r increases. So for larger sources the clearance mechanisms are able to reduce the range of influence, having a localising effect (Figure 3.6c). As the range of influence is primarily determined by diffusion, it means that increases in the basal tone or reductions in the volume fraction (which would both reduce the amount of additional adenosine required to reach the IC_{50}) would greatly increase the range of influence for a constant point source. Conversely, inhibiting transporters *e.g.* with alcohol, or reduction in purine metabolism would have a relatively minor effect on the range of influence.

The steady-state for the diffusion model (Eq. 2.17) can be solved analytically

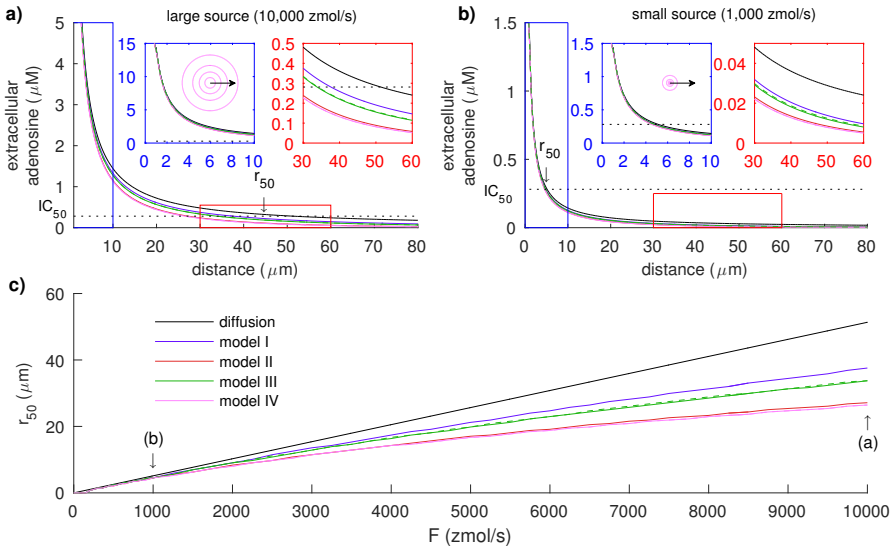

Figure 3.6: **The concentration of extracellular adenosine for an isolated point source is primarily determined by diffusion**. Two numerical solutions of the steady-state concentration profiles resulting from a constant point source. The extracellular adenosine concentration is primarily determined by diffusion, with the clearance mechanisms having a relatively minor effect. As the model assumes spherical symmetry the concentration profiles are given for the radial distance from the source. **a)** shows the extracellular adenosine concentration resulting from a large source $F = 10,000$zmol/s and **b)** small source $F = 1,000$zmol/s. Inserts show an enlargement of the concentration close (blue box) and far (red box) from the source, with contour plots showing the inhibitory concentration of 20%, 40%, 60% and 80% of A_1R, with scale arrow of 50μm. While the concentrations in **a)** are far greater than **b)** the shape of the profile is very similar, as diffusion dilutes the concentration in tissue so the concentration profile is well approximated by the linear low concentration limit (Eq. 3.15). The furthest distance from the source where the concentration exceeds the IC_{50} of A_1R r_{50} (*i.e.* the distance a synapses could be from the source where the EPSPs amplitude would be halved due to the extracellular adenosine concentration), is indicated in **a)** and **b)** and in **c)** it is shown as a function of source intensity. The behaviour is dominated by diffusion with the clearance mechanisms having a more prominent role for larger source intensities. Fast removal of breakdown products $\mu_8 = 5$/s (solid) and slow $\mu_8 = 5 \times 10^{-4}$/s (dashed).

(section B.5). For a constant point source the steady-state concentration A_e, scales as $\sim\frac{1}{r}$ (Eq. 3.13), where r is the distance from the source. This result also provides an estimate for the range of influence, r_{50}, the furthest distance where the concentration exceeds the IC_{50}, this distance grows linearly with the source intensity F (Eq. 3.14).

$$A_e = \frac{F}{4\alpha\pi Dr} \tag{3.13}$$

$$r_{50} = \frac{F}{4\alpha\pi DIC_{50}} \tag{3.14}$$

When the concentrations are lower than the MM constants, the nonlinear clearance kinetics are well approximated by linear rates (Figure B.1c), (given by the ratio of the maximum velocity and MM constant), this low concentration limit (section 3.2) can be solved analytically (section B.3). The constant point source A_e (Eq. 3.15), provides a good steady-state approximation over the source range considered. As with the solution for the diffusion model it also provides an estimate of the range of influence, which grows logarithmically rather than linearly with source intensity F (Eq. 3.16), where W is the product-log function.

$$A_e = \frac{F}{4\alpha\pi Dr}\exp\left(-\frac{r}{\lambda}\right) \tag{3.15}$$

$$r_{50} = \lambda W\left(\frac{F}{4\alpha\pi D\lambda IC_{50}}\right) \tag{3.16}$$

The limit (Eq. 3.15) and range (Eq. 3.16) are given in terms of characteristic distance, λ, the square root of the ratio of the removal rate and the diffusion coefficient (Eq. 3.2), the average distance an extracellular adenosine molecule diffuses before it is cleared for the ECS. Comparison with the diffusion result (Eq. 3.13) shows the relatively rapid removal of adenosine, (Table 3.1), *e.g.* the distance λ is as low as $\sim 40\mu$m for model IV, which

suggests endogenous adenosine has a local effect and also shows the dominant role neurons play in the clearance of adenosine. However this assumes that intracellular concentrations are the result of transport from the extracellular space. If for example, neuronal release via ENTs were the source of extracellular adenosine, the length scale would be similar to model III.

3.4 Brief endogenous and activity-dependent release

Extracellular adenosine concentration can change rapidly due to insult or neuronal activity. These are described in the model with a brief source. A uniform source is considered, which is comparable to multiple releases distributed throughout this tissue corresponding to a short insult, such as oxygen-glucose deprivation or a seizure. The model hierarchy (section 2.8) is used to determine the relative importance of the different clearance mechanisms. An isolated point source, comparable to activity-dependent release, is also considered. In this case both the range of influence and the efficacy of the different clearance mechanisms are evaluated and as before the adenosine signal is found to be highly localised and the dominant clearance mechanism is neuronal uptake and metabolism.

3.4.1 Uniform sources

Activity-dependent and spontaneous release events have been observed in several brain regions, including the cerebellum (Klyuch et al. 2012b) and striatum (Cechova et al. 2010; Nguyen et al. 2014). The release mechanisms vary with brain region and stimulus, often involving multiple pathways *e.g.* half of the increase in extracellular adenosine concentration in the cerebellum is due to extracellular metabolism of ATP whereas the other half is due to direct exocytosis (Klyuch et al. 2012a). The release events are characterised by a rapid increase in the extracellular adenosine concentration followed by a much slower decay due to diffusion and clearance (Klyuch et al. 2011). Here an instantaneous rise in extracellular adenosine concentration is considered and the model is used to study the role of the various clearance mechanisms.

Unlike the constant source, the duration of the extracellular adenosine concentration also has to be taken into account. If the concentration rapidly diminishes it will not have time to bind to A_1Rs. To account for this a single state model of the A_1R, is used (Eq. 2.15), to estimate the percentage of inhibition resulting for the proportion of bound A_1R (section 2.7).

Examples are given of a relatively large source $C_0 = 100\mu$M, where the initial clearance velocity is near its maximum value, (Table 3.2), and a small source of $C_0 = 1\mu$M. Note the sources here are given as a relative concentration *i.e.* multiplied by the free volume fraction, so that $\frac{S(x,t)}{\alpha} = C_0$ [μM] in (Eqs. 2.20, 2.22, 2.28, and 2.34).
Neuronal transport is clearly the dominant clearance mechanism for a brief uniform source. This is apparent by the rapid clearance of extracellular adenosine in models (II and IV) with neuronal uptake, compared to models (I and III) lacking neuronal uptake Figure 3.7a,e. *E.g.* The concentration arising from a small source (Figure 3.7a) falling below IC_{50} in ~7s in model II compared with ~35s for model III. Neuronal adenosine (Figure 3.7b,f) peaks as neurons become a source of breakdown products, competitively inhibiting further adenosine uptake. While the neuronal adenosine concentration remains less than the extracellular adenosine concentration, the combination of adenosine and breakdown products within neurons can rapidly exceed the extracellular combination, saturating ENTs (Figure 3.7e,f), this occurs between 11s $C_0\alpha = 1$nM and 80s $C_0\alpha = 100\mu$M. Neurons then act as a source of breakdown products, as neuronal ADA is faster than ecto-ADA. Similarly glial transport peaks where influx is balanced by ADK (Figure 3.7c,g), the rapid removal of breakdown products prevents them accumulating within glia.

With larger initial concentrations, all models show an initial exponential decline in extracellular adenosine (Figure 3.7a), with the additional mechanisms simply increasing the clearance velocity, and neuronal clearance having the greatest effect. The duration of the adenosine signal can be characterised by the time required for the estimated activation of the single site model of the A_1R to fall below 50% (Figure 3.8a), similar to the low concentration clearance rate τ (Table 3.1) for small sources. Alternatively the

duration of the signal could be quantified by the average survival time of a molecule of adenosine released as part of an initial concentration (Figure 3.8b). For small sources this is equal to the steady-state characteristic scale given in (3.1). This relatively long time scale suggests that the adenosine could mix throughout the whole uniform volume, (as the mean displacement of a molecule scales as $\sqrt{6Dt}$ and the uniform volume will be comparatively small).

The separation between models with (II and IV) and without (I and III) neuronal uptake is also apparent from the initial clearance velocity (Figure 3.8c), where even for small concentration neuronal uptake has a substantial effect on the clearance velocity. The effective $V_{\max}$ and K_m (Table 3.2) are determined by a nonlinear fit of the saturating MM kinetics (Eq. 2.9) to these initial velocities. There is a dramatic increase in the velocity in model II, combined with a reduction of K_m, (Table 3.2), again highlighting the dominant role of neuronal clearance. The removal rate of breakdown products in glia (μ_8) has almost no effect on this single MM reaction approximation, because of the relatively slow transport into glia. These single MM reactions are a poor approximation of the clearance dynamics for model II-IV, particularly for a small source because of the relatively rapid saturation of ENTs.

Model	K_m (μM)	$V_{\max}$ (μM/s)	Ratio (s^{-1})
I	80.72 ($\pm$0.18)	1.42 ($\pm 6.28\times10^{-7}$)	0.018
II	13.58 ($\pm$0.36)	2.63 ($\pm 1.34\times10^{-2}$)	0.194
III	56.57 ($\pm$0.30)	2.05 ($\pm 1.97\times10^{-3}$)	0.036
IV	15.86 ($\pm$0.37)	3.28 ($\pm 1.45\times10^{-2}$)	0.207

Table 3.2: **Neuronal uptake dramatically increases the maximum removal velocity**. The MM parameters obtained via a nonlinear fit to initial clearance velocity (Figure 3.8c) with a 95% confidence interval of the fit given in brackets. Notice that the μ_8 parameter has little effect on the parameter estimates because of the relatively slow transport into glia.

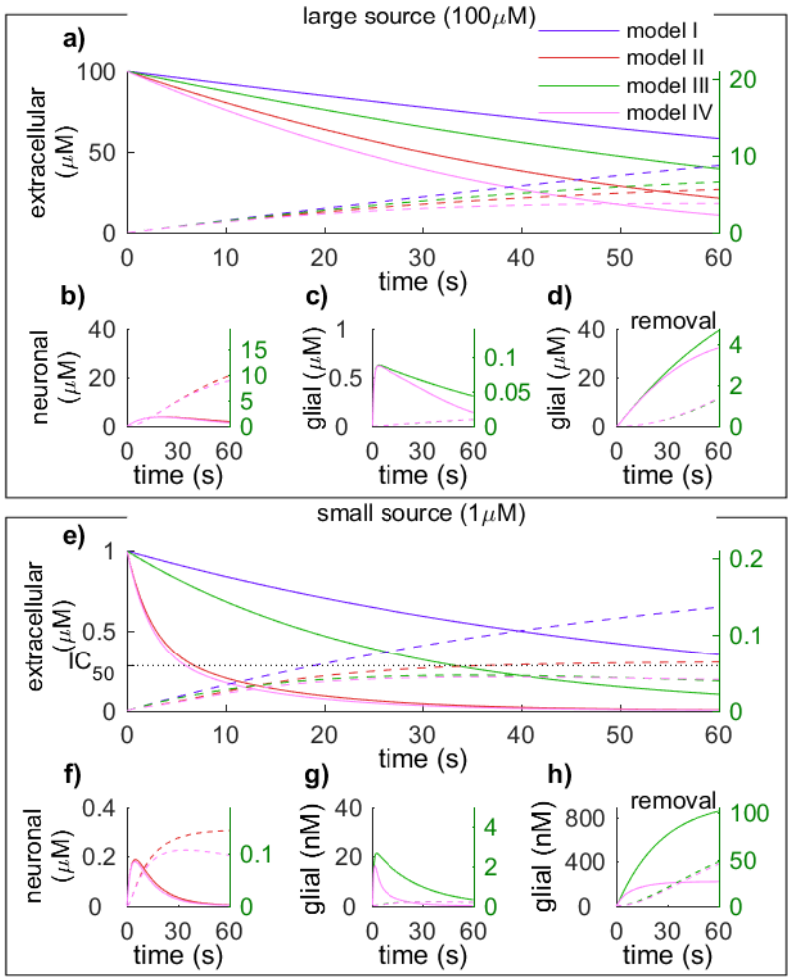

Figure 3.7: **Neuronal uptake is the dominant clearance mechanism for a brief uniform source.** Examples of the concentration dynamics for a large **a)-d)** 100μM and small **e)-h)** 1μM source. Relative concentrations are shown on the left, while total concentrations are shown on the right to allow direct comparison between extracellular, neuronal and glial adenosine. Adenosine (solid) and breakdown products (dashed) in **a)-c)**, **e)-g)**, while **d)** and **h)** show the removal in glia of adenosine by ADK (solid lines) or by the unsaturating clearance of breakdown products (dashed lines). Examples shown have the rapid removal of breakdown products in glia ($\mu_8 = 5$/s).

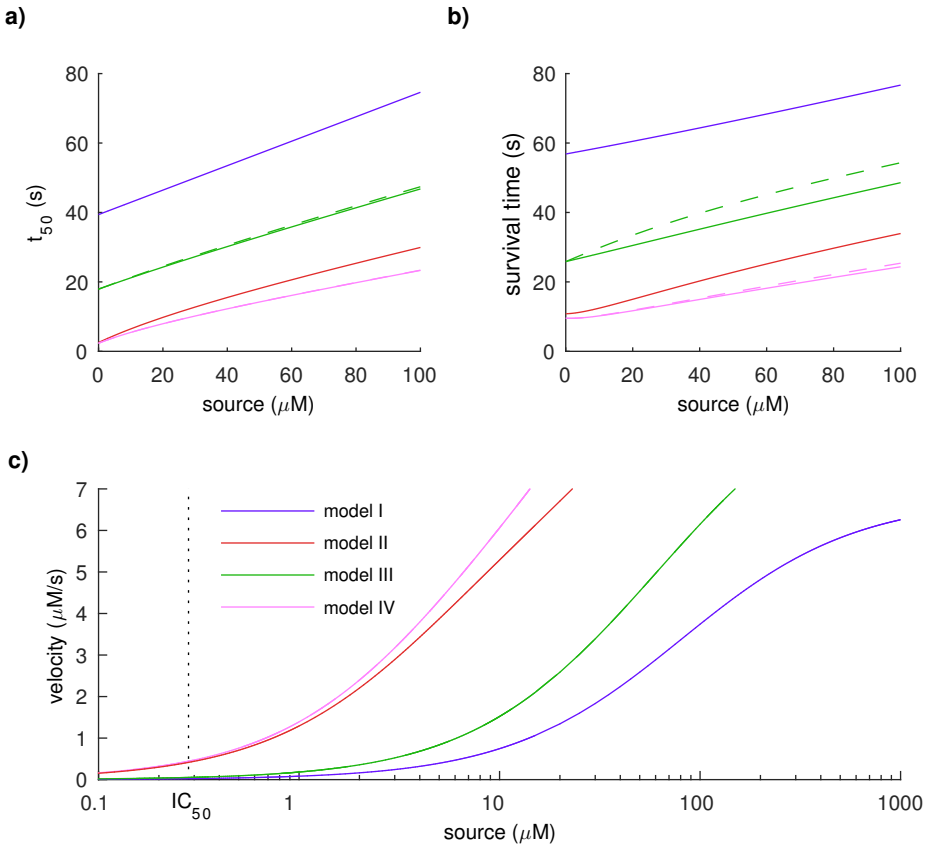

Figure 3.8: **Neuronal uptake is the dominant clearance mechanism for a large range of brief uniform source intensities. a)** the duration of the adenosine signal, characterised as the time required for the estimated activation of A_1R to fall below 50%. **b)** the average survival time of a molecule of adenosine. **c)** the initial clearance velocity, the removal rate in glia has very little impact on the initial clearance velocity. With rapid removal of breakdown products in glia ($\mu_8 = 5/s$) shown by solid lines and slow removal ($\mu_8 = 5 \times 10^{-4}/s$) is shown by dashed lines.

3.4.2 Isolated point source

There are multiple pathways implicated in activity-dependent release, with evidence for direct neuronal adenosine release, *e.g.* postsynaptically in the hippocampus (Lovatt et al. 2012), glia release, or extracellular ATP metabolising enzymes (Wall and Dale 2008). Here these mechanisms are modelled with a brief point source of adenosine and its range of influence is considered using a simple model of the A_1R (section 2.7). It is found to be highly localised reaching $\sim 25\mu$m with a relatively large source $F_0 = 50,000$zmol and primarily determined by diffusion. By integrating over the concentration profiles, the total amount of adenosine in the intracellular and extracellular spaces can be compared with the clearance of a brief uniform source, because of rapid diffusion in the extracellular space the removal clearance of both the large and small source are very similar.

While any brief point source will increase the concentration above the IC_{50} of A_1R sufficiently close to the source, 200zmol is required to achieve half activation within 1μm (Figure 3.9n). The range of influence of adenosine scales with volume, as $F_0^{\frac{1}{3}}$ and is primarily determined by diffusion, (regardless of whether the range is based on the IC_{50} concentration or proportion of bound receptors), with clearance mechanisms having a minor effect. Diffusion rapidly dilutes the adenosine source, so for a small source clearance mechanisms have very little influence on range, (Figure 3.9i,k) or duration (Figure 3.9j,l). However, a larger source takes longer to be diluted by diffusion, so clearance mechanisms can have a more substantial effect, especially neuronal transport, (Figure 3.9b-f). There is a clear separation between models with (II and IV) and without (I and III) neuronal uptake.

The receptor model results in both a slower rise and decay compared to the concentration profiles (Figure 3.9a,b,g,h). The duration of the adenosine signal, characterised as the time required for the extracellular concentration to fall below IC_{50} throughout the tissue, scales as $\sim F_0^{2/3}$ (for the diffusive case, section B.5). Whereas the time required for inhibition due to A_1R to fall below 50%, rapidly increases to $\sim 5s$ (Figure 3.10o).

The dominant role of neuronal uptake on adenosine clearance can be seen by the clear separation between the profiles for models with (II and IV) and

without (I and III) neuronal clearance (Figure 3.9a,g). This is also apparent from the percentage inhibition *i.e.* the reduction in amplitude of an EPSP for a synapse located at the source of adenosine (Figure 3.9b,h), this is also apparent in the duration of the adenosine signal (charterised either by the time above the IC_{50} or the time taken for percentage inhibition to fall bellow 50%) and peak inhibition. However the primary factor in determining the adenosine profile is diffusion, particularly apparent from the peak adenosine concentration which is almost identical for all models (Figure 3.9c,i).

A comparison of the clearance mechanisms is given by integrating over the concentration profiles to obtain the amount of purines in tissue at a given time (Figure 3.10). This has a very similar form to the small brief uniform source (Figure 3.7e), because diffusion is able to rapidly dilute the concentrations. As before models II and IV deviate from this form because of the rapid neuronal uptake, which suggests the neuronal ENTs saturate after the initial burst, as in the uniform case.

The rate of removal of breakdown products within glia (μ_8) has only a minor effect on the extracellular amounts. Initially removal of breakdown products in glia dominates for rapid removal (μ_8=5/s), (Figure 3.10d,h), but as breakdown products build up the salvage pathway surpasses it, with the crossover time in both model III and IV of 40s. This suggests the model is able to adequately quantify extracellular concentration, but can only give a qualitative description of the glial dynamics, without a better estimate of the dynamics of the purine metabolism in glia.

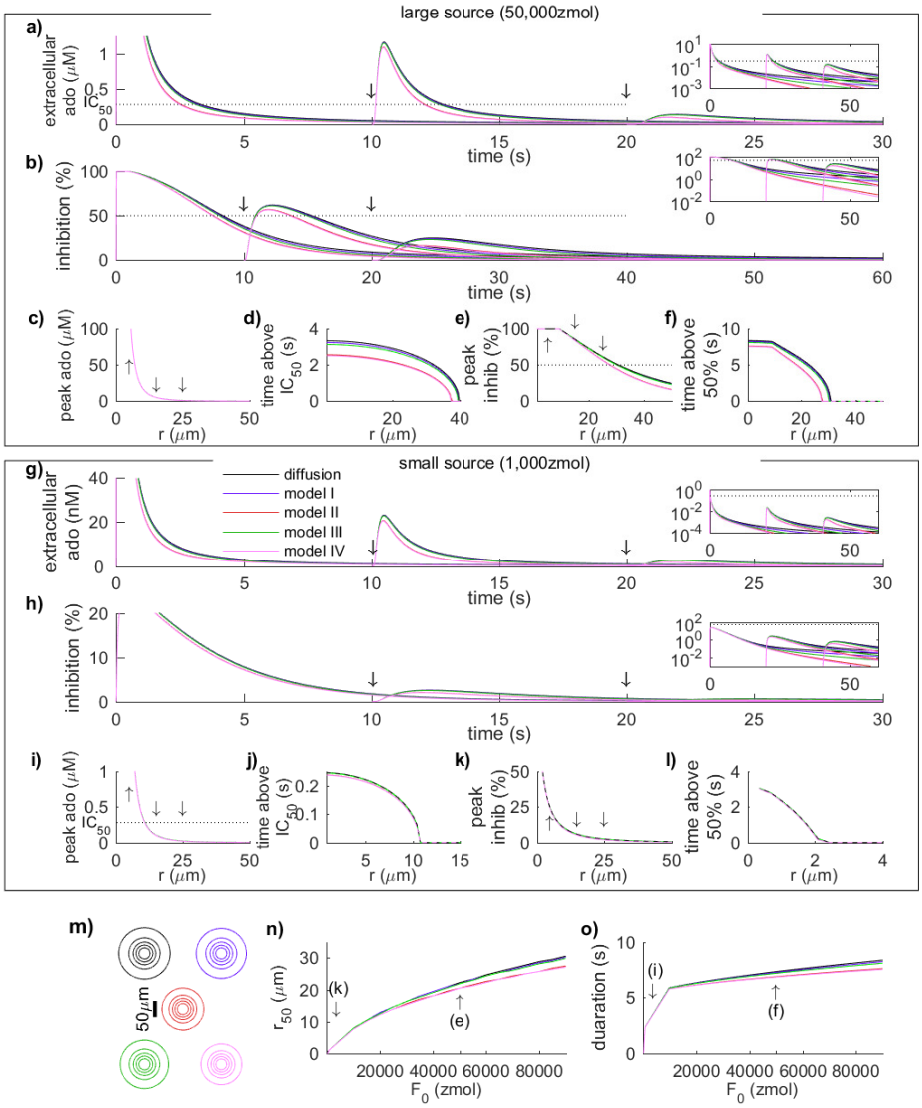

Figure 3.9: **For a brief point source, the range of influence of adenosine is primarily determined by diffusion with clearance mechanisms only having a substantial impact for relatively large sources.** A relatively large source $F_0 = 50,000$zmol **a)-f)** is compared with a small source $F_0 = 1,000$zmol **g)-l)** in both cases there is rapid removal of breakdown products in glia ($\mu_8 = 5$/s). **a)** and **g)** are concentration profiles of extracellular adenosine at 5μm, 15μm and 25μm with inset of a log-linear plot. **b)** and **h)** the percentage inhibition based on the proportion of bound A_1R with inset of a log-linear plot. **c)** and **i)** the peak adenosine concentration is determined by diffusion. **d)** and **j)** the duration of the adenosine signal. **e)** and **k)** the peak inhibition. **f)** and **l)** the duration of the adenosine signal. **m)** example contour plots for the large source showing 10%, 30%, 50% 70% and 90% inhibition. **n)** the range of influence of adenosine. **o)** the duration of the adenosine signal.

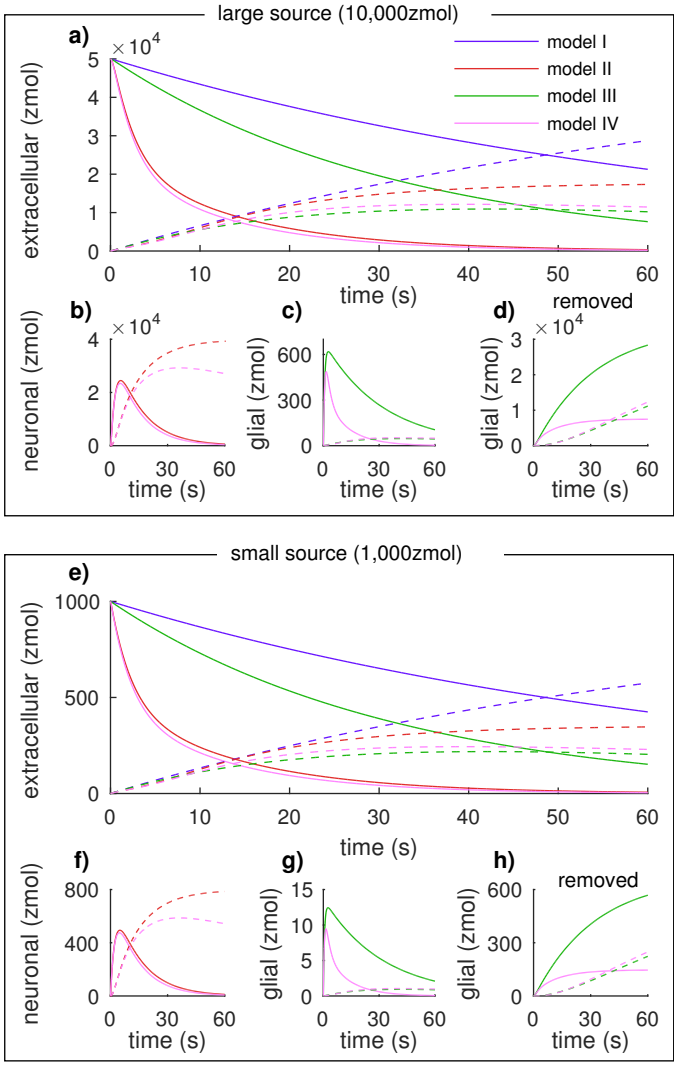

Figure 3.10: **Neuronal uptake is the dominant clearance mechanism for a brief point source.** **a)** and **e)** extracellular adenosine (solid) and breakdown products (dashed) indicate a substantial difference between models with (II and IV) and without (I and III) neuronal transport. **b)** and **f)** neuronal adenosine (solid) rapidly peaks at ∼5s and becomes a source of breakdown products (dashed). **c)** and **g)** glial adenosine (solid) also reaches a peak at ∼3s for model III, or ∼7 for model IV. Break-down products (dashed) do not accumulate due to the rapid removal mechanism. **d)** and **h)** initially glia are primarily removing adenosine by creating AMP (solid) due to the large amount of extracellular adenosine, but removal of breakdown products (dashed) becomes dominant as they accumulate extracellularly. With rapid removal of breakdown products in glia $\mu_8 = 5/\text{s}$.

3.5 Bath applied adenosine

The models developed here are applicable to experimental conditions. For example bath application of adenosine to a tissue slice has been used extensively to study the effect of adenosine on synaptic transmission and has produced estimates of the efficacy of adenosine clearance, suggesting ∼20 fold less adenosine at the synapse than the bath (Dunwiddie and Diao 1994; Kerr et al. 2013; Zhang et al. 2015).

Here the models are used to obtain a steady-state concentration profile when 100μM or 10μM are applied at both the top and bottom of a 400μm slice. When 100μM is applied the inhibitory effect of A_1R exceeds 99% in the steady state (Figure 3.11b) and reaches 50% throughout the slice within ∼15s. Whereas with 10μM applied in model IV the concentration is reduced to 0.3μM in the middle of the slice, but due to the high affinity of the A_1R, this still achieves at least 50% inhibition (Figure 3.11d). The breakdown products penetrate the slice more easily due to relatively slow uptake by glia, so the total amount gradually exceeds the adenosine in the slice even with relatively fast removal in glia ($\mu_8 = 5/s$). The high applied concentration may have unwanted side effects, for example activating low density $A_{2B}R$ and A_3R which require ∼70 and ∼90 fold higher concentration of adenosine than A_1R (Fredholm et al. 2011). The use of high applied concentration have been avoided in several studies, by using a net so that the applied adenosine reaches both the top and bottom of the slice (Dunwiddie and Diao 1994; Stutzmann et al. 2001; Kerr et al. 2013) or more commonly using A_1R antagonists that are not susceptible to the purine metabolism.

The time for the whole slice to exceed 50% activation with 100μM applied is around 25s for model I and III and 85s for models II and 310s for model IV. Bath applied adenosine studies typically allow several minutes for the synaptic adenosine concentration to become stable (Dunwiddie and Diao 1994), these models confirm that this is clearly adequate. The breakdown products rapidly accumulate in the slice in models II and IV due to relatively rapid metabolism of neuronal ADA, with 100μM applied, the total amount of breakdown products exceeds the extracellular adenosine concentration in models II (by 140s) and IV (by 155s). Similarly the extracellular concen-

tration breakdown products in the steady state is greater than adenosine through the middle of the slice in models IV (between $177 - 223\mu$m) and II (between $155 - 245\mu$m).

The steady-state extracellular concentrations in model IV are similar for both slow ($\mu_8 = 5 \times 10^{-4}$/s) and fast ($\mu_8 = 5$/s) breakdown product removal. The glia concentration of adenosine are also slightly higher with fast removal, with 100μM applied, model III has a minimum steady-state concentration of 0.3μM for fast removal compared with 0.15μM for slow removal, similarly 0.2μM and 0.1μM for model IV. So while the model can quantify the extracellular concentration of adenosine in tissue, it does not adequately describe the glial adenosine dynamics.

3.5.1 Effective dose response curve

Here the model is indirectly compared with an experimental operative. The local dose-response to extracellular adenosine of A1 receptors can be determined from the response to agonists and their binding affinity *e.g.* N^6-Cyclopentyladenosine (CPA). The model gives a concentration profile of adenosine resulting for a bath applied concentration, by assuming a uniform distribution of synapses and receptors, the dose-response to bath applied adenosine to be calculated and compared with experimental observations (Stutzmann et al. 2001). The bath applied IC_{50} is 2.7μM for adenosine and $10n$M for CPA which is shifted for the higher potency of CPA to give an estimated 100nM IC_{50} for adenosine in the absence of any clearance mechanisms. The model of clearance then shifts this response curve further to an IC_{50} of 1.1μM (Figure 3.12). The discrepancy between this estimate and the observed value could be due to underestimating the impact of clearance mechanisms. However, it could also be due to heterogeneities in the distribution of synapses and adenosine receptors. Synapses near the surfaces of the slice, where the model predicts the highest concentration of adenosine, are less likely to survive and contribute to the observed inhibition. It could also result from heterogeneities in the clearance mechanisms themselves, ecto-ADA has been shown to colocalize and even form a dimer with A_1R (Gracia et al. 2008) and ENTs may be preferentially located near synapses.

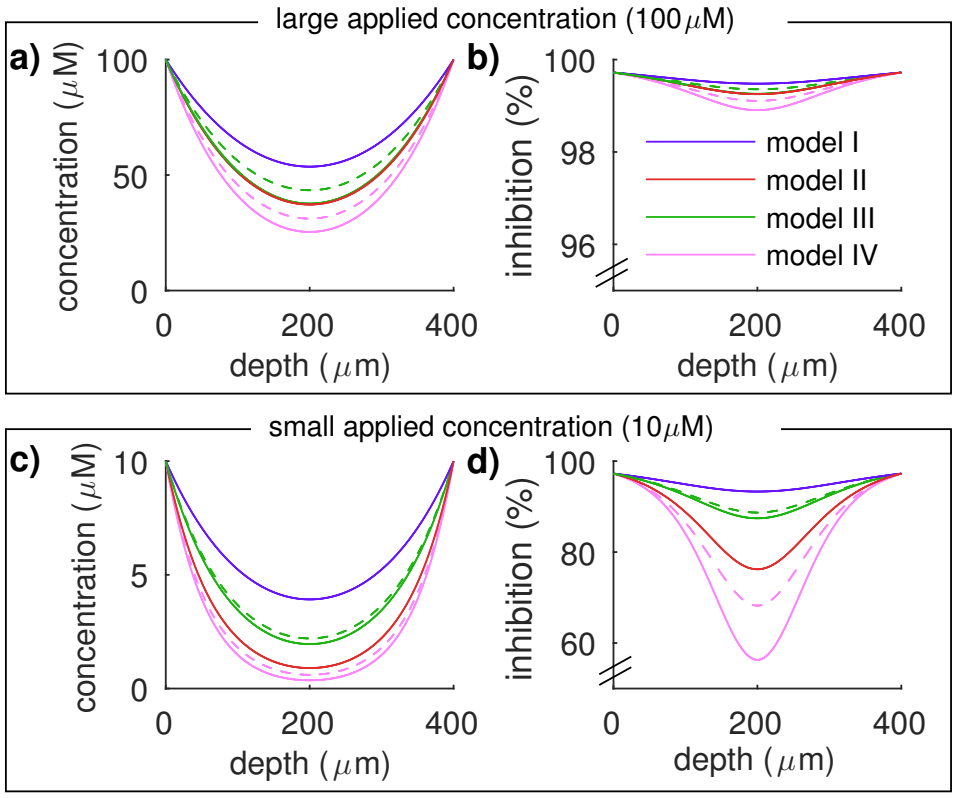

Figure 3.11: **The extracellular adenosine concentration remains comparatively high throughout the slice despite up to a ∼20 fold decrease from the applied concentration.** The steady-state concentration of extracellular adenosine for a large source (100μM) falls to 50%, 35% 35% and 22% of the applied concentration for models I-IV respectively, a small source (10μM) can fall as low as 3%. **a)** Extracellular adenosine concentration and **b)** % inhibition due to A_1R following application of 100μM. Similarly **c)** and **d)** for 10μM application. Removal of breakdown products in glia with rate $\mu_8 = 5/\text{s}$ (solid) or $\mu_8 = 5 \times 10^{-4}/\text{s}$ (dashed).

3.5.2 ENT Blockers

The model predicts that reducing the maximum velocity of ENTs by blocking some of them, will drastically increase the extracellular adenosine concentration (Figure 3.13). Dose response curves suggest 5μM of NBMPR would reduce neuronal uptake by ∼11% and uptake by astrocytes by ∼19% by blocking ENT1s. Similarly 1μM of dipyridamole produces a ∼20% reduction in ENT2 uptake, causing an estimated 17% reduction in neurons and a 14% reduction in glia transport, by interpolation of the data presented in (Yao et al. 1997; Nagai et al. 2005).

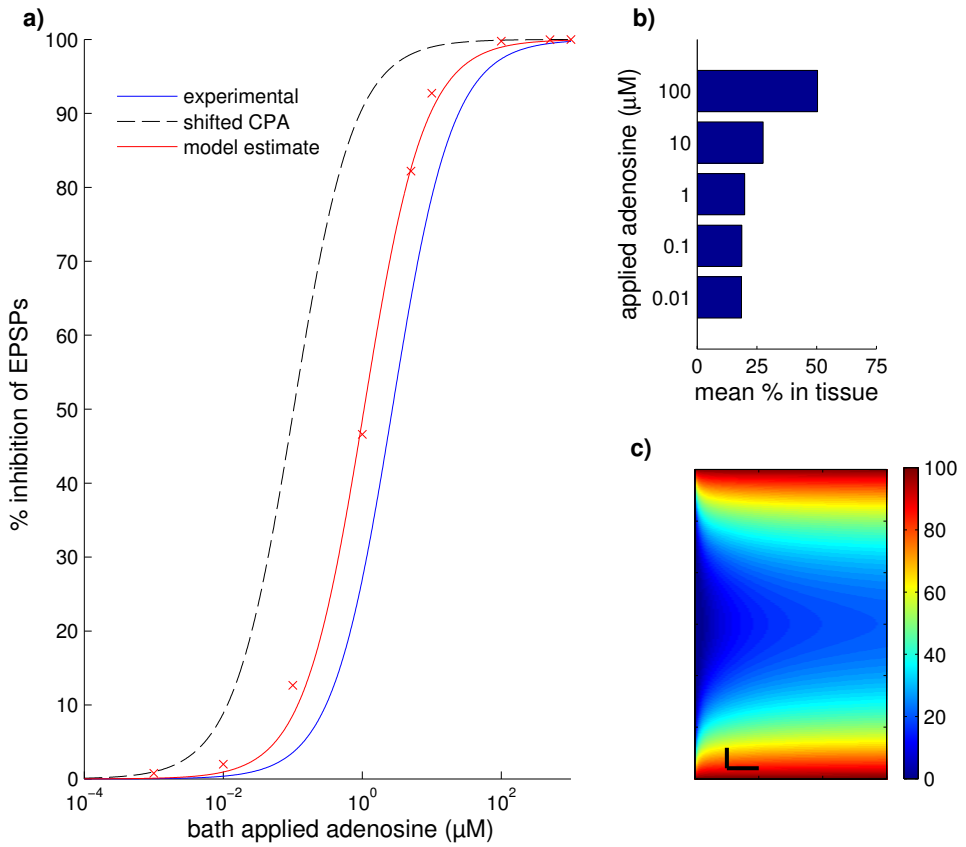

Figure 3.12: **Modelling adenosine clearance shifts the dose response curve closer to the observed inhibition. a)** Bath applied adenosine in (Stutzmann et al. 2001) gives an estimated IC_{50} for adenosine of 2.7μM (blue line) and A_1R agonist CPA of 10nM. The CPA curve is shifted by the relative potency of CPA to adenosine, giving an estimated IC_{50} of adenosine in the absence of clearance (dashed black line). The model (evaluated at points indicted by red crosses) provides a further shift in the CPA dose response curve to account for adenosine clearance (red line). **b)** The average adenosine concentration in the tissue slice and a percentage of the bath applied concentration clearly shows the saturation of clearance mechanisms as the concentration is moved far beyond physiological levels. **c)** The extracellular adenosine concentration with 100μM applied, scale bar shows 10μm vertical and 5s horizontal.

This is not apparent in bath application experiments in the rat cortex or hippocampus, where application of both 5μM of NBMPR and 1μM of dipyridamole had no statistically significant effect on the extracellular concentration of bath applied adenosine. This was measured by subtracting the response of an inosine biosensor (sensitive to inosine and hypoxanthine) from

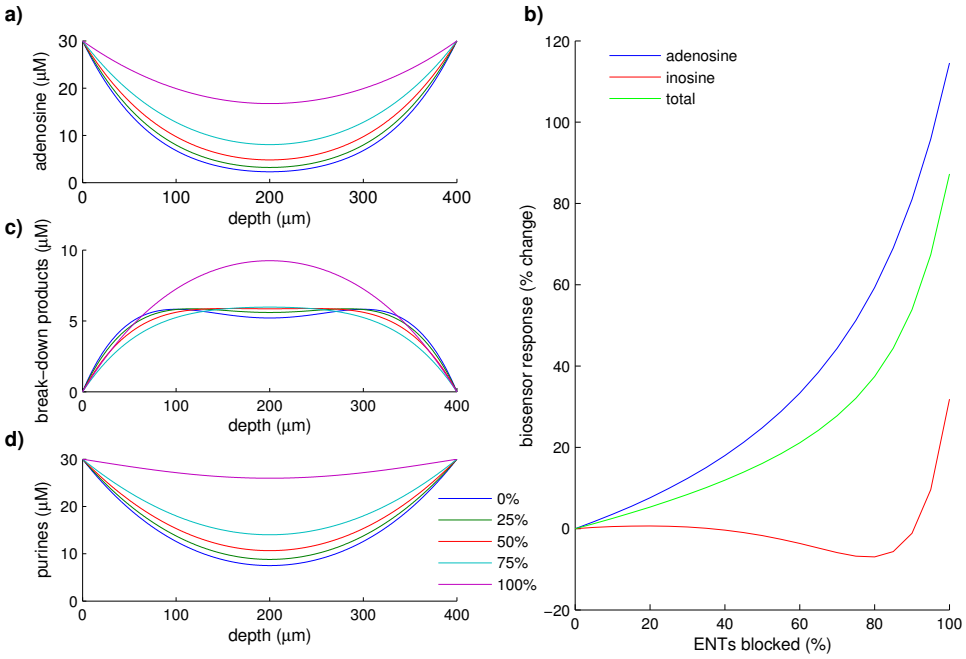

Figure 3.13: **The extracellular concentration of adenosine in the rat cortex is substantially greater as ENTs are blocked, however the combination of adenosine and its breakdown products shows a smaller increase.** Concentration profiles for 30μM bath applied adenosine for a 400μm slice of the rat cortex at 32°C for 3 minutes. **a)** extracellular adenosine **c)** extracellular breakdown products or **d)** the combination of both extracellular adenosine and its breakdown products. The ENT velocities (V_2, V_3, V_5 and V_6) are reduced to represent the proportion that have been inhibited. **d)** The relative change in the average concentration of adenosine, breakdown products and the combination of the two, for reduced transport velocity shows the higher extracellular adenosine concentration offset by a lower concentration of breakdown products, with fast removal of glia breakdown products ($\mu_8 = 5/\text{s}$)

adenosine biosensor (sensitive to adenosine as well as inosine and hypoxanthine). (Data provided by Marianne Cobham, M. J. Wall lab, School of Life Sciences, University of Warwick). This could be due to a greater role for CNTs or other, uninhibited classes of ENTs. However other studies, particularly in the hippocampus have seen a significant decrease in the post-synaptic EPSPs with bath application of transporter inhibitors (Clasadonte et al. 2014), which suggests the failure to observe a change with biosensors could be due to spatial heterogeneities of the clearance mechanisms, or the accumulation of cytosolic ADA around the biosensors. When the biosensors are inserted into tissue, their large diameter $\sim$100μm disrupts cells, this

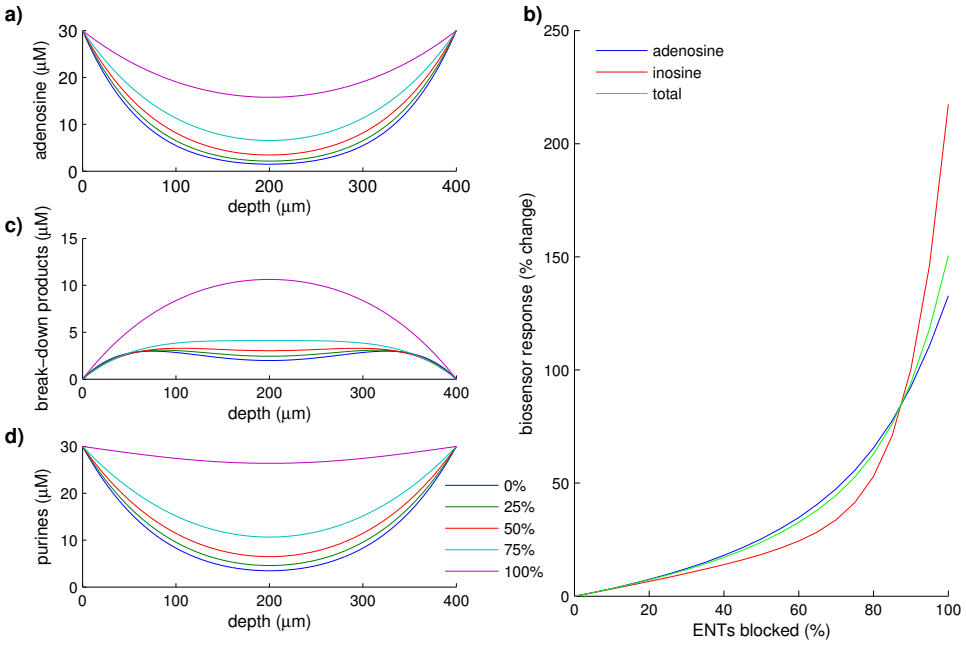

Figure 3.14: **The extracellular concentration of adenosine and inosine are both substantially greater as ENTs are blocked in the rat hippocampus.** Concentration profiles for 30μM bath applied adenosine for a 400μm slice of the rat hippocampus at 32°C. **a)** extracellular adenosine **c)** extracellular breakdown products and **d)** adenosine and its breakdown products combined. The percentage of ENT inhibited is modelled by reducing the transport velocities; V_2, V_3, V_5 and V_6. **b)** The relative change in average concentration of adenosine and breakdown products for reduced transport velocity shows a substantial rise in both adenosine and its breakdown products, with fast glia removal of breakdown products $\mu_8 = 5/\text{s}$

is apparent from the large increase in extracellular adenosine. If cytosolic ADA remains in or around the polymer matrix of the biosensor, then both the inosine and the adenosine biosensor would measure adenosine and the subtraction used to estimate the adenosine concentration would be an underestimate and so unlikely to capture the change due to ENT blockers. Therefore it may be better to consider the change in purine concentration instead, in which case the change resulting from ENT blockers would be far less in the cortex (Figure 3.13) and so more likely to be obscured by experimental variability.

In the rat hippocampus changes in extracellular purine concentrations (adenosine, inosine, hypoxanthine) tone was successfully observed using biosensors,

with 5μM of NBMPR and 10μM of dipyridamole there was an increase in extracellular purines of $0.6 \pm 0.2\mu$M' in 7 of 9 hippocampal slices (Etherington et al. 2009). The combined concentration of adenosine and its breakdown products, show a similar increase to adenosine in response to ENT blockers in the hippocampus (Figure 3.14).

Chapter 4

Modelling biosensors in tortuous environments

4.1 Introduction

Biosensors have become invaluable for both *in vitro* and *in vivo* experiments. Biosensors have been used to measure neurotransmitters and neuromodulators, such as: glutamate (Oldenziel et al. 2006; Hu et al. 1994), acetylcholine (Bruno et al. 2006; Zhang et al. 2010), ATP (Wells et al. 2015; Lopatář et al. 2015; Lalo et al. 2014; Llaudet et al. 2005), adenosine, inosine and hypoxanthine (Wall and Richardson 2014; Van Gompel et al. 2014; Klyuch et al. 2012a; Llaudet et al. 2003). Biosensors consist of three components; a selective biological element, a detector element and a device to record and display the result. Here biosensors which use enzymes to select for the analyte and electrochemically detect the product of the reactions are considered. Such biosensors are typically formed of a microelectrode surrounded by a permeable medium where enzymes are immobilised and will metabolise an analyte to create an electroactive product.

Many biosensors developed for brain tissue use oxidative enzymes, followed by detection via fixed potential amperometry (FPA). There are many considerations in the construction and use of biosensors to ensure that the signal observed provides an accurate measure of the desired substrate. These include; interference from other substrates of the enzyme cascade, interference from O_2, a non-linear enzyme response due to substrate or product inhibi-

tion and a reduction in signal proportional to the sensors size (Dale et al. 2005). However, these difficulties have been overcome for many different substrates, including glutamate, acetylcholine, ATP, glucose, lactate, H_2O_2 and adenosine.

Biosensors are typically formed of a platinum or carbon fibre core, on which a conducting polymer matrix such as pyrrole or paraphenylene are deposited. The electrochemical polymerization is achieved by either holding the core at a constant potential or by cycling the potential. This allows the thickness of the matrix to be controlled and reproduced. A thin layer biosensor is created when the enzyme is attached (immobilised by absorption) to the surface of the polymer matrix (Kobayashi et al. 2001), or by cross-linking the enzyme to create a matrix principally of covalently bonded enzyme (Mikeladze et al. 2002). A thick layer biosensor is made when the enzyme is immobilised by entrapment within the free volume of the polymer matrix, (Llaudet et al. 2003) or covalently bonded to the polymer matrix (Kotanen et al. 2014).

An *in vivo* study of glutamate in the striatum of anaesthetized rats measured the basal tone as $\sim 18\mu$M (Oldenziel et al. 2006), by subtracting the signal from a null sensor and using a flow-injection analysis system (Oldenziel and Westerink 2005) for calibration. Then inserting a micropipette in the vicinity (within 100μm) of the biosensors and applying either; potassium chloride, excitatory amino acid kainate or glutamate reuptake inhibitor DL-threo-beta-Benzyloxyaspartate. All induced dose dependent increases in extracellular glutamate. Finally the sodium channel blocker tetrodotoxine (TTX) was injected, reducing extracellular glutamate by 90%, suggesting most of the basal tone is derived from vesicle release.

Acetylcholine has also been studied with anaesthetized rats (Zhang et al. 2010), using biosensors to show that hippocampal theta oscillations are coupled to acetylcholine (ACh) release. They used amperometric choline sensors in the dorsal CA1 area and separated a low frequency signal containing chemical information with a high frequency signal representing the local field potential (LFP). They induced theta oscillation with a tail pinch and showed an increase in choline concentration to around 100nM, and that the maximal phasic release of ACh in CA1 occurs around the pyramidal layer,

and the releases lag $20 - 50$s behind the onset of theta oscillations.

Biosensors were surgically implanted in the rat cerebral cortex to monitor glucose concentrations during the sleep/wake cycle (Dash et al. 2013). As in the other studies mentioned, the sensor was calibrated *in vitro*, but then *in vivo* injections of the substrate and saline were used as confirmation. The study focused on how brain glucose levels change during periods of high energy need. They compared the normal sleep/wake cycle with 3 hours of sleep deprivation. The glutamate concentration showed a rise during non rapid eye movement (NREM) sleep ($\sim$12mM) and a fall during REM sleep ($\sim$4mM), the onset of the fall is delayed by sleep deprivation.

In many studies biosensors are calibrated in a free environment before and/or after being used in tissue. The calibration is used to estimate the concentration of analyte from the biosensor's response. However, these studies fail to take into account differences in the diffusion characteristics of tissue, where analyte is limited to the ECS and the diffusion coefficient is reduced by tortuosity. Here mathematical and computational models are developed to compare the response of biosensors in both free and tortuous environments. A single enzyme reaction is considered as well as an enzyme cascade, where the product of one reaction is the substrate of another, with multiple reactions required before an electroactive product is detected. Damage caused by biosensor insertion is modelled with additional free space around the biosensor. An estimate is made of a ratio by which the experimental response of the biosensor should be scaled to account for differences between the free-flow calibration and diffusive experimental environments. Finally, the influence that the model parameters have on such a correction is considered.

4.2 Mathematical modelling

In order to characterise the response of biosensors and assist in their design, extensive mathematical and computational modelling has been used, quantifying the influence of substrate and product inhibition (Šimelevičius and Baronas 2010; Šimelevičius and Baronas 2011), geometry (Štikonienė

et al. 2010) and enzyme kinetics (Ivanauskas et al. 2008; Simelevicius et al. 2012). However, the effect that tissue structure can have on the biosensor's response has yet to be considered. Chemicals in tissue must diffuse through the tortuous ECS, which is characterised by a reduced volume fraction or porosity α, (typically $\sim$0.2 in brain tissue) and the tortuosity θ (typically $\sim$1.6). The tortuosity is the proportional increase in the average path length a particle must take because of obstructions. This influences the macroscopic description by reducing the diffusion coefficient. Measurements of these macroscopic characteristics of tissue have been made in many brain regions and species under both physiological and pathological conditions (Syková and Nicholson 2008).

4.2.1 Single enzyme model

A biosensor with a single enzyme in tissue is described by a model in cylindrical coordinates, with radial symmetry, and three regions. The biosensor is centred at the origin, and the radius of the edge of the core is r_b, this is followed by the enzyme which is immobilised in a polymer matrix with thickness w and porosity α_b and diffusion coefficient D_b. Inserting the biosensor may distort the extracellular space around it. This is incorporated into the model with a free volume thickness d with diffusion coefficient D_f. The tissue is modelled with diffusion coefficient D_t and porosity α_t (Figure 4.1). The tissue is modelled as maintaining a constant concentration of the analyte, as a balance between a constant uniform source and endogenous clearance mechanisms. The concentration of the analyte A is described by the partial differential equations;

$$\frac{\partial A}{\partial t} = \begin{cases} D_b \nabla^2 A_b - \dfrac{V_{\max} A_b}{K_m + A_b} & r_b \leq r < r_f \\ D_f \nabla^2 A_f & r_f \leq r \leq r_t \\ D_t \nabla^2 A_t + \mathcal{S} - f(A_t) & r_t \leq r \end{cases} \tag{4.1}$$

Where $V_{\max}$ and K_m are the Michaelis-Menten parameters of the biosensor enzyme, $\mathcal{S}$ is a uniform source of the analyte in tissue and $f(A_t)$ describes the clearance mechanisms. The concentrations of analyte are defined as the amount of analyte in a given volume, ignoring the obstructions such as cells

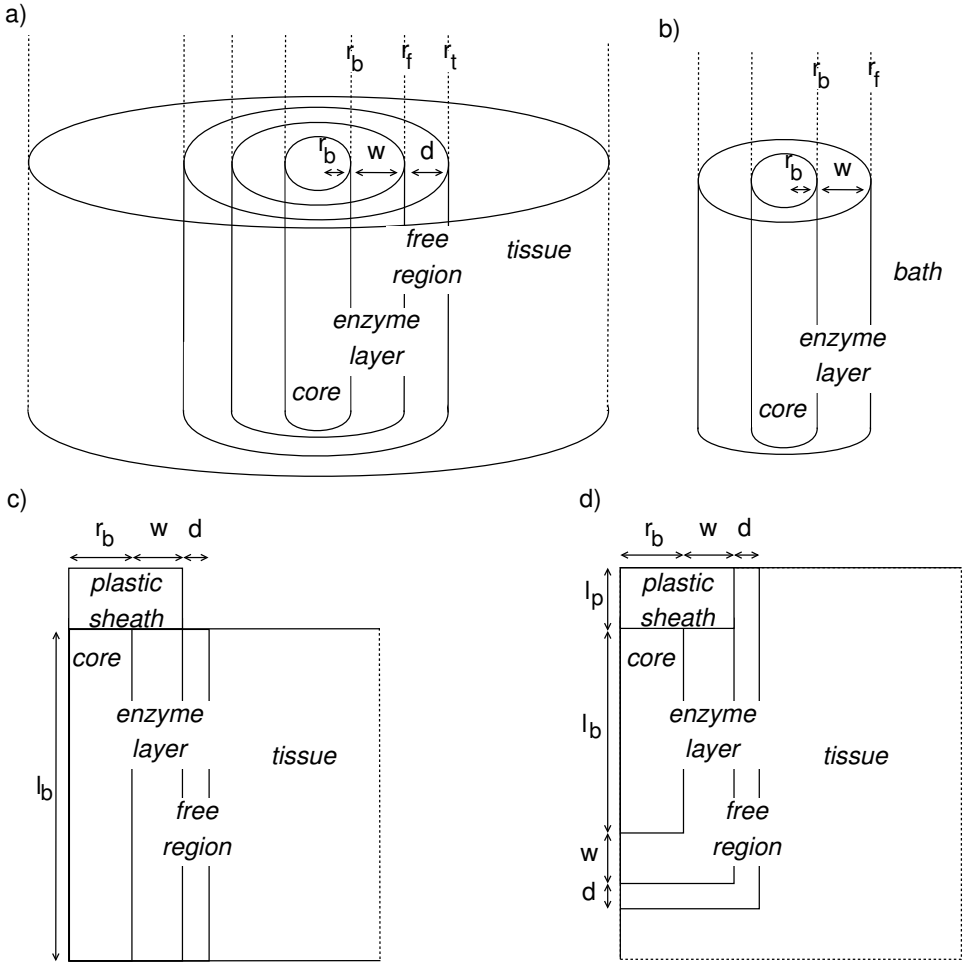

Figure 4.1: **A schematic of the model for a cylindrical biosensor.** The biosensor is comprised of a conducting core, typically platinum or carbon fibre (thickness r_b) surrounded by a polymer matrix with the immobilised enzyme (thickness w) forming the enzyme layer. In the calibration model a boundary condition would be applied to the edge of the polymer matrix. Whereas the tissue model may include a free region (thickness d) representing tissue that has been damaged or distorted by the biosensor, followed by normal tissue. **a)** An idealised model where the biosensor is sufficiently long that boundaries at the top and bottom can be ignored and the concentration is only a function of the radius. **b)** An idealised model for the biosensor in calibration. **c)** An *in vitro* model where the tissue has the same depth as the biosensor ($l_b + w$), this is similar to the idealised model, but with the addition of boundary conditions on the top and bottom of the slice. **d)** An *in vivo* model where the insulating plastic sheath is also inserted a distance l_p into the tissue, the biosensor has length $l_b + w$.

or the polymer matrix *i.e.* total concentration (section 2.5.2). The simplest case is an infinitely long biosensor so that the depth in tissue is not included in the model. Additional radial symmetry means the Laplace operator is;

$$\nabla^2 = \frac{d}{dr^2} + \frac{1}{r}\frac{d}{dr} \tag{4.2}$$

Simulations are used (section 4.3) to confirm that there must be continuity of relative concentrations between regions (Eq. 4.3, 4.5) but the flux between regions depends on the total concentrations (Eq. 4.4, 4.6).

$$\frac{A_b(t, r_f)}{\alpha_b} = A_f(t, r_f) \tag{4.3}$$

$$-D_b \frac{\partial A_b}{\partial r}\bigg|_{r=r_f} = -D_f \frac{\partial A_f}{\partial r}\bigg|_{r=r_f} \tag{4.4}$$

$$A_f(t, r_t) = \frac{A_t(t, r_t)}{\alpha_t} \tag{4.5}$$

$$-D_f \frac{\partial A_f}{\partial r}\bigg|_{r=r_t} = -D_t \frac{\partial A_t}{\partial r}\bigg|_{r=r_t} \tag{4.6}$$

Where the radii are; the biosensors core r_b, the start of the free volume $r_f = r_b + w$ and the start of the tissue $r_t = r_f + d$.

For a range of substrate concentrations the MM kinetics can be approximated by a linear rate $v_b = \frac{V_{\max}}{K_m}$. This is a reasonable approximation as biosensors are designed to operate within their linear regime. In tissue and in the absence of the biosensor there is a steady-state concentration of the analyte A^*, where $\mathcal{S} = f(A^*)$. Consider the series expansion of $\mathcal{S} - f(A_t)$ about A^*;

$$\mathcal{S} - f(A_t) = -v_t(A_t - A_t^*) + \mathcal{O}\left((A_t - A^*)^2\right) \tag{4.7}$$

$$v_t = \frac{df(A_t)}{dA_t}\bigg|_{A=A^*} \tag{4.8}$$

Then a linear model for a single enzyme biosensor is given by;

$$\frac{\partial A}{\partial t} = \begin{cases} D_b \nabla^2 A_b - v_b A_b & r_b \le r < r_f \\ D_f \nabla^2 A_f & r_f \le r \le r_t \\ D_t \nabla^2 A_t - v_t(A_t - A^*) & r_t \le r \end{cases} \tag{4.9}$$

For example if clearance in tissue is due to an enzyme described by MM kinetics;

$$f(A_t) = \frac{V_{\max} A_t}{K_m A_t} \tag{4.10}$$

Then both $\mathcal{S}$ and v_t can be determined;

$$\mathcal{S} = \frac{V_{\max} A^*}{A^* + K_m} \tag{4.11}$$

$$v_t = \frac{(\mathcal{S} - V_{\max})^2}{K_m V_{\max}} \tag{4.12}$$

Or the clearance rate can be obtained directly;

$$v_t = \frac{V_{\max} K_m}{(K_m + A^*)^2} \tag{4.13}$$

Where $V_{\max}$ and K_m are the Michaelis-Menten parameters of the enzyme in tissue. The boundary conditions are;

$$\lim_{r \to \infty} A(t, r) = A^* \tag{4.14}$$

$$\left. \frac{dA(t, r)}{dr} \right|_{r = r_b} = 0 \tag{4.15}$$

The electroactive product, typically hydrogen peroxide (H) formed in the polymer matrix of the biosensor is described by the following PDE;

$$\frac{\partial H}{\partial t} = D_h \nabla^2 H + v_b A_b \tag{4.16}$$

Where D_h is the diffusion coefficient of the electroactive product in the polymer matrix. The rate of the electrochemical reaction is governed by the Butler-Volmer model which is dependent on the holding potential, typically the electrochemical reaction is far faster than the enzymatic reaction. This suggests the concentration of the product at the core of the biosensor will be zero. Hydrogen peroxide is toxic, so is rapidly removed in tissue *e.g.* by catalase which does not saturate for physiological concentrations and has activity of $\sim 19,000$U per ml of brain tissue, where U is the enzyme unit, the amount of enzyme required to catalyse 1μmol of per minute. These assumptions give the following boundary conditions;

$$H(t, r_f) = 0 \tag{4.17}$$

$$H(t, r_b) = 0 \tag{4.18}$$

4.2.1.1 Flow injection calibration

In flow injection calibration, where the biosensor is placed in a bath with applied concentration S_0 flowing through it (Figure 4.1b), if there is a sufficiently rapid flow, the system has the following boundary conditions;

$$\frac{1}{\alpha_b} A_b(r_f) = S_0 \tag{4.19}$$

$$\left.\frac{dA(r)}{dr}\right|_{r=r_b} = 0 \tag{4.20}$$

$$H(r_f) = 0 \tag{4.21}$$

$$H(r_b) = 0 \tag{4.22}$$

The analyte at the edge of the polymer matrix will be replaced far faster than it is metabolised (Eq. 4.19) and as before there is no flux of the analyte at the core (Eq. 4.20). The flow in the bath will remove electroactive product produced in the polymer matrix (Eq. 4.21) and a relativly rapid electrochemical reaction will remove the product at the core (Eq. 4.22).

4.2.2 Two-enzyme and three-enzyme cascade model

The inosine biosensor is composed of two layers of enzymes and the adenosine biosensor of three (Llaudet et al. 2003). In both cases the outer most layer holds xanthine oxidase (XO), and the next layer contains purine nucleoside phosphorylase (PNP). The adenosine biosensor has an additional innermost layer of adenosine deaminase (ADA), so adenosine or inosine has to diffuse through the outer layers before being metabolised. As before, a linear approximation of the reactions with rates v_b for XO, v_{b_2} for PNP and v_{b_3} for ADA in the biosensor are used. Together with v_t, v_{t_2} and v_{t_3} in the tissue and the corresponding steady-state concentration of hypoxanthine A^*, inosine A_2^* and adenosine A_3^*. This model can be solved analytically for the idealised biosensor to give steady-state concentration profiles for

adenosine, inosine, hypoxanthine and the electroactive product for both the two-enzyme inosine biosensor (Figure 4.9) and the three-enzyme adenosine biosensor (Figure 4.9). The solution is used to estimate a correction for the calibration.

4.2.3 Quantifying biosensor responses

There are many characteristics used to quantify and compare biosensors (Baronas et al. 2009), here several are considered in order to compare the operation of biosensors in free and tortuous environments. The biosensor signal or current density $I(t)$ [nA/mm^2];

$$I(t, S_0) = n_e F D_h \left. \frac{\partial H(t,r)}{\partial r} \right|_{r=r_b} \tag{4.23}$$

Where n_e is the charge (in number of electrons) of the electroactive product H [μM], n_e is 2 for hydrogen peroxide, with diffusion coefficient (in the polymer matrix) D_h [m^2/s], $F = 96,485$C/mol is Faraday's constant and S_0 [μM] is the bulk substrate concentration. Let $H^*(r)$ be the steady-state concentration of the product, then the steady-state current density is;

$$I^*(S_0) = n_e F D_h \left. \frac{dH^*(r)}{dr} \right|_{r=r_b} \tag{4.24}$$

The response time can be defined as the rise time; the time required for the signal to reach some proportion ξ of the steady-state response.

$$T = \arg\min_t \left\{ \frac{I(t, S_0)}{I^*(S_0)} \geq \xi \right\} \tag{4.25}$$

Biosensors are used to estimate analyte concentrations by calibrating with a known concentration;

$$C = \frac{I^*(S_0)}{S_0} \tag{4.26}$$

Where I^* is the steady-state signal (Eq. 4.24) with applied concentration S_0 and C [nA/μM] is the calibration which does not depend on the applied concentration (S_0) provided it is within the linear regime, *e.g.* S_0 up to 20μM adenosine (Llaudet et al. 2003).

The diffusion modulus;

$$\sigma^2 = \frac{w^2 V_{\max}}{K_M D_b} \tag{4.27}$$

Where w is the thickness of the enzyme layer, can determine if the biosensor's response is primarily controlled by the enzyme kinetics $\sigma^2 \ll 1$, *i.e.* relatively little enzyme is immobilised around the biosensors, so factors that influence the enzyme kinetics will have a substantial effect on the current response. Whereas if $\sigma^2 \gg 1$ then the enzyme's response is diffusion controlled and is subsequently better for determining the substrate concentration (Baronas et al. 2009).

Models of biosensors are typically applied to the case where the biosensor is placed in a well-stirred medium (Schulmeister 1990). The biosensor may operate under an external diffusion limitation, when transport from the bulk to the biosensors is much slower than the diffusion within the enzyme layer. Conversely, the biosensor may operate under an internal diffusion limitation, where transport through the enzyme layer is far slower. In a well stirred medium there will persist a layer around the biosensor where transport is primarily due to diffusion and not convection. The concentration of substrate will asymptotically increase towards the bulk concentration with distance from the biosensor. The Nernst diffusion layer approximation suggests there is a layer of width δ, where transport is solely due to diffusion, so the flux within the layer is constant, for $r \in [r_f, r_f + \delta)$ The width of the diffusion layer will depend on the flow and viscosity of the medium, provided the flow in the bath is sufficiently rapid, the diffusion layer will be relatively small and so will not substantially alter the biosensor signal. The sensor may also be coated in a permeable membrane, providing an additional diffusion layer (Baronas et al. 2014) in order to reduce interference from other substance that could react electrochemically at the core *e.g.* ascorbate. Such permeable membranes could readily be incorporated into the model, but as interference is not considered, their only influence would be to reduce the signal in both the calibration and tissue models as a function of their thickness.

4.3 Simulations

Particle simulations are used to confirm the choice of continuity conditions (Eq. 4.3-4.6). Let the amount (number of particles) divided by the free volume be the relative concentration C_R while the number of particles divided by the total volume is the total concentration C_T (section 2.5.2). These are related by the free volume fraction or porosity α, with $C_T = \alpha C_R$. Two particle simulations are implemented, the first uses an explicitly discretized grid with square or cubic obstructions, so that a particle takes an integer position. At each time step it tries to move in a direction chosen uniformly at random and remains stationary if obstructed. The second represents the particles position with a vector of floating point numbers. In each there is a region with and without square obstacles. Particles move through regions until they reach an inner boundary, at which point they are replaced by another particle at an outer boundary. This continues until a steady state is reached, the concentration of particles is then used to compare possible continuity conditions. It does not represent a real system, but is used to confirm the intuition about the continuity conditions. The simulation does not give a good representation of tissue, as the tortuosity for a given free volume fraction is far lower than tissue. More biologically plausible obstacles such as Voronoi tessellation, does not greatly increase the tortuosity. However the required tortuosity could be obtained by including lakes (Jin et al. 2008) or dead-space (Hrabe et al. 2004) in the ECS.

4.3.1 Spatially discrete simulations

The discrete simulation can be efficiently implemented by repeating a grid of obstacles, the dimensions are determined by the desired length L of the simulation, the spatial step size Δ_X and the diffusion coefficient as follows;

$$\Delta_X = \frac{2MN}{L} \tag{4.28}$$

$$\Delta_T = 2dD\Delta_X^2 \tag{4.29}$$

Where M is the number of times the $N \times N$ grid is repeated and d is the number of spatial dimensions and D is the diffusion coefficient.

$$D = \lim_{t\to\infty} \frac{1}{2dt} \left\langle (\mathbf{x}(0) - \mathbf{x}(t))^2 \right\rangle \tag{4.30}$$

Where $\mathbf{x}(t)$ is the position of the particle at time step t. The mean squared displacement scales with the number of time steps, so setting the time step (Eq. 4.29), gives the required diffusion coefficient. Alternatively, the mean squared displacement can be used to estimate the tortuosity θ that results from the obstacles.

Here a 2D simulation of three concentric circles is used to confirm the continuity conditions. The largest of radius R is where particles are added to the simulation and cannot move beyond it. Within it are two smaller circles radius r_t and r_b, between r_t and R there are square obstacles creating a tortuous environment. Alternative shaped obstacles or Voronoi tessellation does not greatly alter the relationship between porosity and tortuosity (Tao and Nicholson 2004) and would not effect the continuity conditions. In the simulation between r_b and r_t there is free space (Figure 4.2a). If a particle reaches the inner circle r_b it is removed and a new particle is added at a random point on the outer edge (radius R). In the steady-state the flux at r_b will equal the flux at r_t (Eq. 4.31). The simulation can be used to confirm that the concentration of particles (A), must be the relative concentration in the continuity conditions (Figure 4.2b) and the total concentration for the continuity of the flux (Figure 4.2c), where the steady-state gradient of the total concentration at r_b is approximately equal to the gradient at r_f scaled by the tortuosity.

$$D \left.\frac{dA}{dr}\right|_{r=r_b} = \frac{D}{\theta^2} \left.\frac{dA}{dr}\right|_{r=r_t} \tag{4.31}$$

4.3.2 Spatially continuous simulations

With the spatially continuous simulations time step Δ_T must be sufficiently small so as to approximate the underlying continuous process. It is shown that $\Delta_T = \frac{1}{1024}$ provides a good approximation (Figure 4.3).

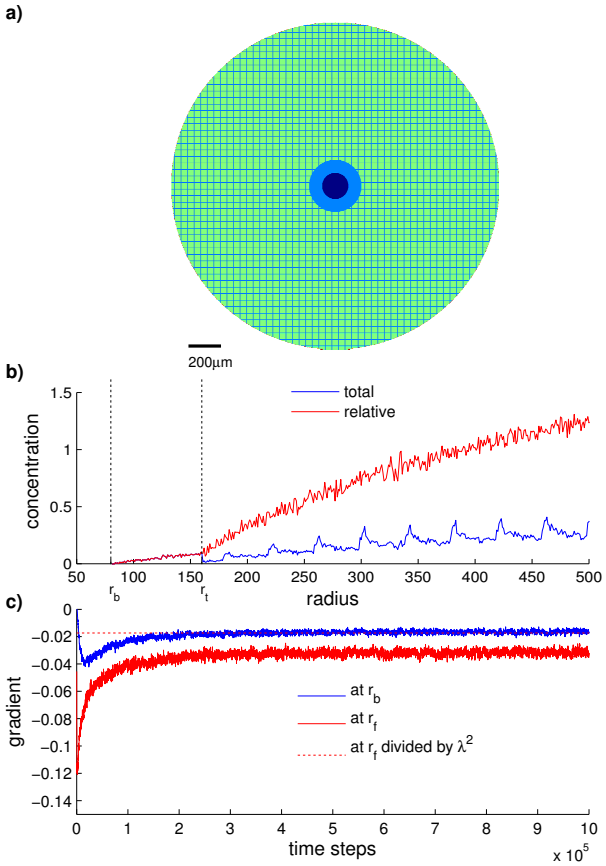

Figure 4.2: **The discrete particle simulation confirms choice of continuity conditions between regions. a)** The 2D grid consists of a circle with square 4×4 obstacles (green) with free space between them (blue) and a region without objects (radius 160). An ensemble of 50 particles are simulated, when a particle reaches the centre radius 80, (dark blue) it is removed and a new particle is added on the edge. **b)** The relative and total concentration as a function of the radius in the steady-state (after 1 million time steps), dashed lines show the start of the outer/tortuous region and the inner edge of the simulation. The pulses in the total concentration results from a greater number of particles at the radii that include more space between objects, this is why they are eliminated in the relative concentration. They could also be removed with a coarser averaging. **c)** Using the total concentration (averaged over a radius of 20), the gradient at both the inner boundary (r_b) and the outer boundary (r_t) are shown. The steady-state gradient at the r_f in the final 1,000 time steps, divided by the estimated tortuosity $\theta = 1.35$ (calculated from the MSD), is approximately equal to the steady-state of the gradient at r_b, confirming the use of total concentration for the flux.

As with the spatially discrete simulation, the continuous simulation can be used to confirm the choice of total concentrations for the continuity of fluxes and relative concentration for the continuity of concentrations (Eq. 4.3)-(Eq.

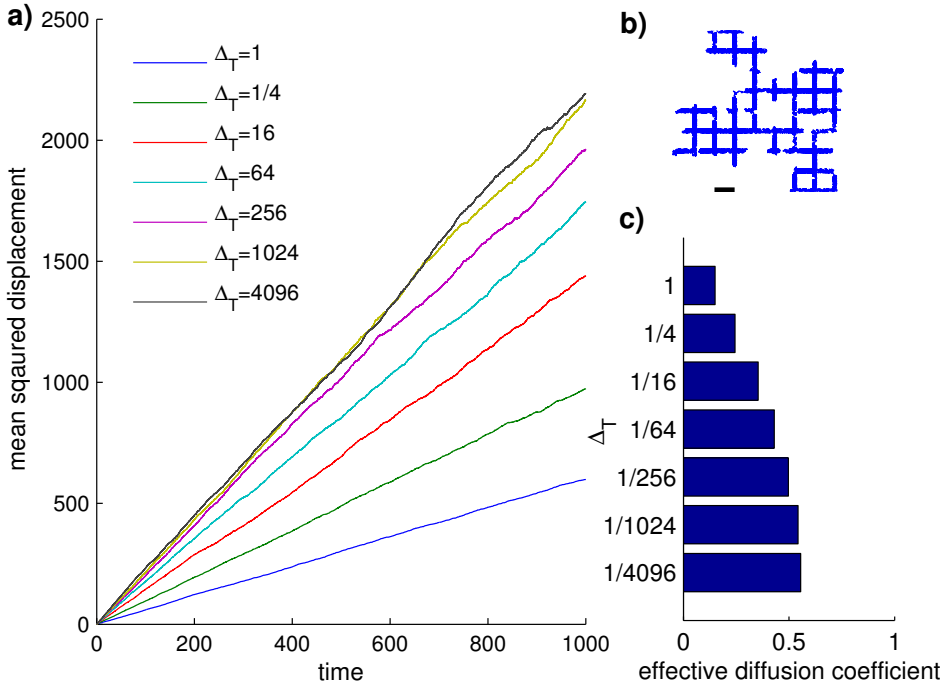

Figure 4.3: **A time step of $\Delta_T = \frac{1}{1024}$ is sufficient to approximate the underlying continous process. a)** Smaller time steps increase the MSD because the distance lost due to collisions is reduced. Each time step shows the average over an ensemble to 3,000 particles moving in a 2D grid with square obstacles. **b)** An example path with $\Delta_T = \frac{1}{1024}$ (scale bar 5 units) **c)** The gradient of the mean square displacement provides an estimate for the effective diffusion coefficient 0.55, extrapolation suggests this will tend to 0.56 as $\Delta_T \to 0$, both give an estimated tortuosity of $\theta = 1.34$

4.6). The simulation uses square objects in a square grid, with free space of length L at the leftmost edge. The concentration is defined by the number of particles at a given distance along the x-axis, divided by either the total space (total concentration) or the free space (relative concentration). As before, in the steady-state the flux into the free region should equal the flux out of it;

$$D\frac{dA}{dx}\bigg|_{x=0} = \frac{D}{\theta^2}\nabla\frac{dA}{dx}\bigg|_{x=L} \tag{4.32}$$

A particle simulation with a 50×50 grid (the length and time scale are arbitrary, such that the free diffusion coefficient $D = 1$), with a free region extending to $L = 10$, followed by a tortuous region with volume fraction

$\alpha = \frac{9}{25}$ and tortuosity$\theta = 1.34$ (calculated from the MSD). Particles are allowed to diffuse through the tortuous region, replacing them when they reach $x = 0$ with a new particle at $x = 50$, until a steady-state is reached. It becomes clear that the condition on the flux (Eq. 4.32) is satisfied by the total and not the relative concentration (Figure 4.4). With the two fluxes in (Eq. 4.32) differing by only ∼1% after 50,000 time steps.

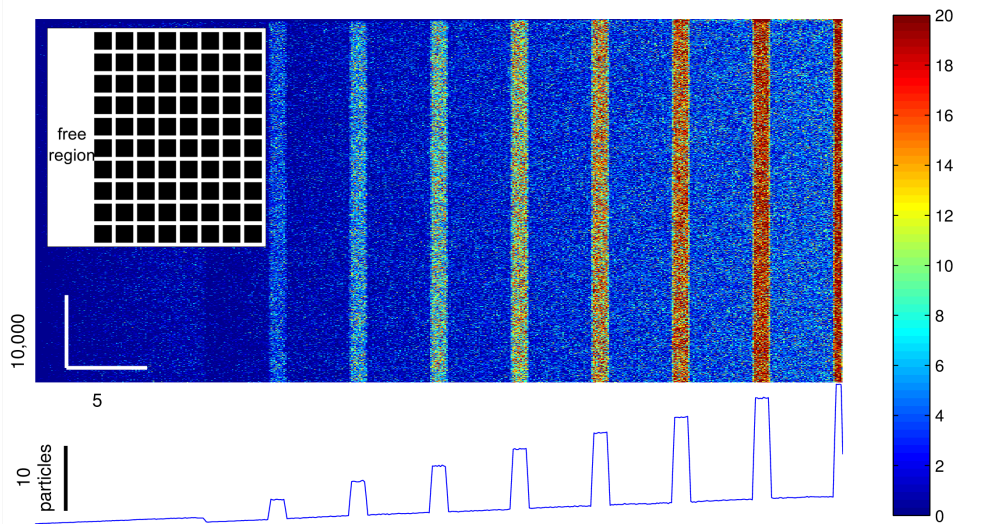

Figure 4.4: **Continuity conditions should be applied to the flux of the total concentration.** An ensemble of $1,700$ particles diffuse in a 2D (50×50) field with a free region extending from $x = 0$ to 10, followed by a region with square (4×4) obstacles (Inset; a schematic of the domain). A particle starts at $x = 50$ and when it passes $x = 0$ it is removed and a new particles is added at $x = 50$. The concentration as a function of the distance along the x-axis (number of particles within a $\frac{1}{10}$ region at a given time step), is shown as a heat map with the initial distribution of particles at the top and the final distribution at the bottom. Below this map are the number of particles as a function of distance along the x-axis, averaged over the final 5,000 time steps, which is proportional to the total concentration. The peaks in the number of particles correspond to vertical gaps between the square obstacles. In this steady-state the gradient of the total concentration at $x = 0$ (-8.2×10^{-4}) and at the start of the tortuous region $x = 10$ (-8.3×10^{-4}) (scaled by the tortuosity $\theta = 1.34$ from MSD) differ by ∼1%. This confirms that continuity conditions of the flux between regions (Eq. 4.32) must be given in terms of total concentrations.

4.4 Parameter estimation

The parameters that describe the biosensor are the radius of the core r_b, the thickness of the enzyme layer w, the tortuosity of the polymer matrix

μ, (used to determine the diffusion coefficients) and the free volume fraction of the enzyme layer α_b. However, an extensive literature review found these values are seldom specified in publications (Table A.1). The free volume fraction in the polypyrrole matrix is difficult to determine, as it is known to depend on deposition conditions, doping agents, inert additives and thickness, with the initial ($<$ 100nm) thickness governed by nuclei growth, whereas later layers follow a 1D transversal growth (Garcia-Belmonte 2003). A comparison of the free volume of polypyrrole with different dopant-ions measured with nitrogen gas (Hallik et al. 2007) has volume fractions between 0.26 and 0.56, but nitrogen is much smaller (14g/mol) than either hydrogen peroxide (34g/mol) or hypoxanthine (136g/mol) so this may overestimate the relevant free volume. Given the diffusion coefficient in the polymer matrix is equal to the free diffusion (Sarissa Biomedical Ltd.). The free volume fraction was estimated as 0.15 from the steady-state calibration response of the hypoxanthine biosensor 2.60 ± 0.28nA ($\pm$ standard error, $n = 4$) with 10μM hypoxanthine applied (Table 4.1).

Parameter	Value		Description
r_b	25	(μm)	Radius of the biosensor core (Llaudet et al. 2003)
w	20	(μm)	Thickness of the enzyme layer (Sarissa Biomedical Ltd.)
d	5	(μm)	Thickness of the damaged layer
v_b	178	(1/s)	Enzyme reaction rate
v_t	43×10^{-3}	(1/s)	Clearance rate of the analyte about the steady-state tissue concentration
D_b	800	(μm^2/s)	Diffusion coefficient of the analyte in the polymer matrix
D_f	800	(μm^2/s)	Diffusion coefficient of the analyte in the free region
D_t	425	(μm^2/s)	Diffusion coefficient of the analyte in tissue
D_h	1700	(μm^2/s)	Diffusion coefficient of hydrogen peroxide in the polymer matrix (van Stroe-Biezen et al. 1993)
α_t	0.21		Free volume fraction of the extracellular space (Rice and Nicholson 1991)
α_b	0.15		Volume fraction of the polymer matrix
A^*	0.75	(μM)	Steady-state concentration of the analyte (Walter et al. 1988)
w_2	20	(μm)	Thickness of the first enzyme layer
v_{b_2}	4.8	(1/s)	Second layer enzyme reaction rate
D_{b_2}	610	(μm^2/s)	Diffusion coefficient of the second analyte in the polymer matrix
D_{f_2}	610	(μm^2/s)	Diffusion coefficient of the second analyte in the free region
D_{t_2}	235	(μm^2/s)	Diffusion coefficient of the second analyte in tissue
A_2^*	0.51	(μM)	Steady-state concentration of the second analyte (Walter et al. 1988)
v_{t_2}	1.14×10^{-3}	(1/s)	Clearance rate of the second analyte about the steady-state tissue concentration
w_3	20	(μm)	Thickness of the third enzyme layer
v_{b_3}	7.0	(1/s)	Third layer enzyme reaction rate
D_{b_3}	610	(μm^2/s)	Diffusion coefficient of the third analyte in the polymer matrix
D_{f_3}	610	(μm^2/s)	Diffusion coefficient of the third analyte in the free region
D_{t_3}	235	(μm^2/s)	Diffusion coefficient of the third analyte in tissue
A_3^*	73.5	(nM)	Steady-state concentration of the third analyte (Walter et al. 1988)
v_{t_3}	17.6×10^{-3}	(1/s)	Clearance rate of the third analyte about the steady-state tissue concentration

Table 4.1: **Parameters of the biosensor models.**

In constructing the hypoxanthine biosensor 10μl containing the pyrrole monomer and $5U$ xanthine oxidase (XO) (Llaudet et al. 2003), the percentage of immobilized enzyme is not estimated although it is suggested that it may be far greater than the 8% (Coche-Guerente et al. 1995) obtained using a similar technique. Then assuming the enzyme is uniformly distributed the activity 5U in 10μl suggests a velocity of 8.34mM/s in the 10μl volume. If only 8% is entrapped the rate for the volume of the enzyme matrix is 0.67mM/s at 25°C. At 32°C the maximum velocity is 71% higher (Mondal and Mitra 1994), suggesting a velocity of 1.14mM/s, together with K_m of 6.41 (Mondal and Mitra 1994), this provides an estimated removal rate of $v_b = 178$/s. Two reactions occur in the hypoxanthine biosensor; hypoxanthine $\rightarrow$ xanthine + H_2O_2 and xanthine $\rightarrow$ urate $+H_2O_2$. Both reactions are catalysed by XO, for simplicity they are modelled as a single reaction, where the analyte (hypoxanthine) produces twice as much of the electroactive product (hydrogen peroxide).

In homogenate of the rat cerebrum and cerebellum, xanthine oxidase activity was found to be 19.5mU/g of tissue at 30°C (Hashimoto 1974). Assuming hypoxanthine clearance is due to xanthine oxidase and this activity is uniformly distributed in the brain, gives an average clearance velocity of 0.31μM/s. Using this value for the maximum clearance together with the K_m of 6.41 (Coche-Guerente et al. 1995), suggests a source rate $\mathcal{S}$ of 24nM/s (Eq. 4.11) and a clearance rate v_t of 43×10^{-3}/s (Eq. 4.12).

In whole rat brain homogenate XO activity was 2.26 nmol/mg protein/hour at 37°C (Betz 1985). Assuming 10mg of tissue produces 1mg of protein suggests an average velocity 0.60μM/s. PNP activity has been found in the CSF but the kinetics have not been determined for inosine but for a 2-amino-6-mercapto-7-methylpurine ribonucleoside (MESG), (Silva et al. 2004). The kinetics are $V_{\max} = 10.2 \pm 0.6$U/g which is approximately 0.17μM/s and $K_m = 142.5 \pm 29.5\mu$M which gives a clearance rate of v_{t_2} of 1.1×10^{-3}/s (Eq. 4.13).

The adenosine biosensor used 1U of ADA in 10μl entrapped in polypyrrole, which suggests a velocity of 1.67mM/s in the 10μl volume. Assuming only 8% is entrapped, gives a velocity of 133μM/s at 25°C. Using the Q_{10} of

ADA 3.74, gives a velocity of 649.8μM/s. ADA from the bovine spleen, has a $K_m = 93 \pm 2.1\mu$M (Sharoyan et al. 2006), which gives a removal rate of $v_{b_3} = 6.99$/s.

4.4.1 Reliability of response

The estimation of parameters from the biosensor calibration responses, and in particular the rise times, were considered. However the peak response of the sensors varies considerably, (Figure 4.5) and the same sensor can show both a decline (*e.g.* calibrations 4-5) or increase (*e.g.* calibration 1-3) in responsiveness after successive experiments. This may be due to a reduction in the thickness of the enzyme layer with use. The rise times (Eq. 4.25) and fall times vary considerably between calibrations (Figure 4.6), which is more likely to reflect nonlinear flow in the bath than characteristics of the sensors, and means that rise time data is unlikely to be useful in determining the sensor parameters. (Data provided by Marianne Cobham, M. J. Wall lab, School of Life Sciences, University of Warwick).

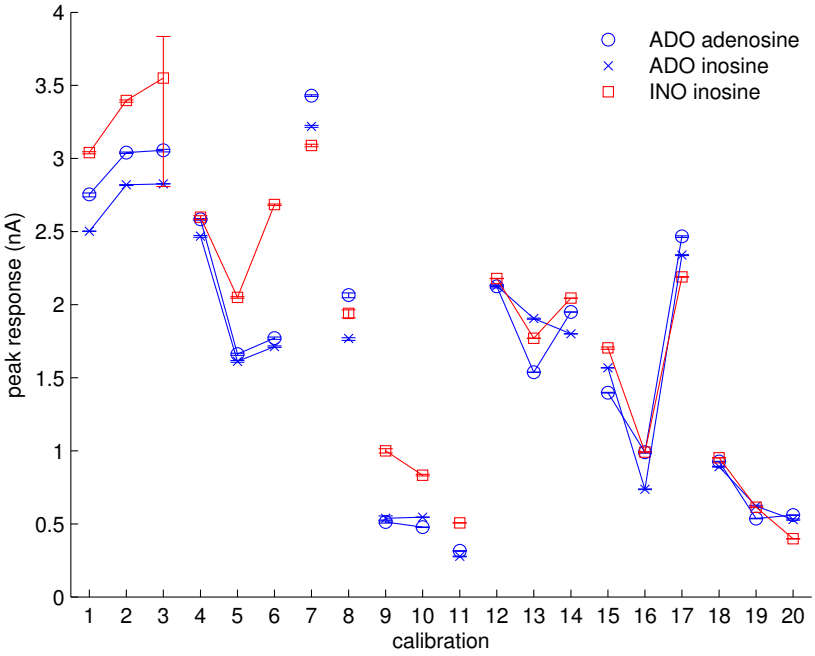

Figure 4.5: **Peak adenosine biosensor response during calibration.** The peak response is the average over a 1s window, with error bars showing the maximum and minimum response within the window. Lines join successive calibrations performed with the same biosensors before and after it is used in tissue. The peak calibration responses are quite variable, even for the same biosensor, which limits the extent calibration data could be used to infer the parameters. Data provided by Marianne Cobham, M. J. Wall lab, School of Life Sciences, University of Warwick

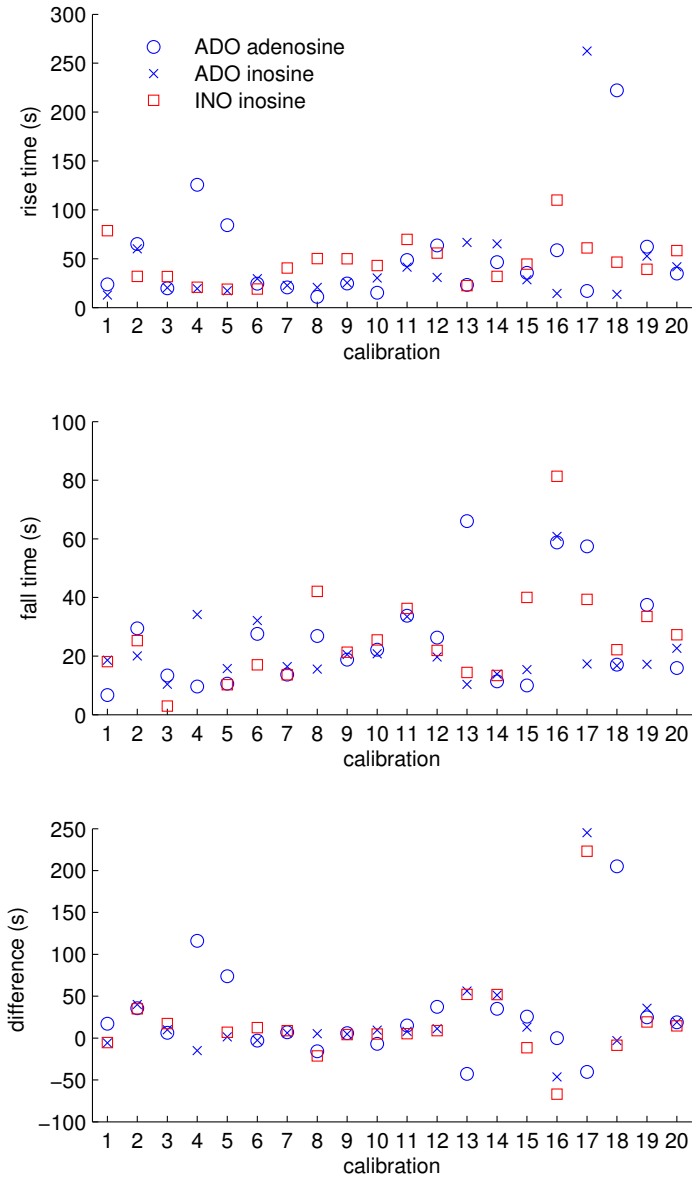

Figure 4.6: **Time required for adenosine biosensors to reach peak response and to return to baseline during calibration.** The rise time is the duration between 10% and 90% of the peak response, conversely the fall time is the duration of 90% to 10%. The three layer adenosine biosensor (ADO) is calibrated with either adenosine or inosine, while the two-layer inosine biosensor (INO) is calibrated with inosine. The variability in **a)** the rise time and **b)** fall time may be the result of nonlinear flow in the bath and it suggests that calibration data can not be used to reliably infer the biosensor parameters. The difference (rise time - fall time) shows the rise time tends to be greater than the fall time. Data provided by Marianne Cobham, M. J. Wall lab, School of Life Sciences, University of Warwick

4.5 Model response and calibration multiplier

The dynamics of the tissue and calibration models are determined by the PDE (Eq. B.165), this is solved numerically (code C.2). There is a rapid rise time in calibration reaching 95% of the steady-state response within 0.1s. The tissue models overshoot the steady-state response, as the biosensor metabolises all the nearby analyte, after which there is a slow decay to the steady-state response, reaching 105% within $20s$ (Figure 4.7). The addition of a free region diminishes the initial peak and increases the time required to reach the steady-state response, this is because the analyte generated in the tissue has to diffuse further to be detected.

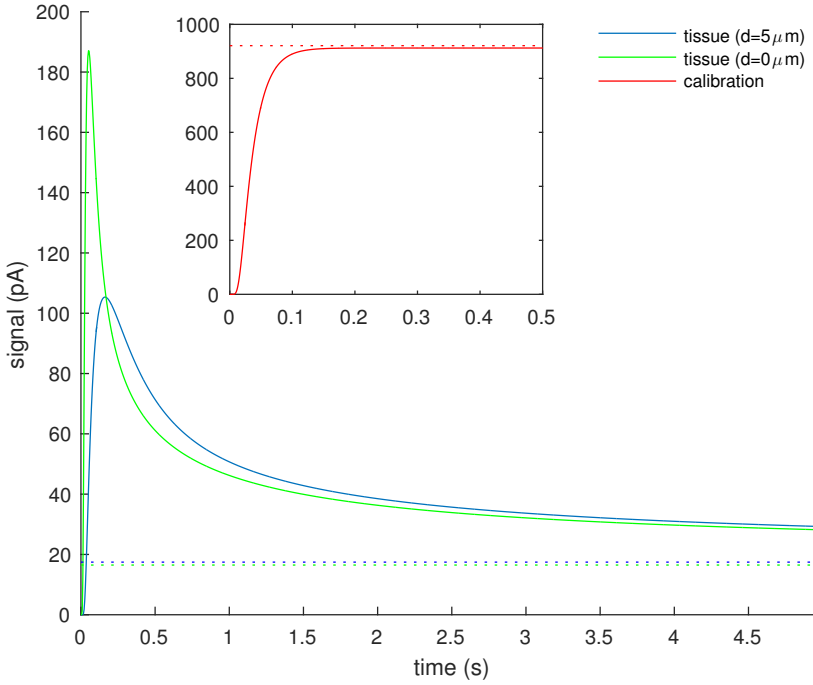

Figure 4.7: **The response of the tissue model is both quantitatively and qualitatively different from calibration.** The dotted lines show the steady-state response and the inset shows the calibration model. The signal for the calibration model rapidly reaches the steady-state response. Whereas the tissue models with ($d = 5\mu$m) and without ($d = 0\mu$m) a free region have an initial peak as the biosensor reacts with all the available analyte. The tissue response then slowly decays towards the steady-state, as the analyte has to diffuse further to reach the biosensor.

Biosensors connect currents to concentration by calibrating with a known concentration (Eq. 4.26). Biosensors are typically calibrated in a free-flow environment, however the models show this will produce a substantially larger signal than would be observed in tissue for the same analyte concentration (Figure 4.8b). Let the calibration multiplier be;

$$m = \frac{I_t^*\left(A^*\right)}{I_c^*\left(\frac{A^*}{\alpha_t}\right)} \tag{4.33}$$

Where I_t^* is the steady-state signal (Eq. 4.24) of the tissue model (Figure 4.1a) and I_c^* the steady-state signal of the calibration model (Figure 4.1b), for the same relative concentration *i.e.* A^* in tissue and $\frac{A^*}{\alpha_t}$ in the free-flow environment. The relative concentration is used as it is more relevant than the total concentration for quantifying chemical signals and ensures $m \in [0, 1]$. As the models are both linear A^* factors out, so a similar multiplier matched for the total concentrations $\frac{I_t^*\left(A^*\right)}{I_c^*\left(A^*\right)}$ is obtained by multiplying m by $\alpha_t \approx \frac{1}{5}$.

The calibration multiplier is the amount by which the free-flow steady-state current should be multiplied to provide an estimate of the calibration signal for the tissue environment;

$$\hat{C} = \frac{mI^*\left(S_0\right)}{S_0} \tag{4.34}$$

Where $\hat{C}$ [nA/μM] is the calibration corrected for differences in the free-flow and tissue environment. The inverse of the calibration multiplier ($\frac{1}{m}$) is the proportion of tissue concentration that would be underestimated using conventional calibration (Eq. 4.26).

Idealised biosensors with two or three-enzyme layers are considered and analytic solutions were obtained for the steady-state concentration profiles and responses. The calibration multiplier for the two-enzyme biosensor depends on both the second analyte and the analyte concentration (Eq. 4.35). Similarly the calibration multiplier for the three-enzyme biosensor depends on all three analyte concentrations (Eq. 4.36). The calibration multiplier is 0.05 for the two-enzyme biosensor and 0.03 for three-enzyme sensor, (pa-

rameter values from Table 4.1). Typically biosensors that are sensitive to multiple analytes are calibrated to each separately, in which case different calibration multipliers are estimated for each analyte. However the amalgamated multiplier estimated here is sufficient to demonstrate the need for such a correction and for comparison between one, two and three-enzyme biosensors.

$$m^b = \frac{I_t^*\left(A^*, A_2^*\right)}{I_c^*\left(\frac{A^*}{\alpha_t}, \frac{A_2^*}{\alpha_t}\right)} \tag{4.35}$$

$$m^c = \frac{I_t^*\left(A^*, A_2^*, A_3^*\right)}{I_c^*\left(\frac{A^*}{\alpha_t}, \frac{A_2^*}{\alpha_t}, \frac{A_3^*}{\alpha_t}\right)} \tag{4.36}$$

Where m^b is the calibration multiplier of the two-enzyme biosensor with steady-state tissue concentration of the first analyte A^* *e.g.* hypoxanthine and the second analyte A_2^* *e.g.* inosine. Similarly the calibration multiplier for the three-enzyme biosensor m^c also depends on the concentration of the third analyte A_3^* *e.g.* adenosine.

Calibration multipliers can be obtained for each analyte separately. Let C be the calibration of the single-enzyme biosensor as before and C_1 and C_2 are the calibration for the first and second analyte of the two-enzyme biosensor;

$$C_1^{(2)} = \frac{I^*\left(S_0, 0\right)}{S_0} \tag{4.37}$$

$$C_2^{(2)} = \frac{I^*\left(0, S_0^b\right)}{S_0^b} \tag{4.38}$$

These are obtained experimentally by placing the biosensor in a free-flow environment and applying S_0 of the first analyte (Eq. 4.37) or S_0^b of the second analyte (Eq. 4.38). Then in an experiment the concentration of the second analyte would be estimated as;

$$A_2 = \frac{1}{C_2^{(2)}}\left(I_2^* - I_1^*\frac{C_1^{(2)}}{C}\right) \tag{4.39}$$

Where I_2^* the steady-state current of the two-enzyme biosensor and I^* the response of the corresponding single-enzyme biosensor. Subtraction is nec-

essary as the two-enzyme biosensor is sensitive to both analytes. To account for the difference between the free-flow calibration environment and the tortuous tissue environment two calibration multipliers are required;

$$m_1^b = \frac{I_t^*\left(A^*, 0\right)}{I_c^*\left(\frac{A^*}{\alpha_t}, 0\right)} \tag{4.40}$$

$$m_2^b = \frac{I_t^*\left(0, A_2^*\right)}{I_c^*\left(0, \frac{A_2^*}{\alpha_t}\right)} \tag{4.41}$$

Whereas (Eq. 4.40-4.41) are obtained from the models of the biosensor in tissue and the calibration environments. Then a better estimate of the concentration of the second analyte can be obtained by subtraction;

$$A_2 = \frac{1}{m_2^b C_2^{(2)}}\left(I_2^* - I_1^* \frac{m_1^b C_1^{(2)}}{mC}\right) \tag{4.42}$$

Similarly for the three-enzyme adenosine biosensor;

$$C_1^{(3)} = \frac{I^*\left(S_0, 0, 0\right)}{S_0} \tag{4.43}$$

$$C_2^{(3)} = \frac{I^*\left(0, S_0^b, 0\right)}{S_0^b} \tag{4.44}$$

$$C_2^{(3)} = \frac{I^*\left(0, 0, S_0^c\right)}{S_0^c} \tag{4.45}$$

Where S_0 is the applied concentration of the first analyte (Eq. 4.37) , S_0^b of the second analyte (Eq. 4.38) and S_0^c of the third analyte. Then in an experiment the concentration of the third analyte would be estimated as;

$$A_3 = \frac{1}{C_3^{(3)}}\left(I_3^* - \frac{C_2^{(3)}}{C_2^{(2)}}\left(I_2^* - I_1^* \frac{C_1^{(2)}}{C}\right) - \frac{C_3^{(3)}}{C} I_1^*\right) \tag{4.46}$$

Where I_3^* the steady-state current of the three-enzyme biosensor, I_2^* the response of the corresponding two-enzyme biosensor and I^* the response of the single-enzyme biosensor. Their calibration multipliers are required to

account for the difference between the free-flow and tissue environments;

$$m_1^c = \frac{I_t^*\left(A^*, 0, 0\right)}{I_c^*\left(\frac{A^*}{\alpha_t}, 0, 0\right)} \tag{4.47}$$

$$m_2^c = \frac{I_t^*\left(0, A_2^*, 0\right)}{I_c^*\left(0, \frac{A_2^*}{\alpha_t}, 0\right)} \tag{4.48}$$

$$m_3^c = \frac{I_t^*\left(0, 0, A_3^*\right)}{I_c^*\left(0, 0, \frac{A_3^*}{\alpha_t}\right)} \tag{4.49}$$

The multipliers are obtained from the models of the three-enzyme biosensor in tissue (I_t^*) and the calibration (I_c^*) environments. An improved estimated of the concentration of the third analyte is;

$$A_3 = \frac{1}{m_3^c C_3^{(3)}}\left(I_3^* - \frac{m_2^c C_2^{(3)}}{m_2^b C_2^{(2)}}\left(I_2^* - I_1^* \frac{m_1^b C_1^{(2)}}{mC}\right) - \frac{m_1^c C_1^{(3)}}{mC} I_1^*\right) \tag{4.50}$$

Where I_3^* is the steady-state response of the three-enzyme biosensor, I_2^* the two-enzyme biosensor and I_1^* the single-enzyme biosensor. The multipliers for a model of a three-enzyme adenosine biosensor (with the parameters in Table 4.1) are given in Table 4.2.

The calibration multipliers determined for models of a single, two and three layer biosensor are very small, suggesting the tissue concentration obtained using conventional calibration would underestimate the analyte concentration by up to $\sim$40 fold. The multiplier is determined by the model parameters (Table 4.1), so this may be exaggerated, but does emphasise the necessity of accounting for the tortuous environment in which biosensors are used.

Biosensor	hypoxanthine	inosine	adenosine	combined
single-enzyme	0.024	-	-	0.024
two-enzyme	0.021	0.148	-	0.046
three-enzyme	0.019	0.056	0.120	0.028

Table 4.2: **Calibration multipliers for each biosensor model.** Either the combined calibration multiplier (Eqs, 4.33, 4.35 and 4.36), or the calibration multiplier when the biosensor is exposed to the first analyte (hypoxanthine), second analyte (inosine) or third analyte (adenosine) separately.

4.5.1 Steady-state solutions

The steady-state solutions in cylindrical coordinates (section B.9) are given in terms of modified Bessel functions;

$$M_0(r) = I_0(\kappa r) + \gamma K_0(\kappa r) \tag{4.51}$$

$$M_1(r) = I_1(\kappa r) - \gamma K_1(\kappa r) \tag{4.52}$$

$$\gamma = \frac{I_1(\kappa r_b)}{K_1(\kappa r_b)} \tag{4.53}$$

$$\kappa = \sqrt{\frac{v_b}{D_b}} \tag{4.54}$$

Where $\sigma = \kappa w$ is the root of the diffusion module (Eq. 4.27), a dimensionless characteristic of the biosensor. The parameters suggest $\sigma = 9.4$, as $\sigma^2 \gg 1$ the response of the biosensor is controlled by diffusion not the enzyme kinetics, allowing the biosensor to accurately measure the analyte concentration. For calibration the steady-state solution is;

$$A_b(r) = B_b M_0(r) \tag{4.55}$$

$$B_b = \frac{\alpha_b}{M_0(r_f)} \tag{4.56}$$

In the case where there is no tissue damage, *i.e.* $r_f = r_t$, the steady-state

solution is;

$$A(r) = \begin{cases} B_b M_0(r) & r_b \leq r < r_t \\ A^* + B_t K_0(cr) & r_t \leq r \end{cases} \tag{4.57}$$

$$c = \sqrt{\frac{v_t}{D_t}} \tag{4.58}$$

$$B_b = \frac{A^*}{\alpha_t}\left[\frac{M_1(r_t)}{\alpha_b} + \frac{D_b}{D_t}\frac{\kappa M_1(r_t) K_0(cr_t)}{\alpha_t c K_1(cr_t)}\right]^{-1} \tag{4.59}$$

$$B_t = -B_b \frac{D_b}{D_t}\frac{\kappa M_1(r_t)}{cK_1(cr_t)} \tag{4.60}$$

Finally the addition of a free diffusion layer around the biosensor has the following steady-state solution;

$$A(r) = \begin{cases} B_b M_0(r) & r_b \leq r < r_f \\ \dfrac{A^*}{\alpha_t} + \dfrac{B_t}{\alpha_t}\left(K_0(cr_t) - a\log\left(\dfrac{r}{r_t}\right)\right) & r_f \leq r < r_t \\ A^* + B_t K_0(cr) & r_t \leq r \end{cases} \tag{4.61}$$

$$B_t = -B_b \frac{D_b}{D_t}\frac{r_f \kappa M_1(r_f)}{r_t c K_1(cr_t)} \tag{4.62}$$

$$\begin{aligned} B_b = \frac{A*}{\alpha_t}\Bigg[&\frac{M_0(r_f)}{\alpha_b} - \frac{D_f}{D_b}(r_f \kappa M_1(r_f)) \\ &\times\left(\log\left(\frac{r_f}{r_t}\right) - \frac{D_f}{D_t}\frac{K_0(cr_t)}{\alpha_t r_t c K_1(cr_t)}\right)\Bigg]^{-1} \end{aligned} \tag{4.63}$$

$$a = \frac{D_t}{D_f} r_t c K_1(cr_t) \tag{4.64}$$

In each case;

$$\begin{aligned} H(r) = 2B_b \frac{D_b}{D_h}\Bigg[&\left(M_0(r_f) - M_0(r_b)\right)\frac{\log\left(\frac{r}{r_b}\right)}{\log\left(\frac{r_f}{r_b}\right)} \\ &+ M_0(r_b) - M_0(r)\Bigg] \end{aligned} \tag{4.65}$$

Where B_b is given be (Eq. 4.56) for calibration and (Eq. 4.59) for the tissue model without damage and (Eq. 4.63) for the tissue model with, and free region around the biosensor.

Analytic solutions to the two and three-enzyme sensor have been obtained

and have a similar form to (Eq. 4.65). The steady-state concentration (Figure 4.8) shows the limited influence an additional free region has for the single enzyme model. The influence of the biosensor is also relatively limited, reaching 95% of the unperturbed tissue concentration (A^*) within 250μm. The calibration multiplier for the single enzyme biosensor is 0.02, which implies that the concentration found in tissue through using conventional calibration should be ∼40 fold greater.

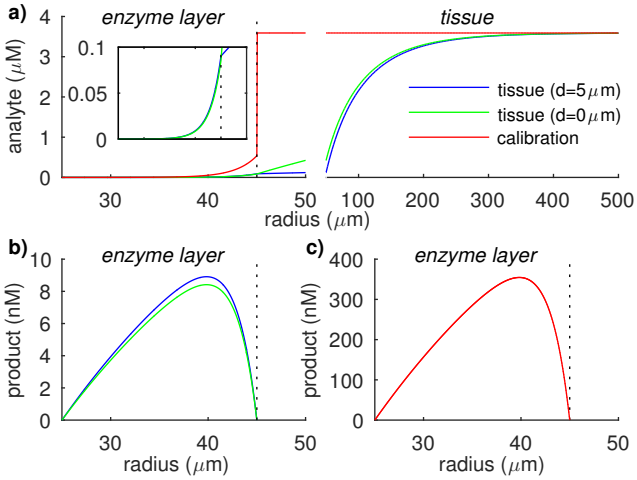

Figure 4.8: **The relative concentrations of both the analyte and product within the enzyme layer ($25-45\mu$m) are far greater in the free-flow environment than in tissue, where the applied concentration in the free-flow environment is the relative steady-state tissue concentration $\frac{A^*}{\alpha_t}$.** The rapid metabolism in the enzyme later (rate v_b) substantially diminishes the concentration in the surrounding tissue. **a)** The analyte in the polymer matrix ($25-45\mu$m) is vastly greater for the calibration model (Eq. 4.55) than either tissue model with (Eq. 4.61) or without (Eq. 4.57) a free region around the biosensor caused by tissue damage. The inset shows that the additional free region has little effect and both tissue models result in a very low concentration in the enzyme layer. The concentration in tissue approaches the steady-state concentration in the absence of the biosensor ($\frac{A^*}{\alpha_t}$) within a relatively short distance determined by the rate of activity in tissue v_t. **b)** The electroactive product is also substantially greater during calibration, the inset shows the concentration for the two tissue models is ∼25 fold lower than calibration. This plot show the relative concentrations, so they are continuous between regions. Parameter values from Table 4.1.

The concentration profile of analyte for an idealised two-enzyme biosensor is similar to (Figure 4.8a), but with contribution from both tissue on the right and the reaction of the second analyte on the left. The second reaction rate in the biosensor (v_{b_2}) is far slower than the first (v_b), subsequently the second

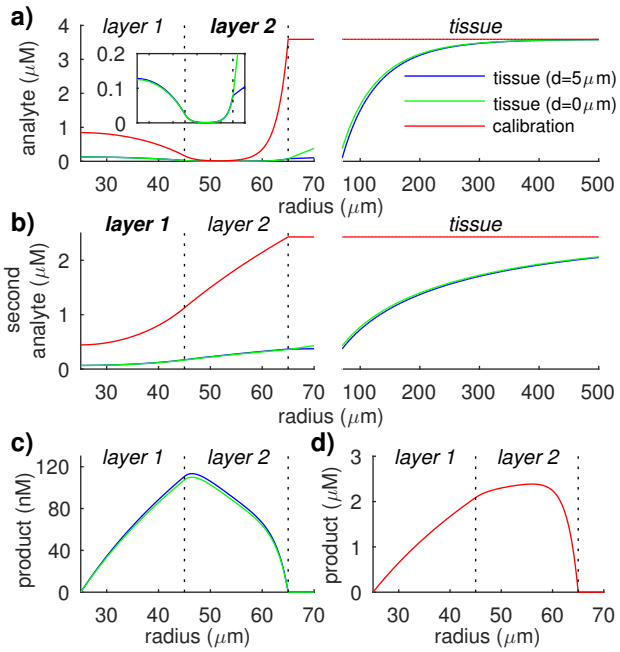

Figure 4.9: **The steady-state tissue concentrations around the biosensor is greatly reduced, resulting in far less electroactive product than the free-flow environment, where the applied concentration is the relative steady-state tissue concentration $\frac{A^*}{\alpha_t}$.** The two-layer biosensor has a region of the enzyme layer ($25-45\mu$m layer 1) that reacts with the second analyte (inosine) and a region ($45-65\mu$m layer 2) that reacts with the analyte (hypoxanthine). **a)** the analyte concentration. **b)** The second analyte (inosine) **c)** The electroactive product is the result of the reaction in layer 3, it either diffuses though layer 1 to be detected at the biosensor or diffuses into tissue and is destroyed. **d)** The concentration of electroactive product for a model of the free-flow environment. This plot show the relative concentrations, so they are continuous between regions. Parameter values from Table 4.1.

analyte penetrates the enzyme layer and the concentration in tissue is not as dramatically reduced. However the biosensor effects a larger region due to the slower reaction rate in tissue v_{t_2} (Figure 4.9b). As with the single-enzyme biosensor a free-flow environment with the same relative concentrations as tissue (far from the biosensor) results in far more electroactive product in the steady-state.

The concentration profile of the analyte in the three-layer biosensor (Figure 4.10), in layer 1 is almost half that of the two-layer biosensor (Figure 4.9a), because it has a larger region to fill (layers 1 and 2). The second analyte and has a much greater concentration ($\sim$3 fold) than in the two-layer biosensor

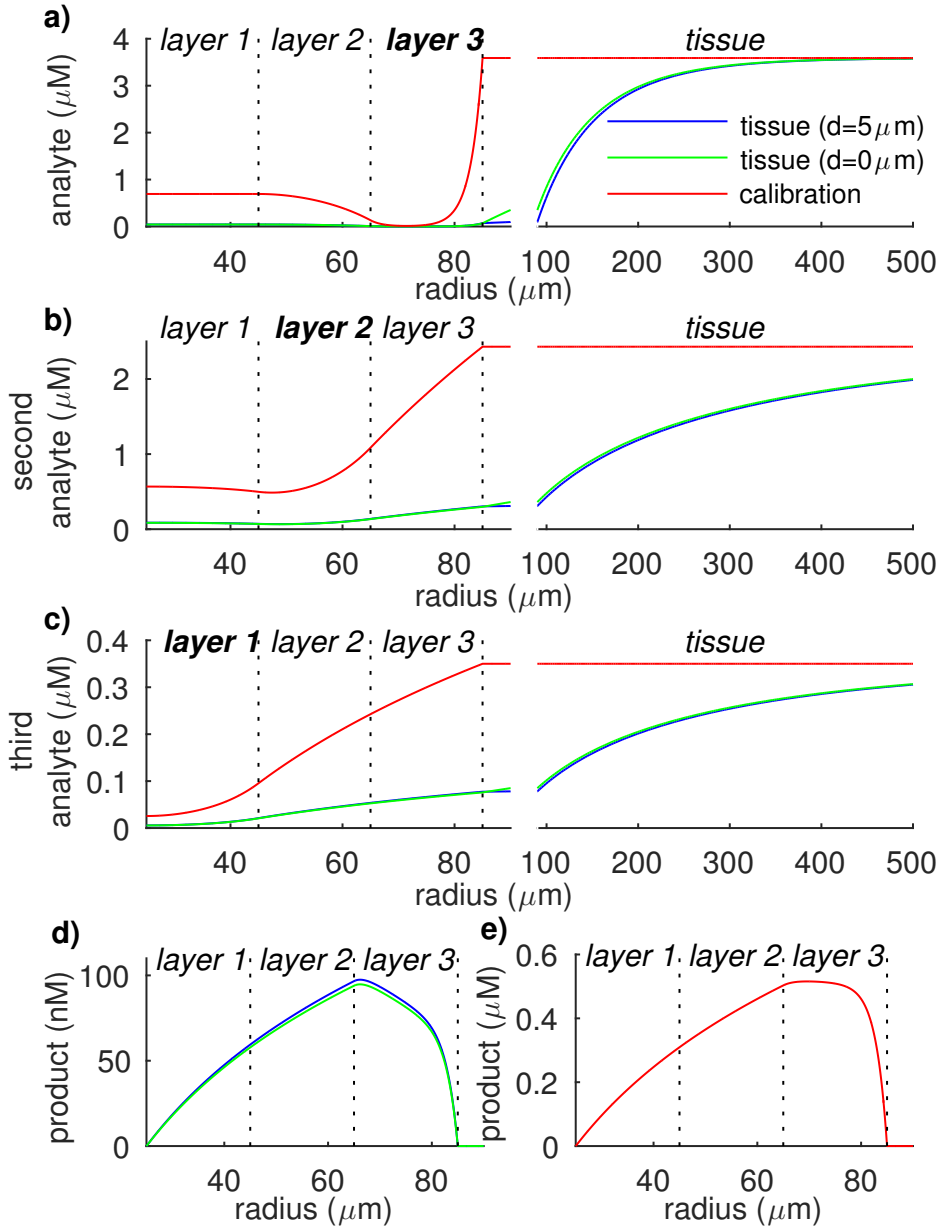

Figure 4.10: **The greater volume of enzyme layers for the three-enzyme biosensor reduces the concentration of the electroactive product close to the biosensor.** **a)** The analyte (hypoxanthine) reacts within layer 3 forming the electroactive product. **b)** The second analyte (inosine) reacts within layer 2. **c)** The third analyte (adenosine) within layer 1, producing the second analyte. **d)** The steady-state concentration electroactive product in the tissue environment with (d=5μm) and without (d=0μm) a free region is substantially lower than a free-flow environment **d)** with the same relative concentration. These plots show the relative concentrations, so they are continuous between regions. Parameter values from Table 4.1.

(Figure 4.9b), as it is produced in tissue and by reaction of the third analyte. The concentration of electroactive product is less than for the two-layer biosensor, because the analyte has to travel further to reach the core, more is lost to tissue or the free-flow environment, so the product concentration in layer 1 is almost 3/4 that of the two-layer biosensor (Figure 4.9c,d).

4.6 Sensitivity analysis

The calibration multiplier (Eq. 4.33) depends on the parameters of the model. Here the multiplier is determined for a range of values for each parameter in turn, while the others remain fixed at the values given in Table 4.1.

4.6.1 Single enzyme biosensor

The signal in both the calibration and tissue models is lower for wider cores, but the core width has a similar effect on both models, so core radius has almost no effect on the calibration multiplier (Figure 4.11a). The thickness of the enzyme layer influences both the calibration and tissue models. There is a peak in the steady-state signal for a layer of thickness $\sim 2\mu$m in calibration and $\sim 0.5\mu$m in the tissue model. The signal diminishes with a thicker layer, as more of the product is lost as it diffuses into tissue, or the bath and is removed. Conversely a thinner layer also reduces the signal as fewer reactions can take place to produce the electroactive product. As the signal for both the calibration and the tissue model is reduced for thinner layers, the calibration multiplier increases, *e.g.* $m = 0.95$ for a layer thickness of 1nm.

The steady-state gradient of the electroactive product at the core of the biosensor is almost unaffected by tortuosity. Whereas the same gradient in the tissue model is greater the more tortuous the enzyme layer, as the influence of the biosensor on the concentration of analyte around the biosensor is diminished. This is apparent in the calibration multiplier, (Figure 4.11f) *e.g.* $m \approx 0.5$ for a matrix tortuosity of 25.

The reaction rate in tissue v_t obviously does not influence the calibration

model, but the faster v_t the greater the signal for the tissue model, as the biosensor will have less of an influence on the analyte concentration in tissue, which is being removed and replaced more rapidly. However, v_t only appears in the model as a ratio of the relatively large diffusion coefficient in tissue (Eq. 4.58), so small changes in v_t have little effect on the calibration multiplier (Figure 4.11d). *E.g.* v_t ~100 for m ~0.5. While the tortuosity of the tissue (Figure 4.11g) has a substantial influence, it has been estimated for many species, brain regions and experimental conditions (Nicholson 2005), so it may be known prior to the experiment.

The steady-state response of the calibration model is larger when the enzyme reaction in the biosensor is faster, reaching 95% of the maximum response at $v_b \approx 30$/s. The signal from the tissue model has a maximum at $v_b \approx 5$/s, the signal in the tissue model is diminished if the reaction rate is faster than this, as the concentration of analyte in tissue is reduced. When v_b is slow, both models have a similar response and the calibration multiplier is larger (Figure 4.11e) *e.g.* For $v_b = 1$/s then m ~0.5. However, in constructing a biosensor it is not desirable to have a slow reaction rate and subsequently a small diffusion module (Eq. 4.27), as the response is controlled by the enzyme kinetics in the biosensor rather than the substrate concentrations around it.

The steady-state response of the calibration model is linearly dependent on the volume fraction of the enzyme layer α_b, whereas the steady-state response of the tissue model is substantially greater with a larger volume fraction when $\alpha_b < 0.1$, but almost unaffected by changes in volume fraction when $\alpha_b > 0.2$. So for a small volume fraction, both the calibration and tissue response are diminished as the calibration multiplier is increased (Figure 4.11h), *e.g.* m ~0.5 for α_b ~0.003.

The tortuosity and porosity of tissue gives rise to substantially lower steady-state concentrations in the matrix around the biosensor. This difference is exacerbated by rapid metabolism in the biosensor (v_b). However, a rapid reaction in the biosensor is desirable in biosensor design. Consider the diffusion module (Eq. 4.27), for a slow reaction $\sigma^2 \ll 1$ and the response becomes dependent on the enzyme kinetics of the sensor rather than the analyte con-

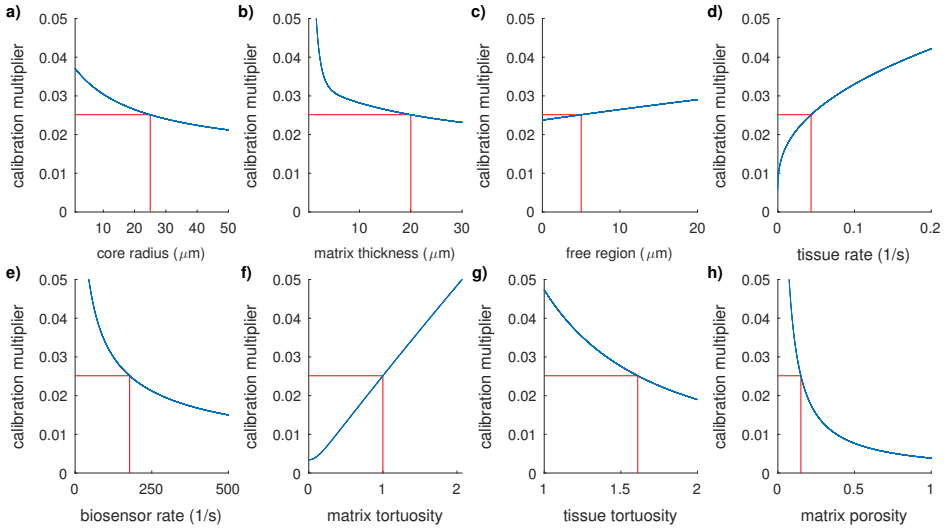

Figure 4.11: **The calibration multiplier is dependent on the parameters, however it remains relatively small for a wide range of values.** The estimated calibration multiplier of 0.02 for the parameters given in Table 4.1 is shown in red, while a single parameter is varied to see the impact it has on the calibration multiplier. **a)** The radius biosensor core (r_b) can vary from ∼7μm using carbon fibre to over ∼50μm with platinum, but this has a similar effect on both the calibration and tissue model, so has little influence on the calibration multiplier. **b)** For a very thin matrix width both the calibration model and tissue model have a very low response. **c)** The free region has little effect on the tissue model response (Figure 4.8c). **d)** The velocity of removal in tissue v_t has a limited effect on the response, its unlikely to reach very large values as this would mean the tissue was producing and destroying the analyte very rapidly. **e)** A slow reaction rate in the biosensor v_b means the response in both models is determined more by the enzyme than the analyte, so the response is similar and the calibrate multiple closer to 1. **f)** The matrix tortuosity has a greater impact on the tissue model than the calibration model as it determines the effect the biosensor has on analyte concentration in tissue, for larger values this effect is diminished and the biosensor response in tissue is closer to the response in calibration. **g)** While the tissue volume fraction influences the response, it is unlikely to vary greatly during an experiment and estimates are available in the literature for many brain regions (Nicholson 2005). **h)** It is difficult to estimate the matrix volume fraction and it can have a substantial impact on the required calibration multiplier.

centration. The diffusion module for the single-enzyme biosensor is $\sigma = 9.4$, as $\sigma^2 \gg 1$ the response of the biosensor is controlled by diffusion not the enzyme kinetics, allowing the biosensor to accurately measure the analyte

concentration in calibration, but also gives rise to a calibration multiplier of 0.02. The parameters for biosensors are rarely published and may vary between biosensors and with use *e.g.* the polymer matrix is known to decay with repeated use.

4.6.2 Two-enzyme biosensor

The two-enzyme biosensor has an estimated calibration multiplier of 0.05 for the parameters (Table 4.1). The solution can be used as before to determine the influence each parameter has on the calibration multiplier. Unlike the single enzyme case, here the calibration multiplier is based on calibration with a combination of the two analytes (Eq. 4.35). As with the single enzyme layer, the matrix properties have the greatest effect on the calibration multiplier. With a greater matrix tortuosity the signal in the tissue model is closer to the signal in the calibration model (Figure 4.12i), similarly for a smaller matrix volume fraction (Figure 4.12j).

4.6.3 Three-enzyme biosensor

An adenosine biosensor with three-enzyme layers is considered. As before analytic solutions are obtained for the concentration of each substrate and used to determine the signal during calibration, tissue, and the corresponding calibration multiplier, $m^c = 0.02$. As before there are several parameters determining the enzyme layer thickness, biosensor reaction rate and matrix porosity (Figure 4.13) which when reduced slow the reaction in both calibration and tissue to such an extent that the calibration multiplier is close to 1.

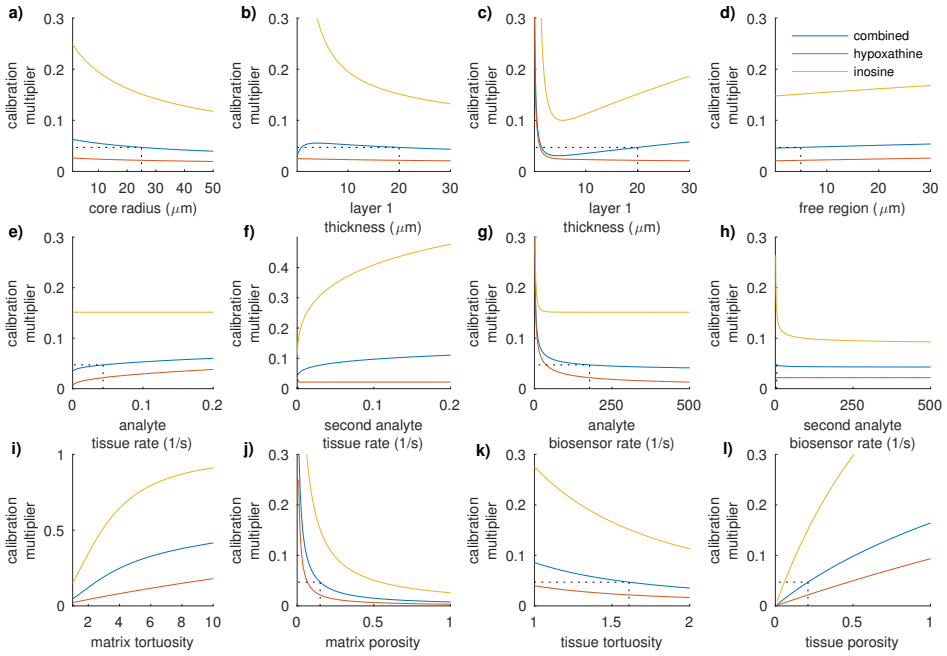

Figure 4.12: **The matrix thickness, tortuosity and volume fraction have the greatest impact on the calibration multiplier.** **a)** The radius biosensor core (r_b) has a similar effect on both calibration and tissue models. **b)** The thickness of layer 1, (where the reaction of the second analyte occurs) has little effect, unlike **c)** the thickness of the second layer (where the reaction of the analyte occurs), as it is this reaction that produces the electroactive product. If this is slow, both calibration and tissue model will produce a similar response. **d)** The thickness of free region has little effect on the concentration of product in the sensor, so does not substantially influence the response (Figure 4.9). **e)** The reaction rate of the analyte in tissue (v_t) has a greater impact on the multiplier than **f)** the second analyte v_{t_2}, due to the comparatively slow reaction in the biosensor of the second analyte compared with the first. **g)** Similarly changing the reaction rate of the analyte v_b in the biosensor has a greater impact than changing the rate of the second analyte **h)** v_{b_2}, as the second analyte has to go though both reactions to result in electroactive product. **i)** The matrix tortuosity, **j)** the matrix volume fraction, **k)** tissue tortuosity and **l)** tissue volume fraction have the same effect on the multiplier as the single layer biosensor (Figure 4.11). The combined calibration multiplier of 0.05 for parameters in Table 4.1 is shown with a dashed line.

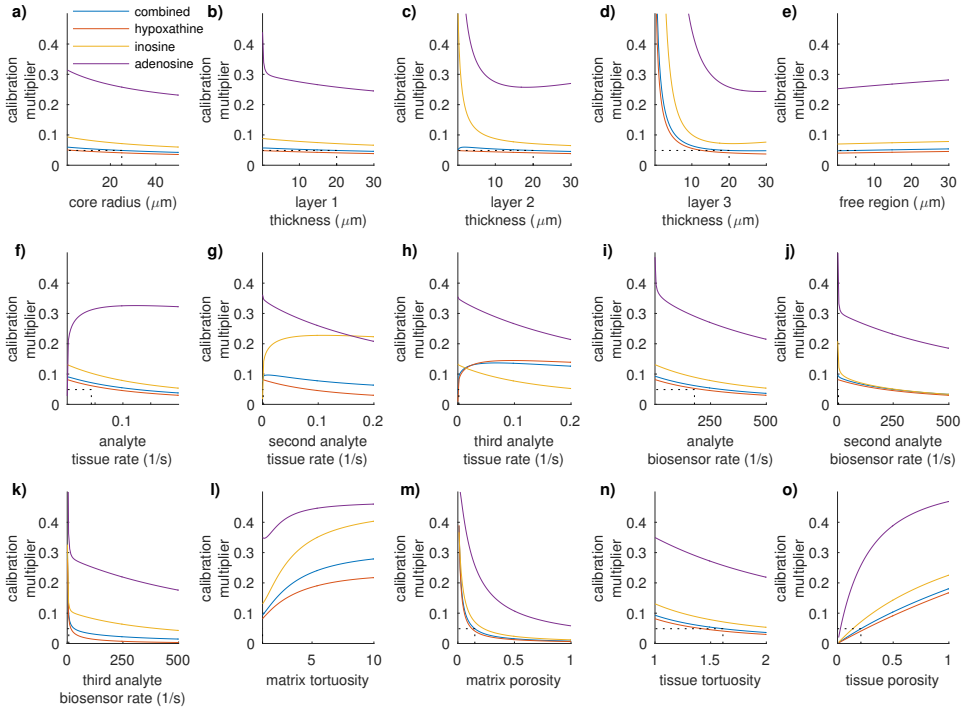

Figure 4.13: **The three-enzyme biosensor has more parameters so their individual influence on the calibration multiplier is diminished.** As before, the parameters of the enzyme layer have the greatest impact on the calibration multiplier. **a)** The radius of the biosensor core (r_b) has a similar effect on both calibration and tissue models, so has little impact on the calibration multiplier. **b)** The thickness of layer one (the inner most layer where the reaction of the third analyte occurs) and **c)** layer two (the middle layer where the reaction of the second analyte occurs) have little influence on the calibration multiplier compared with **d)** the third layer thickness (where the reaction of the first analyte occurs producing the electroactive product), as this layer is a bottleneck, where all three analytes must react to be detected. **e)** The free region has little effect on the concentration of product in the enzyme layer (Figure 4.8b). The reaction rate in tissue of the **f)** analyte v_t, **g)** second analyte v_{t_2} and **h)** third analyte v_{t_3} determine the range of influence the biosensor has on the analyte concentrations and so influence on the calibration multiplier. As with layer width, the reaction rate in the biosensor of **i)** the analyte v_b is a bottleneck for the formation of the electroactive product, so has a far greater impact on the combined calibration multiplier than either the **j)** second analyte v_{b_2} or **k)** third analyte v_{b_3}. **l)** The matrix tortuosity **m)** the biosensor volume fraction, **n)** the tissue tortuosity and **o)** volume fraction have the same effect on the combined multiplier as for the single layer biosensor (Figure 4.11). The estimated combined calibration multiplier of 0.02 for parameters in Table 4.1 is shown by the dashed line.

4.7 Tissue depth

The idealised model (Figure 4.1a) can be expanded to account for the finite length of a biosensor inserted into tissue. Here a single-enzyme biosensor is considered. As before the analyte A is described by the PDE (Eq. 4.1) and by making linear approximations (Eq. B.165). However, in this case the Laplace operator is;

$$\nabla^2 = \frac{1}{r}\frac{\partial}{\partial r}\left(r^2\frac{\partial}{\partial r}\right) + \frac{\partial}{\partial z^2} \tag{4.66}$$

Additional boundary conditions are needed for the slice surfaces. A simple *in vitro* case is consider where the whole biosensor length (l_b) is inserted into a slice of tissue with the same depth (l_b). The tissue is in a bath with artificial cerebrospinal fluid (aCSF) flowing over both the top ($\frac{l_b}{2}$) and bottom (-$\frac{l_b}{2}$). The insulation on the biosensor is assumed to cover the enzyme layer at the top and there is no polymer matrix at the base of the sensor (Figure 4.1b). Typically a tissue slice will have a far greater length than depth as thick slices can become hypoxic, so a boundary condition is applied in the limit $r \to \infty$. These assumptions give the boundary conditions;

$$A\left(t, r, \frac{l_b}{2}\right) = 0 \qquad r_f < r \tag{4.67}$$

$$\left.\frac{dA(t,r,z)}{dz}\right|_{z=\frac{l_b}{2}} = 0 \qquad r_b < r \leq r_f \tag{4.68}$$

$$A\left(t, r, -\frac{l_b}{2}\right) = 0 \tag{4.69}$$

$$\lim_{r\to\infty} A(t,r,z) = A_0(z) \tag{4.70}$$

$$\left.\frac{dA(t,r,z)}{dr}\right|_{r=r_b} = 0 \tag{4.71}$$

$$\left.\frac{dH(t,r,z)}{dz}\right|_{z=\frac{l_b}{2}} = 0 \qquad r_b < r \leq r_f \tag{4.72}$$

$$H\left(t, r, -\frac{l_b}{2}\right) = 0 \tag{4.73}$$

$$H\left(t, r_b, z\right) = 0 \tag{4.74}$$

$$H\left(t, r_f, z\right) = 0 \tag{4.75}$$

Where $A_0(z)$ is the steady-state concentration of analyte in the tissue slice without the biosensor, it is given by;

$$A_0(z) = A^* \left(1 - \frac{\cosh(cz)}{\cosh\left(c\frac{l_b}{2}\right)} \right) \tag{4.76}$$

$$c = \sqrt{\frac{v_t}{D_t}} \tag{4.77}$$

Where the boundaries are at $\pm\frac{l_b}{2}$, this is also the initial condition of the tissue. In the initial condition for the free region, and enzyme layer, both the analyte and the product are zero. The continuity conditions are the same as (Eq. 4.3-4.6) for all z.

An *in vivo* case is also considered where a biosensor of length l_b is inserted at depth l_p into tissue and plastic insulation covers the top of the polymer matrix, which extends around the whole sensor (Figure 4.1c). The boundary conditions require zero flux of the analyte at the core, at $r = 0$ and at the surface. The analyte concentration is fixed at A^* as the depth or radius tends to infinity. The boundary conditions on the product require it to be zero at both the core and at the edge between the enzyme layer and the free region, with zero flux at $r = 0$ and at the top of the enzyme layer, where it meets the plastic sheath. The analyte concentration is initially A^* in the tissue and zero in the free region and enzyme layer. The product concentration is initially zero. The continuity conditions are similar to (Eq. 4.3-4.6) with continuity of the relative concentrations between regions and continuity of the flux of the total concentrations.

4.7.1 Model response

More realistic *in vitro* and *in vivo* models are considered (Figure 4.1c,d). The concentration in each model are determined numerically, (code C.3) and used to infer the biosensor's response. As with the time-dependent response for the idealised model, there is a sharp initial rise, (Figure 4.14) followed by a slow decay as the sensor removes the nearby analyte, until it reaches the steady-state response. The heat maps show that the analyte does not penetrate far into the enzyme layer, as it is rapidly converted to the electroactive product.

Steady-state responses for the *in vivo* model give a calibration multiplier of 0.041 similar to the idealised model, which does not include depth. Similarly the *in vitro* model has a calibration multiplier of 0.034. While the model response differs from the idealised biosensor, it still demonstrates the need to account for differences between the calibration and the experimental environments, quantified by the calibration multiplier (Eq. 4.33).

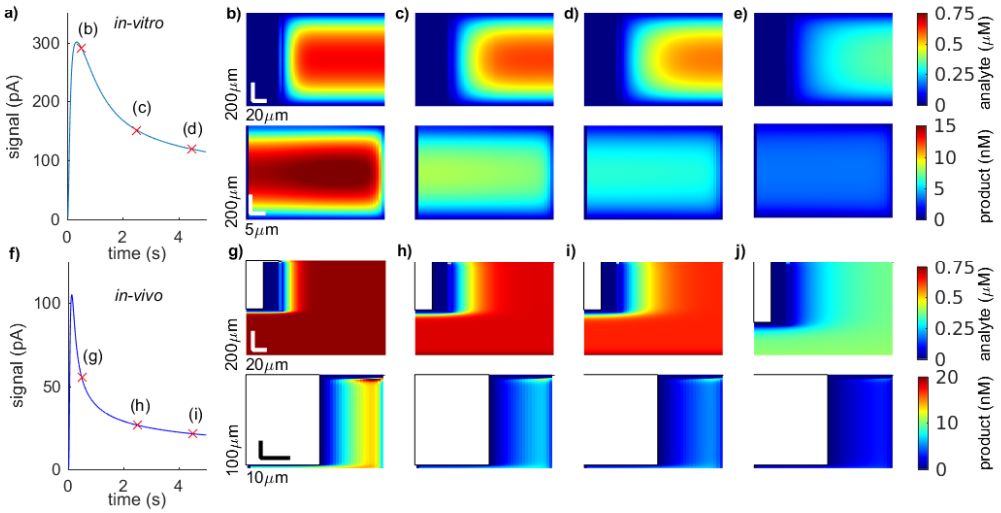

Figure 4.14: **The signal obtained from the *in vitro* and *in vivo* model has a similar form to the idealised model, but it is quantitatively different.** **a)** the time-dependent response for the *in vitro* model is far smaller than both the idealised and *in vivo* model, in part due to a lower concentration of analyte in tissue. There are three time points (indicated by red crosses) where the concentration profiles of the analyte (top) and product (bottom) are shown, **b)** at 0.5s, **c)** at 2.5s and **d)** at 5s. These show the decline in the concentration of analyte and product towards **e)** the steady-state concentrations. The electroactive product is only shown in the enzyme layer, as it is not in tissue, so the length scale is much smaller. Notice that the initial distribution in tissue has a depth dependent concentration profile (Eq. 4.76). **f)** the time-dependent response for the *in vivo* case also with three time points (indicated by red crosses) where the concentration profiles of the analyte (top) and product (bottom) are shown, **g)** at 0.5s, **h)** at 2.5s and **i)** at 5s. Which tend towards **j)** the steady-state concentrations. Here the biosensor core and plastic sheath are included in the model (Figure 4.1d), indicated by the white area in the top right. The concentration of electroactive product is shown in the enzyme layer, hence the smaller length scale. Time step 1μs and $\Delta_R = \Delta_Z = 1\mu$m. The grid size $500 \times 500\mu$m for the *in vitro* model and $1000 \times 1000\mu$m for the *in vivo* model with insertion depth 20μm and sensor length 500μm.

Chapter 5

Conclusion

The interactions between transport and metabolism of the neuromodulator adenosine have not previously been well quantified. This study provides the first detailed model of the spatiotemporal dynamics of adenosine in tissue. The mechanisms included in the model are; diffusion and breakdown by adenosine deaminase (ADA) in the extracellular space; competitive transport between the extracellular and intracellular space by equilibrative nucleoside transporters (ENT); neuronal breakdown by ADA and glial metabolism via adenosine kinase. A hierarchy of models was considered, starting with extracellular metabolism only, then including neurons, or glia, or both. Analysis of these models determines that the concentration following local adenosine release is primarily determined by diffusion through the tortuous extracellular space (chapter 3). The literature search provided estimates of the model parameters as well as identifying aspects of the purine transport and metabolism that have yet to be experimentally quantified (chapter 2). The model predicts the range of influence of an isolated adenosine source, characterised as the maximum distance where the amplitude of an EPSP would be halved due to the activation of A_1Rs, the most abundant class of adenosine receptors in the neocortex. The greatest influences on this effective range are the tortuous diffusion coefficient, extracellular volume fraction, and the endogenous adenosine tone (chapter 3). Purine biosensors measure both adenosine and its breakdown products inosine and hypoxanthine by an enzymatic cascade that produces hydrogen peroxide which is electrochemically detected. The response of the sensor is typically compared with flow-injection calibration to estimate the concentra-

tion in tissue. In chapter 4 mathematical models of the biosensors allowed the response to be correctly scaled to account for the tortuosity and volume fraction of the tissue.

5.1 Adenosine clearance

It is shown that the range of influence of a point source of adenosine is primarily determined by diffusion. The model indicates that neuronal metabolism is the dominant clearance mechanism due to its rapid uptake and breakdown of adenosine, *e.g.* for a small constant point source in the steady state, neuronal clearance reduces the total amount of extracellular adenosine to around 12% of model I, compared to around 50% by glia. This suggests that the role played by glia in maintaining the endogenous tone of adenosine is predominately as a release mechanism. In the bath applied case the clearance mechanisms frustrate penetration through the tissue slice, however, experimental work is able to mitigate this effect by applying far higher concentrations of adenosine than occur endogenously, by using adenosine receptor agonists that are not affected by uptake and metabolism and by using a perfusion system to increase the flow of adenosine through the slice.

5.1.1 Diffusion

The model predicts that for quantities of adenosine expected during normal brain function, the primary factor determining the range of influence is diffusion. Subsequently factors that influence diffusion will have a substantial effect on the adenosine signal. The diffusion coefficient is influenced both by temperature and by the tortuosity of the ECS. Adenosine has a neuroprotective role, with studies that focus on pathological conditions such as epilepsy and ischemia, which reduce the extracellular volume fraction and increase tortuosity of the ECS (Syková et al. 1994), decreasing the rate of diffusion through the tissue, and localising the influence of adenosine release. Additionally the tortuosity of the ECS varies with species and brain region (Syková and Nicholson 2008). Lastly several slice preparation and experimental procedures can also alter tortuosity and extracellular volume fraction (Wetherington et al. 2008; Aitken et al. 1995).

Extracellular adenosine concentrations are correlated with the need for sleep (Sims et al. 2013; Clasadonte et al. 2014) with the ECS having been shown to increase substantially from $\sim$15% in awake to $\sim$25% in anaesthetised mice, while the tortuosity is unchanged (Xie et al. 2013). The extracellular concentrations and cellular transport will be reduced in the anaesthetised state, decreasing both the gradient of the curve and the influence of clearance mechanisms, thus increasing the range of influence (Figure 3.6c, Figure 3.9n).

5.1.2 Clearance mechanisms

The clearance mechanisms have a significant effect for uniform sources and bath applied adenosine. They only have a substantial impact on point sources that are sufficiently large to compensate for rapid dilution due to diffusion. Previous work has suggested that the dominant removal mechanism for adenosine is via ADK: based on it higher binding affinity (Boison 2006). The substantial increase in the endogenous tone of adenosine when it is inhibited with iodotubercidin (Etherington et al. 2009) and overexpression of ADK in transgenic mice causes both spontaneous seizure activity (Fedele et al. 2005) and more damage during ischemia (Pignataro et al. 2006). Whereas ADA has a lower binding affinity and inhibition with erythro-9-(2-hydroxy-3-nonyl)adenine (EHNA), it does not have a significant impact on adenosine signalling in physiological conditions, depending on brain region (Latini and Pedata 2001), consistent with variations in expression of ADA between regions (Yamamoto et al. 1987). The models presented here only consider clearance of adenosine, and as glia play only a minor role in clearance, they predict that blocking ADK will have little effect. However this does not contradict previous findings. Breaking the cycle between AMP and adenosine mediated by ADK and 5′N, would turn glia into a source of adenosine. This has been demonstrated in the rat cerebellum, where the increase in endogenous tone following application of iodotubercidin, was prevented when ENT blockers, NBTI and dipyrimole were applied (Wall et al. 2007).

Transport of adenosine is known to be a vital clearance mechanism (Dunwiddie and Diao 1994), consistent with the model results. Clearance of the

endogenous adenosine during physiological conditions could be accomplished by cellular transport and the relatively slow glia clearance, even with diminished ADA activity. While ADA remains important for clearance of larger more pathological concentrations (Dunwiddie and Masino 2001). For bath applied adenosine the salvage of breakdown products by glia is clearly significant, experimentally glia may be ablated (Bush et al. 1998) or the salvage pathway may be blocked with an XO inhibitor, such as febuxostat (Honorat et al. 2013). In either case the extracellular concentration of breakdown products may be sufficient to cause unwanted side effects, such as increases in brain-derived neurotrophic factor (Muto et al. 2014) or activation of a signal transduction pathway that regulates axonal growth (Dachir et al. 2014).

5.1.3 Parameters

The simplified salvage pathway used in these models attempts to account for removal of inosine and xanthine through the blood brain barrier (BBB), however it ignores both direct removal of adenosine in glia through the BBB and the creation of AMP via hypoxanthine and inosine monophosphate (IMP). It is difficult to test the validity of this simplification. There is a cycle between inosine and IMP, and in pathological conditions conversion of IMP to inosine is believed to be the main source of astrocytic inosine rather than uptake from the ECS (Schultz and Lowenstein 1978). However, given the difficulties of obtaining parameter estimates for the speed and affinity of inosine transport, a more detailed model of the salvage pathway would not improve the accuracy of these models. Experiments of the kind used to establish the parameters of adenosine transport *e.g.* using radiolabeled adenosine molecules in cell cultures, could be conducted for inosine allowing the effect of competitive inhibition to be accurately modelled. Given this data it may be constructive to separate the breakdown products into inosine and hypoxanthine, as hypoxanthine is known to have a very low transport affinity, K_m ~1mM. The models here primarily focus on adenosine, but inosine can also bind to A_1R, $A_{2A}R$ or A_3R (Haskó et al. 2004) and may have significant cognitive effect (Kaster et al. 2013).

5.1.4 Model hierarchy

The spatial resolution of macroscopic models are limited, requiring around $\sim 10\mu$m for the averages over spatial structures to be valid. This makes it inappropriate for studying heterogeneities in adenosine concentration that may occur about a synapse. Similarly, diffusion is not modelled in the intracellular space.

Without knowing the source of extracellular adenosine it is difficult to estimate the minimum release required to affect multiple synapses. Given the synaptic density in the rat parietal cortex gives an average distance between synapses of 1.6μm (Calverley et al. 1988). An alternative is to use the spine density to estimate an average upper bound on the distance between synapses, 1.7 ± 0.3 μm of dendrite per spine for thick tufted layer 5 pyramidal neurons of the rat visual cortex (Larkman 2004). In both cases the method here is inappropriate at this scale, as it fails to account for the local microstructures around the synapse.

It would be desirable to be able to further subdivide the tissue by type of glia, *i.e.* oligodendrocytes, microglia and astrocytes, as well as the classes of neurons, *e.g.* inhibitory interneurons and excitatory primary neurons. This could be achieved using cell cultures to perform transport and uptake studies of adenosine. Transport focuses on the short time scale so as not to include intracellular metabolism, whereas uptake looks over longer time scales. Experimental validation of such a model will be challenging, given the small spatial scales involved.

5.1.5 Brain regions and sources

This model could easily be adapted for other species and brain regions by changing the parameters, although there are substantial difference in the purine metabolism *e.g.* neuronal ADA is restricted to a subset of neurons and is most prominent in the tuberomamillary nucleus and is more abundant in glia than neurons in mice. Adenosine influence on neuronal activity is primarily mediated by the A_1R; however in the striatum the $A_{2A}R$ also has a prominent effect. It is not clear that the simple receptor model used

here would adequately capture the effect of adenosine. Adenosine receptors are also influenced by several endogenous proteins and other GPCRs. A fascinating extension is to incorporate the growing body of work on activity-dependent adenosine release, with the goal of coupling the slow diffusive dynamics and fast network dynamics.

As the first detailed model of adenosine dynamics in neural tissue, several assumptions have been made to produce a parsimonious model. Several parameters could not be inferred from the literature, in particular estimates of kinetics AK in glia and ENTs velocity and affinity for inosine, while others are highly uncertain, such as the removal rate of breakdown products in glia. The models predict concentration profiles are primarily determined by diffusion, while clearance mechanism have a substantial impact for large point sources that are able to persist despite rapid diffusion, and for uniform sources. Neuronal uptake is the dominant clearance mechanism due the relatively rapid neuronal ADA compared with ecto-ADA. They also occupy a greater volume and have faster transporters than glia.

5.2 Biosensor modelling

The modelling performed in chapter 4 for hypoxanthine, inosine and adenosine biosensors (Llaudet et al. 2003), could readily be applied to any of the biosensors used in tissue (Table A.1) or other tortuous media. The main barrier for such analysis is the paucity of published information regarding the properties of the biosensors. The advantage of modelling biosensors in tissue is the ability to more accurately estimate the concentration of analytes in tissue, which is essential for any quantitative understanding of chemical signalling. The modelling suggests tissue concentration could be up to $\sim$40 fold greater than the estimates obtained by conventional calibration. Although this is on the parameters of the biosensor, for a wide range of parameters this underestimation is still substantial. It may be that biosensors are less well suited to detecting the analyte where the calibration and tissue signal are similar, *e.g.* the model suggests a slower reaction rate for the enzyme in the biosensor will reduce the underestimation of tissue concentration, however this will also mean the biosensor response will

be more dependent on the enzyme than the analyte concentration around it.

Additionally layers could be added to the model, for example an additional Nafion layer is often used to reduce interference from negatively charged molecules like ascorbate, or the Nernst diffusion layer could be included in calibration. These inactive layers would have a solution following the logarithm of the radius, and as they are relatively thin would have little influence on the calibration multiplier. In particular the thickness of the Nernst diffusion layer, (used to account for the depletion of analyte about the electrode), is obtained by extrapolating the concentration gradient at the electrode surface to a radius where the bulk concentration is reached. While it is relevant during calibration, its thickness will diminish with the flow rate and so will not have an influence on the signal for sufficiently rapid flow.

This study only considered cylindrical biosensors, however many other shapes are often used, for example disk shapes are quite common (Table A.1) and the analysis could readily be repeated for such shapes. However more complex geometries are also used, for example the plate-gap model describes a biosensor created by depositing the enzyme into a porous electrode *e.g.* carbon paste electrode (Gavalas et al. 1998), where there is an outer membrane over multiple enzymes deposits which are surrounded by the electrode. While both mathematical and numerical modelling has been performed for the plate-gap biosensor (Baronas et al. 2006; Ivanauskas and Baronas 2008), the diffusion characteristics of tissue have not been taken into account.

In conclusion, this work includes both the first detailed model of adenosine clearance in tissue and a mathematical model of the biosensors that are frequently used to measure adenosine. While there are limitations in both the models developed, principally in estimating parameter values, together they provide a foundation for the quantitative study of adenosine signalling in the brain.

Appendix A

Biosensors review

An extensive literature review of many of the biosensors available for various neurochemical species, shows that the key parameters necessary for modelling the response of the biosensor are rarely published. These paramters are liklely to vary greatly given the wide range of techniques that are used to form the enzyme layer and the variety of enzymes used to select a specific analyte.

Sensor		Layers	Enzymes	Parameters	
ATP	(Llaudet et al. 2005)	silicate layer	glycerol kinase (GK)	r_b	3.5μm (carbon fibre)
			glycerol-3-phosphate oxidase (G3POx)		12.5μm or 25μm (platinum)
			ascorbate oxidase (20U/10μl)	w	unknown
			Cosubstrate: glycerol	μ	unknown
			Electroactive product: 1 H_2O_2	α_b	unknown
				GK	$V_{\max}$ = 420fmol/s K_m = 165μM
				G3POx	$V_{\max}$ = 590fmol/s K_m = 133μM
ATP	(Patel et al. 2011)	poly-phenol film	glucose oxidase (GOx)	r_b	25μm platinum disc
			hexokinase (HEX)	w	unknown
			Compete for glucose	μ	unknown
			Electroactive product: 1 H_2O_2	α_b	unknown
				GOx	$V_{\max}$ unknown K_m = 10.69μM
				HEX	$V_{\max}$ unknown K_m unknown
Glucose	(Endo et al. 2010)	Nafion layer	glucose oxidase (GOx)	r_b	88μm
		2 layers cross linked GOx and BSA	Electroactive product: 1 H_2O_2	w	unknown
				μ	unknown
				α_b	unknown
				GOx	$V_{\max}$ unknown K_m unknown
Glucose	(Chen et al. 2002)	polyphenol layer	glucose oxidase (GOx)	r_b	42.5μm

		with cross-linked GOx, BSA and 3-ATS outer polyurethane layer	Electroactive product: 1 H_2O_2	w μ α_b GOx	0.5μm unknown unknown $V_{\max}$ unknown K_m unknown
Hypoxanthine	(Li et al. 2008)	FeTPPNPs layer cross-linked XO, BSA and GA layer	xanthine oxidase (XO) Electroactive product: 2 H_2O_2	r_b w μ α_b X0	1.5mm glassy carbon core unknown unknown unknown $V_{\max}$ unknown K_m unknown
Hypoxanthine	(Coche-Guerente et al. 1995)	amphiphilic pyrrole	xanthine oxidase (XO) Electroactive product: 2 H_2O_2	r_b w μ α_b X0	2.5mm disk unknown unknown unknown $V_{\max}$ unknown K_m unknown
Hypoxanthine	(Llaudet et al. 2003)	lactobionamide pyrrole amphiphillic pyrrole anti-fouling layer	xanthine oxidase (XO) Electroactive product: 2 H_2O_2	r_b w μ α_b X0	3.5μm (carbon fibre) 12.5μm or 25μm (platinum) $\sim$20μm unknown unknown $V_{\max}$ unknown K_m unknown
Inosine	As above	additional layer amphiphillic pyrrole	Purine nucleoside phosphorylase (PNP) ‘	w_i PNP	unknown $V_{\max}$ unknown K_m unknown
Adenosine	As above	additional layer amphiphillic pyrrole	adenosine deaminase (ADA) ‘	w_a ADA	unknown $V_{\max}$ unknown K_m unknown
Glutamate	(Hu et al. 1994)	Nafion layer cellulose acetate layer cross-linked BSA, GA and enzyme layer	glutamate oxidase (GO) ascorbic acid oxidase (AAO) Electroactive product: 1 H_2O_2	r_b w μ α_b GO	88μm unknown unknown unknown $V_{\max}$ unknown K_m unknown
Glutamate	(Tian et al. 2009)	poly(phenylene diamine) sol-gel later	glutamate oxidase (GO) Electroactive product: 2 H_2O_2	r_b w μ α_b GO	3.5μm (carbon fibre) 12.5μm or 25μm (platinum) unknown unknown unknown $V_{\max}$ unknown $K_m = 776\mu$mol/L
Glutamate	(Mikeladze et al. 2002)	redox polymer ($PVI_1$9-dmeOs) cross-linked poly(ethylene glycol) enzyme layer	glutamate oxidase (GlOx) horseradish peroxidase (HRP) Electroactive product: 1 H_2O_2	r_b w μ α_b	1.5mm graphite core (13% porosity) unknown unknown unknown

				GO	$V_{\max}$ unknown K_m = 3 or 7mM
Glucose	(Kotanen et al. 2014)	polypyrrole (PPy) with SBA covalently bonded to GOx	glucose oxidase (GOx)	r_b 50μm	
and Lactate		PPy(SBA-con-GOx) or P(Py-co-PyBA-con-GOx)	lactate oxidase (LOx)	w	unknown
		Second layer Py PyBA with entrapped LOx	Electroactive product: 1 H_2O_2 each	μ	unknown
				α_b	unknown
				GOx	$V_{\max}$ unknown K_m = 7.2 or 19.7mM
				LOx	$V_{\max}$ unknown K_m unknown
Lactate	(Kobayashi et al. 2001)	2 thin films of concanavalin A with attached LOx	lactate oxidase (LOx)	r_b	1.5mm disk
			Electroactive product: 1 H_2O_2	w	∼0
				μ	unknown
				α_b	unknown
				LOx	$V_{\max}$ unknown K_m unknown
Acetylcholine	(Chen et al. 1998)	20 monolayers alternating between avidin an attached ChOx additional layer of avidin and attached ChE	choline esterase (ChE)	r_b	1.5mm disk
			choline oxidase (ChOx)	w	∼210nm[a]
			Electroactive product: 3 H_2O_2	μ	unknown
				α_b	unknown
				ChE	$V_{\max}$ unknown K_m unknown
				ChOx	$V_{\max}$ unknown K_m unknown
D-serine	(Zain et al. 2010)	poly-ortho-phenylenediamine (PPD) layer	d-amino acid oxidase (DAAO)	r_b	1.5mm graphite core (13% porosity)
		Nafion layer	Electroactive product: 1 H_2O_2	w	unknown
		GA and DAAO later		μ	unknown
				α_b	unknown
				DAAO	$V_{\max}$ unknown K_m = 3 or 7mM
Choline	(Razola et al. 2003)	BSA crosslinked to HRP with GA, paraffin and PHZ	horseradish peroxidase (HRP)	r_b	1.5mm disk
		CHOx with dialysismembrane	choline oxidase (CHOx)	w	unknown
			Electroactive product: 2 H_2O_2	μ	unknown
				α_b	unknown
				HRP	$V_{\max}$ unknown K_m unknown
				CHOx	$V_{\max}$ unknown K_m unknown
D-Serine	(Shigetomi et al. 2013)		D-amino acid oxidase (DAAO)	r_b	25μm

		Electroactive product: 1 H_2O_2	w	unknown
			μ	unknown
			α_b	unknown
			DAAO	$V_{\max}$ unknown K_m unknown

Table A.1: **Review of published information for a variety of biosensors.** Where K_m is given it is based on K_m^{app} of the biosensors response. a] estimated form (Gokel 1997). The following acronyms are used; (3- aminopropyl)trimethoxysilane (3-ATS), bovine serum albumin (BSA), iron (III) mesotetraphenylporphyrin nanoparticles (FeTPPNPs), glutaraldehyde (GA),4-sulfobenzoic acid (SBA), pyrrol (Py), 4-(3-pyrrolyl)butyric acid (PyBA), Phenothiazine base (PHZ)

Appendix B

Mathematics appendix

B.1 Enzyme kinetics

$$E + S \underset{k_{-1}}{\overset{k_1}{\rightleftharpoons}} ES \overset{k_2}{\rightarrow} E + P \tag{B.1}$$

Where E is the enzyme and S is the substrate. By assuming the total enzyme concentration does not change (E_0) and that the concentration of the complex ES does not change on the same timescale as the product formation;

$$E_0 = [E] + [ES] \tag{B.2}$$

$$\frac{d[ES]}{dt} = 0 \tag{B.3}$$

Then the ODE for the complex can be written as;

$$\frac{d[ES]}{dt} = k_1[E][S] - k_1[ES] - k_2[ES] \tag{B.4}$$

$$= 0 \tag{B.5}$$

$$[ES] = k_1(E_0 - [ES])[S] - k_{-1}[ES] - k_2[ES] \tag{B.6}$$

$$= \frac{k_1 E_0[S]}{k_2 + k_{-1} + k_1[S]} \tag{B.7}$$

$$= \frac{E_0[S]}{K_m + [S]} \tag{B.8}$$

$$K_m = \frac{k_2 + k_{-1}}{k_1} \tag{B.9}$$

Then the rate of product formation is given by;

$$\frac{d[P]}{dt} = k_2 [ES] \tag{B.10}$$

$$= \frac{V_{\max}[S]}{K_m + [S]} \tag{B.11}$$

$$V_{\max} = k_2 E_0 \tag{B.12}$$

B.2 Transporter kinetics

Suppose the transporters have the following kinetics;

$$E + A_e \underset{k_2}{\overset{k_1}{\rightleftharpoons}} EA \underset{k_1}{\overset{k_2}{\rightleftharpoons}} E + A_i \tag{B.13}$$

$$E + P_e \underset{k_4}{\overset{k_3}{\rightleftharpoons}} EP \underset{k_3}{\overset{k_4}{\rightleftharpoons}} E + P_i \tag{B.14}$$

Assume the total concentration of transporters does not change and that the concentrations of the complex changes on a slower timescale than the equilibration of the intracellular and extracellular concentration of adenosine and it's breakdown products.

$$E_0 = [E] + [EA] + [EP] \tag{B.15}$$

$$\frac{d[EA]}{dt} = 0 \tag{B.16}$$

$$\frac{d[EP]}{dt} = 0 \tag{B.17}$$

Suppose the intracellular and extracellular space occupy the same volume fraction, then let $A = [A_e] + [A_i]$ be the total adenosine concentration.

$$\frac{d[EA]}{dt} = k_1 [A_e][E] + k_1 [A_i][E] - 2k_2 [EA] \tag{B.18}$$

$$= 0 \tag{B.19}$$

$$[EA] = \frac{k_1}{2k_2}[E]([A_e] + [A_i]) \tag{B.20}$$

$$= \frac{k_1}{2k_2}(E_0 - [EA] - [EP])A \tag{B.21}$$

$$= \frac{E_0 - [EP]}{\frac{2k_2}{k_1} + A}A \tag{B.22}$$

$$= \frac{E_0 - [EP]}{K_A + A}A \tag{B.23}$$

Similarly

$$[EP] = \frac{E_0 - [EA]}{\frac{2k_4}{k_3} + P}P \tag{B.24}$$

$$= \frac{E_0 - [EA]}{K_P + P}P \tag{B.25}$$

Substituting (Eq. B.25) into (Eq. B.23) gives

$$[EA] = \frac{E_0(K_P + P)A - E_0AP}{(K_A + A)(K_P + P) - AP} \tag{B.26}$$

$$= \frac{E_0K_PA}{K_AK_P + K_AP + K_PA} \tag{B.27}$$

Similarly

$$[EP] = \frac{E_0K_AP}{K_AK_P + K_PA + K_AP} \tag{B.28}$$

Where $K_A = \frac{2k_2}{k1}$ and $K_P = \frac{2k_4}{k_3}$. The concentration transported is then given by;

$$\frac{d[A_i]}{dt} = k_2[EA] - k_1[E][A_i] \tag{B.29}$$

$$= k_2[EA] - k_1(E_0 - [EA] - [EP])[A_i] \tag{B.30}$$

$$= \frac{(k_2 + k_1[A_i])E_0K_PA - k_1E_0[A_i](K_AK_P + K_PA + K_AP) + k_1E_0K_AP}{K_AK_P + K_PA + K_AP} \tag{B.31}$$

$$= \frac{k_2E_0K_PA - k_1E_0[A_i]K_AK_P}{K_AK_P + K_PA + K_AP} \tag{B.32}$$

$$= \frac{k_2E_0K_PA - 2k_2E_0[A_i]K_P}{K_AK_P + K_PA + K_AP} \tag{B.33}$$

$$= \frac{k_2E_0K_P([A_e] - [A_i])}{K_AK_P + K_PA + K_AP} \tag{B.34}$$

$$= \frac{V_A([A_e] - [A_i])}{K_A\left(1 + \frac{P}{K_P}\right) + A} \tag{B.35}$$

Where $V_A = k_2E_0$, similarly with $V_P = k_4E_0$;

$$\frac{d[P_i]}{dt} = \frac{V_P([P_e] - [P_i])}{K_P\left(1 + \frac{A}{K_A}\right) + P} \tag{B.36}$$

B.2.1 Volume fractions

The above derivation is valid if the extracellular volume fraction (α) is equal to the intracellular volume fraction (β). The concentrations are given by their relative volumes (2.5.2) and the second order reaction rates (with units $\mu\mathrm{M}^{-1}\mathrm{s}^{-1}$) may be scaled by the relevant volume fraction. Let the transporter $[E]$ and bound transporter $[EA]$ and $[EP]$ be represented by their total concentration, while adenosine and its breakdown products are represented by the relative concentration. Again using the quasi-steady-state assumptions (Eqs. B.15-B.17) gives;

$$\frac{d[EA]}{dt} = \frac{k_1}{\alpha}\alpha[A_e][E] + \frac{k_1}{\beta}\beta[A_i][E] - 2k_2[EA] \tag{B.37}$$

$$= 0 \tag{B.38}$$

Where $[A_e]$ is scaled by α to give the total concentration, similarly $[A_i]$ is scaled by β, as the reactions are then given in terms of total concentrations, the reactions rate k_1 is also scaled by the corresponding volume fraction. This is identical to (Eq. B.18), so $[EA]$ is given by (Eq. B.27) and $[EP]$ by (Eq. B.28). Then;

$$\frac{d\left[A_i\right]}{dt} = k_2 \frac{1}{\beta}\left[EA\right] - k_1 \frac{1}{\beta}\left[E\right]\left[A_i\right] \tag{B.39}$$

$$= \frac{1}{\beta} \frac{V_A\left(\left[A_e\right] - \left[A_i\right]\right)}{K_A\left(1 + \frac{P}{K_P}\right) + A} \tag{B.40}$$

Where $[EA]$ and $[E]$ are scaled by $\frac{1}{\beta}$ to give the relative concentration, as the reaction is in terms of the relative concentration, k_1 is not scaled by the volume fraction. Similarly;

$$\frac{d\left[A_i\right]}{dt} = \frac{1}{\alpha} k_2 \left[EA\right] - \frac{k_1}{\alpha}\left[E\right]\left[A_e\right] \tag{B.41}$$

$$= \frac{1}{\alpha} \frac{V_A\left(\left[A_i\right] - \left[A_e\right]\right)}{K_A\left(1 + \frac{P}{K_P}\right) + A} \tag{B.42}$$

Notice that as E_0 represents a total concentration, so unlike the enzyme kinetics V_A and V_P do not need to be scaled by the volume fraction (section 2.5.2). While k_1 and k_3 represent the relative rates

B.3 Low concentration limit

In low concentration limit the Michaelis-Manton kinetics are equal to first order removal rates $\mu_i = \frac{V_i}{K_i}$ and the description of the transporters (Eq.

B.43-B.46) are given by (Eq. B.47-B.50).

$$J_n^A = \frac{V_2 K_3 \left(A_n - A_e\right)}{K_2 K_3 + K_2 \left(P_e + P_n\right) + K_3 \left(A_e + A_n\right)} \tag{B.43}$$

$$J_n^P = \frac{V_3 K_2 \left(P_n - P_e\right)}{K_2 K_3 + K_2 \left(P_e + P_n\right) + K_3 \left(A_e + A_n\right)} \tag{B.44}$$

$$J_g^A = \frac{V_5 K_6 \left(A_g - A_e\right)}{K_5 K_6 + K_5 \left(P_e + P_g\right) + K_6 \left(A_e + A_g\right)} \tag{B.45}$$

$$J_g^P = \frac{V_6 K_5 \left(P_g - P_e\right)}{K_5 K_6 + K_5 \left(P_e + P_g\right) + K_6 \left(A_e + A_g\right)} \tag{B.46}$$

$$j_n^A = \mu_2 \left(A_n - A_e\right) \tag{B.47}$$

$$j_n^P = \mu_3 \left(P_n - P_e\right) \tag{B.48}$$

$$j_g^A = \mu_5 \left(A_g - A_e\right) \tag{B.49}$$

$$j_g^P = \mu_6 \left(P_g - P_e\right) \tag{B.50}$$

The low concentration limit for model IV is;

$$\frac{\partial A_e}{\partial t} = D\nabla^2 A_e - \mu_1 A_e + \frac{1}{\alpha}\left(j_n^A + j_g^A\right) + \frac{S}{\alpha}\delta\left(r\right) \tag{B.51}$$

$$\frac{\partial P_e}{\partial t} = D\nabla^2 A_e + \mu_1 A_e + \frac{1}{\alpha}\left(j_n^P + j_g^P\right) \tag{B.52}$$

$$\frac{dA_n}{dt} = -\frac{1}{\beta_n} j_n^A - \mu_4 A_n \tag{B.53}$$

$$\frac{dP_n}{dt} = -\frac{1}{\beta_n} j_n^P + \mu_4 A_n \tag{B.54}$$

$$\frac{dA_g}{dt} = -\frac{1}{\beta_g} j_g^A - \mu_7 A_g \tag{B.55}$$

$$\frac{dP_g}{dt} = -\frac{1}{\beta_g} j_g^P - \mu_8 P_g \tag{B.56}$$

In the steady-state the intracellular concentrations are proportional to the extracellular concentrations;

$$A_n^* = \frac{\mu_2}{\beta_n \mu_4 + \mu_2} A_e^* \tag{B.57}$$

$$P_n^* = P_e^* + \frac{\beta_n \mu_4}{\mu_3 \left(\beta_n \mu_4 + \mu_2\right)} A_e^* \tag{B.58}$$

$$A_g^* = \frac{\mu_5}{\mu_5 + \beta_g \mu_7} A_e^* \tag{B.59}$$

$$P_g^* = \frac{\mu_6}{\beta_g \mu_8 + \mu_6} P_e^* \tag{B.60}$$

Which gives the following steady-state transport by the ENTs;

$$\bar{j}_n^A = -\frac{\beta_n \mu_2 \mu_4}{\beta_n \mu_4 + \mu_2} A_e^* \tag{B.61}$$

$$\bar{j}_n^P = \frac{\beta_n \mu_3 \mu_4}{\beta_n \mu_4 + \mu_2} A_e^* \tag{B.62}$$

$$\bar{j}_g^A = -\frac{\beta_g \mu_5 \mu_7}{\mu_5 + \beta_g \mu_7} A_e^* \tag{B.63}$$

$$\bar{j}_g^P = -\frac{\beta_g \mu_6 \mu_8}{\beta_g \mu_8 + \mu_6} P_e^* \tag{B.64}$$

So the steady-state extracellular concentration are determined by two ODEs;

$$0 = D\nabla^2 A_e^* - \mu_1 A_e^* + \frac{1}{\alpha}\left(\bar{j}_n^A + \bar{j}_g^A\right) + \frac{S}{\alpha}\delta\left(r\right) \tag{B.65}$$

$$0 = D\nabla^2 A_e^* + \mu_1 A_e^* + \frac{1}{\alpha}\left(\bar{j}_n^P + \bar{j}_g^P\right) \tag{B.66}$$

Which can be rearranged as follows;

$$0 = \nabla^2 A_e^* - \frac{A_e^*}{\lambda^2} + \frac{S}{\alpha D}\delta\left(r\right) \tag{B.67}$$

$$0 = \nabla^2 P_e^* + \frac{A_e^*}{\kappa_1^2} - \frac{P_e^*}{\kappa_2^2} \tag{B.68}$$

Where;

$$\lambda = \sqrt{D\left(\mu_1 + \frac{1}{\alpha}\left(\frac{\beta_n \mu_2 \mu_4}{\beta_n \mu_4 + \mu_2} + \frac{\beta_g \mu_5 \mu_7}{\mu_5 + \beta_g \mu_7}\right)\right)^{-1}} \tag{B.69}$$

$$\kappa_1 = \sqrt{D\left(\mu_1 + \frac{1}{\alpha}\frac{\beta_n \mu_3 \mu_4}{\beta_n \mu_4 + \mu_2}\right)^{-1}} \tag{B.70}$$

$$\kappa_2 = \sqrt{D\alpha\frac{\beta_g \mu_8 + \mu_6}{\beta_g \mu_6 \mu_8}} \tag{B.71}$$

Solutions in spherical coordinates are found by using the boundary condition $A_e^*(r) \to 0$ as $r \to \infty$ and by using the divergence theorem to equate the surface integrated of the ODE with the volume integral of the source term as the radium of the volume goes to zero. The same approach yields a solutions

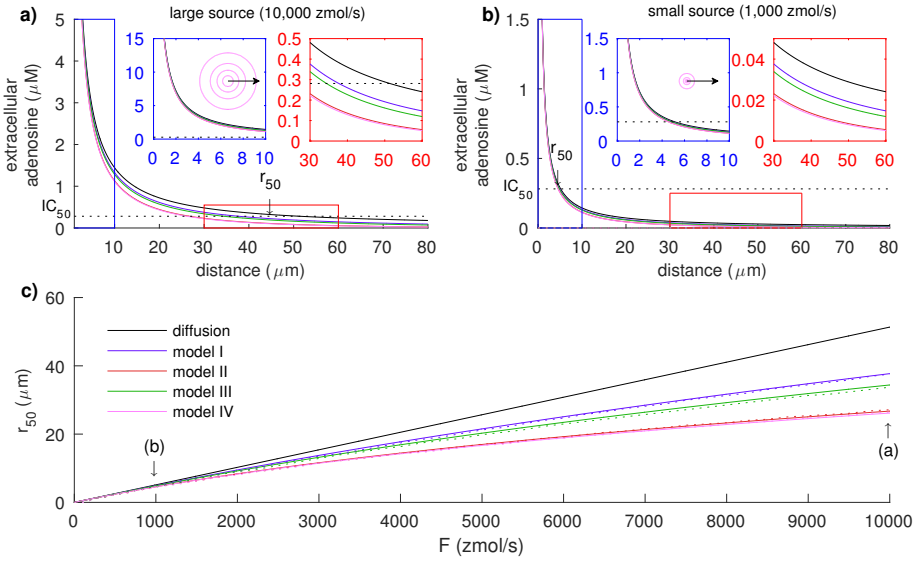

Figure B.1: **The low concentration limit provides a good approximation for a wide range of sources because the concentration is rapidly diminished by diffusion.** Examples of relatively; **a)** large source $(10,000\text{zmol/s})$ and **b)** small source $(1,000\text{zmol/s})$ are shown with enlargements close (blue box) and far (red box) from the source. The radius at which the concentration reaches IC_{50} is indicated with an arrow labelled r_{50}. Contour plots show the inhibitory concentration of 20%, 40%, 60% and 80% of A_1R, with scale arrow of $50\mu\text{m}$. **c)** Shows how the maximum distance at which the concentration exceeds the IC_{50} increases with the source intensity in the low concentration limit (solid lines) for each of the models. The dashed show the numerical solution are almost identical to the low concentration limit.

for P_e, as follows;

$$A_e^*(r) = \frac{S}{4\pi D\alpha r}\exp\left(-\frac{r}{\lambda}\right) \tag{B.72}$$

$$P_e^*(r) = \frac{S\kappa_2^2\lambda^2}{4\pi D\alpha\kappa_1^2\left(\kappa_2^2-\lambda^2\right)r}\left(\exp\left(-\frac{r}{\kappa_2}\right)-\exp\left(-\frac{r}{\lambda}\right)\right) \tag{B.73}$$

These solutions (Figure B.1a,b) are obtained from the general solution, which has the form;

$$A_e(r) = K_1\frac{e^{-\frac{r}{\lambda}}}{r} + K_2\frac{e^{\frac{r}{\lambda}}}{r} \tag{B.74}$$

$$\lim_{r\to\infty} A_e(r) = 0 \tag{B.75}$$

So

$$A_e(r) = K_1 \frac{e^{-\frac{r}{\lambda}}}{r} \tag{B.76}$$

Then by considering an integral of a sphere about the source of radius epsilon;

$$\int\int\int_{V_\epsilon} dV A_e = \int\int\int_{V_\epsilon} dV \frac{F}{D\alpha}\delta(r) \tag{B.77}$$

by the Divergence theorem;

$$4\pi \left[r^2 \nabla \cdot A_e(r)\right]_0^\epsilon = -\frac{F}{D\alpha} \tag{B.78}$$

$$4K\pi e^{-\frac{\epsilon}{\lambda}} \left(1 - \frac{\epsilon}{\lambda}\right) = -\frac{F}{D\alpha} \tag{B.79}$$

Taking the limit $\epsilon \to 0$

$$K = \frac{F}{4\pi D\alpha} \tag{B.80}$$

The range of influence (r_{50}), characterised by the distance where the concentration exceeds the IC_{50}, is determined as;

$$\frac{F}{4\pi\alpha D r_{50}} \exp\left(-\frac{r_{50}}{\lambda}\right) = IC_{50} \tag{B.81}$$

$$\frac{r_{50}}{\lambda} \exp\left(-\frac{r_{50}}{\lambda}\right) = \frac{F}{4\pi\alpha D\lambda IC_{50}} \tag{B.82}$$

Let $z = \frac{r_{50}}{\lambda}$ then;

$$ze^z = \frac{F}{4\pi\alpha D\lambda IC_{50}} \tag{B.83}$$

$$r_{50} = \frac{1}{\lambda} W\left(\frac{F}{4\pi\alpha D\lambda IC_{50}}\right) \tag{B.84}$$

Where W is the product-log function (Figure B.1c). The low concentration limit for the other models are determined by removing the terms for the appropriate clearance mechanisms and provides a good approximation for a wide range of source terms Figure B.1c.

B.4 High concentration limit

A similar limit can be found for high extracellular concentration of adenosine. In this case

$$\frac{\partial A_e}{\partial t} = D\nabla^2 A_e - V_1 - \frac{1}{\alpha}\left(\phi_n^A + \phi_g^A\right) + \frac{S(t,r)}{\alpha} \tag{B.85}$$

$$\phi_n^A = V_2 \frac{1}{A_e}\left[\frac{K_2K_3 + K_2\left(P_e + P_n\right) + 2K_3A_n - K_3A_e}{K_3A_e}\right] + O\left(\frac{1}{A_e^2}\right) \tag{B.86}$$

$$\phi_n^A = V_5 \frac{1}{A_e}\left[\frac{K_5K_6 + K_5\left(P_e + P_g\right) + 2K_6A_g - K_6A_e}{K_3A_e}\right] + O\left(\frac{1}{A_e^2}\right) \tag{B.87}$$

If the concentration of the breakdown products is far lower than that of extracellular adenosine then the transport occurs at its maximum velocity and the model IV is;

$$\frac{\partial A_e}{\partial t} = D\nabla^2 A_e - V_{\max} + \frac{S(t,r)}{\alpha} \tag{B.88}$$

$$V_{\max} = V_1 + \frac{1}{\alpha}\left(V_2 + V_5\right) \tag{B.89}$$

Where V_2 is the maximum uptake by neurons and V_5 is the maximum uptake by glia (these terms can be removed to given the maximum velocity in models I, II and III). If the concentration of breakdown products is also high, this approximation is invalid as transport between the intracellular and extracellular space will be far slower.

B.5 Solution for the diffusion model

For model zero, where only diffusion is included the solution for a constant point source F [zmol/s] is found in the same way as the solution of the low concentration limit (section B.3. The general solution is;

$$A_e(r) = \frac{K}{r} \tag{B.90}$$

By integrating over a small sphere about the origin;

$$\int\int\int_{V_\epsilon} dV\, A_e = \int\int\int_{V_\epsilon} dV \frac{F}{D\alpha}\delta(r) \tag{B.91}$$

Using the divergence theorem on the left-hand side

$$\lim_{\epsilon \to 0} 4\pi \left[r^2 \nabla \cdot A_e(r) \right]_0^{\epsilon} = \frac{F}{D\alpha} \tag{B.92}$$

$$4\pi K = \frac{F}{D\alpha} \tag{B.93}$$

$$A_e(r) = \frac{F}{4\pi D\alpha r} \tag{B.94}$$

For a brief point source at the origin, the solution to the diffusion equation in spherical coordinates is given by;

$$A_e(t, r) = \frac{F_0 \exp\left(-\frac{r^2}{4Dt}\right)}{\sqrt{6\pi}\alpha \left(Dt\right)^{\frac{3}{2}}} \tag{B.95}$$

So the peak concentration at $r = 0$ has the form;

$$A_e(t, 0) = \frac{F_0}{\sqrt{6\pi}\alpha \left(Dt\right)^{\frac{3}{2}}} \tag{B.96}$$

$$t_{50} = \frac{F_0^{\frac{2}{3}}}{\left(6\pi D^3 \alpha^2 I C_{50}^2\right)^{\frac{1}{3}}} \tag{B.97}$$

Which gives the scaling $t_{50} \sim F_0^{\frac{2}{3}}$ observed (Figure 3.9o).

B.6 Intracellular steady-state concentrations

B.6.1 Neuronal intracellular steady-state

Suppose the extracellular concentration is fixed by altering the source intensity and glial metabolism. Then the neuronal steady state solution is determined from the extracellular concentration of adenosine A_e and its breakdown products P_e by solving a cubic. Using the equation for the steady state of intracellular breakdown products, allows P_n to be written in terms of A_n

$$0 = -\frac{K_2 V_3 \left(P_n - P_e\right)}{K_2 K_3 + K_2 \left(P_e + P_n\right) + K_3 \left(A_e + A_n\right)} + \beta_n \frac{V_4 A_n}{K_4 + A_n} \tag{B.98}$$

$$P_n = \frac{q_0 A_n^2 + q_1 A_n + q_2}{q_3 A_n + q_4} \tag{B.99}$$

Where

$$q_0 = \beta_n K_3 V_4 \tag{B.100}$$

$$q_1 = K_2 V_3 P_e + \beta_n V_4 \left(K_2 K_3 + K_2 P_e + K_3 A_e\right) \tag{B.101}$$

$$q_2 = K_2 K_4 V_3 P_e \tag{B.102}$$

$$q_3 = K_2 V_3 - \beta_n K_2 V_4 \tag{B.103}$$

$$q_4 = K_2 K_4 V_3 \tag{B.104}$$

Then by substituting into the equation for the steady state of neuronal adenosine, the neuronal concentration of adenosine is given by roots of the cubic;

$$0 = \frac{K_2 V_3 \left(A_n - A_e\right)}{K_2 K_3 + K_2 \left(P_e + P_n\right) + K_3 \left(A_e + A_n\right)} + \beta_n \frac{V_4 A_n}{K4 + A_n} \tag{B.105}$$

$$0 = b_3 A_n^3 + b_2 A_n^2 + b_1 A_n + b_0 \tag{B.106}$$

Where

$$b_3 = K_2 K_3 \left(V_2 V_3 + \beta_n V_4 \left(V_3 - V_2\right)\right) \tag{B.107}$$

$$\begin{aligned} b_2 = {} & K_2 K_3 V_2 V_3 \left(2K_4 - A_e\right) \\ & + \beta_n K_2 V_4 \left(K_3 V_2 \left(A_e - K_4\right) + V_3 \left(K_3 \left(K_2 + K_4 + A_e\right) + 2K_2 P_e\right)\right) \end{aligned} \tag{B.108}$$

$$\begin{aligned} b_1 = {} & K_2 K_4 \left(K_3 V_2 V_3 \left(K_4 + A_e - 2\right)\right. \\ & \left. + \beta_n V_3 \left(K_2 \left(K_3 + 2P_e\right) + K_3 V_4 \left(V_2 + V_3\right) A_e\right)\right) \end{aligned} \tag{B.109}$$

$$b_0 = -K_2 K_3 K_4^2 V_2 V_3 A_e \tag{B.110}$$

Numerical evaluation of this solution for a physiological range of extracellular concentrations, shows three real solutions, one positive and two negative. As the discriminant is always greater than zero for any extracellular concentration (with parameters given in Table 2.3 and Table 2.2), by considering the sum and product of the roots, it is clear that there is only one positive root for all extracellular concentrations. The product of the roots is given

by;

$$-\frac{b_0}{b_3} = \frac{K_4^2 V_2 V_3}{V_2 V_3 + \beta_n V_4 (V_3 - V_2)} A_e \tag{B.111}$$

$$\approx 1300 A_e \tag{B.112}$$

Notice that the denominator is positive for the parameters for the rat cortex, and will be non-negative provided;

$$V_3 \geq \beta_n V_4 \tag{B.113}$$

Or if

$$V_3 < \beta_n V_4 \tag{B.114}$$

$$V_2 \geq \frac{\beta_n V_3 V_4}{\beta_n V_4 - V_3} \tag{B.115}$$

The parameters used have $V_2 = V_3$ so as $A_e \geq 0$ there could either be one positive and two negative roots or three positive roots. The sum of the roots is;

$$-\frac{b_2}{b_3} = \frac{K_3 V_2 V_3 (A_e - 2K_4) - \beta_n V_4 (K_3 V_2 (A_e - K_4) + V_3 (K_3 (A_e + K_2 + K_4) + 2K_2 P_e))}{K_3 V_4 (V_2 V_3 + \beta_n (V_3 - V_2))} \tag{B.116}$$

$$\approx -12A - 13P - 100 < 0 \tag{B.117}$$

The sum of the roots must be negative, so there cannot be three positive roots, therefore there must always be one positive and two negative roots with the parameters values found for the rat cortex. The parameters found for the rat cortex give $b_3 > 0$, instead if $b_3 < 0$ then (B.111) is negative so there is either one negative and two positive roots or three negative roots, if additionally $K_3 > \frac{\beta_n V_4 (V_2 + V_3)}{V_2 V_3}$ then (B.116) is positive, so there must be one negative and two positive roots.

There is a bifurcation at $b_3 = 0$ where the intracellular steady state are roots of a quadratic rather than a cubic and the value of b_3 depend on the balance between adenosine transport V_2 and intracellular ADA V_4, these vary considerably with species brain region, *e.g.* no intracellular ADA observed

red in the hippocampus (Yamamoto et al. 1987), ENT also varies between brain regions *e.g.* Western blots show around a 10% decrease in ENT1 and a 150% in ENT2 in the rat hypothalamus compared to the cortex (Alanko et al. 2006).

Numerical solutions for the intracellular concentrations are found with 100nM of extracellular adenosine and 100nM of breakdown products over a range of V_2 and V_4 (Figure B.2), similar results are found for equal concentration of adenosine and breakdown products and with more adenosine then breakdown products. The stability of these steady states are determined by evaluating eigenvalues of model II (section B.7). There is only one non-negative solution for both adenosine and the breakdown products and it is stable, the unstable solution (Figure B.2a,b) has positive adenosine but negative breakdown products, whereas the unstable solution (Figure B.2c,d) has positive breakdown products by negative adenosine. Notice when $b_3 = 0$ (shown by the contour) the solutions are equal. There is a third solution of the cubic, where both adenosine and the breakdown products are negative, such that the denominators of both the terms for the transports and for ADA are zero. The neuronal steady-state has only one valid solution and it is stable, regardless of the balance between transport and metabolism.

B.6.2 Glial intracellular steady-state

The glial intracellular steady-state concentration can be determined, again by fixing the extracellular concentrations and solving the intracellular steady-state. It can be shown that there is at most one steady-state solution for

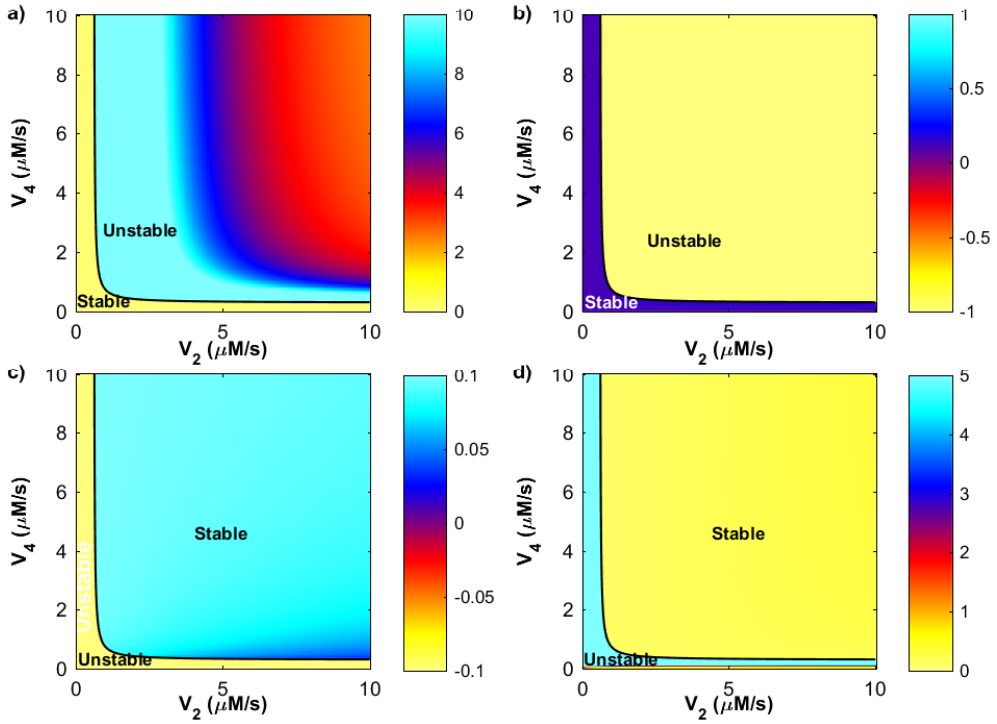

Figure B.2: **The steady-state neuronal concentrations for a range of transport and V_2 and metabolism V_4 maximum velocities show there is only one valid stable solution.** With 100μM extracellular adenosine and 100μM extracellular breakdown products. The neuronal adenosine concentrations **a), c)** and breakdown product concentrations **b), d)** are shown for two solutions of (Eq. B.106), with a contour $b_3 = 0$ where the two solutions are equal. Labels indicate the stability of the regions determined by the eigenvalues of model II.

the intracellular concentration.

$$0 = r_3 A_g P_g + r_2 P_g^2 + r_1 P_g + r_0 \tag{B.118}$$

$$r_3 = \beta_g \mu_8 K_6 \tag{B.119}$$

$$r_2 = \beta_g \mu_8 K_5 \tag{B.120}$$

$$r_1 = \beta_g \mu_8 K_6 A_e + K_5 \left(V_6 + \beta_g \mu_8 \left(K_6 + P_e\right)\right) \tag{B.121}$$

$$r_0 = -K_5 V_6 P_e \tag{B.122}$$

$$0 = c_3 A_g P_g + c_2 A_g^2 + c_1 A_g + c_0 \tag{B.123}$$

$$c_3 = -\beta_g K_5 V_7 \tag{B.124}$$

$$c_2 = K_6 \left(\beta_g V_7 + V_5\right) \tag{B.125}$$

$$c_1 = K_6 K_7 V_5 + \beta_g K_5 \left(K_6 + P_E\right) V_7 + K_6 \left(\beta_g V_7 - V_5\right) A_e \tag{B.126}$$

$$c_0 = -K_6 K_7 V_5 A_e \tag{B.127}$$

By equating (Eq. B.118) and (Eq. B.123) the glial adenosine steady-state concentration is given by the roots of a quadratic for some concentration of the breakdown products;

$$0 = \frac{c_2}{c_3} A_g^2 + \frac{c_1}{c_3} A_g + f(P_g) \tag{B.128}$$

The sum of the roots is given by $-\dfrac{c_1}{c_2} < 0$ as c_1 and c_2 are positive as $\beta_g V_7 > V_5$ for the rat cortex, this means that for any $f\left(P_g\right)$ there is at most one positive solution for the steady-state concentration of adenosine. Conversely P_g can be expressed as a quadratic of the form;

$$0 = \frac{r_2}{r_3} P_g^2 + \frac{r_1}{r_3} A_g + f(A_g) \tag{B.129}$$

The sum of the roots is given by $-\dfrac{r_1}{r_2} < 0$ as r_1 and r_2 are positive, so for any steady-state concentration of adenosine, there is at most one positive solution for the steady-state concentration of the breakdown products.

Substitution of (Eq. B.118) into (Eq. B.123) yields a quartic in A_g;

$$0 = a_4 A_g^4 + a_3 A_g^3 + a_2 A_g^2 + a_1 A_g^1 + a_0 \tag{B.130}$$

$$a_4 = \beta_g^2 K_5^2 K_6 \mu_8^2 V_5 \tag{B.131}$$

$$\begin{aligned} a_3 = {} & \beta_g K_5 K_6 \mu_8 \left[2K_5 V_5 V_6 + \beta_g K_5 V_6 V_7 \right. \\ & \left. + \beta_g \mu_8 V_5 \left(3A_e K_6 - K_6 K_7 + 2K_5 \left(K_6 + P_e\right)\right)\right] \end{aligned} \tag{B.132}$$

$$\begin{aligned} a_2 = {} & K_6 \left[2A_e^2 \beta_g^2 K_6^2 \mu_8^2 V_5 \right. \\ & + A_e \beta_g K_6 \mu_8 \left(\beta_g \mu_8 \left(-2K_6 K_7 + 3K_5 \left(K_6 + P_e\right)\right) V_5 + 3K_5 V_5 V_6 + \beta_g K_5 V_6 V_7\right) \\ & + K_5 \left[V_5 \left(\beta_g^2 \mu_8^2 \left(K_6 + P_e\right) \left(-K_6 K_7 + K_5 \left(K_6 + P_e\right)\right) + \beta_g K_6 \left(2K_5 - K_7\right) \mu_8 V_6 + K_5 V_6^2\right)\right. \\ & \left. \left. + \beta_g K_5 V_6 \left(\beta_g K_6 \mu_8 + V_6\right) V_7\right]\right] \end{aligned} \tag{B.133}$$

$$\begin{aligned} a_1 = {} & K_5 P_e V_6 \left[-2K_6 \left(A_e \beta_g K_6 \mu_8 + K_5 \left(\beta_g \mu_8 \left(K_6 + P_e\right) + V_6\right)\right) \left(V_5 + \beta_g V_7\right) \right. \\ & \left. + \beta_g K_6 \mu_8 \left(K_6 K_7 V_5 + \beta_g K_5 \left(K_6 + P_e\right) V_7 + A_e K_6 \left(-V_5 + \beta_g V_7\right)\right)\right] \end{aligned} \tag{B.134}$$

$$a_0 = K_5^2 K_6 P_e^2 V_6^2 \left(V_5 + \beta_g V_7\right) \tag{B.135}$$

Numerically evaluating the discriminant suggests it is positive for any extracellular concentration (for the parameters of the rat cortex), so there are four distinct real solutions.

The product of the roots $\frac{a_4}{a_0}$ is positive as both a_4 and a_0 are positive, while the sum of the roots $-\frac{a_3}{a_4}$ is negative as a_3 is also positive (for the parameters of the rat cortex). So there must be two positive and two negative roots. Therefore there is exactly one solution of (Eq. B.118) and (Eq. B.123) where both A_g and P_g are positive. The stability of the solution is determined by considering the eigenvalues for model III, which are all negative so it is a stable solution (section B.7).

B.7 Stability of the steady-state solutions

The simplest case to consider is that of a constant uniform of intensity C [nM/s]. The concentration of breakdown products in models I and II clearly diverge, however there is still a steady-state solution for the extracellular

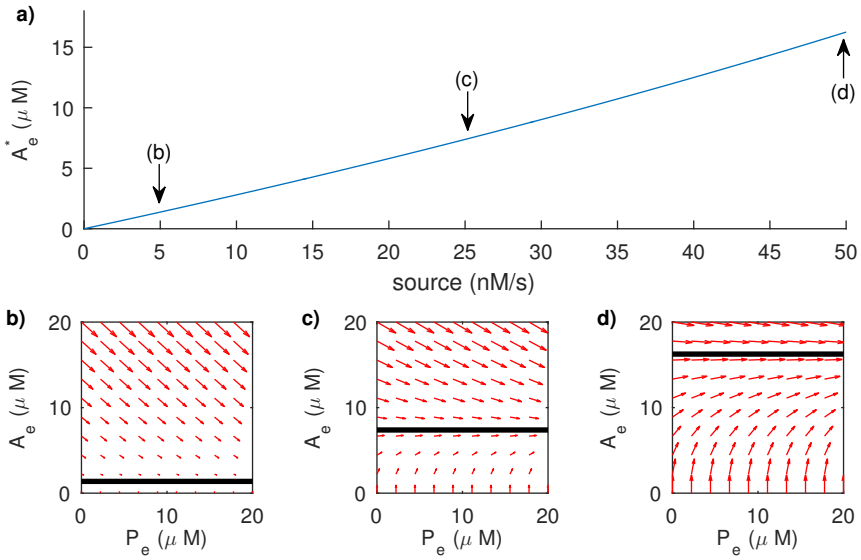

Figure B.3: **For constant uniform source in models I and II, the extracellular adenosine concentration reaches a steady-state (A_e^*) but the breakdown products accumulate indefinitely. a)** shows the steady-state extracellular adenosine concentration resulting from a given source intensity. With example phase portraits for a source of **b)** 5nM/s **c)** 25nM/s and **d)** 50nM/s. In each case there is a steady-state solution of extracellular adenosine (A_e), but not for the breakdown products (P_e).

adenosine, shown by the phase portraits (Figure B.3).

The models with the parameters for the rat cortex (Table 2.3 and Table 2.2) have only one steady-state solution (section B.6) and it is stable. The solution of characteristic equation for the Jacobian about the steady-state can be found algebraically, however the resulting expression for the eigenvalues for model II-IV are uninformative, (as roots of a 4th-6th order polynomial). Instead the numerical values of the eigenvalues are determined for the model with the current parameter values.

In this case model I and II are equivalent and have eigenvalue;

$$\tau_1 = -\frac{V_1 K_1}{(K_1 + A_e^*)^2} \tag{B.136}$$

In general the eigenvalues, (Figure B.4) are obtained from the Jacobian;

$$N_d = \left(K_2K_3 + K_3\left(A_e^* + A_n^*\right) + K_2\left(P_e^* + P_n^*\right)\right)^2 \tag{B.137}$$

$$G_d = \left(K_5K_6 + K_6\left(A_e^* + A_g^*\right) + K_5\left(P_e^* + P_g^*\right)\right)^2 \tag{B.138}$$

$$\mu_1 = \frac{V_1K_1}{\left(K_1 + A^*\right)^2} \tag{B.139}$$

$$\mu_{2a} = K_3V_2\frac{2A_n^*K_3 + K_2K_3 + K_2\left(P_e^* + P_n^*\right)}{N_d} \tag{B.140}$$

$$\mu_{2b} = K_3V_2\frac{2A_e^*K_3 + K_2K_3 + K_2\left(P_e^* + P_n^*\right)}{N_d} \tag{B.141}$$

$$\mu_{2p} = K_2K_3V_2\frac{A_e^* - A_n^*}{N_d} \tag{B.142}$$

$$\mu_{3p} = V_3K_2\frac{2P_n^*K_2 + K_2K_3 + K_3\left(A_e^* + A_n^*\right)}{N_d} \tag{B.143}$$

$$\mu_{3q} = V_3K_2\frac{2P_e^*K_2 + K_2K_3 + K_3\left(A_e^* + A_n^*\right)}{N_d} \tag{B.144}$$

$$\mu_{3a} = K_2K_3V_3\frac{P_e^* - P_n^*}{N_d} \tag{B.145}$$

$$\mu_4 = \frac{V_4K_4}{\left(K_4 + A_n^*\right)^2} \tag{B.146}$$

$$\mu_{5a} = K_6V_5\frac{2A_g^*K_6 + K_5K_6 + K_5\left(P_e^* + P_g^*\right)}{G_d} \tag{B.147}$$

$$\mu_{5c} = V_5K_6\frac{2A_e^*K_6 + K_5K_6 + K_5\left(P_e^* + P_g^*\right)}{G_d} \tag{B.148}$$

$$\mu_{5p} = K_5K_6V_5\frac{A_e^* - A_g^*}{G_d} \tag{B.149}$$

$$\mu_{6p} = V_6K_5\frac{2P_g^*K_5 + K_5K_6 + K_6\left(A_e^* + A_g^*\right)}{G_d} \tag{B.150}$$

$$\mu_{6q} = V_6K_5\frac{2P_e^*K_5 + K_5K_6 + K_6\left(A_e^* + A_g^*\right)}{G_d} \tag{B.151}$$

$$\mu_{6a} = K_5K_6V_6\frac{P_e^* - P_g^*}{G_d} \tag{B.152}$$

Model	τ_1 (min^{-1})	τ_2 (min^{-1})	τ_3 (min^{-1})	τ_4 (min^{-1})	τ_5 (min^{-1})	τ_6 (min^{-1})
I) Extracellular only	1.06					
II) Extracellular & neuronal	1.06					
III) Extracellular & glial						
Slow Removal $\mu_8 = 5\times10^{-4}$/s	0.011	2.32	3.62	96.53		
Fast Removal $\mu_8 = 5$/s	0.022	0.039	1.61	5.04		
IV) Extracellular, neuronal & glial						
Slow Removal $\mu_8 = 5\times10^{-4}$/s	0.0044	2.63	5.17	28.01	30.82	96.54
Fast Removal $\mu_8 = 5$/s	0.38	5.17	27.91	30.81	96.54	302.31

Table B.1: **All models have a stable steady-state solution.** Decay rates at which small perturbations form the low concentration limit will decay to the stable steady-state solution.

$$J = \begin{pmatrix} -\mu_1 - \frac{\mu_{2a}}{\alpha} - \frac{\mu_{5a}}{\alpha} & \frac{\mu_{5p}}{\alpha} + \frac{\mu_{2p}}{\alpha} & \frac{\mu_{2b}}{\alpha} & \frac{\mu_{2p}}{\alpha} & \frac{\mu_{5c}}{\alpha} & \frac{\mu_{5p}}{\alpha} \\ \mu_1 + \frac{\mu_{3a}}{\alpha} + \frac{\mu_{6a}}{\alpha} & -\frac{\mu_{3p}}{\alpha} - \frac{\mu_{6p}}{\alpha} & \frac{\mu_{3a}}{\alpha} & \frac{\mu_{3q}}{\alpha} & \frac{\mu_{6a}}{\alpha} & \frac{\mu_{6q}}{\alpha} \\ \frac{\mu_{2a}}{\beta_n} & -\frac{\mu_{2p}}{\beta_n} & -\mu_4 - \frac{\mu_{2b}}{\beta_n} & -\frac{\mu_{2p}}{\beta_n} & 0 & 0 \\ -\frac{\mu_{3a}}{\beta_n} & \frac{\mu_{3p}}{\beta_n} & \mu_4 - \frac{\mu_{3a}}{\beta_n} & -\frac{\mu_{3q}}{\beta_n} & 0 & 0 \\ \frac{\mu_{5a}}{\beta_g} & -\frac{\mu_{5p}}{\beta_g} & 0 & 0 & -\mu_7 - \frac{\mu_{5c}}{\beta_g} & -\frac{\mu_{5p}}{\beta_g} \\ -\frac{\mu_{6a}}{\beta_g} & \frac{\mu_{6p}}{\beta_g} & 0 & 0 & -\frac{\mu_{6a}}{\beta_g} & -\frac{\mu_{6q}}{\beta_g} - \mu_8 \end{pmatrix} \tag{B.153}$$

Where the values of μ_i depend on the steady state concentrations and are given by equations (Eq. B.139)-(Eq. B.152). In the low concentration limit this is given by (Eq. B.154) which gives the eigenvalues in Table B.1.

$$J = \begin{pmatrix} -\mu_1 - \frac{\mu_2}{\alpha} - \frac{\mu_5}{\alpha} & 0 & \frac{\mu_2}{\alpha} & 0 & \frac{\mu_5}{\alpha} & 0 \\ \mu_1 & -\frac{\mu_3}{\alpha} - \frac{\mu_6}{\alpha} & 0 & \frac{\mu_3}{\alpha} & 0 & \frac{\mu_6}{\alpha} \\ \frac{\mu_2}{\beta_n} & 0 & -\mu_4 - \frac{\mu_2}{\beta_n} & 0 & 0 & 0 \\ 0 & \frac{\mu_3}{\beta_n} & \mu_4 & -\frac{\mu_3}{\beta_n} & 0 & 0 \\ \frac{\mu_5}{\beta_g} & 0 & 0 & 0 & -\mu_7 - \frac{\mu_5}{\beta_g} & 0 \\ 0 & \frac{\mu_6}{\beta_g} & 0 & 0 & 0 & -\frac{\mu_6}{\beta_g} - \mu_8 \end{pmatrix} \tag{B.154}$$

Where the values of $\mu_i = \frac{V_i}{K_i}$.

B.8 Model sensitivity

The local sensitivity is determined for by taking the partial derivative of the state of the model with respect to each parameter in turn. For a constant

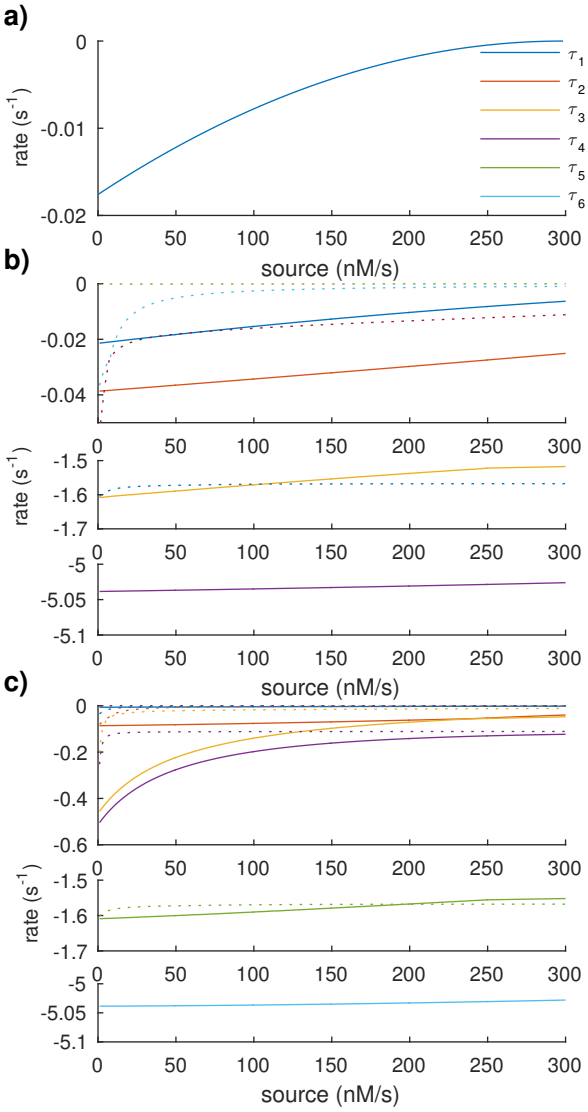

Figure B.4: **All the eigenvalues are negative and tend towards zero as the source intensity increases**. The eigenvalues of **a)** models I and II, **b)** model III **c)** model IV. The dashed lines show the eigenvalues for slow removal of breakdown products in glia ($\mu_8 = 5 \times 10^{-4}$/s) while solid lines show the eigenvalues with fast removal ($\mu_8 = 5$/s)

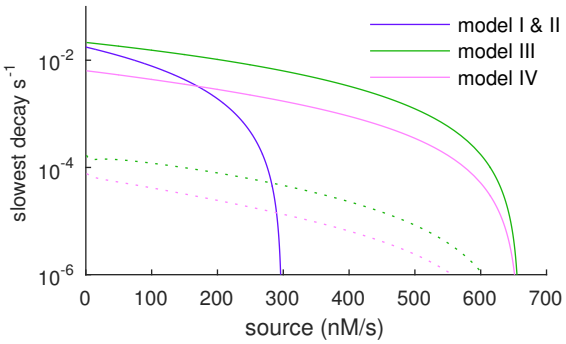

Figure B.5: **The slowest decay rate for each model tends to zero as the source intensity increases and overwhelms the clearance mechanisms.** The dashed lines for models III and IV indicate the slowest decay rate with slow breakdown products in glia ($\mu_8 = 5 \times 10^{-4}$/s) while solid lines correspond with fast removal ($\mu_8 = 5$/s)

uniform source the derivative of steady-state adenosine with respect to each parameter is shown in (Figure B.6) and (Figure B.7). For model I these are;

$$\left|\frac{\partial A_e^*}{\partial V_1}\right| = \frac{\alpha C K_1}{\alpha V_1 - C} \tag{B.155}$$

$$\left|\frac{\partial A_e^*}{\partial K_1}\right| = \frac{C}{\alpha V_1 - C} \tag{B.156}$$

where C [μM/s] is the source. Like the steady-state extracellular concentration of adenosine, the senility of parameters V_1 (Eq. B.155) and K_1 (Eq. B.156) diverges when the source intensity is greater than the maximum removal velocity. They increase monotonically with the adenosine concentration (Figure B.6a,e) and the sensitivities are greater for model I than models III and IV (for the same source) as there are no other clearance mechanisms. However a larger source is required in models III and IV to achieve the same adenosine tone, so models III and IV are more sensitive to changes in V_1 at a given steady-state adenosine concentration. Local sensitivity of the parameters in models III and IV are determined for the PDE

for A_e as follows;

$$\frac{\partial A_e}{\partial t} = \frac{J_n^A(A_e, A_n, P_e, P_n) + J_g^A(A_e, A_g, P_e, P_g}{\alpha} - \frac{V_1}{K_1 + A_e} + \frac{C}{\alpha} \tag{B.157}$$

$$\left|\frac{\partial A_e^*}{\partial p_i}\right| = \left|\frac{\frac{\partial}{\partial p_1}\frac{\partial A_e}{\partial t}}{\frac{\partial}{\partial A_e}\frac{\partial A_e}{\partial t}}\right| \tag{B.158}$$

where p_i is the parameter being considered. In model IV the neuronal transport of breakdown products (Figure B.6c,g) are the most sensitive parameters, as the breakdown products from the neurons need to be transported to the extracellular space so they can be removed by glia. The steady-state is less sensitive to changes in the parameters for transport of adenosine (Figure B.6b,f) and the neuronal metabolism by ADA (Figure B.6d,h). The sensitivities reach a peak value and then decline for increasing adenosine tone, this is because the intracellular neuronal concentration of adenosine reaches a peak as the transporters saturate. There is greater sensitivity for the maximum velocity of breakdown products in glia V_6 than adenosine transport V_5 (Figure B.6i,j), as the primary role of glia in the steady-state arising from a uniform source, is the removal of breakdown products. The sensitivity to the unsaturating removal rate μ_8 is relatively small except for model IV with slow removal, where the accumulation of breakdown products inhibits transport (Figure B.6l).

While the volume fractions were used in determining the correct MM parameters for the relative concentration (Table 2.3), here the MM parameters are fixed and the changes in volume fraction only influence transport between intracellular and extracellular space. The neuronal volume fraction β_n is the least sensitive volume fraction (Figure B.7b), as the steady-state is primarily determined by the removal of breakdown products by glia. With slow removal of breakdown products $\mu_8 = 5 \times 10^{-4}$/s the steady-state is far less senility to changes in the glial volume fraction β_g (Figure B.7c), as the clearance of breakdown products limited by the slow removal rather than transporters.

The same local sensitivity analysis can be applied to steady-state resulting from a constant point source in the low concentration limit, which provides

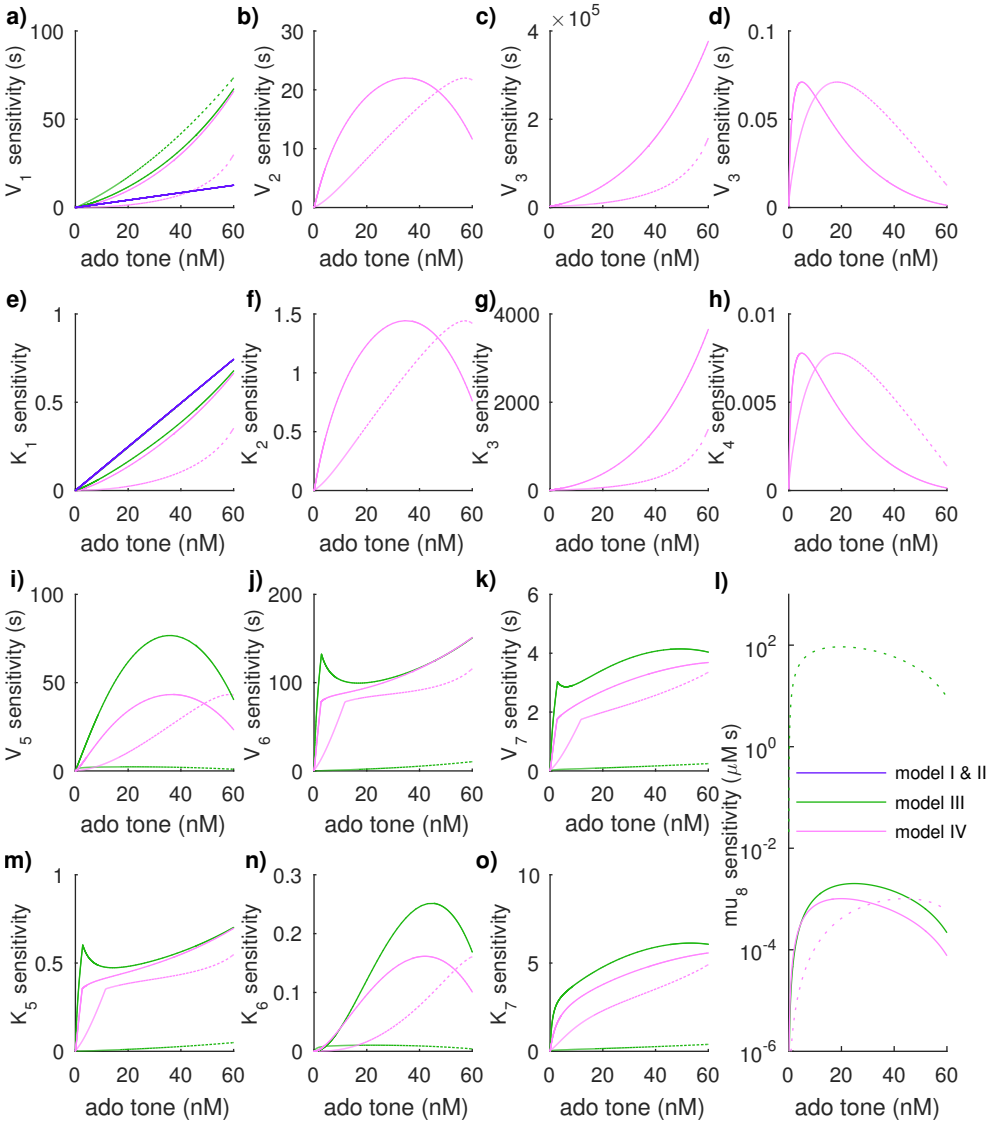

Figure B.6: **The adenosine tone in model IV is most sensitive to changes in neuronal transport of breakdown products**. Because the adenosine tone is dependant on neuronally derived breakdown products being removed by glia. Sensitivity of parameters for; **a), e)** ecto-ADA, **b), f)** neuronal adenosine transport, **c), g)** neuronal transport of breakdown products, **d), h)** neuronal ADA, **i),m)** glial adenosine transport, **j), n)** glial transport of breakdown products, **k), o)** glial ADK and **l)** unsaturating removal of breakdown products in glia. The dashed lines show the sensitivity for slow removal of breakdown products in glia ($\mu_8 = 5 \times 10^{-4}$/s) while solid lines show the sensitivity with fast removal ($\mu_8 = 5$/s)

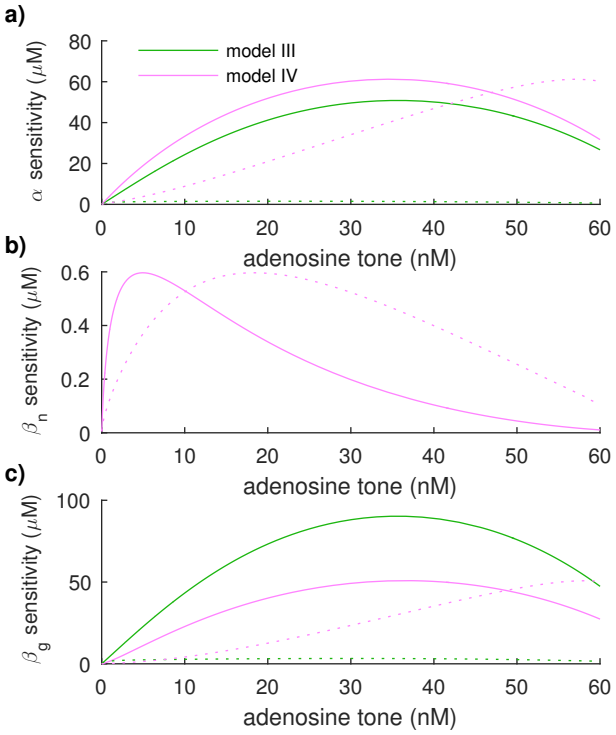

Figure B.7: **The adenosine tone is more sensitive to the extracellular or glial volume fraction than the neuronal volume fraction**. Sensitivity of the adenosine tone to volume fraction; **a)** extracellular, **b)** neuronal, **c)** glial. The dashed lines show the sensitivity for slow removal of breakdown products in glia ($\mu_8 = 5 \times 10^{-4}$/s) while solid lines show the sensitivity with fast removal ($\mu_8 = 5$/s)

a good approximation for a range of source intensities because of rapid diffusion in the ECS (section 3.2). The characteristic length scale is a function of the parameters $\lambda(p)$, so the local sensitivity of the range of influence is given by;

$$\frac{\partial A_e(r_{50})}{\partial p_i} = \left(W\left(\frac{F}{4\pi D\alpha IC_{50}\lambda(p)}\right)^2 \frac{\partial \lambda(p)}{\partial p_i} \right) \left(1 + W\left(\frac{F}{4\pi D\alpha IC_{50}\lambda(p)}\right)\right)^{-1} \tag{B.159}$$

$$= \frac{r_{50}\dfrac{\partial \lambda(p)}{\partial p_i}}{\lambda(p) + r_{50}} \tag{B.160}$$

Where p_i is one of the clearance parameters IC_{50} is the concentration that will halve an EPSP. The sensitivities increase monotonically with source intensity (Figure B.8). To determine the sensitivity to the diffusion coefficient, the

$$\frac{\partial A_e(r_{50})}{\partial D} = \frac{W\left(\dfrac{F}{4\pi\alpha IC_{50}\lambda}\right)\left(\dfrac{\partial \lambda}{\partial D} DW\left(\dfrac{F}{4\pi\alpha IC_{50}\lambda}\right) - \lambda\right)}{D\left(1 + W\left(\dfrac{F}{4\pi\alpha IC_{50}}\right)\right)} \tag{B.161}$$

$$= \frac{r_{50}\left(\dfrac{\partial \lambda}{\partial D}\dfrac{D}{\lambda(p)} r_{50} - \lambda\right)}{D\left(\lambda(p) + r_{50}\right)} \tag{B.162}$$

The models are far more sensitive to changes in the ECS volume fraction (α) than either the neuronal or glial volume fraction (Figure B.8i,m,n). This is because the amount of adenosine required to reach the IC_{50} is inversely proportional ECS volume fraction. The sensitivity is greater for changes in neuronal volume fraction than glial volume fraction consistent with the dominant role of neuronal uptake in adenosine clearance clearance. Similarly model IV is more sensitive to changes in neuronal adenosine transport than any of the other clearance mechanisms (Figure B.8b).

B.9 Biosensor analytic solutions

The single enzyme biosensor model (Eq. B.165), let $a_t(r) = A(r) - A^*$ where A^* is has steady-state concentration in tissue. Then the solution has the form;

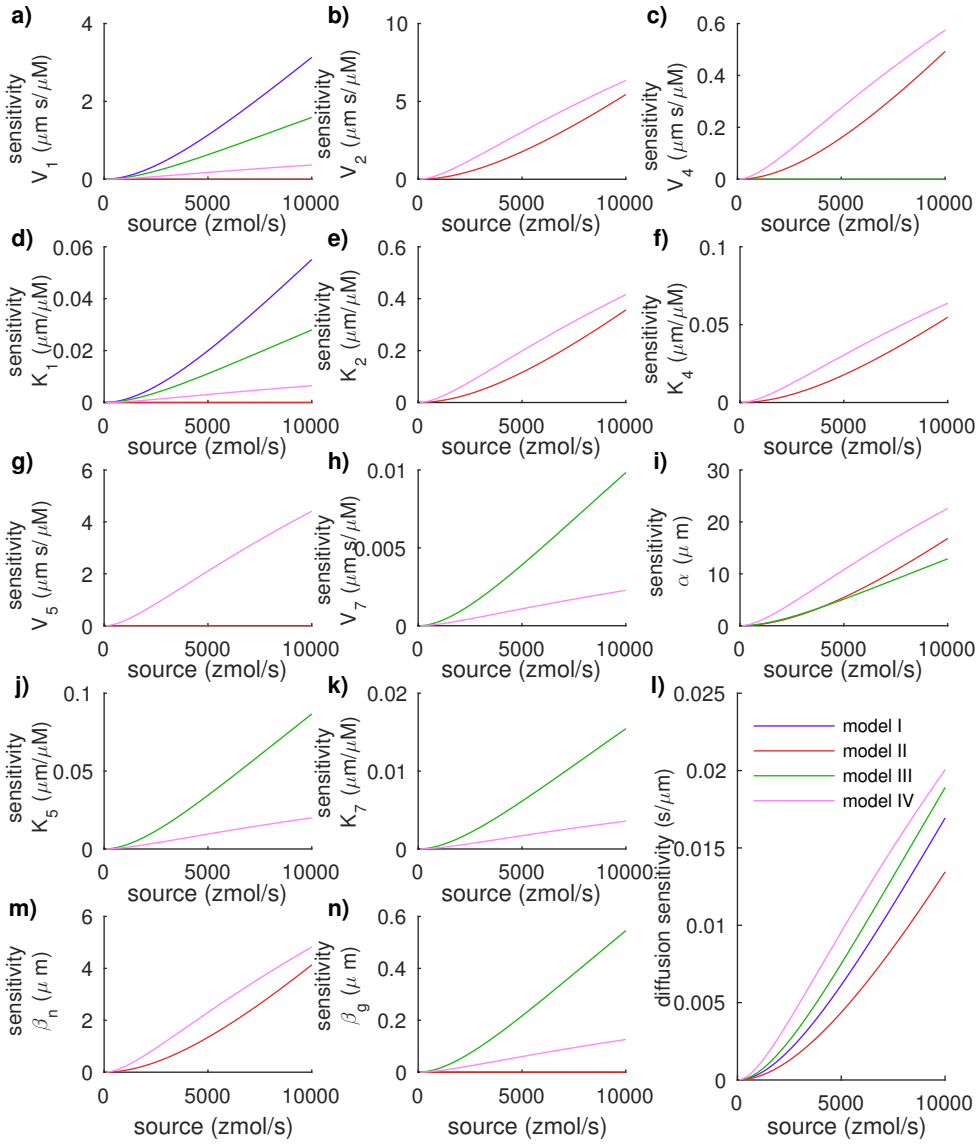

Figure B.8: **Sensitivity of the range of influence (r_{50}) of low concentration limit for a constant point source**. Sensitivity to changes in the; **a)** maximum velocity of ecto-ADA, **b)** maximum velocity of neuronal adenosine transporters, **c)** maximum velocity of neuronal ADA, **d)** MM constant of ecto-ADA, **e)** MM constant of neuronal adenosine transporters, **f)** MM constant of neuronal ADA, **g)** maximum velocity of glial adenosine transporters, **h)** maximum velocity of ADK, **i)** ECS volume fraction, **j)** MM constant of glial adenosine transporters, **k)** MM constant of ADK, **l)** diffusion coefficient, **m)** neuronal volume fraction, **n)** glial volume fraction.

$$a(r) = b_1 K_0(cr) + b_2 I_0(cr) \qquad r_t \leq r \tag{B.163}$$

$$\lim_{r\to\infty} a(r) = 0 \tag{B.164}$$

So $b_2 = 0$ and c is given by (Eq. 4.58). Then the steady-state solution has the form;

$$A(r) \quad = \quad \begin{cases} b_4 I_0(\kappa r) + b_5 K_0(\kappa r) & r_b \leq r < r_f \\ b_2 \log(r) + b_3 & r_f \leq r \leq r_t \\ b_1 K_0(cr) + A^* & r_t \leq r \end{cases} \tag{B.165}$$

Where κ is given by (Eq. 4.54). The constants b_1 to b_5 are found by applying the boundary (Eq. 4.15) and continuity conditions (Eq. 4.3-4.6) to give the analytic steady-state solution for the idealised biosensor (Eq. 4.61). The solution for the electroactive product (H) is obtained by rearranging the solution for the analyte in the enzyme layer;

$$0 = D_b \nabla^2 A(r) - v_b A(r) \tag{B.166}$$

$$v_b A(r) = D_b \nabla^2 A(r) \tag{B.167}$$

Substituting into (Eq. 4.16);

$$0 = D_h \nabla^2 \left(H(r) + \frac{D_b}{D_h} A(r) \right) \tag{B.168}$$

Let $P(r) = H(r) + \frac{D_b}{D_h} A(r)$ then the solution has the form;

$$P(r) = b_6 \log(r) + b_7 \tag{B.169}$$

So;

$$H(r) = b_6 \log(r) + b_7 - \frac{D_b}{D_h} A(r) \tag{B.170}$$

The constants b_6 and b_7 are determined by applying the boundary conditions (Eqs. 4.17, 4.18) to give the solution (Eq. 4.65). A similar approach is used for the two-enzyme biosensor and the three-enzyme biosensor.

Appendix C

Code

C.1 Adenosine clearance from a point source

The following C code is used to compute a numerical solution for a brief point source of adenosine and provides the concentration profiles (Figure 3.9) and totals amounts (Figure 3.10) of adenosine and breakdown products in tissue. Similar code is used for the steady-state solution to a constant point source and the bath applied case.

```
#include <stdio.h>
#include <stdlib.h>
#include <math.h>

/*macros*/
#define SQ(x) ((x)*(x))
#define CU(x) ((x)*(x)*(x))
#define MAX(a,b) ((a)>(b)?(a):(b))
#define MIN(a,b) ((a)<(b)?(a):(b))

/*trapezoid rule for integration*/
#define TRAP(xc,xp,Ac,Ap)          2.*M_PI*((xc)-(xp))*(SQ(xc)*(Ac) + SQ(xp)*(Ap))

/*state vectors*/
/*extracellular adenosine*/
#define AOLD(i)       A[j%2][i]
#define ANEW(i)       A[(j+1)%2][i]

/*neuronal adenosine*/
#define BOLD(i)       B[j%2][i]
#define BNEW(i)       B[(j+1)%2][i]

/*glial adenosine*/
#define COLD(i)       C[j%2][i]
#define CNEW(i)       C[(j+1)%2][i]

/*extracellular break-down products*/
#define POLD(i)       P[j%2][i]
#define PNEW(i)       P[(j+1)%2][i]
```

```
/*neuronal break-down products*/
#define QOLD(i)          Q[j%2][i]
#define QNEW(i)       Q[(j+1)%2][i]

/*glial break-down products*/
#define ROLD(i)          R[j%2][i]
#define RNEW(i)       R[(j+1)%2][i]

/*additional vectors*/
/*loss due to ADK*/
#define LOLD(i)          L[j%2][i]
#define LNEW(i)       L[(j+1)%2][i]

/*loss due to removal of break-down products*/
#define SOLD(i)          S[j%2][i]
#define SNEW(i)       S[(j+1)%2][i]

/*proportion of bound A1R*/
#define TOLD(i)          Theta[j%2][i]
#define TNEW(i)       Theta[(j+1)%2][i]


/*ENTs*/
#define TransAn(A,B,P,Q)            (V2*(B−A)/(K2*(1. + (P+Q)/K3) + (A+B)))
#define TransPn(A,B,P,Q)            (V3*(Q−P)/(K3*(1. + (A+B)/K2) + (P+Q)))
#define TransAg(A,C,P,R)            (V5*(C−A)/(K5*(1. + (P+R)/K6) + (A+R)))
#define TransPg(A,C,P,R)            (V6*(R−P)/(K6*(1. + (A+C)/K5) + (P+R)))

/*Diffusion*/
#define RK4DIFFBULK(A,Ap,Am,x,xn,xp)
          (D*dt/(x*SQ(dx)))*(Ap*xn −2.*x*A + Am*xp)                                    SQ
#define RK4DIFF(A,Ap,Am,x)
          (i>0?RK4DIFFBULK(A,Ap,Am,x,(x+dx),(x−dx)):(2.*D*dt*(Ap−A)/(SQ(dx))))

/*d/dt macros for*/
/*extracellular adenosine*/
#define RK4A(A,B,C,P,Q,R,Ap,Am,x) (RK4DIFF((A),(Ap),(Am),(x))                          \
                                 + dt*(−V1*((A)/(K1+(A)))                            \
                                 + (1./alpha)*TransAn((A),(B),(P),(Q))               \
                                 + (1./alpha)*TransAg((A),(C),(P),(R))))

/*neuronal adenosine*/
#define RK4B(A,B,C,P,Q,R)            dt*(−V4*(B)/((B)+K4)                           \
                                     − (1./betan)*TransAn((A),(B),(P),(Q)))

/*glial adenosine*/
#define RK4C(A,B,C,P,Q,R)            dt*(−V7*(C)/(K7+(C))                           \
                                     − (1./betag)*TransAg((A),(C),(P),(R)))

/*extracellular break-down products*/
#define RK4P(A,B,C,P,Q,R,Pp,Pm,x) (RK4DIFF((P),(Pp),(Pm),(x))                          \
                                     + dt*( V1*((A)/(K1+(A)))                       \
                                     + (1./alpha)*TransPn((A),(B),(P),(Q))          \
                                     + (1./alpha)*TransPg((A),(C),(P),(R))))

/*neuronal break-down products*/
#define RK4Q(A,B,C,P,Q,R)            dt*(V4*(B)/((B)+K4)                            \
                                     − (1./betan)*TransPn((A),(B),(P),(Q)))

/*glial break-down products*/
#define RK4R(A,B,C,P,Q,R)            −dt*(mu8*R + (1./betag)*TransPg((A),(C),(P),(R)))

/*loss due to ADK*/
#define RK4L(A,B,C,P,Q,R)            (dt*V7*(C)/(K7 + (C)))

/*loss due to removal of break-down products*/
#define RK4S(A,B,C,P,Q,R)            dt*mu8*R
```

```
/*proportion of bound A1R*/
#define RK4T(A,B,C,P,Q,R,T)              dt*(kon*A*(1.-T)-koff*T)


/*RK4 update rule*/
#define RKSUM(x)        (RK4[x][0] + 2.*RK4[x][1] + 2.*RK4[x][2] + RK4[x][3])/6.


/*macros for debugging used when compiled with -DDEBUG
 * check for NaN or negative values which indicates a problem with the parameters provided
 */
#ifdef DEBUG
#define checkNAN(A,B,P,Q,C,R,L)                                                    \
          if(isnan(A)||isnan(B)||isnan(P)||isnan(Q)||isnan(C)||isnan(R)||isnan(L))
          {
               fprintf(stderr,"Warning: NaNs in solution at r=%le t=%le time-step %le\n",x[i],t,dt);
               fprintf(stderr,"%le\t%1.20e\t%1.20e\t%1.20e\t%1.20e\t%1.20e\t%1.20e\t%1.20e\n",x[i],A,B,P,Q,C,R,L);
               return -1;                                                                  \
          }
#define checkNEG(A,B,P,Q,C,R,L)
          if(A<0||B<0||P<0||Q<0||C<0||R<0||M<0||L<0)                                    if
          {
               fprintf(stderr,"Warning: Negative solution at r=%le t=%le time-step %le\n",x[i],t,dt);
               fprintf(stderr,"%le\t%1.20e\t%1.20e\t%1.20e\t%1.20e\t%1.20e\t%1.20e\t%1.20e\n",x[i],A,B,P,Q,C,R,L);
               fprintf(stderr,"Failed!\n");                                            \
               return -2;                                                              \
          }
#define check(A,B,P,Q,C,R,L)                                                       \
          {                                                                        \
               checkNAN(A,B,P,Q,C,R,L);                                            \
               checkNEG(A,B,P,Q,C,R,L);                                            \
          }
#define DPRINT(str,fmt)                  fprintf(stderr,str,fmt);
#else
#define check(A,B,P,Q,C,R,L)                {}
#define DPRINT(str,fmt)                     {}
#endif


/* global variables */

double Rmin,              /*radius of the source in the ECS*/
       Rmax,              /*boundary far from the source*/
       minStep,           /*time step*/
       /*model parameters (see chapter 2)*/
       V1,V2,V3,V4,V5,V6,V7,mu8,kon,koff,
       K1,K2,K3,K4,K5,K6,K7,K8,alpha,betan,betag,F,D,IC50;

int N,                   /*number of grid points*/
    MidStep,             /*number of subdivision of Rmin*/
    printStep,           /*number of grid points to skip when printing output*/
    printTimeStep;/*number of time steps to skip when printing output*/


/*forward time centred space RK4 method*/
double FTCS(FILE* out, FILE* outREM, FILE* outIC50)                                FTCS
{
  double dx=Rmin/MidStep;          /*space step size*/
  double dt = minStep;               /*time step size*/
  double ret=0;                      /*return value*/
  double t=0;                      /*time*/
  int i,j;                           /*indices*/
  double tA=0,tB=0,tP=0,tQ=0,tC=0,tR=0,tL=0,tS=0;
                           /*totals in tissue*/
  double Kd=koff/kon, Occ=IC50/(Kd+IC50);
                             /*parameters of the A1R*/
  int maxR=0;                /*maxim distance where A(r)>IC50*/
  int Profile[10];             /*profiles*/
```

```
170
        /*peak adenosine at each grid point (Figure 3.9 c,e,i,k) */
        double *peakA    = (double*) calloc(N+1,sizeof(double*));
        double *peakT    = (double*) calloc(N+1,sizeof(double*));

175     /*signal duration at each grid point (Figure 3.9 d,f,j,l) */
        double *peakTa =    (double*) calloc(N+1,sizeof(double*));
        double *peakAa =    (double*) calloc(N+1,sizeof(double*));

        /*time to reach peak at each grid point*/
180     double *peakAt =    (double*) calloc(N+1,sizeof(double*));
        double *peakTt =    (double*) calloc(N+1,sizeof(double*));

        /*allocate vectors*/
        double** A = (double**) malloc(2*sizeof(double*));
185     A[0] = (double*)calloc(N+1,sizeof(double));
        A[1] = (double*)calloc(N+1,sizeof(double));
        double** B = (double**) malloc(2*sizeof(double*));
        B[0] = (double*)calloc(N+1,sizeof(double));
        B[1] = (double*)calloc(N+1,sizeof(double));
190     double** P = (double**) malloc(2*sizeof(double*));
        P[0] = (double*)calloc(N+1,sizeof(double));
        P[1] = (double*)calloc(N+1,sizeof(double));
        double** Q = (double**) malloc(2*sizeof(double*));
        Q[0] = (double*)calloc(N+1,sizeof(double));
195     Q[1] = (double*)calloc(N+1,sizeof(double));
          double** R = (double**) malloc(2*sizeof(double*));
        R[0] = (double*)calloc(N+1,sizeof(double));
        R[1] = (double*)calloc(N+1,sizeof(double));
          double** C = (double**) malloc(2*sizeof(double*));
200     C[0] = (double*)calloc(N+1,sizeof(double));
        C[1] = (double*)calloc(N+1,sizeof(double));
        double** L = (double**) malloc(2*sizeof(double*));
        L[0] = (double*)calloc(N+1,sizeof(double));
        L[1] = (double*)calloc(N+1,sizeof(double));
205     double** S = (double**) malloc(2*sizeof(double*));
        S[0] = (double*)calloc(N+1,sizeof(double));
        S[1] = (double*)calloc(N+1,sizeof(double));
        double *x = (double*)malloc((N+1)*sizeof(double));
        double **RK4 = (double**)malloc(10*sizeof(double));
210     double** Theta = (double**) malloc(2*sizeof(double*));
        Theta[0] = (double*)calloc(N+1,sizeof(double));
        Theta[1] = (double*)calloc(N+1,sizeof(double));
        for(i=0;i<9;i++)
          RK4[i] = (double*)malloc(4*sizeof(double));
215
        /*initialize grid and profile points*/
        x[0] = dx;
        for(i=1;i<=N;i++)
        {
220       x[i] = x[i-1]+dx;
          if(x[i]<=5e-6)
            Profile[0]=i;
          if(x[i]<=10e-6)
            Profile[1]=i;
225       if(x[i]<=15e-6)
            Profile[2]=i;
          if(x[i]<=20e-6)
            Profile[3]=i;
          if(x[i]<=25e-6)
230         Profile[4]=i;
          if(x[i]<=30e-6)
            Profile[5]=i;
          if(x[i]<=40e-6)
            Profile[6]=i;
235       if(x[i]<=50e-6)
            Profile[7]=i;
          if(x[i]<=75e-6)
            Profile[8]=i;
```

```
    if(x[i]<=100e-6)
240     Profile[9]=i;
}

DPRINT("Sampling at %le (%i) %le (%i) %le (%i) %le (%i)\n",
      x[Profile[0]],Profile[0],x[Profile[1]],Profile[1],x[Profile[2]],Profile[2],x[Profile[3]],Profile[3]);
245
/*integral source over volume of ECS Rmin^3*/
double source = (3.*F*1e-18/(4.*M_PI*alpha*CU(Rmin)))/(1 + 3./((double)MidStep*2.) + 1./(2.*SQ((double)MidStep)));
for(i=0;i<MidStep;i++)
{
250 A[0][i]=source;
}
    fprintf(outREM,"%le\t%1.20e\t%1.20e\t%1.20e\t%1.20e\t%1.20e\t%1.20e\t%1.20le\n",t,F*1e-18,tB,tP,tQ,tC,tR,tL,tS);
for(j=0;t<60;j++)
{
255     /*Neumann BC with imaginary point at -dx*/
        for(i=0;i<N;i++)
        {

            /*RK4 method - step 1*/
260         RK4[0][0] = RK4A(AOLD(i),BOLD(i),COLD(i),POLD(i),QOLD(i),ROLD(i),
                             AOLD(i+1),AOLD(i-1),x[i]);
            RK4[1][0] = RK4B(AOLD(i),BOLD(i),COLD(i),POLD(i),QOLD(i),ROLD(i));
            RK4[2][0] = RK4C(AOLD(i),BOLD(i),COLD(i),POLD(i),QOLD(i),ROLD(i));
            RK4[3][0] = RK4P(AOLD(i),BOLD(i),COLD(i),POLD(i),QOLD(i),ROLD(i),
265                          POLD(i+1),POLD(i-1),x[i]);
            RK4[4][0] = RK4Q(AOLD(i),BOLD(i),COLD(i),POLD(i),QOLD(i),ROLD(i));
            RK4[5][0] = RK4R(AOLD(i),BOLD(i),COLD(i),POLD(i),QOLD(i),ROLD(i));
            RK4[6][0] = RK4L(AOLD(i),BOLD(i),COLD(i),POLD(i),QOLD(i),ROLD(i));
            RK4[7][0] = RK4T(AOLD(i),BOLD(i),COLD(i),POLD(i),QOLD(i),ROLD(i),
270                          TOLD(i));
            RK4[8][0] = RK4S(AOLD(i),BOLD(i),COLD(i),POLD(i),QOLD(i),ROLD(i));

            /*RK4 method - step 2*/
        RK4[0][1] = RK4A(AOLD(i)+RK4[0][0]/2.,BOLD(i)+RK4[1][0]/2.,
275                          COLD(i)+RK4[2][0]/2.,POLD(i)+RK4[3][0]/2.,
                             QOLD(i)+RK4[4][0]/2.,ROLD(i)+RK4[5][0]/2.,
                             AOLD(i+1),AOLD(i-1),x[i]);
            RK4[1][1] = RK4B(AOLD(i)+RK4[0][0]/2.,BOLD(i)+RK4[1][0]/2.,
                             COLD(i)+RK4[2][0]/2.,POLD(i)+RK4[3][0]/2.,
280                          QOLD(i)+RK4[4][0]/2.,ROLD(i)+RK4[5][0]/2.);
            RK4[2][1] = RK4C(AOLD(i)+RK4[0][0]/2.,BOLD(i)+RK4[1][0]/2.,
                             COLD(i)+RK4[2][0]/2.,POLD(i)+RK4[3][0]/2.,
                             QOLD(i)+RK4[4][0]/2.,ROLD(i)+RK4[5][0]/2.);
            RK4[3][1] = RK4P(AOLD(i)+RK4[0][0]/2.,BOLD(i)+RK4[1][0]/2.,
285                          COLD(i)+RK4[2][0]/2.,POLD(i)+RK4[3][0]/2.,
                             QOLD(i)+RK4[4][0]/2.,ROLD(i)+RK4[5][0]/2.,
                             POLD(i+1),POLD(i-1),x[i]);
            RK4[4][1] = RK4Q(AOLD(i)+RK4[0][0]/2.,BOLD(i)+RK4[1][0]/2.,
                             COLD(i)+RK4[2][0]/2.,POLD(i)+RK4[3][0]/2.,
290                          QOLD(i)+RK4[4][0]/2.,ROLD(i)+RK4[5][0]/2);
            RK4[5][1] = RK4R(AOLD(i)+RK4[0][0]/2.,BOLD(i)+RK4[1][0]/2.,
                             COLD(i)+RK4[2][0]/2.,POLD(i)+RK4[3][0]/2.,
                             QOLD(i)+RK4[4][0]/2.,ROLD(i)+RK4[5][0]/2.);
            RK4[6][1] = RK4L(AOLD(i)+RK4[0][0]/2.,BOLD(i)+RK4[1][0]/2.,
295                          COLD(i)+RK4[2][0]/2.,POLD(i)+RK4[3][0]/2.,
                             QOLD(i)+RK4[4][0]/2.,ROLD(i)+RK4[5][0]/2.);
            RK4[7][1] = RK4T(AOLD(i)+RK4[0][0]/2.,BOLD(i)+RK4[1][0]/2.,
                             COLD(i)+RK4[2][0]/2.,POLD(i)+RK4[3][0]/2.,
                             QOLD(i)+RK4[4][0]/2.,ROLD(i)+RK4[5][0]/2.,
300                          TOLD(i)+RK4[7][0]/2.);
            RK4[8][1] = RK4S(AOLD(i)+RK4[0][0]/2.,BOLD(i)+RK4[1][0]/2.,
                             COLD(i)+RK4[2][0]/2.,POLD(i)+RK4[3][0]/2.,
                             QOLD(i)+RK4[4][0]/2.,ROLD(i)+RK4[5][0]/2.);

305         /*RK4 method - step 3*/
            RK4[0][2] = RK4A(AOLD(i)+RK4[0][1]/2.,BOLD(i)+RK4[1][1]/2.,
                             COLD(i)+RK4[2][1]/2.,POLD(i)+RK4[3][1]/2.,
```

```
                                QOLD(i)+RK4[4][1]/2.,ROLD(i)+RK4[5][1]/2.,
                                AOLD(i+1),AOLD(i-1),x[i]);
310           RK4[1][2] = RK4B(AOLD(i)+RK4[0][1]/2.,BOLD(i)+RK4[1][1]/2.,
                                COLD(i)+RK4[2][1]/2.,POLD(i)+RK4[3][1]/2.,
                                QOLD(i)+RK4[4][1]/2.,ROLD(i)+RK4[5][1]/2.);
              RK4[2][2] = RK4C(AOLD(i)+RK4[0][1]/2.,BOLD(i)+RK4[1][1]/2.,
                                COLD(i)+RK4[2][1]/2.,POLD(i)+RK4[3][1]/2.,
315                             QOLD(i)+RK4[4][1]/2.,ROLD(i)+RK4[5][1]/2.);
              RK4[3][2] = RK4P(AOLD(i)+RK4[0][1]/2.,BOLD(i)+RK4[1][1]/2.,
                                COLD(i)+RK4[2][1]/2.,POLD(i)+RK4[3][1]/2.,
                                QOLD(i)+RK4[4][1]/2.,ROLD(i)+RK4[5][1]/2.,
                                POLD(i+1),POLD(i-1),x[i]);
320           RK4[4][2] = RK4Q(AOLD(i)+RK4[0][1]/2.,BOLD(i)+RK4[1][1]/2.,
                                COLD(i)+RK4[2][1]/2.,POLD(i)+RK4[3][1]/2.,
                                QOLD(i)+RK4[4][1]/2.,ROLD(i)+RK4[5][1]/2.);
              RK4[5][2] = RK4R(AOLD(i)+RK4[0][1]/2.,BOLD(i)+RK4[1][1]/2.,
                                COLD(i)+RK4[2][1]/2.,POLD(i)+RK4[3][1]/2.,
325                             QOLD(i)+RK4[4][1]/2.,ROLD(i)+RK4[5][1]/2.);
              RK4[6][2] = RK4L(AOLD(i)+RK4[0][1]/2.,BOLD(i)+RK4[1][1]/2.,
                                COLD(i)+RK4[2][1]/2.,POLD(i)+RK4[3][1]/2.,
                                QOLD(i)+RK4[4][1]/2.,ROLD(i)+RK4[5][1]/2.);
              RK4[7][2] = RK4T(AOLD(i)+RK4[0][1]/2.,BOLD(i)+RK4[1][1]/2.,
330                             COLD(i)+RK4[2][1]/2.,POLD(i)+RK4[3][1]/2.,
                                QOLD(i)+RK4[4][1]/2.,ROLD(i)+RK4[5][1]/2.,
                                TOLD(i)+RK4[7][1]/2.);
              RK4[8][2] = RK4S(AOLD(i)+RK4[0][1]/2.,BOLD(i)+RK4[1][1]/2.,
                                COLD(i)+RK4[2][1]/2.,POLD(i)+RK4[3][1]/2.,
335                             QOLD(i)+RK4[4][1]/2.,ROLD(i)+RK4[5][1]/2.);


              /*RK4 method - step 4*/
              RK4[0][3] = RK4A(AOLD(i)+RK4[0][2],BOLD(i)+RK4[1][2],
340                             COLD(i)+RK4[2][2],POLD(i)+RK4[3][2],
                                QOLD(i)+RK4[4][2],ROLD(i)+RK4[5][2],
                                AOLD(i+1),AOLD(i-1),x[i]);
              RK4[1][3] = RK4B(AOLD(i)+RK4[0][2],BOLD(i)+RK4[1][2],
                                COLD(i)+RK4[2][2],POLD(i)+RK4[3][2],
345                             QOLD(i)+RK4[4][2],ROLD(i)+RK4[5][2]);
              RK4[2][3] = RK4C(AOLD(i)+RK4[0][2],BOLD(i)+RK4[1][2],
                                COLD(i)+RK4[2][2],POLD(i)+RK4[3][2],
                                QOLD(i)+RK4[4][2],ROLD(i)+RK4[5][2]);
              RK4[3][3] = RK4P(AOLD(i)+RK4[0][2],BOLD(i)+RK4[1][2],
350                             COLD(i)+RK4[2][2],POLD(i)+RK4[3][2],
                                QOLD(i)+RK4[4][2],ROLD(i)+RK4[5][2],
                                POLD(i+1),POLD(i-1),x[i]);
              RK4[4][3] = RK4Q(AOLD(i)+RK4[0][2],BOLD(i)+RK4[1][2],
                                COLD(i)+RK4[2][2],POLD(i)+RK4[3][2],
355                             QOLD(i)+RK4[4][2],ROLD(i)+RK4[5][2]);
              RK4[5][3] = RK4R(AOLD(i)+RK4[0][2],BOLD(i)+RK4[1][2],
                                COLD(i)+RK4[2][2],POLD(i)+RK4[3][2],
                                QOLD(i)+RK4[4][2],ROLD(i)+RK4[5][2]);
              RK4[6][3] = RK4L(AOLD(i)+RK4[0][2],BOLD(i)+RK4[1][2],
360                             COLD(i)+RK4[2][2],POLD(i)+RK4[3][2],
                                QOLD(i)+RK4[4][2],ROLD(i)+RK4[5][2]);
              RK4[7][3] = RK4T(AOLD(i)+RK4[0][2],BOLD(i)+RK4[1][2],
                                COLD(i)+RK4[2][2],POLD(i)+RK4[3][2],
                                QOLD(i)+RK4[4][2],ROLD(i)+RK4[5][2],
365                             TOLD(i)+RK4[7][2]);
              RK4[8][3] = RK4S(AOLD(i)+RK4[0][2],BOLD(i)+RK4[1][2],
                                COLD(i)+RK4[2][2],POLD(i)+RK4[3][2],
                                QOLD(i)+RK4[4][2],ROLD(i)+RK4[5][2]);

370           /*RK4 method - sum terms*//
              BNEW(i) = BOLD(i) + RKSUM(1);
              CNEW(i) = COLD(i) + RKSUM(2);
              QNEW(i) = QOLD(i) + RKSUM(4);
              RNEW(i) = ROLD(i) + RKSUM(5);
375           ANEW(i) = AOLD(i) + RKSUM(0);
              PNEW(i) = POLD(i) + RKSUM(3);
```

```
            LNEW(i) = LOLD(i) + RKSUM(6);
            TNEW(i) = MIN(1.,TOLD(i) + RKSUM(7));
            SNEW(i) = SOLD(i) + RKSUM(8);

            check(A,B,P,Q,C,R,L);


            /*peak adenosine at grid point x[i]*/
            if(ANEW(i)>peakA[i])
            {
               peakA[i] = ANEW(i);
               peakAt[i] = t+dt;
            }

            /*peak inhibition at grid point x[i]*/
            if(TNEW(i)>peakT[i])
            {
               peakT[i] = TNEW(i);
               peakTt[i] = t+dt;
            }

            /*duration above IC50 at grid point x[i]*/
            if(ANEW(i)>=IC50)
               peakAa[i] += dt;

            /*duration above 50% inhibition at grid point x[i]*/
            if(TNEW(i)>=Occ)
               peakTa[i] += dt;


            if(j%printTimeStep==0)
            {
               /*integrate to find total amounts*/
               if(i==0)
               {
                  tA = TRAP(x[0],0,ANEW(0),0);
                  tB = TRAP(x[0],0,BNEW(0),0);
                  tC = TRAP(x[0],0,CNEW(0),0);
                  tP = TRAP(x[0],0,PNEW(0),0);
                  tQ = TRAP(x[0],0,QNEW(0),0);
                  tR = TRAP(x[0],0,RNEW(0),0);
                  tL = TRAP(x[0],0,LNEW(0),0);
                  tS = TRAP(x[0],0,SNEW(0),0);

               }
               else
               {
                  tA += TRAP(x[i],x[i-1],ANEW(i),ANEW(i-1));
                  tB += TRAP(x[i],x[i-1],BNEW(i),BNEW(i-1));
                  tC += TRAP(x[i],x[i-1],CNEW(i),CNEW(i-1));
                  tP += TRAP(x[i],x[i-1],PNEW(i),PNEW(i-1));
                  tQ += TRAP(x[i],x[i-1],QNEW(i),QNEW(i-1));
                  tR += TRAP(x[i],x[i-1],RNEW(i),RNEW(i-1));
                  tL += TRAP(x[i],x[i-1],LNEW(i),LNEW(i-1));
                  tS += TRAP(x[i],x[i-1],SNEW(i),SNEW(i-1));

               }
            }

            /*stop iteration if all states at x[i] are zero*/
            if(ANEW(i) ==0 && BNEW(i)==0 && CNEW(i) == 0 && PNEW(i)==0 && QNEW(i)==0 && RNEW(i)==0)
            {
                break;
            }

         }

          t+=dt;
```

```
        if(j%printTimeStep==0)
        {
            tA*=alpha;tP*=alpha;        /*scale extracellular totals*/
            tB*=betan;tQ*=betan;        /*scale neuronal totals*/
            tC*=betag;tR*=betag;        /*scale glial totals*/
            tL*=betag;tS*=betag;        /*scale removal totals*/

            /*write the profiles and totals*/
            fprintf(outREM,"%le\t%1.20e\t%1.20e\t%1.20e\t%1.20e\t%1.20e\t%1.20e\t%1.20e\t%1.20le\n",t,tA,tB,tP,tQ,tC,tR,tL,tS);
            fprintf(out,"%le",t);
            for(i=0;i<10;i++)
                fprintf(out,"\t%le\t%le\t%le",ANEW(Profile[i]),PNEW(Profile[i]),TNEW(Profile[i]));
            fprintf(out,"\n");
        }

        ret = x[maxR];
    }


    DPRINT("%le\t%le\t%i\n",ret,t,maxR);

    /*write peaks and durations to file*/
    for(i=0;i<N;i++)
    {
        fprintf(outIC50,"%1.20e\t%1.20e\t%1.20e\t%1.20e\t%1.20e\t%1.20e\t%1.20e\n",
                x[i],peakA[i],peakAt[i],peakAa[i],peakT[i],peakTt[i],peakTa[i]);
    }


    /*free allocated memory*/
    free(A[0]);
    free(A[1]);
    free(A);
    free(B[0]);
    free(B[1]);
    free(B);
    free(P[0]);
    free(P[1]);
    free(P);
    free(Q[0]);
    free(Q[1]);
    free(Q);
    free(C[0]);
    free(C[1]);
    free(C);
    free(R[0]);
    free(R[1]);
    free(R);
    free(L[0]);
    free(L[1]);
    free(L);
    free(S[0]);
    free(S[1]);
    free(S);
    free(x);

    return ret;
}


/*Read parameters from file*/
int readParameters(char *filename)                                  readParameters
{
    FILE *pf;
    pf = fopen(filename,"r");
    if(pf==NULL)
        return -1;
    if(fscanf(pf,"MidStep=%i\n",&MidStep)<0)
```

```
515         return -2;
        if(fscanf(pf,"N=%i\n",&N)<0)
            return -2;
        if(fscanf(pf,"minStep=%le\n",&minStep)<0)
            return -2;
520     if(fscanf(pf,"PrintStep=%i\n",&printStep)<0)
            return -2;
        if(fscanf(pf,"PrintTimeStep=%i\n",&printTimeStep)<0)
            return -2;
        if(fscanf(pf,"V1=%lf\n",&V1)<0)
525         return -2;
        if(fscanf(pf,"V2=%lf\n",&V2)<0)
            return -2;
        if(fscanf(pf,"V3=%lf\n",&V3)<0)
            return -2;
530     if(fscanf(pf,"V4=%lf\n",&V4)<0)
            return -2;
        if(fscanf(pf,"V5=%lf\n",&V5)<0)
            return -2;
        if(fscanf(pf,"V6=%lf\n",&V6)<0)
535         return -2;
        if(fscanf(pf,"V7=%lf\n",&V7)<0)
            return -2;
        if(fscanf(pf,"V8=%lf\n",&V8)<0)
            return -2;
540     if(fscanf(pf,"V9=%lf\n",&V9)<0)
            return -2;
        if(fscanf(pf,"mu8=%lf\n",&mu8)<0)
            return -2;
        if(fscanf(pf,"K1=%lf\n",&K1)<0)
545         return -2;
        if(fscanf(pf,"K2=%lf\n",&K2)<0)
            return -2;
        if(fscanf(pf,"K3=%lf\n",&K3)<0)
            return -2;
550     if(fscanf(pf,"K4=%lf\n",&K4)<0)
            return -2;
        if(fscanf(pf,"K5=%lf\n",&K5)<0)
            return -2;
        if(fscanf(pf,"K6=%lf\n",&K6)<0)
555         return -2;
        if(fscanf(pf,"K7=%lf\n",&K7)<0)
            return -2;
        if(fscanf(pf,"K8=%lf\n",&K8)<0)
            return -2;
560     if(fscanf(pf,"D=%le\n",&D)<0)
            return -2;
        if(fscanf(pf,"alpha=%lf\n",&alpha)<0)
            return -2;
        if(fscanf(pf,"betan=%lf\n",&betan)<0)
565         return -2;
        if(fscanf(pf,"betag=%lf\n",&betag)<0)
            return -2;
        if(fscanf(pf,"F=%lf\n",&F)<0)
            return -2;
570     if(fscanf(pf,"IC50=%lf\n",&IC50)<0)
            return -2;
        if(fscanf(pf,"kon=%lf\n",&kon)<0)
            return -2;
        if(fscanf(pf,"koff=%lf\n",&koff)<0)
575         return -2;
        Rmin=pow(3./(4.*M_PI*alpha),1./3.)*1e-6;
        return 0;

    }
580
    /*echo parameters*/
    int printParameters(FILE *fp)                                    printParameters
    {
```

```
    fprintf(fp,"\nRmin=%le\n",Rmin);
    fprintf(fp,"Rmax=%le\n",(double)N*Rmin/(double)MidStep);
    fprintf(fp,"N=%i\n",N);
    fprintf(fp,"minStep=%le\n",minStep);
    fprintf(fp,"PrintStep=%i\n",printStep);
    fprintf(fp,"PrintTimeStep=%i\n",printTimeStep);
    fprintf(fp,"V1=%le\n",V1);
    fprintf(fp,"V2=%le\n",V2);
    fprintf(fp,"V3=%le\n",V3);
    fprintf(fp,"V4=%le\n",V4);
    fprintf(fp,"V5=%le\n",V5);
    fprintf(fp,"V6=%le\n",V6);
    fprintf(fp,"V7=%le\n",V7);
    fprintf(fp,"mu8=%le\n",mu8);
    fprintf(fp,"K1=%le\n",K1);
    fprintf(fp,"K2=%le\n",K2);
    fprintf(fp,"K3=%le\n",K3);
    fprintf(fp,"K4=%le\n",K4);
    fprintf(fp,"K5=%le\n",K5);
    fprintf(fp,"K6=%le\n",K6);
    fprintf(fp,"K7=%le\n",K7);
    fprintf(fp,"K8=%le\n",K8);
    fprintf(fp,"D=%le\n",D);
    fprintf(fp,"alpha=%lf\n",alpha);
    fprintf(fp,"betan=%lf\n",betan);
    fprintf(fp,"betag=%lf\n",betag);
    fprintf(fp,"IC50=%lf\n",IC50);
    fprintf(fp,"koff=%lf\n",koff);
    fprintf(fp,"kon=%lf\n",kon);
    fprintf(fp,"F=%le\n",F);
    fflush(fp);
    return 0;
}

int main(int argc, char** argv)                                                    main
{
  FILE *outIC50, *outTRACE,*outREM;
  int err;
  if(argc<5)
  {
    fprintf(stderr, "Insufficient arguments.\n"
                    "REQUIRED:\t parameterfile ouputIC50 outTRACE outREM F\n");
    return -1;
  }
  /*open the parameter file and read the parameters*/
  err=readParameters(argv[1]);
  if(err==-1)
  {
    fprintf(stderr,"Failed to open file %s.\n",argv[1]);
  return -1;
  }
  else if(err==-2)
  {
    fprintf(stderr,"Failed to read a parameter from %s.\n",argv[1]);
  return -1;
  }

  /*open the output file for the peaks and durations*/
  outIC50 = fopen(argv[2],"a");
  if(outIC50 == NULL)
  {
    fprintf(stderr,"Failed to open file %s.\n",argv[2]);
  return -1;
  }

  /*open the output file for the profiles*/
  outTRACE = fopen(argv[3],"w");
  if(outTRACE == NULL)
  {
```

```
        fprintf(stderr,"Failed to open file %s.\n",argv[3]);
        return -1;
    }

    /*open the output file for the totals*/
    outREM = fopen(argv[4],"w");
    if(outTRACE == NULL)
    {
        fprintf(stderr,"Failed to open file %s.\n",argv[4]);
        return -1;
    }
    /*set the source intensity [zmol]*/
    F=atof(argv[5]);
    printParameters(stderr);

    /*Call FTCS method*/
    FTCS(outTRACE,outREM,outIC50);
    /*close all the files*/
    fflush(outIC50);
    fflush(outTRACE);
    fclose(outIC50);
    fclose(outTRACE);
    fflush(outREM);
    fclose(outREM);
    return 0;

}
```

C.2 Model of an idealised biosensor

The following C code provides a numeric solution for the PDEs (Eq. B.165) and (Eq. 4.16) using the Runge-Kutta method (RK4). The parameters are read from a parameter file and the solution is used to calculate the gradient of electroactive product at biosensor, which is scaled to give the signal (Eq. 4.23) (Figure 4.7). In addition to the gradient profiles of the analyte and product are output at regular time intervals, specified in the parameters file.

```
#include <stdio.h>
#include <stdlib.h>
#include <math.h>

/*simple macros*/
#define SQ(x) ((x)*(x))
#define MAX(a,b) ((a)>(b)?(a):(b))
#define MIN(a,b) ((a)<(b)?(a):(b))

/*access arrays representing the analyte and product*/
#define AOLD(i)      A[j%2][i]
#define ANEW(i)      A[(j+1)%2][i]
#define POLD(i)          P[j%2][i]
#define PNEW(i)      P[(j+1)%2][i]


/*Macros for the RK4 steps given the state (A) at position (x) and at x+dx (Ap) and x-dx (Am)*/
/*reaction-diffusion in tissue*/
```

```
#define STEPA0(A,Ap,Am,x)            dt*(                                          \
    (D/SQ(lambda))*((Ap -2.*A + Am)/(SQ(dx)) + (Ap - Am)/(2.*dx*x))                 \
    - Vt*(A-A0))

/*diffusion in the free region*/
#define STEPA1(A,Ap,Am,x)            dt*(                                          \
    D*((Ap -2.*A + Am)/(SQ(dx)) + (Ap - Am)/(2.*dx*x)))

/*reaction-diffusion in the enzyme-layer*/
#define STEPA2(A,Ap,Am,x)            dt*(                                          \
    (D /SQ(mu))*( (Ap -2.*A + Am)/(SQ(dx)) + (Ap - Am)/(2.*dx*x)) - (Vb*A))

/*reaction-diffusion of the electroactive product*/
#define STEPP2(P,Pp,Pm,x,A)            dt*(                                        \
    (Dh/SQ(mu))*( (Pp -2.*P + Pm)/(SQ(dx)) + (Pp - Pm)/(2.*dx*x)) + (Vb*A))

#define RKSUM(x)        (RK4[x][0] + 2.*RK4[x][1] + 2.*RK4[x][2] + RK4[x][3])/6.


/*When compiled with -DDEBUG check for negative or NaN state variables
  * that usually occur if the is a problem with the parameters*/
#ifdef DEBUG
#define checkNAN(A)                          if(isnan(A)){                          \
    fprintf(stderr,"Warning: NaNs in solution");                                    \
    fprintf(stderr,"\nx=%le t=%le timestep %le\n",x[i],t,dt);                       \
    return -1;}
#define checkNEG(A)                          if(A<0){                               \
    fprintf(stderr,"Warning: Negative solution");                                   \
    fprintf(stderr,"\nx=%le t=%le timestep %le\n",x[i],t,dt);                       \
    return -2;}
#define checkS(X)                             {checkNAN(X);}
#define check(A)                              {checkS(A);}
#else
#define checkS(X)                             {}
#define check(A)                              {}
#endif


/*
  * Global variables
  */
double    dx1,dx2,dx,          /*step sizes close to the biosensor and in tissue*/
          Vt,                  /*tissue rate (v_t)*/
          D,                   /*analyte free diffusion coefficient (D_f)*/
          Dh,                  /*product free diffusion coefficient*/
          R3,                  /*outer edge of the solution*/
          R2,                  /*boundary between tissue and the free region (r_t)*/
          R1,                  /*boundary between the free region and enzyme layer (r_f)*/
          R0,                  /*radius of the biosensor core (r_b)*/
          lambda,              /*tissue tortuosity (D_t = D/λ^2)*/
          mu,                  /*enzyme-layer tortuosity (D_b = D/μ^2)*/
          Vb,                  /*reaction rate in enzyme later*/
          dt,                  /*time step*/
          T,                   /*maximum solution time*/
          A0,                  /*tissue steady-state concentration without the biosensor*/
          alphaB,              /*enzyme layer porosity (α_b)*/
          alphaT;              /*tissue porosity (α_t)*/

int N,                         /*number of grid points*/
    printStep,                 /*number of gird points to skip when writing output*/
    printTimeStep,             /*number of time steps to skip when writing output*/
    I0,                        /*grid point corresponding to R1*/
    I1;                        /*grid point corresponding to R2*/
unsigned char CAL;             /*flag indicates solve for calibration case*/

/*solve numerically using Forward-Time Central-Space method*/
int FTCS(FILE* outProfile, FILE* outSensor, FILE* outFinal)
{
```

SQ

FTCS

```
        double t=0,                 /*time*/
               maxdiff=0;           /*difference in continuity conditions*/
90      int I0,                     /*grid point corresponding to R1*/
            A0E,                    /*fake grid point I0+1 used for continuity conditions*/
            A1S,                    /*fake grid point I0+2 used for continuity conditions*/
            I1,                     /*grid point corresponding to R2*/
            A1E,                    /*fake grid point I1+1 used for continuity conditions*/
95          A2S;                    /*fake grid point I1+2 used for continuity conditions*/
        /*indices*/
        unsigned int i,j,k;
        unsigned char DMG = R1<R2;      /*flag if problem includes a free region*/
        unsigned char LAST;             /*continuity conditions unchanged in an iteration*/
100
        /*arrays for the analyte and product*/
        double** A = (double**) malloc(2*sizeof(double*));
        A[0] = (double*)calloc(N+1,sizeof(double));
        A[1] = (double*)calloc(N+1,sizeof(double));
105     double** P = (double**) malloc(2*sizeof(double*));
        P[0] = (double*)calloc(N+1,sizeof(double));
        P[1] = (double*)calloc(N+1,sizeof(double));

        /*array of grid points*/
110     double *x = (double*)malloc((N+1)*sizeof(double));

        /*array to store RK4 terms*/
        double **RK4 = (double**)malloc(2*sizeof(double));
        for(i=0;i<2;i++)
115         RK4[i] = (double*)malloc(4*sizeof(double));

        /*initialise grid*/
        dx=dx1;
        x[0] = R0-dx;
120     if(CAL)
        {
            for(i=1;i<=N;i++)
            {
                x[i]=x[i-1]+dx;
125             if(x[i]<=R1 && x[i]+dx>R1)
                {
                    I0=i;
                    x[i+1]=x[i];i++;I1=i;
                    break;
130             }
            }
            A[0][I1]=alphaB*A0;
            A[1][I1]=alphaB*A0;
        }
135     else
        {
            if(DMG)
            {
                for(i=1;i<=N;i++)
140             {
                    x[i] = x[i-1]+dx;
                    if(x[i]<=R1 && x[i]+dx>R1)
                    {
                        I0=i;
145                     x[i+1]=x[i];i++;A0E=i;
                        x[i+1]=x[i];i++;A1S=i;
                    }
                    if(x[i]<=R2 && x[i]+dx>R2)
                    {
150                     I1=i;
                        x[i+1]=x[i];i++;A1E=i;
                        x[i+1]=x[i];i++;A2S=i;
                        A[0][i]=A0;A[1][i]=A0;
                        dx=dx2;
155                 }
                    if(x[i]>R2)
```

```
                {
                    A[0][i]=A0;
                    A[1][i]=A0;
                }
            }
        }
        else
        {
            for(i=1;i<=N;i++)
            {
                x[i] = x[i-1]+dx;
                if(x[i]<=R1 && x[i]+dx>R1)
                {
                    I0=i;
                    x[i+1]=x[i];i++;A0E=i;
                    x[i+1]=x[i];i++;A1S=i;
                    dx=dx2;
                }
                if(x[i]>R1)
                {
                    A[0][i]=A0;
                    A[1][i]=A0;
                }
            }
            A2S=A1S;
        }

    }

    for(j=0;t<T;j++)
    {
        for(k=0,LAST=1;LAST||maxdiff>0;k++)
        {
            /*solve once after the continuity conditions are unchanged*/
            if(k>0 && maxdiff==0)
                LAST=0;
            else
                LAST=1;

            dx=dx1;         /*use the smaller step size for solving near the biosensor*/
            for(i=1;i<=I0;i++)
            {
                /*RK4 method for analyte and product in the enzyme layer*/
                RK4[0][0] = STEPA2(AOLD(i),AOLD(i+1),AOLD(i-1),x[i]);
                RK4[1][0] = STEPP2(POLD(i),POLD(i+1),POLD(i-1),x[i],AOLD(i));

                RK4[0][1] = STEPA2(AOLD(i)+RK4[0][0]/2.,AOLD(i+1),AOLD(i-1),x[i]);
                RK4[1][1] = STEPP2(POLD(i)+RK4[1][0]/2.,POLD(i+1),POLD(i-1),x[i],AOLD(i)+RK4[0][0]/2.);

                RK4[0][2] = STEPA2(AOLD(i)+RK4[0][1]/2.,AOLD(i+1),AOLD(i-1),x[i]);
                RK4[1][2] = STEPP2(POLD(i)+RK4[1][1]/2.,POLD(i+1),POLD(i-1),x[i],AOLD(i)+RK4[0][1]/2.);

                RK4[0][3] = STEPA2(AOLD(i)+RK4[0][2],AOLD(i+1),AOLD(i-1),x[i]);
                RK4[1][3] = STEPP2(POLD(i)+RK4[1][2],POLD(i+1),POLD(i-1),x[i],AOLD(i)+RK4[0][2]);

                ANEW(i) = AOLD(i) + RKSUM(0);
                PNEW(i) = POLD(i) + RKSUM(1);

                /*check solution if complied with -DDEBUG*/
                check(ANEW(i));
                check(PNEW(i));

            }
            /*if solving for calibration then apply the boundary conditions*/
            if(CAL)
            {
                ANEW(I0)=A0*alphaB;
                PNEW(I0)=0;
```

```
        ANEW(0)=ANEW(1);        /*Neumann boundary for analyte at the core*/
        PNEW(1)=0;                /*x[1]=R0*/
    }
    else
    {
        if(DMG)
        {
            /*if there is a free region solve for it using RK4 method*/
            for(i=A1S+1;i<=I1;i++)
            {
                RK4[0][0] = STEPA1(AOLD(i),AOLD(i+1),AOLD(i-1),x[i]);
                RK4[0][1] = STEPA1(AOLD(i)+RK4[0][0]/2.,AOLD(i+1),AOLD(i-1),x[i]);
                RK4[0][2] = STEPA1(AOLD(i)+RK4[0][1]/2.,AOLD(i+1),AOLD(i-1),x[i]);
                RK4[0][3] = STEPA1(AOLD(i)+RK4[0][2],AOLD(i+1),AOLD(i-1),x[i]);

                ANEW(i) = AOLD(i) + RKSUM(0);
                checkS(ANEW(i));
            }
        }
        dx=dx2;         /*using the larger step size*/
        /*solve for tissue using the RK4 method*/
        for(i=A2S+1;i<N;i++)
        {

            RK4[0][0] = STEPA0(AOLD(i),AOLD(i+1),AOLD(i-1),x[i]);
            RK4[0][1] = STEPA0(AOLD(i)+RK4[0][0]/2.,AOLD(i+1),AOLD(i-1),x[i]);
            RK4[0][2] = STEPA0(AOLD(i)+RK4[0][1]/2.,AOLD(i+1),AOLD(i-1),x[i]);
            RK4[0][3] = STEPA0(AOLD(i)+RK4[0][2],AOLD(i+1),AOLD(i-1),x[i]);

            ANEW(i) = AOLD(i) + RKSUM(0);
            checkS(ANEW(i));
        }
        /*apply the boundary conditons*/
        ANEW(0) = ANEW(1);
        PNEW(1) = 0;
        ANEW(N)    = ANEW(N-1);
        PNEW(I0)   = 0;

        if(DMG)
        {
            /*continuity between the enzyme-layer and free-region
              * using 5 point stencils for the gradient*/
            ANEW(A1S) = AOLD(I0)/alphaB;
            ANEW(A0E) = ((18.*AOLD(I0-1) - 6.*AOLD(I0-2) +
                          AOLD(I0-3) -10.*AOLD(I0)) +
                          SQ(mu)*(48.*AOLD(A1S+1) -36.*AOLD(A1S+2)
                                +16.*AOLD(A1S+3) -3.*AOLD(A1S+4)-
                                25.*AOLD(A1S)))/3.;

            /*continuity between the free-region and tissue using 5
              * point stencils for the gradient*/
            ANEW(A2S) = alphaT*AOLD(I1);
            ANEW(A1E) = ((18.*AOLD(I1-1) - 6.*AOLD(I1-2) + AOLD(I1-3)
                                -10.*AOLD(I1)) + SQ(1./lambda)*(
                                    48.*AOLD(A2S+1) -36.*AOLD(A2S+2)
                                    +16.*AOLD(A2S+3) -3.*AOLD(A2S+4)
                                    -25.*AOLD(A2S))*(dx1/dx2))/3.;
            /*check how much continuity conditions have not changed*/
            maxdiff = fabs(ANEW(A1S)-AOLD(A1S));
            maxdiff +=fabs(ANEW(A0E)-AOLD(A0E));
            maxdiff +=fabs(ANEW(A2S)-AOLD(A2S));
            maxdiff +=fabs(ANEW(A1E)-AOLD(A1E));
            /*update the fake grid points*/
            AOLD(A1S) = ANEW(A1S);
            AOLD(A0E) = ANEW(A0E);
            AOLD(A2S) = ANEW(A2S);
            AOLD(A1E) = ANEW(A1E);

        }
```

```
295                     else
                        {
                            /*continuity between the enzyme-layer and tissue using 5
                              * point stencils for the gradient*/
                            ANEW(A1S) = alphaT*AOLD(I0)/alphaB;
300                         ANEW(A0E) = ((18.*AOLD(I0-1) - 6.*AOLD(I0-2) + AOLD(I0-3)
                                        -10.*AOLD(I0)) + SQ(mu/lambda)*(48.*AOLD(A1S+1)
                                            -36.*AOLD(A1S+2) +16.*AOLD(A1S+3)
                                           -3.*AOLD(A1S+4)
                                           - 25.*AOLD(A1S))*(dx1/dx2))/3.;
305                         /*check how much continuity conditions have not changed*/
                            maxdiff = fabs(ANEW(A1S)-AOLD(A1S));
                            maxdiff += fabs(ANEW(A0E)-AOLD(A0E));
                            /*update the fake grid points*/
                            AOLD(A1S) = ANEW(A1S);
310                         AOLD(A0E) = ANEW(A0E);

                        }
                        /*check if the continuity conditions are converging in a
                          * reasonable number of iterations*/
315                     if(k>100)
                        {
                            fprintf(stderr,"%i\tmaxdiff=%le (%i)\n",j,maxdiff,k);
                        }
                    }
320
                }

                t+=dt;          /*update the time*/
                if(j%printTimeStep==0)
325             {
                    /*initially write the grid being used (including fake points)*/
                    if(j==0)
                    {
                        fprintf(outProfile,"%le\t",t);
330                     for(i=0;i<=I1;i++)
                            fprintf(outProfile,"%le\t",x[i]);
                        for(;i<=N;i+=printStep)
                            fprintf(outProfile,"%le\t",x[i]);
                        fprintf(outProfile,"\n");
335
                    }

                    /*output a profile of the solution at the current time*/
                    fprintf(outProfile,"%le\t",t);
340                 for(i=0;i<=I1;i++)
                        fprintf(outProfile,"%1.20e\t",AOLD(i));
                    for(;i<=N;i+=printStep)
                        fprintf(outProfile,"%1.20e\t",AOLD(i));
                    fprintf(outProfile,"\n");
345


                    fprintf(outProfile,"%le\t",t);
                    for(i=0;i<=I1;i++)
                        fprintf(outProfile,"%1.20e\t",POLD(i));
350                 for(;i<=N;i+=printStep)
                        fprintf(outProfile,"%1.20e\t",POLD(i));
                    fprintf(outProfile,"\n");

                    /*output the gradient of the electroactive product at the biosensor
355                   * core*/
                    fprintf(outSensor,"%le\t%1.20e\t%1.20e\n",t,PNEW(2)/dx1);
                }
            }

360         /*output the profile at time T*/
            for(i=0;i<N;i++)
            {
                fprintf(outFinal,"%1.20e\t%1.20e\t%1.20e\n",x[i],AOLD(i),POLD(i));
```

```
365         }


            /*free allocated memory*/
            free(A[0]);
370         free(A[1]);
            free(A);
            free(P[0]);
            free(P[1]);
            free(P);
375         free(x);
            free(RK4[0]);
            free(RK4[1]);
            free(RK4);
            return 0;
380     }


        /*load the parameter values from a file*/
385     int readParameters(char *filename)                                    readParameters
        {
            FILE *pf;
            pf = fopen(filename,"r");
            if(pf==NULL)
390             return -1;
            if(fscanf(pf,"dx1=%lf\n",&dx1)<0)
                return -2;
            if(fscanf(pf,"dx2=%lf\n",&dx2)<0)
                return -2;
395         if(fscanf(pf,"T=%lf\n",&T)<0)
                return -2;
            if(fscanf(pf,"dt=%le\n",&dt)<0)
                return -2;
            if(fscanf(pf,"PrintStep=%i\n",&printStep)<0)
400             return -2;
            if(fscanf(pf,"PrintTimeStep=%i\n",&printTimeStep)<0)
                return -2;
            if(fscanf(pf,"R3=%lf\n",&R3)<0)
                return -2;
405         if(fscanf(pf,"R2=%lf\n",&R2)<0)
                return -2;
            if(fscanf(pf,"R1=%lf\n",&R1)<0)
                return -2;
            if(fscanf(pf,"R0=%lf\n",&R0)<0)
410             return -2;
            if(fscanf(pf,"D=%lf\n",&D)<0)
                return -2;
            if(fscanf(pf,"Dh=%lf\n",&Dh)<0)
                return -2;
415         if(fscanf(pf,"Lambda=%lf\n",&lambda)<0)
                return -2;
            if(fscanf(pf,"Mu=%lf\n",&mu)<0)
                return -2;
            if(fscanf(pf,"Vb=%lf\n",&Vb)<0)
420             return -2;
            if(fscanf(pf,"Vt=%lf\n",&Vt)<0)
                return -2;
            if(fscanf(pf,"alphaB=%lf\n",&alphaB)<0)
                return -2;
425         if(fscanf(pf,"alphaT=%lf\n",&alphaT)<0)
                return -2;
            N = (int)ceil((R3-R2)/dx2             + (R2/dx1));
            N+=4;       /*increase the number of grid point to include fake points for
                          continuity conditions*/
430         fclose(pf);
            return 0;
```

```
}

/*echo parameter values*/
int printParameters(FILE *fp)                                          printParameters
{
    fprintf(fp,"N=%i\n",N);
    fprintf(fp,"T=%lf\n",T);
    fprintf(fp,"dx=%le\n",dx);
    fprintf(fp,"dt=%le\n",dt);
    fprintf(fp,"PrintStep=%i\n",printStep);
    fprintf(fp,"PrintTimeStep=%i\n",printTimeStep);
    fprintf(fp,"R3=%le\n",R3);
    fprintf(fp,"R2=%le\n",R2);
    fprintf(fp,"R1=%le\n",R1);
    fprintf(fp,"R0=%le\n",R0);
    fprintf(fp,"D=%le\n",D);
    fprintf(fp,"Dh=%le\n",Dh);
    fprintf(fp,"Lambda=%lf\n",lambda);
    fprintf(fp,"Mu=%lf\n",mu);
    fprintf(fp,"Vb=%lf\n",Vb);
    fprintf(fp,"Vt=%lf\n",Vt);
    fprintf(fp,"A*=%lf\n",A0);
    fprintf(fp,"alphaB=%lf\n",alphaB);
    fprintf(fp,"alphaT=%lf\n",alphaT);
    fflush(fp);
    return 0;
}

int main(int argc, char** argv)                                        main
{
    FILE *outProfile, *outSensor,*outFinal;
    int err;
    if(argc<6)
    {
        fprintf(stderr, "Insufficient arguments.\n"
                        "REQUIRED:\t parameterFile, profileOutput sensorOutput"
                        " finalProfile A0 calibrationFlag\n");
      return -1;
    }
    err=readParamters(argv[1]);
    if(err==-1)
    {
        fprintf(stderr,"Failed to open file %s.\n",argv[1]);
      return -1;
    }
    else if(err==-2)
    {
        fprintf(stderr,"Failed to read a parameter from %s.\n",argv[1]);
      return -1;
    }

    dx=MIN(dx1,dx2);
    if(D*dt/SQ(dx)>0.5 || D*dt/SQ(lambda*dx)>0.5 || MAX(D,Dh)*dt/SQ(mu*dx)>0.5)
    {
        fprintf(stderr,
            "Error: Parameters are unstable\nD*dt/SQ(dx)>0.5\n(%le %le %le)\n",
            D*dt/SQ(dx), D*dt/SQ(lambda*dx),D*dt/SQ(lambda*dx));
      return -1;
    }
    outProfile = fopen(argv[2],"w");
    if(outProfile == NULL)
    {
        fprintf(stderr,"Failed to open file %s.\n",argv[2]);
      return -1;
    }
    outSensor = fopen(argv[3],"w");
    if(outSensor == NULL)
    {
        fprintf(stderr,"Failed to open file %s.\n",argv[3]);
```

```
        return -1;
    }
    outFinal = fopen(argv[4],"w");
    if(outFinal == NULL)
    {
        fprintf(stderr,"Failed to open file %s.\n",argv[4]);
        return -1;
    }

    A0=atof(argv[5]);
    CAL=atoi(argv[6]);
    printParameters(stderr);


    /*Call the actual method*/
    err = FTCS(outProfile,outSensor,outFinal);
    fprintf(stderr, "Function returned %i",err);
    fflush(outProfile);
    fflush(outSensor);
    fflush(outFinal);
    fclose(outProfile);
    fclose(outSensor);
    fclose(outFinal);
    return 0;

}
```

C.3 Model of a biosensor *in vivo*

The Alternating Direction Implicit (ADI) method is applied to the problem of a biosensor in 3 dimensions, the code provided is for the *in vivo* model (Figure 4.1d), a similar approach is used to the *in vitro* model (Figure 4.1c). The GNU Scientific Library is used to solve the tridiagonal system, first for a system where the radial direction is taken implicit, then for a system where the vertical direction is taken implicit. The code provides output at intervals specified in a parameters file, with the gradient at the core (Figure 4.14f) and profiles of the total concentrations of analyte and product (Figure 4.14g,h,k,j).

```
#include <stdio.h>
#include <stdlib.h>
#include <math.h>
#include <gsl/gsl_linalg.h>
#include <gsl/gsl_vector.h>
#include <gsl/gsl_errno.h>
#include <zlib.h>
#include <string.h>
#include <assert.h>

/*simple macros*/
#define SQ(x) ((x)*(x))
#define MAX(a,b) ((a)>(b)?(a):(b))
```

```
15
#define AOLD(i,k)       A[0][i][k]
#define ANEW(i,k)       A[1][i][k]
#define POLD(i,k)       P[1][i][k]
#define PNEW(i,k)       P[1][i][k]
20
/*wrappers for functions that give a detailed error messages,
  * used when compiled with -DDEBUG*/
#ifdef DEBUG
#define DBPRINT(x)                              fprintf(stderr,"%s",x)
25
#define GSL_V_SET(vec,idx,val)                  {lineno=__LINE__;                                   \
                                                gsl_vector_set(vec,idx,val);}

#define GSL_V_GET(vec,idx)                      my_vector_get(vec,idx,__LINE__)
30 #else
#define DBPRINT(x)                              {}
#define GSL_V_SET(vec,idx,val)                  gsl_vector_set(vec,idx,val)
#define GSL_V_GET(vec,idx)                      gsl_vector_get(vec,idx)
#endif
35
/*wrappers for functions that check memory is successfully allocated*/
#define SCALLOC(n,sz)                           safe_calloc(n,sz,__LINE__)
#define SMALLOC(sz)                             safe_malloc(sz,__LINE__)

40
/*report and error using the scientific library (gsl)*/
#define ERR_REP(x)          {lineno=__LINE__;                                                   \
                        if(x!=0){                                                               \ if
                            fprintf(stderr, "GSL error: %s\n\tin %s at (%d)\n",                 \
45                              gsl_strerror(x), __FILE__, __LINE__);                           \
                        return -1;}}
/*report and error using the compression library (zlib)*/
#define ERR_ZLIB(x) {if(x<0){                                                                   \
                            fprintf(stderr,                                                     \ fprintf
50                          "Zlib error %s:%d: %s returned a bad status of %d.\n", \
                            __FILE__, __LINE__,#x, x);                                          \
                        exit(x);}}

/*constants used when compressing output*/
55 #define CHUNK 32768
#define windowBits 15
#define GZIP_ENCODING 16
#define MESG_SIZE 16384

60



/*
  * Global variables
65  */

double dx,dz,           /*grid step sizes*/
       dt,              /*time step*/
       depth,           /*depth of the solution*/
70     length,          /*length of the biosensor core (l_b)*/
       width,           /*thickness of the enzyme-layer (w)*/
       dmg,             /*thickness of the free-region (d)*/
       T,               /*duration of the solution*/
       R0,              /*radius of the biosensor core (r_b)*/
75     R1,              /*boundary between the enzyme-layer and free-region (r_f)*/

       R2,              /*boundary between the free-region and tissue (r_t)*/

       R3,              /*maximum radius of the solution*/
80     Pz,              /*length of the plastic sheath inserted into tissue (l_p)*/
       Cz,              /*depth of the biosensor core (l_p + l_b)*/
       Ez,              /*depth of the enzyme layer (l_p + l_b + w))*/
```

```
            Fz,             /*depth of the free-region (l_p + l_b + w + d))*/
            D,              /*analyte free-diffusion coefficient (D_g)*/
            Dp,             /*product free-diffusion coefficient)*/
            lambda,         /*tissue tortuosity (D_t = D/λ^2)*/
            mu,             /*product tortuosity (D_b = D/μ^2)*/
            Vt,             /*tissue reaction rate (v_t)*/
            Vb,             /*enzyme-layer reaction rate (v_b)*/
            A0,             /*steady-state tissue concentration (A*)*/
            alphaT,         /*tissue porosity (α_t)*/
            alphaB;         /*enzyme-layer porosity (α_b)*/

    int     N,M,            /*number of grid points in the r and z direction*/
            I0,             /*column number of grid corresponding to R0*/
            I1,             /*column number of grid corresponding to R1*/
            K0,             /*row number of grid corresponding to the base of the plastic
                              sheath*/
            K1,             /*row number of grid corresponding to the base of the
                              biosensor core*/
            K2,             /*row number of grid corresponding to the base of the
                              free-region*/
            K3,             /*row number of grid corresponding to the base of the
                              enzyme layer*/
            lineno;         /*line number reported in debug messages*/

    int printSensorStep,            /*frequency of output to sensor file*/
        printTimeStep;              /*frequency of output of profile files*/

    /*array used for writing compressed output*/
    unsigned char zout[CHUNK];

    typedef struct zfile
    {
        FILE*    file;
        z_stream stream;
    }zfile;


    /*function reports an error with in the scientific library (gsl)*/
    void errHandler (const char * reason, const char * file, int line,          errHandler
        int gsl_errno)
    {
        fprintf(stderr,"GSL Error occurred: %s \t(%s)\nFile: %s at %d [from %d]\n",
            reason,gsl_strerror(gsl_errno),file,line,lineno);
        exit(-1);
    }

    /*wrapper for calloc function that checks memory has been allocated*/
    void* safe_calloc(size_t nmemb, size_t size, int line)                      safe_calloc
    {
        void* ptr = calloc(nmemb,size);
        if(ptr==NULL)
        {
            fprintf(stderr,"Error occurred: calloc failed at line %d\n",line);
        }
        return ptr;
    }
    /*wrapper for malloc function that checks memory has been allocated*/
    void* safe_malloc(size_t size, int line)                                    safe_malloc
    {
        void* ptr = malloc(size);
        if(ptr==NULL)
        {
            fprintf(stderr,"Error occurred: malloc failed at line %d\n",line);
        }
        return ptr;
    }


    /*function initialised stream for compressed output*/
```

zstream_init

```
int zstream_init(z_stream * strm)
{
      strm->zalloc = Z_NULL;
      strm->zfree  = Z_NULL;
      strm->opaque = Z_NULL;
      ERR_ZLIB(deflateInit2(strm, Z_DEFAULT_COMPRESSION, Z_DEFLATED,
            windowBits | GZIP_ENCODING, 8, Z_DEFAULT_STRATEGY));
      return 0;
}

/*function opens a file for compressed output*/
```

zfopen

```
zfile* zfopen(const char * name)
{
      zfile* zf = (zfile*)SCALLOC(1,sizeof(struct zfile));
      zf->file = fopen(name,"w");
      if(zf->file == NULL)
         {
             fprintf(stderr,"Failed to create file %s.\n",name);
         exit(-1);
         }
      zstream_init(&zf->stream);
      return zf;
}

/*function writes compressed output*/
```

zprint

```
int zprint(zfile* F, char * msg)
{
      F->stream.next_in = (unsigned char*)msg;
      int have;

      F->stream.avail_in = strlen(msg);
      do {
            F->stream.avail_out = CHUNK;
            F->stream.next_out = zout;
            ERR_ZLIB(deflate(&F->stream, Z_NO_FLUSH));
            have = CHUNK - F->stream.avail_out;
            fwrite(zout, sizeof(char), have, F->file);
      }
      while (F->stream.avail_out == 0);
      bzero(msg,MESG_SIZE*sizeof(unsigned char));
      return 0;
}


/*function closes file used for compressed output*/
```

zfclose

```
int zfclose(zfile* F, char* msg)
{
      int flag;
      int have;
      F->stream.avail_in = strlen(msg);
      do {
            F->stream.avail_out = CHUNK;
            F->stream.next_out = zout;
            flag = deflate(&F->stream, Z_FINISH);
            ERR_ZLIB(flag)
            have = CHUNK - F->stream.avail_out;
            fwrite(zout, sizeof(char), have, F->file);
      }
      while (F->stream.avail_out == 0 && flag == Z_OK);
      fflush(F->file);
      fclose(F->file);
      deflateEnd(&F->stream);
      free(F);
      bzero(msg,MESG_SIZE*sizeof(unsigned char));
      return 0;
}

/*function wrapper for gsl_vector_get that checks for NaN, only used when
  * compiled with -DDEBUG*/
```

my_vector_get

```
double my_vector_get(gsl_vector* v, int idx,int lineno)
{
    double ret = gsl_vector_get(v,idx);
    if(isnan(ret))
    {
        fprintf(stderr,"Error: %ith value is NaN at %d\n",idx,lineno);
        exit(-1);
    }
    return ret;
}

/*function computes the solution and writes the sensor output (outSensor) and
  * a series of profiles to files that start with file name*/
```

solver

```
int solver(FILE* outSensor, char* filename)
{
    /*set a function for reporting GSL errors*/
    gsl_set_error_handler(&errHandler);

    double t=0,                          /*time*/
           cb=Vb*SQ(mu*dx)/D,            /*enzyme-layer reaction*/
           ct=Vt*SQ(lambda*dx)/D;         /*tissue reaction*/

    unsigned int i,j,k;                  /*indices*/

    int IC,          /*column number of fake grid points for boundary condition at
                       * biosensor core (r_b)*/
        A0E,A1S, /*column numbers of fake grid points for continuity conditions
                       * at the edge of the enzyme-layer (r_f)*/
        A1E,A2S, /*column numbers of fake grid points for continuity conditions
                       * at the edge of the free-region (r_t)*/
        EzE,FzS, /*row numbers of fake grid points for continuity conditions at
                       * the edge of the enzyme-layer (l_p + l_b + w)*/
        FzE,TzS; /*row numbers of fake grid points for continuity conditions at
                       * the edge of the free region (l_p + l_b + w + d)*/

    /*file names for writing profiles of the analyte and product*/
    char* fname = (char*)SCALLOC((strlen(filename)+35),sizeof(char));

    /*buffer for writing compressed output*/
    char* msg = (unsigned char*)SCALLOC(MESG_SIZE,sizeof(unsigned char*));
    /*zip file pointer for compressed output*/
    zfile* zf;

    /*grids for the analyte and product*/
    double*** A = (double***)SMALLOC(2*sizeof(double**));
    double*** P = (double***)SMALLOC(2*sizeof(double**));
    for(j=0;j<2;j++)
    {
        A[j] = (double**)SMALLOC((N+1)*sizeof(double*));
        for(i=0;i<=N;i++)
            A[j][i] = (double*)SCALLOC(M+1,sizeof(double));
    }
    double *z = (double*)SMALLOC((M+1)*sizeof(double));
    double *x = (double*)SMALLOC((N+1)*sizeof(double));


    /*set the spatial directions, including fake points for the boundaries
      * between regions*/
    z[0] = -dz/2.;
    for(k=1;k<=M;k++)
    {
        z[k]=z[k-1]+dz;
        if(z[k]<=Pz && z[k]+dz>Pz)
        {
            K0=k;
        }
        if(z[k]<=Cz && z[k]+dz>Cz)
        {
            K1=k;
```

```
290             }
                if(z[k]<=Ez  &&  z[k]+dz>Ez)
                {
                        K2=k;
                        z[k+1]=z[k];k++;EzE=k;
295                     FzS=k+1;
                }
                if(z[k]<=Fz  &&  z[k]+dz>Fz)
                {
                        K3=k;
300                     z[k+1]=z[k];k++;FzE=k;
                        TzS=k+1;
                }
        }
        x[0] = -dx/2.;
305     unsigned char DMG = R1<R2;
        unsigned char LAST;
        for(i=1;i<=N;i++)
        {
                x[i] = x[i-1]+dx;
310             if(x[i]<=R0  &&  x[i]+dx>R0)
                {
                    IC=i;
                }
                if(x[i]<=R1  &&  x[i]+dx>R1)
315             {
                        I0=i;
                        x[i+1]=x[i];i++;A0E=i;
                        A1S=i+1;
                }
320             if(x[i]<=R2  &&  x[i]+dx>R2)
                {
                        I1=i;
                        x[i+1]=x[i];i++;A1E=i;
                        A2S=i+1;
325             }
        }

        /*set the initial conditions*/
        for(i=0;i<=N;i++)
330     {
                for(k=0;k<=M;k++)
                {
                        A[0][i][k]=0;
                        A[1][i][k]=0;
335             }
        }
        for(i=A2S;i<=N;i++)
        {
                for(k=0;k<=M;k++)
340             {
                        A[0][i][k]=A0;
                        A[1][i][k]=A0;
                }
        }
345     for(k=TzS;k<=M;k++)
        {
                for(i=1;i<=N;i++)
                {
                        A[0][i][k]=A0;
350                     A[1][i][k]=A0;
                }
        }
        int Wx = I0+1,          /*reduced grid directions for electroactive product*/
                Wz = K2+1;      /*which is limited to the enzyme layer*/
355     for(j=0;j<2;j++)
        {
                P[j] = (double**)SMALLOC((Wx+1)*sizeof(double*));
                for(i=0;i<=Wx;i++)
```

```
                P[j][i] = (double*)SCALLOC(Wz+1,sizeof(double));
360     }
        for(j=0;j<2;j++)
        {
            for(i=0;i<=Wx;i++)
            {
                for(k=0;k<=Wz;k++)
                    P[j][i][k]=0;
            }
        }
        fprintf(stderr,"R2=x[%i]=%e (%i %i) R1=x[%i]=%e (%i %i) R0=x[%i]=%e\n",I1,x[I1],A0E,A1S,I0,x[I0],A1E,A2S,IC,x[IC]);
370     fprintf(stderr,"K3=z[%i]=%e (%i %i) K2=z[%i]=%e (%i %i) K1=z[%i]=%e                                    K0=z[%i]=%e\n",K3,z[K3],FzE,TzS,K2,z[K2],EzI

        /*allocate vectors used to form and solve the tridiagonal system
          *vectors for the radial direction*/
        gsl_vector* MrDiag          = gsl_vector_alloc(N+1);
375     gsl_vector* MrUpper         = gsl_vector_alloc(N);
        gsl_vector* MrLower         = gsl_vector_alloc(N);
        gsl_vector* bk              = gsl_vector_alloc(N+1);
        gsl_vector* MrDiagP         = gsl_vector_alloc(N+1);
        gsl_vector* MrUpperP = gsl_vector_alloc(N);
380     gsl_vector* MrLowerP = gsl_vector_alloc(N);
        gsl_vector* bkP             = gsl_vector_alloc(N+1);
        gsl_vector* MrDiagE         = gsl_vector_alloc(N+1);
        gsl_vector* MrUpperE = gsl_vector_alloc(N);
        gsl_vector* MrLowerE = gsl_vector_alloc(N);
385     gsl_vector* bkE             = gsl_vector_alloc(N+1);
        gsl_vector* MrDiagT         = gsl_vector_alloc(N+1);
        gsl_vector* MrUpperT = gsl_vector_alloc(N);
        gsl_vector* MrLowerT = gsl_vector_alloc(N);
        gsl_vector* bkT             = gsl_vector_alloc(N+1);
390     gsl_vector* MrDiagF         = gsl_vector_alloc(N+1);
        gsl_vector* MrUpperF = gsl_vector_alloc(N);
        gsl_vector* MrLowerF = gsl_vector_alloc(N);
        gsl_vector* bkF             = gsl_vector_alloc(N+1);
        gsl_vector* xk              = gsl_vector_alloc(N+1);
395
        /*vectors for the vertical direction*/
        gsl_vector* MzDiagF         = gsl_vector_alloc(M+1);
        gsl_vector* MzUpperF = gsl_vector_alloc(M);
        gsl_vector* MzLowerF = gsl_vector_alloc(M);
400     gsl_vector* biF             = gsl_vector_alloc(M+1);
        gsl_vector* MzDiagE         = gsl_vector_alloc(M+1);
        gsl_vector* MzUpperE = gsl_vector_alloc(M);
        gsl_vector* MzLowerE = gsl_vector_alloc(M);
        gsl_vector* biE             = gsl_vector_alloc(M+1);
405     gsl_vector* MzDiagB         = gsl_vector_alloc(M+1);
        gsl_vector* MzUpperB = gsl_vector_alloc(M);
        gsl_vector* MzLowerB = gsl_vector_alloc(M);
        gsl_vector* biB             = gsl_vector_alloc(M+1);
        gsl_vector* MzDiagT         = gsl_vector_alloc(M+1);
410     gsl_vector* MzUpperT = gsl_vector_alloc(M);
        gsl_vector* MzLowerT = gsl_vector_alloc(M);
        gsl_vector* biT             = gsl_vector_alloc(M+1);
        gsl_vector* xi              = gsl_vector_alloc(M+1);

415     /*vectors for the product in the radial direction*/
        gsl_vector* PrDiag          = gsl_vector_alloc(Wx+1);
        gsl_vector* PrUpper         = gsl_vector_alloc(Wx);
        gsl_vector* PrLower         = gsl_vector_alloc(Wx);
        gsl_vector* bPk             = gsl_vector_alloc(Wx+1);
420     gsl_vector* PrDiagC         = gsl_vector_alloc(Wx+1);
        gsl_vector* PrUpperC = gsl_vector_alloc(Wx);
        gsl_vector* PrLowerC = gsl_vector_alloc(Wx);
        gsl_vector* bPkC            = gsl_vector_alloc(Wx+1);
        gsl_vector* xPk             = gsl_vector_alloc(Wx+1);
425
        /*vectors for the product in the vertical direction*/
        gsl_vector* PzDiag          = gsl_vector_alloc(Wz+1);
```

```
gsl_vector* PzUpper          = gsl_vector_alloc(Wz);
gsl_vector* PzLower          = gsl_vector_alloc(Wz);
gsl_vector* bPi              = gsl_vector_alloc(Wz+1);
gsl_vector* PzDiagP          = gsl_vector_alloc(Wz+1);
gsl_vector* PzUpperP = gsl_vector_alloc(Wz);
gsl_vector* PzLowerP = gsl_vector_alloc(Wz);
gsl_vector* bPiP             = gsl_vector_alloc(Wz+1);
gsl_vector* xPi              = gsl_vector_alloc(Wz+1);


/*
 *
 *
 * Create Vectors
 *
 *
 */

/*
 *
 * Tri-diagonal system for the analyte in the radial direction
 * There are 5 different cases depending on the depth there are;
 * 1) biosensor core followed by the enzyme-layer, free-region and tissue
 * 2) plastic sheath followed by the free-region and the tissue
 * 3) enzyme-layer followed by free-region and tissue
 * 4) free-region followed by tissue
 * 5) tissue
 *
 * Vectors for the RHS of the tri-diagonal system are created in turn with
 * the corresponding boundary and continuity conditions.
 */

 /*
 * Core—-Enzyme—-Free—Tissue
 */
/*Zero in core*/
for(i=0;i<IC-1;i++)
{
      GSL_V_SET(MrDiag,i,1);
      GSL_V_SET(MrUpper,i,0);
      GSL_V_SET(MrLower,i,0);
}

/*Zero flux at core*/
GSL_V_SET(MrDiag,IC-1,1);
GSL_V_SET(MrUpper,IC-1,-1);

for(i=IC;i<=I0;i++)
{
      GSL_V_SET(MrDiag,i,1.+(D*dt/(2.*SQ(mu*dx)))*(2.+cb));
      GSL_V_SET(MrUpper,i,-(D*dt/(2.*SQ(mu*dx)))*(1.+(dx/2.*x[i])));
      GSL_V_SET(MrLower,i-1,-(D*dt/(2.*SQ(mu*dx)))*(1.-(dx/2.*x[i])));
}

/*Continuity condition are not time dependant*/
GSL_V_SET(MrDiag,A0E,-1);
GSL_V_SET(MrUpper,A0E,SQ(mu));
GSL_V_SET(MrLower,A0E-1,1.-SQ(mu)/alphaB);

GSL_V_SET(MrDiag,A1S,1.+(D*dt/(2.*SQ(dx)))*(2.
      +(SQ(mu)/(alphaB-SQ(mu)))*(1.-(dx/2.*x[A1S]))));
GSL_V_SET(MrUpper,A1S,-(D*dt/(2.*SQ(dx))));
GSL_V_SET(MrLower,A1S-1,  -(D*dt/(2.*SQ(dx)))*
      (1./(alphaB-SQ(mu)))*(1.-(dx/2.*x[A1S])));


for(i=A1S+1;i<=I1;i++)
{
      GSL_V_SET(MrDiag,i,1.+2.*(D*dt/(2.*SQ(dx))));
```

```
        GSL_V_SET(MrUpper,i,-(D*dt/(2.*SQ(dx)))*(1.+(dx/2.*x[i])));
        GSL_V_SET(MrLower,i-1,-(D*dt/(2.*SQ(dx)))*(1.-(dx/2.*x[i])));
    }

    GSL_V_SET(MrDiag,A1E,-1);
    GSL_V_SET(MrUpper,A1E,1./SQ(lambda));
    GSL_V_SET(MrLower,A1E-1,1.-alphaT/SQ(lambda));

    GSL_V_SET(MrDiag,A2S, 1+(D*dt/(2.*SQ(dx*lambda)))*
        (2.+ct+(1.-(dx/2.*x[A2S]))*alphaT/(SQ(lambda)-alphaT)));
    GSL_V_SET(MrUpper,A2S, -(D*dt/(2.*SQ(dx*lambda)))*(1.+(dx/2.*x[A2S])));
    GSL_V_SET(MrLower,A2S-1, -(D*dt/(2.*SQ(dx*lambda)))*
        (1.-(dx/2.*x[A2S]))*alphaT*SQ(lambda)/(SQ(lambda)-alphaT));

    for(i=A2S+1;i<N;i++)
    {
        GSL_V_SET(MrDiag,i,1+(D*dt/(2.*SQ(dx*lambda)))*(2.+ct));
        GSL_V_SET(MrUpper,i,-(D*dt/(2.*SQ(dx*lambda)))*(1.+(dx/2.*x[i])));
        GSL_V_SET(MrLower,i-1,-(D*dt/(2.*SQ(dx*lambda)))*(1.-(dx/2.*x[i])));
    }

    GSL_V_SET(MrLower,N-1,0);
    GSL_V_SET(MrDiag,N,1);

    for(i=0;i<IC;i++)
        GSL_V_SET(bk,i,0);              /*Zero in core*/

    GSL_V_SET(bk,A0E,0);                /*Continuity conditions*/
    GSL_V_SET(bk,A1E,0);
    GSL_V_SET(bk,N,A0);                 /*Zero flux*/

    DBPRINT("Created vectors for first row:\tCore---Enzyme---Free---Tissue\n");

    /*
      * Plastic—Free—-Tissue
      */
    /*Zero in plastic*/
    for(i=0;i<=I0;i++)
    {
        GSL_V_SET(MrDiagP,i,1);
        GSL_V_SET(MrUpperP,i,0);
        GSL_V_SET(MrLowerP,i,0);
    }

    /*Zero flux at the boundary with the plastic sheath*/
    GSL_V_SET(MrDiagP,A0E,1);
    GSL_V_SET(MrUpperP,A0E,-1);

    for(i=A1S;i<=I1;i++)
    {
        GSL_V_SET(MrDiagP,i,1.+2.*(D*dt/(2.*SQ(dx))));
        GSL_V_SET(MrUpperP,i,-(D*dt/(2.*SQ(dx)))*(1.+(dx/2.*x[i])));
        GSL_V_SET(MrLowerP,i-1,-(D*dt/(2.*SQ(dx)))*(1.-(dx/2.*x[i])));
    }
    GSL_V_SET(MrDiagP,A1E,-1);
    GSL_V_SET(MrUpperP,A1E,1./SQ(lambda));
    GSL_V_SET(MrLowerP,A1E-1,1.-alphaT/SQ(lambda));

    GSL_V_SET(MrDiagP,A2S, 1+(D*dt/(2.*SQ(dx*lambda)))*
        (2.+ct+(1.-(dx/2.*x[A2S]))*alphaT/(SQ(lambda)-alphaT)));
    GSL_V_SET(MrUpperP,A2S, -(D*dt/(2.*SQ(dx*lambda)))*(1.+(dx/2.*x[A2S])));
    GSL_V_SET(MrLowerP,A2S-1, -(D*dt/(2.*SQ(dx*lambda)))*
        (1.-(dx/2.*x[A2S]))*alphaT*SQ(lambda)/(SQ(lambda)-alphaT));

    for(i=A2S+1;i<N;i++)
    {
        GSL_V_SET(MrDiagP,i,1.+(D*dt/(2.*SQ(dx*lambda)))*(2.+ct));
        GSL_V_SET(MrUpperP,i,-(D*dt/(2.*SQ(dx*lambda)))*(1.+(dx/2.*x[i])));
        GSL_V_SET(MrLowerP,i-1,-(D*dt/(2.*SQ(dx*lambda)))*(1.-(dx/2.*x[i])));
```

```
}

GSL_V_SET(MrLowerP,N-1,0);
GSL_V_SET(MrDiagP,N,1);

for(i=0;i<=I0;i++)
    GSL_V_SET(bkP,i,0);          /*Zero in plastic*/

GSL_V_SET(bkP,A0E,0);            /*Continuity conditions*/
GSL_V_SET(bkP,A1E,0);
GSL_V_SET(bkP,N,A0);             /*A(N)=A**/

DBPRINT("Created vectors for second row:\tPlastic---Free---Tissue\n");


/*
  * Enzyme—-Free—Tissue
  */
/*Zero flux at zero*/
GSL_V_SET(MrDiagE,0,1);
GSL_V_SET(MrUpperE,0,-1);

for(i=1;i<=I0;i++)
{
    GSL_V_SET(MrDiagE,i,1.+(D*dt/(2.*SQ(mu*dx)))*(2.+cb));
    GSL_V_SET(MrUpperE,i,-(D*dt/(2.*SQ(mu*dx)))*(1.+(dx/2.*x[i])));
    GSL_V_SET(MrLowerE,i-1,-(D*dt/(2.*SQ(mu*dx)))*(1.-(dx/2.*x[i])));
}

/*Continuity condition are not time dependant*/
GSL_V_SET(MrDiagE,A0E,-1);
GSL_V_SET(MrUpperE,A0E,SQ(mu));
GSL_V_SET(MrLowerE,A0E-1,1.-SQ(mu)/alphaB);

GSL_V_SET(MrDiagE,A1S,1.+(D*dt/(2.*SQ(dx)))*(2.
    +(SQ(mu)/(alphaB-SQ(mu)))*(1.-(dx/2.*x[A1S]))));
GSL_V_SET(MrUpperE,A1S,-(D*dt/(2.*SQ(dx))));
GSL_V_SET(MrLowerE,A1S-1, -(D*dt/(2.*SQ(dx)))*
    (1./(alphaB-SQ(mu)))*(1.-(dx/2.*x[A1S])));


for(i=A1S+1;i<=I1;i++)
{
    GSL_V_SET(MrDiagE,i,1.+2.*(D*dt/(2.*SQ(dx))));
    GSL_V_SET(MrUpperE,i,-(D*dt/(2.*SQ(dx)))*(1.+(dx/2.*x[i])));
    GSL_V_SET(MrLowerE,i-1,-(D*dt/(2.*SQ(dx)))*(1.-(dx/2.*x[i])));
}

GSL_V_SET(MrDiagE,A1E,-1);
GSL_V_SET(MrUpperE,A1E,1./SQ(lambda));
GSL_V_SET(MrLowerE,A1E-1,1. - alphaT/SQ(lambda));

GSL_V_SET(MrDiagE,A2S, 1+(D*dt/(2.*SQ(dx*lambda)))*
    (2.+ct+(1.-(dx/2.*x[A2S]))*alphaT/(SQ(lambda)-alphaT)));
GSL_V_SET(MrUpperE,A2S, -(D*dt/(2.*SQ(dx*lambda)))*(1.+(dx/2.*x[A2S])));
GSL_V_SET(MrLowerE,A2S-1, -(D*dt/(2.*SQ(dx*lambda)))*
    (1.-(dx/2.*x[A2S]))*alphaT*SQ(lambda)/(SQ(lambda)-alphaT));

for(i=A2S+1;i<N;i++)
{
    GSL_V_SET(MrDiagE,i,1.+(D*dt/(2.*SQ(dx*lambda)))*(2.+ct));
    GSL_V_SET(MrUpperE,i,-(D*dt/(2.*SQ(dx*lambda)))*(1.+(dx/2.*x[i])));
    GSL_V_SET(MrLowerE,i-1,-(D*dt/(2.*SQ(dx*lambda)))*(1.-(dx/2.*x[i])));
}

GSL_V_SET(MrLowerE,N-1,0);
GSL_V_SET(MrDiagE,N,1);

GSL_V_SET(bkE,0,0);              /*Zero flux at zero*/
```

```
635     GSL_V_SET(bkE,A0E,0);           /*Continuity conditions*/
        GSL_V_SET(bkE,A1E,0);
        GSL_V_SET(bkE,N,A0);            /*A(N)=A* */

        DBPRINT("Created vectors for third row:\tEnzyme---Free---Tissue\n");
640

        /*
         * Free—Tissue
         */
645     /*Zero flux at zero*/
        GSL_V_SET(MrDiagF,0,1);
        GSL_V_SET(MrUpperF,0,-1);

        for(i=1;i<=I1;i++)
650     {
            GSL_V_SET(MrDiagF,i,1.+2.*(D*dt/(2.*SQ(dx))));
            GSL_V_SET(MrUpperF,i,-(D*dt/(2.*SQ(dx)))*(1.+(dx/2.*x[i])));
            GSL_V_SET(MrLowerF,i-1,-(D*dt/(2.*SQ(dx)))*(1.-(dx/2.*x[i])));
        }
655
        /*Bridge over the fake grid point*/
        GSL_V_SET(MrDiagF,I0,1.+(3.+(dx/2.*x[I0]))*(D*dt/(2.*SQ(dx))));
        GSL_V_SET(MrUpperF,I0,-2.*(D*dt/(2.*SQ(dx)))*(1.+(dx/2.*x[I0])));
        GSL_V_SET(MrDiagF,A0E,-1);
660     GSL_V_SET(MrUpperF,A0E,0.5);
        GSL_V_SET(MrLowerF,A0E-1,0.5);
        GSL_V_SET(MrDiagF,A1S,1.+(3.-(dx/2.*x[A1S]))*(D*dt/(2.*SQ(dx))));
        GSL_V_SET(MrLowerF,A1S-1,-2.*(D*dt/(2.*SQ(dx)))*(1.-(dx/2.*x[A1S])));

665
        GSL_V_SET(MrDiagF,A1E,-1);
        GSL_V_SET(MrUpperF,A1E,1./SQ(lambda));
        GSL_V_SET(MrLowerF,A1E-1,1. - alphaT/SQ(lambda));

670     GSL_V_SET(MrDiagF,A2S, 1+(D*dt/(2.*SQ(dx*lambda)))*
            (2.+ct+(1.-(dx/2.*x[A2S]))*alphaT/(SQ(lambda)-alphaT)));
        GSL_V_SET(MrUpperF,A2S, -(D*dt/(2.*SQ(dx*lambda)))*(1.+(dx/2.*x[A2S])));
        GSL_V_SET(MrLowerF,A2S-1, -(D*dt/(2.*SQ(dx*lambda)))*
            (1.-(dx/2.*x[A2S]))*alphaT*SQ(lambda)/(SQ(lambda)-alphaT));
675
        for(i=A2S+1;i<N;i++)
        {
            GSL_V_SET(MrDiagF,i,1+(D*dt/(2.*SQ(dx*lambda)))*(2.+ct));
            GSL_V_SET(MrUpperF,i,-(D*dt/(2.*SQ(dx*lambda)))*(1.+(dx/2.*x[i])));
680         GSL_V_SET(MrLowerF,i-1,-(D*dt/(2.*SQ(dx*lambda)))*(1.-(dx/2.*x[i])));
        }

        GSL_V_SET(MrLowerF,N-1,0);
        GSL_V_SET(MrDiagF,N,1);
685
        GSL_V_SET(bkF,0,0);             /*Zero flux at zero*/
        GSL_V_SET(bkF,A0E,0);           /*Continuity conditions*/
        GSL_V_SET(bkF,A1E,0);
        GSL_V_SET(bkF,N,A0);            /*A(N)=A* */
690
        DBPRINT("Created vectors for fourth row:\tFree---Tissue\n");

        /*
         * Tissue
695      */
        /*Zero flux at zero*/
        GSL_V_SET(MrDiagT,0,1);
        GSL_V_SET(MrUpperT,0,-1);

700     for(i=1;i<N;i++)
        {
            GSL_V_SET(MrDiagT,i,1.+(D*dt/(2.*SQ(dx*lambda)))*(2.+ct));
            GSL_V_SET(MrUpperT,i,-(D*dt/(2.*SQ(dx*lambda)))*(1.+(dx/2.*x[i])));
```

```
        GSL_V_SET(MrLowerT,i-1,-(D*dt/(2.*SQ(dx*lambda)))*(1.-(dx/2.*x[i])));
}

/*Bridge over the extra points*/
GSL_V_SET(MrDiagT,I0,1.+(3.+ct+(dx/2.*x[I0]))*(D*dt/(2.*SQ(dx*lambda))));
GSL_V_SET(MrUpperT,I0,-2.*(D*dt/(2.*SQ(dx*lambda)))*(1.+(dx/2.*x[I0])));
GSL_V_SET(MrDiagT,A0E,-1);
GSL_V_SET(MrUpperT,A0E,0.5);
GSL_V_SET(MrLowerT,A0E-1,0.5);
GSL_V_SET(MrDiagT,A1S,1.+(3.+ct-(dx/2.*x[A1S]))*(D*dt/(2.*SQ(dx*lambda))));
GSL_V_SET(MrLowerT,A1S-1,-2.*(D*dt/(2.*SQ(dx*lambda)))*(1.-(dx/2.*x[A1S])));

GSL_V_SET(MrDiagT,I1,1.+(3.+ct+dx/x[I1])*(D*dt/(2.*SQ(dx*lambda))));
GSL_V_SET(MrUpperT,I1,-2.*(D*dt/(2.*SQ(dx*lambda)))*(1.+dx/x[I1]));
GSL_V_SET(MrDiagT,A1E,-1);
GSL_V_SET(MrUpperT,A1E,0.5);
GSL_V_SET(MrLowerT,A1E-1,0.5);
GSL_V_SET(MrDiagT,A2S,1.+(3.+ct-(dx/2.*x[A2S]))*(D*dt/(2.*SQ(dx*lambda))));
GSL_V_SET(MrLowerT,A2S-1,-2.*(D*dt/(2.*SQ(dx*lambda)))*(1.-(dx/2.*x[A2S])));


GSL_V_SET(MrLowerT,N-1,0);              /*Zero flux*/
GSL_V_SET(MrDiagT,N,1);

GSL_V_SET(bkT,0,0);             /*Zero flux at 0*/
GSL_V_SET(bkT,A0E,0);           /*Continuity conditions*/
GSL_V_SET(bkT,A1E,0);
GSL_V_SET(bkT,N,A0);            /*A(N)=A* */

DBPRINT("Created vectors for fifth row:\tTissue\n");

/*
 *
 * Tri-diagonal system for the               product in the radial direction
 * As the product is limited to the enzyme layer, there are only 2 cases;
 * 1) biosensor core followed by the enzyme-layer
 * 2) enzyme layer
 *
 * Vectors for the RHS of the tri-diagonal system are created in turn with
 * the corresponding boundary and continuity conditions.
 */

/*
 * Core—Enzyme
 */
for(i=0;i<IC;i++)
{
        GSL_V_SET(PrDiagC,i,1);
        GSL_V_SET(PrUpperC,i,0);
        GSL_V_SET(PrLowerC,i,0);
}

GSL_V_SET(PrDiagC,IC,1);                /*BC - zero at core */
GSL_V_SET(PrUpperC,IC,0);

for(i=IC+1;i<Wx;i++)
{
        GSL_V_SET(PrDiagC,i,1.+2.*(Dp*dt/(2.*SQ(dx*mu))));
        GSL_V_SET(PrUpperC,i,-(Dp*dt/(2.*SQ(dx*mu)))*(1.+(dx/2.*x[i])));
        GSL_V_SET(PrLowerC,i-1,-(Dp*dt/(2.*SQ(dx*mu)))*(1.-(dx/2.*x[i])));
}

GSL_V_SET(PrDiagC,Wx,1);                /*BC - zero at free-region*/
GSL_V_SET(PrLowerC,Wx-1,0);

for(i=0;i<=IC;i++)
{
        GSL_V_SET(bPkC,i,0);
}
```

```
GSL_V_SET(bPkC,Wx,0);

/*
 * Enzyme
 */
for(i=1;i<Wx;i++)
{
      GSL_V_SET(PrDiag,i,1.+2.*(Dp*dt/(2.*SQ(dx*mu))));
      GSL_V_SET(PrUpper,i,-(Dp*dt/(2.*SQ(dx*mu)))*(1.+(dx/2.*x[i])));
      GSL_V_SET(PrLower,i-1,-(Dp*dt/(2.*SQ(dx*mu)))*(1.-(dx/2.*x[i])));
}

GSL_V_SET(PrDiag,0,1);              /*BC zero flux at r=0*/
GSL_V_SET(PrUpper,0,-1);

GSL_V_SET(PrDiag,Wx,1);
GSL_V_SET(PrLower,Wx-1,0);

GSL_V_SET(bPk,0,0);
GSL_V_SET(bPk,Wx,0);



/*
 *
 *
 * Tridiagonal system for the vertical direction
 *
 * There are 4 cases to consider for columns in the system
 * 1) Plastic sheath followed by biosensor core, enzyme-layer, free-region
 *      and tissue.
 * 2) Plastic sheath followed by enzyme-layer, free-region and tissue.
 * 3) Free region followed by tissue.
 * 4) Tissue.
 *
 * Vectors for the RHS of the tri-diagonal system are created for each of
 * these cases with the corresponding boundary and continuity conditions.
 */


/*
 * Plastic—Core—Enzyme—Free—Tissue
 */

/*No analyte in plastic and core*/
for(k=0;k<K1;k++)
{
      GSL_V_SET(MzDiagB,k,1);
      GSL_V_SET(MzUpperB,k,0);
      GSL_V_SET(MzLowerB,k,0);
}

/*Zero flux at core*/
GSL_V_SET(MzDiagB,K1,1);
GSL_V_SET(MzUpperB,K1,-1);

for(k=K1+1;k<=K2;k++)
{
      GSL_V_SET(MzDiagB, k, 1.+2.*(D*dt/(2.*SQ(dz*mu))));
      GSL_V_SET(MzUpperB,k,      -(D*dt/(2.*SQ(dz*mu))));
      GSL_V_SET(MzLowerB,k-1,-(D*dt/(2.*SQ(dz*mu))));
}

GSL_V_SET(MzDiagB,EzE,-1);
GSL_V_SET(MzUpperB,EzE,SQ(mu));
GSL_V_SET(MzLowerB,EzE-1,1.-SQ(mu)/alphaB);

GSL_V_SET(MzDiagB,FzS,          1.+(D*dt/(2.*SQ(dz)))*(2.+SQ(mu)/(alphaB-SQ(mu))));
```

```
GSL_V_SET(MzUpperB,FzS,          -(D*dt/(2.*SQ(dz))));
GSL_V_SET(MzLowerB,FzS-1,-(D*dt/(2.*SQ(dz)))*(SQ(mu)/(alphaB-SQ(mu))));

for(k=FzS+1;k<=K3;k++)
{
      GSL_V_SET(MzDiagB,  k,  1.+2.*(D*dt/(2.*SQ(dz))));
      GSL_V_SET(MzUpperB,k,            -(D*dt/(2.*SQ(dz))));
      GSL_V_SET(MzLowerB,k-1,-(D*dt/(2.*SQ(dz))));
}

GSL_V_SET(MzDiagB,FzE,-1);
GSL_V_SET(MzUpperB,FzE,1./SQ(lambda));
GSL_V_SET(MzLowerB,FzE-1,1.-alphaT/SQ(lambda));

GSL_V_SET(MzDiagB,TzS,          1.+(D*dt/(2.*SQ(dz*lambda)))*
      (2.+alphaT/(SQ(lambda)-alphaT)));
GSL_V_SET(MzUpperB,TzS,          -(D*dt/(2.*SQ(dz*lambda))));
GSL_V_SET(MzLowerB,TzS-1,-(D*dt/(2.*SQ(dz*lambda)))*
      alphaT*SQ(lambda)/(SQ(lambda)-alphaT));

for(k=TzS+1;k<M;k++)
{
      GSL_V_SET(MzDiagB,  k,  1.+2.*(D*dt/(2.*SQ(dz*lambda))));
      GSL_V_SET(MzUpperB,k,        -(D*dt/(2.*SQ(dz*lambda))));
      GSL_V_SET(MzLowerB,k-1,-(D*dt/(2.*SQ(dz*lambda))));
}


/*A=A*  at  lower  boundary*/
GSL_V_SET(MzDiagB,M,1);
GSL_V_SET(MzLowerB,M-1,0);

for(k=0;k<=K1;k++)
{
      GSL_V_SET(biB,k,0);
}
GSL_V_SET(biB,EzE,0);
GSL_V_SET(biB,FzE,0);
GSL_V_SET(biB,M,A0);

DBPRINT("Created vectors for first column:\t"
      "Plastic---Core---Enzyme---Free---Tissue\n");


/*
  *  Plastic—Enzyme—Free—Tissue
  */

/*Zero  in  plastic*/
for(k=0;k<K0;k++)
{
      GSL_V_SET(MzDiagE,k,1);
      GSL_V_SET(MzUpperE,k,0);
      GSL_V_SET(MzLowerE,k,0);
}

/*Zero  flux  at  plastic*/
GSL_V_SET(MzDiagE,K0,1);
GSL_V_SET(MzUpperE,K0,-1);

for(k=K0+1;k<=K2;k++)
{
      GSL_V_SET(MzDiagE,  k,  1.+2.*(D*dt/(2.*SQ(dz*mu))));
      GSL_V_SET(MzUpperE,k,            -(D*dt/(2.*SQ(dz*mu))));
      GSL_V_SET(MzLowerE,k-1,-(D*dt/(2.*SQ(dz*mu))));
}

GSL_V_SET(MzDiagE,EzE,-1);
GSL_V_SET(MzUpperE,EzE,SQ(mu));
```

```
GSL_V_SET(MzLowerE,EzE-1,1.-SQ(mu)/alphaB);

GSL_V_SET(MzDiagE,FzS,          1.+(D*dt/(2.*SQ(dz)))*(2.+SQ(mu)/(alphaB-SQ(mu))));
GSL_V_SET(MzUpperE,FzS,         -(D*dt/(2.*SQ(dz))));
GSL_V_SET(MzLowerE,FzS-1,-(D*dt/(2.*SQ(dz)))*SQ(mu)/(alphaB-SQ(mu)));


for(k=FzS+1;k<M;k++)
{
    GSL_V_SET(MzDiagE, k, 1.+2.*(D*dt/(2.*SQ(dz))));
    GSL_V_SET(MzUpperE,k,           -(D*dt/(2.*SQ(dz))));
    GSL_V_SET(MzLowerE,k-1,-(D*dt/(2.*SQ(dz))));
}

GSL_V_SET(MzDiagE,FzE,-1);
GSL_V_SET(MzUpperE,FzE,1./SQ(lambda));
GSL_V_SET(MzLowerE,FzE-1,1.-alphaT/SQ(lambda));

GSL_V_SET(MzDiagE,TzS,          1.+(D*dt/(2.*SQ(dz*lambda)))*
    (2.+alphaT/(SQ(lambda)-alphaT)));
GSL_V_SET(MzUpperE,TzS,         -(D*dt/(2.*SQ(dz*lambda))));
GSL_V_SET(MzLowerE,TzS-1,-(D*dt/(2.*SQ(dz*lambda)))*
    alphaT*SQ(lambda)/(SQ(lambda)-alphaT));

for(k=TzS+1;k<M;k++)
{
    GSL_V_SET(MzDiagE, k, 1.+2.*(D*dt/(2.*SQ(dz*lambda))));
    GSL_V_SET(MzUpperE,k,           -(D*dt/(2.*SQ(dz*lambda))));
    GSL_V_SET(MzLowerE,k-1,-(D*dt/(2.*SQ(dz*lambda))));
}

/* A* at lower boundary*/
GSL_V_SET(MzDiagE,M,1);
GSL_V_SET(MzLowerE,M-1,0);

for(k=0;k<=K0;k++)
{
    GSL_V_SET(biE,k,0);
}
GSL_V_SET(biE,EzE,0);
GSL_V_SET(biE,FzE,0);
GSL_V_SET(biE,M,A0);

DBPRINT("Created vectors for second column:\tEnzyme---Free---Tissue\n");


/*
 * Free—Tissue
 */

/*Zero flux at surface*/
GSL_V_SET(MzDiagF,0,1);
GSL_V_SET(MzUpperF,0,-1);

for(k=1;k<=K3;k++)
{
    GSL_V_SET(MzDiagF, k, 1.+2.*(D*dt/(2.*SQ(dz))));
    GSL_V_SET(MzUpperF,k,          -(D*dt/(2.*SQ(dz))));
    GSL_V_SET(MzLowerF,k-1,-(D*dt/(2.*SQ(dz))));
}

/*Bridge over extra point*/
GSL_V_SET(MzDiagF, K2, 1.+3.*(D*dt/(2.*SQ(dz))));
GSL_V_SET(MzUpperF,K2,-2.*(D*dt/(2.*SQ(dz))));
GSL_V_SET(MzDiagF,EzE,-1);
GSL_V_SET(MzUpperF,EzE,0.5);
GSL_V_SET(MzLowerF,EzE-1,0.5);
GSL_V_SET(MzDiagF, FzS, 1.+3.*(D*dt/(2.*SQ(dz))));
GSL_V_SET(MzLowerF,FzS-1, -2.*(D*dt/(2.*SQ(dz))));
```

```
980
        GSL_V_SET(MzDiagF,FzE,-1);
        GSL_V_SET(MzUpperF,FzE,1./SQ(lambda));
        GSL_V_SET(MzLowerF,FzE-1,1.-alphaT/SQ(lambda));

985     GSL_V_SET(MzDiagF,TzS,          1.+(D*dt/(2.*SQ(dz*lambda)))*
              (2.+alphaT/(SQ(lambda)-alphaT)));
        GSL_V_SET(MzUpperF,TzS,         -(D*dt/(2.*SQ(dz*lambda))));
        GSL_V_SET(MzLowerF,TzS-1,-(D*dt/(2.*SQ(dz*lambda)))*
                alphaT*SQ(lambda)/(SQ(lambda)-alphaT));
990
        for(k=TzS+1;k<M;k++)
        {
              GSL_V_SET(MzDiagF,  k,  1.+2.*(D*dt/(2.*SQ(dz*lambda))));
              GSL_V_SET(MzUpperF,k,           -(D*dt/(2.*SQ(dz*lambda))));
995           GSL_V_SET(MzLowerF,k-1,-(D*dt/(2.*SQ(dz*lambda))));
        }

        /* A* at lower boundary*/
        GSL_V_SET(MzDiagF,M,1);
1000    GSL_V_SET(MzLowerF,M-1,0);

            GSL_V_SET(biF,0,0);
        GSL_V_SET(biF,EzE,0);
        GSL_V_SET(biF,FzE,0);
1005    GSL_V_SET(biF,M,A0);

        DBPRINT("Created vectors for third column:\tFree---Tissue\n");


1010    /*
          * Tissue
          */

        /*Zero flux at surface*/
1015    GSL_V_SET(MzDiagT,0,1);
        GSL_V_SET(MzUpperT,0,-1);

        for(k=1;k<M;k++)
        {
1020          GSL_V_SET(MzDiagT,  k,  1.+2.*(D*dt/(2.*SQ(dz*lambda))));
              GSL_V_SET(MzUpperT,k,           -(D*dt/(2.*SQ(dz*lambda))));
              GSL_V_SET(MzLowerT,k-1,-(D*dt/(2.*SQ(dz*lambda))));
        }

1025    /*Bridge over extra points*/
        GSL_V_SET(MzDiagT,  K2,  1.+3.*(D*dt/(2.*SQ(dz*lambda))));
        GSL_V_SET(MzUpperT,K2,          -2.*(D*dt/(2.*SQ(dz*lambda))));
        GSL_V_SET(MzDiagT,EzE,-1);
        GSL_V_SET(MzUpperT,EzE,0.5);
1030    GSL_V_SET(MzLowerT,EzE-1,0.5);
        GSL_V_SET(MzDiagT,  FzS,  1.+3.*(D*dt/(2.*SQ(dz*lambda))));
        GSL_V_SET(MzLowerT,FzS-1,           -2.*(D*dt/(2.*SQ(dz*lambda))));

        GSL_V_SET(MzDiagT,  K3,  1.+3.*(D*dt/(2.*SQ(dz*lambda))));
1035    GSL_V_SET(MzUpperT,K3,          -2.*(D*dt/(2.*SQ(dz*lambda))));
        GSL_V_SET(MzDiagT,FzE,-1);
        GSL_V_SET(MzUpperT,FzE,0.5);
        GSL_V_SET(MzLowerT,FzE-1,0.5);
        GSL_V_SET(MzDiagT,  TzS,  1.+3.*(D*dt/(2.*SQ(dz*lambda))));
1040    GSL_V_SET(MzLowerT,TzS-1,           -2.*(D*dt/(2.*SQ(dz*lambda))));


        /* A* flux lower boundary*/
        GSL_V_SET(MzDiagT,M,1);
1045    GSL_V_SET(MzLowerT,M-1,0);

        GSL_V_SET(biT,0,0);
        GSL_V_SET(biT,EzE,0);
```

```
GSL_V_SET(biT,FzE,0);
GSL_V_SET(biT,M,A0);

DBPRINT("Created vectors for forth column:\tTissue\n");

/*
 *
 * Tri-diagonal system for the product in the vertical direction
 * As the product is limited to the enzyme layer, there are only 2 cases;
 * 1) plastic sheath followed by the biosensor core and the enzyme-layer.
 * 2) plastic sheath followed by the enzyme layer.
 *
 * Vectors for the RHS of the tri-diagonal system are created in turn with
 * the corresponding boundary and continuity conditions.
 */

/*
 * Plastic–Core–Enzyme
 */
for(k=0;k<K1;k++)
{
      GSL_V_SET(PzDiag,k,1);
      GSL_V_SET(PzUpper,k,0);
      GSL_V_SET(PzLower,k,0);
}
GSL_V_SET(PzDiag,K1,1);
GSL_V_SET(PzUpper,K1,0);

for(k=K1+1;k<Wz;k++)
{
      GSL_V_SET(PzDiag,k,1.+2.*(Dp*dt/(2.*SQ(dz*mu))));
      GSL_V_SET(PzUpper,k,-(Dp*dt/(2.*SQ(dz*mu))));
      GSL_V_SET(PzLower,k-1,-(Dp*dt/(2.*SQ(dz*mu))));
}
GSL_V_SET(PzDiag,Wz,1);
GSL_V_SET(PzLower,Wz-1,0);

for(k=0;k<=K1;k++)
{
      GSL_V_SET(bPi,k,0);
}
GSL_V_SET(bPi,Wz,0);


/*
 * Plastic–Enzyme
 */
for(k=0;k<K0;k++)
{
      GSL_V_SET(PzDiagP,k,1);
      GSL_V_SET(PzUpperP,k,0);
      GSL_V_SET(PzLowerP,k,0);
}
GSL_V_SET(PzDiagP,K0,1);
GSL_V_SET(PzUpperP,K0,0);

for(k=K0+1;k<Wz;k++)
{
      GSL_V_SET(PzDiagP,k,1.+2.*(Dp*dt/(2.*SQ(dz*mu))));
      GSL_V_SET(PzUpperP,k,-(Dp*dt/(2.*SQ(dz*mu))));
      GSL_V_SET(PzLowerP,k-1,-(Dp*dt/(2.*SQ(dz*mu))));
}
GSL_V_SET(PzDiagP,Wz,1);
GSL_V_SET(PzLowerP,Wz-1,0);

for(k=0;k<=K0;k++)
{
      GSL_V_SET(bPiP,k,0);
}
```

```
        GSL_V_SET(bPiP,Wz,0);

1120


        for(j=0;t<T;j++)
        {
1125        /*
              *   Alternating direction implicit method, first solve in the radially
              *   For each of 5 cases decried above, create a corresponding LHS and
              *   use the Gnu Scientific Library function gsl_linalg_solve_tridiag
              *   to calculate the solution
1130          */

            /*
              * Plastic-Free-Tissue
              */
1135        for(k=1;k<=K0;k++)
            {
                for(i=A1S;i<=I1;i++)
                    GSL_V_SET(bkP,i,AOLD(i,k)+(D*dt/(2.*SQ(dz)))*
                        (AOLD(i,k-1)-2.*AOLD(i,k)+AOLD(i,k+1)));
1140            for(i=A2S;i<N;i++)
                    GSL_V_SET(bkP,i,AOLD(i,k)+(D*dt/(2.*SQ(lambda*dz)))*
                        (AOLD(i,k-1)-2.*AOLD(i,k)+AOLD(i,k+1))+dt*Vt*A0/2.);

                ERR_REP(gsl_linalg_solve_tridiag(MrDiagP,MrUpperP,MrLowerP,bkP,xk));
1145
                for(i=0;i<N;i++)
                    ANEW(i,k) = GSL_V_GET(xk,i);
            }
            /*
1150          * Core—Enzyme—Free—Tissue
              */
            for(k=K0+1;k<K1;k++)
            {
                for(i=IC;i<=I0;i++)
1155                GSL_V_SET(bk,i,AOLD(i,k)+(D*dt/(2.*SQ(mu*dz)))*
                        (AOLD(i,k+1)-2.*AOLD(i,k)+AOLD(i,k-1)));
                for(i=A1S;i<=I1;i++)
                    GSL_V_SET(bk,i,AOLD(i,k)+(D*dt/(2.*SQ(dz)))*
                        (AOLD(i,k-1)-2.*AOLD(i,k)+AOLD(i,k+1)));
1160            for(i=A2S;i<N;i++)
                    GSL_V_SET(bk,i,AOLD(i,k)+(D*dt/(2.*SQ(lambda*dz)))*
                        (AOLD(i,k-1)-2.*AOLD(i,k)+AOLD(i,k+1))+dt*Vt*A0/2.);


1165            ERR_REP(gsl_linalg_solve_tridiag(MrDiag,MrUpper,MrLower,bk,xk));

                for(i=0;i<N;i++)
                    ANEW(i,k) = GSL_V_GET(xk,i);
            }
1170        /*zero flux at plastic sheath*/
            for(i=1;i<=I0;i++)
                ANEW(i,K0)=ANEW(i,K0+1);
            /*bridge over fake points*/
            k=K1;
1175        {
                for(i=IC;i<=I0;i++)
                    GSL_V_SET(bk,i,AOLD(i,k)+(D*dt/(2.*SQ(mu*dz)))*
                        (AOLD(i,k+1)-2.*AOLD(i,k)+AOLD(i,k-1)));
                for(i=A1S;i<=I1;i++)
1180                GSL_V_SET(bk,i,AOLD(i,k)+(D*dt/(2.*SQ(dz)))*
                        (AOLD(i,k-1)-3.*AOLD(i,k)+2.*AOLD(i,k+1)));
                for(i=A2S;i<N;i++)
                    GSL_V_SET(bk,i,AOLD(i,k)+(D*dt/(2.*SQ(lambda*dz)))*
                        (AOLD(i,k-1)-3.*AOLD(i,k)+2.*AOLD(i,k+1))+dt*Vt*A0/2.);
1185
```

```
        ERR_REP(gsl_linalg_solve_tridiag(MrDiag,MrUpper,MrLower,bk,xk));

        for(i=0;i<N;i++)
            ANEW(i,k) = GSL_V_GET(xk,i);
    }

    /*
     * Enzyme—Free—Tissue
     */
    for(k=K1+1;k<K2;k++)
    {
        for(i=1;i<=I0;i++)
            GSL_V_SET(bkE,i,AOLD(i,k)+(D*dt/(2.*SQ(mu*dz)))*
                (AOLD(i,k-1)-2.*AOLD(i,k)+AOLD(i,k+1)));
        for(i=A1S;i<=I1;i++)
            GSL_V_SET(bkE,i,AOLD(i,k)+(D*dt/(2.*SQ(dz)))*
                (AOLD(i,k-1)-2.*AOLD(i,k)+AOLD(i,k+1)));
        for(i=A2S;i<N;i++)
            GSL_V_SET(bkE,i,AOLD(i,k)+(D*dt/(2.*SQ(lambda*dz)))*
                (AOLD(i,k-1)-2.*AOLD(i,k)+AOLD(i,k+1))+dt*Vt*A0/2.);

        ERR_REP(gsl_linalg_solve_tridiag(MrDiagE,MrUpperE,MrLowerE,bkE,xk));

        for(i=0;i<N;i++)
            ANEW(i,k) = GSL_V_GET(xk,i);
    }
    /*bridge over fake points*/
    k=K2;
    {
        for(i=1;i<=I0;i++)
            GSL_V_SET(bkE,i,AOLD(i,k)+(D*dt/(2.*SQ(mu*dz)))*
                (AOLD(i,k-1)-2.*AOLD(i,k)+AOLD(i,k+1)));
        for(i=A1S;i<=I1;i++)
            GSL_V_SET(bkE,i,AOLD(i,k)+(D*dt/(2.*SQ(dz)))*
                (AOLD(i,k-1)-3.*AOLD(i,k)+2.*AOLD(i,k+1)));
        for(i=A2S;i<N;i++)
            GSL_V_SET(bkE,i,AOLD(i,k)+(D*dt/(2.*SQ(lambda*dz)))*
                (AOLD(i,k-1)-3.*AOLD(i,k)+2.*AOLD(i,k+1))+dt*Vt*A0/2.);

        ERR_REP(gsl_linalg_solve_tridiag(MrDiagE,MrUpperE,MrLowerE,bkE,xk));

        for(i=0;i<N;i++)
            ANEW(i,k) = GSL_V_GET(xk,i);
    }

    /*
     * Free—Tissue
     */
    /*apply continuity conditions*/
    k=FzS;
    {
        for(i=1;i<=I0;i++)
            GSL_V_SET(bkF,i,AOLD(i,k) +
                (D*dt/(2.*SQ(mu*dz)))*(AOLD(i,k-1)*(1./(alphaB-SQ(mu)))
                - (2.+SQ(mu)/(alphaB-SQ(mu)))*AOLD(i,k) + AOLD(i,k+1)));
        for(i=A1S;i<=I1;i++)
            GSL_V_SET(bkF,i,AOLD(i,k)+(D*dt/(2.*SQ(dz)))*
                (2.*AOLD(i,k-1)-3.*AOLD(i,k)+AOLD(i,k+1)));
        for(i=A2S;i<N;i++)
            GSL_V_SET(bkF,i,AOLD(i,k)+(D*dt/(2.*SQ(lambda*dz)))*
                (2.*AOLD(i,k-1)-3.*AOLD(i,k)+AOLD(i,k+1))+dt*Vt*A0/2.);

        ERR_REP(gsl_linalg_solve_tridiag(MrDiagF,MrUpperF,MrLowerF,bkF,xk));

        for(i=0;i<N;i++)
            ANEW(i,k) = GSL_V_GET(xk,i);
    }
    for(k=FzS+1;k<=K3;k++)
    {
```

```
        for(i=1;i<=I0;i++)
            GSL_V_SET(bkF,i,AOLD(i,k)+(D*dt/(2.*SQ(dz)))*
                (AOLD(i,k-1)-2.*AOLD(i,k)+AOLD(i,k+1)));
        for(i=A1S;i<=I1;i++)
            GSL_V_SET(bkF,i,AOLD(i,k)+(D*dt/(2.*SQ(dz)))*
                (AOLD(i,k-1)-2.*AOLD(i,k)+AOLD(i,k+1)));
        for(i=A2S;i<N;i++)
            GSL_V_SET(bkF,i,AOLD(i,k)+(D*dt/(2.*SQ(lambda*dz)))*
                (AOLD(i,k-1)-2.*AOLD(i,k)+AOLD(i,k+1))+dt*Vt*A0/2.);

        ERR_REP(gsl_linalg_solve_tridiag(MrDiagF,MrUpperF,MrLowerF,bkF,xk));

        for(i=0;i<N;i++)
            ANEW(i,k) = GSL_V_GET(xk,i);
    }
    /*bridge over fake points*/
    k=K3;
    {
        for(i=1;i<=I0;i++)
            GSL_V_SET(bkF,i,AOLD(i,k)+(D*dt/(2.*SQ(dz)))*
                (AOLD(i,k-1)-2.*AOLD(i,k)+AOLD(i,k+1)));
        for(i=A1S;i<=I1;i++)
            GSL_V_SET(bkF,i,AOLD(i,k)+(D*dt/(2.*SQ(dz)))*
                (AOLD(i,k-1)-2.*AOLD(i,k)+AOLD(i,k+1)));
        for(i=A2S;i<N;i++)
            GSL_V_SET(bkF,i,AOLD(i,k)+(D*dt/(2.*SQ(lambda*dz)))*
                (AOLD(i,k-1)-3.*AOLD(i,k)+2.*AOLD(i,k+1))+dt*Vt*A0/2.);

        ERR_REP(gsl_linalg_solve_tridiag(MrDiagF,MrUpperF,MrLowerF,bkF,xk));

        for(i=0;i<N;i++)
            ANEW(i,k) = GSL_V_GET(xk,i);
    }

    /*
     * Tissue
     */
    /*apply continuity conditions*/
    k=TzS;
    {
        for(i=1;i<=I0;i++)
            GSL_V_SET(bkT,i,AOLD(i,k)+
                (D*dt/(2.*SQ(lambda*dz)))*
                (AOLD(i,k-1)*alphaT*SQ(lambda)/(SQ(lambda)-alphaT)
                -(2.+alphaT/(SQ(lambda)-alphaT))*AOLD(i,k)
                + AOLD(i,k+1)) + dt*Vt*A0/2.);
        for(i=A1S;i<=I1;i++)
            GSL_V_SET(bkT,i,AOLD(i,k)+(D*dt/(2.*SQ(lambda*dz)))*
                (2.*AOLD(i,k-1)-3.*AOLD(i,k)+AOLD(i,k+1))+dt*Vt*A0/2.);
        for(i=A2S;i<N;i++)
            GSL_V_SET(bkT,i,AOLD(i,k)+(D*dt/(2.*SQ(lambda*dz)))*
                (2.*AOLD(i,k-1)-3.*AOLD(i,k)+AOLD(i,k+1))+dt*Vt*A0/2.);

        ERR_REP(gsl_linalg_solve_tridiag(MrDiagT,MrUpperT,MrLowerT,bkT,xk));

        for(i=0;i<N;i++)
            ANEW(i,k) = GSL_V_GET(xk,i);
    }

    for(k=TzS+1;k<M;k++)
    {
        for(i=1;i<=I0;i++)
            GSL_V_SET(bkT,i,AOLD(i,k)+(D*dt/(2.*SQ(lambda*dz)))*
                (AOLD(i,k-1)-2.*AOLD(i,k)+AOLD(i,k+1))+dt*Vt*A0/2.);
        for(i=A1S;i<=I1;i++)
            GSL_V_SET(bkT,i,AOLD(i,k)+(D*dt/(2.*SQ(lambda*dz)))*
                (AOLD(i,k-1)-2.*AOLD(i,k)+AOLD(i,k+1))+dt*Vt*A0/2.);
        for(i=A2S;i<N;i++)
            GSL_V_SET(bkT,i,AOLD(i,k)+(D*dt/(2.*SQ(lambda*dz)))*
```

```
                    (AOLD(i,k-1)-2.*AOLD(i,k)+AOLD(i,k+1))+dt*Vt*A0/2.);

        ERR_REP(gsl_linalg_solve_tridiag(MrDiagT,MrUpperT,MrLowerT,bkT,xk));

        for(i=0;i<N;i++)
            ANEW(i,k) = GSL_V_GET(xk,i);
    }

    /*
     *  Alternating direction implicit method, solve for the product in the
     *  radial direction
     */

    /*
     * Core--Enzyme
     */
    for(k=K0+1;k<=K1;k++)
    {
        for(i=IC+1;i<Wx;i++)
            GSL_V_SET(bPkC,i,POLD(i,k)+(Dp*dt/(2.*SQ(mu*dz)))*
                (POLD(i,k-1)-2.*POLD(i,k)+POLD(i,k+1))
                + Vb*dt*AOLD(i,k)/2.);

        ERR_REP(gsl_linalg_solve_tridiag(PrDiagC,PrUpperC,PrLowerC,bPkC,
            xPk));

        for(i=IC+1;i<Wx;i++)
            PNEW(i,k) = GSL_V_GET(xPk,i);
    }


    /*
     * Enzyme
     */
    for(k=K1;k<K2;k++)
    {
        for(i=1;i<Wx;i++)
            GSL_V_SET(bPk,i,POLD(i,k)+(Dp*dt/(2.*SQ(mu*dz)))*
                (POLD(i,k-1)-2.*POLD(i,k)+POLD(i,k+1))
                + Vb*dt*AOLD(i,k)/2.);

        ERR_REP(gsl_linalg_solve_tridiag(PrDiag,PrUpper,PrLower,bPk,xPk));

        for(i=1;i<Wx;i++)
            PNEW(i,k) = GSL_V_GET(xPk,i);
    }


    for(i=0;i<N;i++)
        ANEW(i,0)=ANEW(i,1);
      for(k=0;k<M;k++)
        ANEW(0,k)=ANEW(1,k);

    /*
     *  Alternating direction implicit method, next solve in the vertical
     *  direction using the solutions found for the radial direction.
     *  For each of 4 cases decried above, create a corresponding LHS and
     *  use the Gnu Scientific Library function gsl_linalg_solve_tridiag
     *  to calculate the solution
     */

    /*
     * Plastic--Core--Enzyme--Free--Tissue
     */
    for(i=1;i<IC;i++)
    {
        for(k=K1+1;k<=K2;k++)
            GSL_V_SET(biB,k,ANEW(i,k)+(D*dt/(2.*SQ(mu*dx)))*
            (ANEW(i+1,k)*(1.+(dx/2.*x[i]))
```

```
                - (2.+cb)*ANEW(i,k)+ANEW(i-1,k)*(1.-(dx/2.*x[i])));

        for(k=FzS;k<=K3;k++)
                GSL_V_SET(biB,k,ANEW(i,k)+(D*dt/(2.*SQ(dx)))*
                        (ANEW(i+1,k)*(1.+(dx/2.*x[i]))-2.*ANEW(i,k)
                          + ANEW(i-1,k)*(1.-(dx/2.*x[i]))));

        for(k=TzS;k<M;k++)
                GSL_V_SET(biB,k,ANEW(i,k)+(D*dt/(2.*SQ(lambda*dx)))*
                        (ANEW(i+1,k)*(1.+(dx/2.*x[i]))-(2.+ct)*ANEW(i,k)+ANEW(i-1,k)*
                        (1.-(dx/2.*x[i])))+dt*Vt*A0/2.);

        ERR_REP(gsl_linalg_solve_tridiag(MzDiagB,MzUpperB,MzLowerB,biB,xi));

        for(k=0;k<M;k++)
                AOLD(i,k) = GSL_V_GET(xi,k);
}

/*
 * Plastic—Enzyme—Free—Tissue
 */
for(i=IC;i<I0;i++)
{
        for(k=K0+1;k<=K2;k++)
                GSL_V_SET(biE,k,ANEW(i,k)+(D*dt/(2.*SQ(mu*dx)))*
                        (ANEW(i+1,k)*(1.+(dx/2.*x[i]))-(2.+cb)*ANEW(i,k)+ANEW(i-1,k)*
                        (1.-(dx/2.*x[i])));

        for(k=FzS;k<=K3;k++)
                GSL_V_SET(biE,k,ANEW(i,k)+(D*dt/(2.*SQ(dx)))*
                        (ANEW(i+1,k)*(1.+(dx/2.*x[i]))-2.*ANEW(i,k)+ANEW(i-1,k)*
                        (1.-(dx/2.*x[i])));

        for(k=TzS;k<M;k++)
                GSL_V_SET(biE,k,ANEW(i,k)+(D*dt/(2.*SQ(lambda*dx)))*
                        (ANEW(i+1,k)*(1.+(dx/2.*x[i]))-(2.+ct)*ANEW(i,k)+ANEW(i-1,k)*
                        (1.-(dx/2.*x[i])))+dt*Vt*A0/2.);

        ERR_REP(gsl_linalg_solve_tridiag(MzDiagE,MzUpperE,MzLowerE,biE,xi));
        for(k=K0+1;k<M;k++)
                AOLD(i,k) = GSL_V_GET(xi,k);
}
/*bridge over fake points*/
i=I0;
{
        for(k=K0+1;k<=K2;k++)
                GSL_V_SET(biE,k,ANEW(i,k)+(D*dt/(2.*SQ(mu*dx)))*
                        (ANEW(i+1,k)*(1.+(dx/2.*x[i]))-(2.+cb)*ANEW(i,k)+ANEW(i-1,k)*
                        (1.-(dx/2.*x[i])));

        for(k=FzS;k<=K3;k++)
                GSL_V_SET(biE,k,ANEW(i,k)+(D*dt/(2.*SQ(dx)))*
                        (2.*ANEW(i+1,k)*(1.+(dx/2.*x[i]))-(3+(dx/2.*x[i]))*ANEW(i,k)
                        +ANEW(i-1,k)*(1.-(dx/2.*x[i]))));

        for(k=TzS;k<M;k++)
                GSL_V_SET(biE,k,ANEW(i,k)+(D*dt/(2.*SQ(lambda*dx)))*
                        (2.*ANEW(i+1,k)*(1.+(dx/2.*x[i]))-(3.+ct+(dx/2.*x[i]))*ANEW(i,k)+
                        ANEW(i-1,k)*(1.-(dx/2.*x[i])))+dt*Vt*A0/2.);

        ERR_REP(gsl_linalg_solve_tridiag(MzDiagE,MzUpperE,MzLowerE,biE,xi));
        for(k=K0+1;k<M;k++)
                AOLD(i,k) = GSL_V_GET(xi,k);
}


/*
 * Free—Tissue
 */
```

```
        /*apply continuity conditions*/
        i=A1S;
1465    {
            for(k=K0;k<=K2;k++)
                GSL_V_SET(biF,k,ANEW(i,k) +
                    (D*dt/(2.*SQ(dx)))*(ANEW(i+1,k)*(1.+(dx/2.*x[i]))
                    - (2.+(SQ(mu)/(alphaB-SQ(mu)))*(1.-(dx/2.*x[i])))*ANEW(i,k)
1470                + ANEW(i-1,k)*(1.-(dx/2.*x[i]))*(1./(alphaB-SQ(mu)))));

            for(k=FzS;k<=K3;k++)
                GSL_V_SET(biF,k,ANEW(i,k)+(D*dt/(2.*SQ(dx)))*(ANEW(i+1,k)*
                    (1.+(dx/2.*x[i]))-(3.-(dx/2.*x[A1S]))*ANEW(i,k)+2.*ANEW(i-1,k)*
1475                (1.-(dx/2.*x[i]))));

            for(k=TzS;k<M;k++)
                GSL_V_SET(biF,k,ANEW(i,k)+(D*dt/(2.*SQ(lambda*dx)))*
                    (ANEW(i+1,k)*(1.+(dx/2.*x[i]))-(3.+ct-(dx/2.*x[A1S]))*ANEW(i,k)
1480                + 2.*ANEW(i-1,k)*(1.-(dx/2.*x[i])))+dt*Vt*A0/2.);

            ERR_REP(gsl_linalg_solve_tridiag(MzDiagF,MzUpperF,MzLowerF,biF,xi));

            for(k=0;k<M;k++)
1485            AOLD(i,k) = GSL_V_GET(xi,k);
        }
        /*zero flux at plastic sheath*/
        for(k=0;k<=K0;k++)
            AOLD(A0E,k)=AOLD(A1S,k);
1490
        for(i=A1S+1;i<I1;i++)
        {
            for(k=1;k<=K2;k++)
                GSL_V_SET(biF,k,ANEW(i,k)+(D*dt/(2.*SQ(dx)))*
1495                (ANEW(i+1,k)*(1.+(dx/2.*x[i]))-2.*ANEW(i,k)
                    + ANEW(i-1,k)*(1.-(dx/2.*x[i]))));

            for(k=FzS;k<=K3;k++)
                GSL_V_SET(biF,k,ANEW(i,k)+(D*dt/(2.*SQ(dx)))*
1500                (ANEW(i+1,k)*(1.+(dx/2.*x[i]))-2.*ANEW(i,k)
                    + ANEW(i-1,k)*(1.-(dx/2.*x[i]))));

            for(k=TzS;k<M;k++)
                GSL_V_SET(biF,k,ANEW(i,k)+(D*dt/(2.*SQ(lambda*dx)))*
1505                (ANEW(i+1,k)*(1.+(dx/2.*x[i]))-(2.+ct)*ANEW(i,k)
                    + ANEW(i-1,k)*(1.-(dx/2.*x[i])))+dt*Vt*A0/2.);

            ERR_REP(gsl_linalg_solve_tridiag(MzDiagF,MzUpperF,MzLowerF,biF,xi));

1510
            for(k=0;k<M;k++)
                AOLD(i,k) = GSL_V_GET(xi,k);
        }
        /*bridge over fake points*/
1515    i=I1;
        {
            for(k=1;k<=K2;k++)
                GSL_V_SET(biF,k,ANEW(i,k)+(D*dt/(2.*SQ(dx)))*
                    (ANEW(i+1,k)*(1.+(dx/2.*x[i]))-2.*ANEW(i,k)
1520                + ANEW(i-1,k)*(1.-(dx/2.*x[i]))));

            for(k=FzS;k<=K3;k++)
                GSL_V_SET(biF,k,ANEW(i,k)+(D*dt/(2.*SQ(dx)))*
                    (ANEW(i+1,k)*(1.+(dx/2.*x[i]))-(3.+(dx/2.*x[i]))*ANEW(i,k)
1525                + ANEW(i-1,k)*(1.-(dx/2.*x[i]))));

              for(k=TzS;k<M;k++)
                GSL_V_SET(biF,k,ANEW(i,k)+(D*dt/(2.*SQ(lambda*dx)))*
                    (2.*ANEW(i+1,k)*(1.+(dx/2.*x[i]))-(3.+ct+(dx/2.*x[i]))*ANEW(i,k)
1530                +ANEW(i-1,k)*(1.-(dx/2.*x[i])))+dt*Vt*A0/2.);
```

```
        ERR_REP(gsl_linalg_solve_tridiag(MzDiagF,MzUpperF,MzLowerF,biF,xi));

1535
        for(k=0;k<M;k++)
            AOLD(i,k) = GSL_V_GET(xi,k);
    }

1540
    /*
     * Tissue
     */
    /*apply continuity conditions*/
1545 i=A2S;
    {
        for(k=1;k<=K2;k++)
          GSL_V_SET(biT,k,ANEW(i,k)+(D*dt/(2.*SQ(lambda*dx)))*
              (ANEW(i+1,k)*(1.+(dx/2.*x[i]))
1550          -(2.+ct+(1.-(dx/2.*x[A2S]))*alphaT/(SQ(lambda)-alphaT))*ANEW(i,k)
              +ANEW(i-1,k)*(1.-(dx/2.*x[i]))*
              alphaT*SQ(lambda)/(SQ(lambda)-alphaT) + dt*Vt*A0/2.));

        for(k=FzS;k<=K3;k++)
1555          GSL_V_SET(biT,k,ANEW(i,k)+(D*dt/(2.*SQ(lambda*dx)))*
              (ANEW(i+1,k)*(1.+(dx/2.*x[i]))
              -(2.+ct+(1.-(dx/2.*x[A2S]))*alphaT/(SQ(lambda)-alphaT))*ANEW(i,k)
              +ANEW(i-1,k)*(1.-(dx/2.*x[i]))*
              alphaT*SQ(lambda)/(SQ(lambda)-alphaT) +dt*Vt*A0/2.));
1560
        for(k=TzS;k<M;k++)
          GSL_V_SET(biT,k,ANEW(i,k) +
              (D*dt/(2.*SQ(lambda*dx)))*(ANEW(i+1,k)*(1.+(dx/2.*x[i]))
                - (3.+ct-(dx/2.*x[A2S]))*ANEW(i,k)+2.*ANEW(i-1,k)*(1.-(dx/2.*x[i])))
1565            + dt*Vt*A0/2.);

        ERR_REP(gsl_linalg_solve_tridiag(MzDiagT,MzUpperT,MzLowerT,biT,xi));

        for(k=0;k<M;k++)
1570          AOLD(i,k) = GSL_V_GET(xi,k);
    }

    for(i=A2S+1;i<N;i++)
    {
1575      for(k=1;k<=K2;k++)
            GSL_V_SET(biT,k,ANEW(i,k) +
              (D*dt/(2.*SQ(lambda*dx)))*(ANEW(i+1,k)*(1.+(dx/2.*x[i]))
                - (2.+ct)*ANEW(i,k)+ANEW(i-1,k)*(1.-(dx/2.*x[i])))+dt*Vt*A0/2.);

1580      for(k=FzS;k<=K3;k++)
            GSL_V_SET(biT,k,ANEW(i,k) +
              (D*dt/(2.*SQ(lambda*dx)))*(ANEW(i+1,k)*(1.+(dx/2.*x[i])) -
              (2.+ct)*ANEW(i,k)+ANEW(i-1,k)*(1.-(dx/2.*x[i])))+dt*Vt*A0/2.);

1585      for(k=TzS;k<M;k++)
            GSL_V_SET(biT,k,ANEW(i,k) +
              (D*dt/(2.*SQ(lambda*dx)))*(ANEW(i+1,k)*(1.+(dx/2.*x[i])) -
              (2.+ct)*ANEW(i,k)+ANEW(i-1,k)*(1.-(dx/2.*x[i])))+dt*Vt*A0/2.);

1590      ERR_REP(gsl_linalg_solve_tridiag(MzDiagT,MzUpperT,MzLowerT,biT,xi));

          for(k=0;k<M;k++)
            AOLD(i,k) = GSL_V_GET(xi,k);
    }
1595 /*
     *  Alternating direction implicit method, solve for the product in
     *  the vertical direction using the solutions from the radial
     *  direction.
     */
1600
```

```
/*
 * Plastic—Core—Enzyme
 */
for(i=1;i<=IC;i++)
{
    for(k=K1+1;k<Wz;k++)
        GSL_V_SET(bPi,k,PNEW(i,k) +
        (Dp*dt/(2.*SQ(mu*dx)))*(PNEW(i+1,k)*(1.+(dx/2.*x[i])) −
        2.*PNEW(i,k)+PNEW(i−1,k)*(1.−(dx/2.*x[i])))+Vb*dt*ANEW(i,k)/2.);

    ERR_REP(gsl_linalg_solve_tridiag(PzDiag,PzUpper,PzLower,bPi,xPi));

    for(k=K1+1;k<Wz;k++)
        POLD(i,k) = GSL_V_GET(xPi,k);
}

/*
 * Plastic—Enzyme
 */
for(i=IC+1;i<I0;i++)
{
    for(k=K0+1;k<Wz;k++)
        GSL_V_SET(bPiP,k,PNEW(i,k) +
            (Dp*dt/(2.*SQ(mu*dx)))*(PNEW(i+1,k)*(1.+(dx/2.*x[i])) −
            2.*PNEW(i,k)+PNEW(i−1,k)*(1.−(dx/2.*x[i])))+Vb*dt*ANEW(i,k)/2.);

    ERR_REP(gsl_linalg_solve_tridiag(PzDiagP,PzUpperP,PzLowerP,bPiP,
        xPi));

    for(k=K0+1;k<Wz;k++)
        POLD(i,k) = GSL_V_GET(xPi,k);
}

/*Zero flux at r=0*/
for(i=0;i<N;i++)
    AOLD(i,0)=AOLD(i,1);
for(k=0;k<M;k++)
    AOLD(0,k)=AOLD(1,k);


/*Update the time*/
t+=dt;

/*write the gradient at the biosensor at time-steps specified in the
 * parameters file. */
if((j+1)%printSensorStep==0)
{
    fprintf(outSensor,"%le\t",t);
    for(k=K0;k<=K1;k++)
        fprintf(outSensor,"%1.20e\t",POLD(IC+1,k)/dx);
    fprintf(outSensor,"\n%le\t",t);
    for(i=0;i<=IC;i++)
        fprintf(outSensor,"%1.20e\t",POLD(i,K1+1)/dz);
    fprintf(outSensor,"\n",t);
}

/*write analyte and product profiles to compressed files*/
if((j+1)%printTimeStep==0)
{
    sprintf(fname,"%s-%f-Analyte.txt.gz",filename,t);
    zf = zfopen(fname);
    for(k=0;k<=M;k++)
    {
        if(k==EzE || k==FzE)
            continue;
        for(i=0;i<=N;i++)
        {
            if(i==A0E||i==A1E)
                continue;
```

```
                        sprintf(msg + strlen(msg),"%1.20e\t",AOLD(i,k));
                        if(strlen(msg)>MESG_SIZE-100)
                            zprint(zf,msg);
                    }
                    sprintf(msg + strlen(msg),"\n");
                }
                zfclose(zf,msg);


                sprintf(fname,"%s-%f-Product.txt.gz",filename,t);
                zf = zfopen(fname);
                for(k=0;k<=Wz;k++)
                {
                    if(k==EzE || k==FzE)
                        continue;
                    for(i=0;i<=Wx;i++)
                    {
                        if(i==A0E||i==A1E)
                            continue;
                        sprintf(msg + strlen(msg),"%1.20e\t",POLD(i,k));
                        if(strlen(msg)>MESG_SIZE-100)
                            zprint(zf,msg);
                    }
                    sprintf(msg + strlen(msg),"\n");
                }
                zfclose(zf,msg);
            }
        }

        /*write the final analyte and product profiles*/
        sprintf(fname,"%sFinalAnalyte.txt.gz",filename);
        zf = zfopen(fname);
        for(k=0;k<=M;k++)
        {
            if(k==EzE || k==FzE)
                continue;
            for(i=0;i<=N;i++)
            {
                if(i==A0E||i==A1E)
                    continue;
                sprintf(msg + strlen(msg),"%1.20e\t",AOLD(i,k));
                if(strlen(msg)>MESG_SIZE-100)
                    zprint(zf,msg);
            }
            sprintf(msg + strlen(msg),"\n");
        }
        zfclose(zf,msg);

        sprintf(fname,"%sFinalProduct.txt.gz",filename);
        zf = zfopen(fname);
        for(k=0;k<=Wz;k++)
        {
            if(k==EzE || k==FzE)
                continue;
            for(i=0;i<=Wx;i++)
            {
                if(i==A0E||i==A1E)
                    continue;
                sprintf(msg + strlen(msg),"%1.20e\t",POLD(i,k));
                if(strlen(msg)>MESG_SIZE-100)
                    zprint(zf,msg);
            }
            sprintf(msg + strlen(msg),"\n");
        }
        zfclose(zf,msg);


        /*free memory allocated for the grid*/
```

```
        for(j=1;j<2;j++)
1740    {
            for(i=0;i<=Wx;i++)
            {
                free(A[j][i]);
            }
1745        for(;i<=N;i++)
                free(A[j][i]);
        }
        for(j=0;j<2;j++)
        {
1750        free(A[j]);
        }
        free(A);

        /*Free all GSL vectors*/
1755    gsl_vector_free(MrDiag);
        gsl_vector_free(MrUpper);
        gsl_vector_free(MrLower);
        gsl_vector_free(bk);
        gsl_vector_free(MrDiagP);
1760    gsl_vector_free(MrUpperP);
        gsl_vector_free(MrLowerP);
        gsl_vector_free(bkP);
        gsl_vector_free(MrDiagE);
        gsl_vector_free(MrUpperE);
1765    gsl_vector_free(MrLowerE);
        gsl_vector_free(bkE);
        gsl_vector_free(MrDiagT);
        gsl_vector_free(MrUpperT);
        gsl_vector_free(MrLowerT);
1770    gsl_vector_free(bkT);
        gsl_vector_free(MrDiagF);
        gsl_vector_free(MrUpperF);
        gsl_vector_free(MrLowerF);
        gsl_vector_free(bkF);
1775    gsl_vector_free(xk);
        gsl_vector_free(MzDiagF);
        gsl_vector_free(MzUpperF);
        gsl_vector_free(MzLowerF);
        gsl_vector_free(biF);
1780    gsl_vector_free(MzDiagE);
        gsl_vector_free(MzUpperE);
        gsl_vector_free(MzLowerE);
        gsl_vector_free(biE);
        gsl_vector_free(MzDiagB);
1785    gsl_vector_free(MzUpperB);
        gsl_vector_free(MzLowerB);
        gsl_vector_free(biB);
        gsl_vector_free(MzDiagT);
        gsl_vector_free(MzUpperT);
1790    gsl_vector_free(MzLowerT);
        gsl_vector_free(biT);
        gsl_vector_free(xi);
        gsl_vector_free(PzDiag);
        gsl_vector_free(PzUpper);
1795    gsl_vector_free(PzLower);
        gsl_vector_free(bPi);
        gsl_vector_free(PzDiagP);
        gsl_vector_free(PzUpperP);
        gsl_vector_free(PzLowerP);
1800    gsl_vector_free(bPiP);
        gsl_vector_free(xPi);
        gsl_vector_free(PrDiag);
        gsl_vector_free(PrUpper);
        gsl_vector_free(PrLower);
1805    gsl_vector_free(bPk);
        gsl_vector_free(PrDiagC);
        gsl_vector_free(PrUpperC);
```

```
        gsl_vector_free(PrLowerC);
        gsl_vector_free(bPkC);
        gsl_vector_free(xPk);
        return 0;
}


/*load the parameter values from a file*/
int readParameters(char *filename)
{
        FILE *pf;
        pf = fopen(filename,"r");
        if(pf==NULL)
                return -1;
        if(fscanf(pf,"dx=%lf\n",&dx)<0)
                return -2;
        if(fscanf(pf,"dz=%lf\n",&dz)<0)
                return -2;
        if(fscanf(pf,"T=%lf\n",&T)<0)
                return -2;
        if(fscanf(pf,"dt=%le\n",&dt)<0)
                return -2;
        if(fscanf(pf,"PrintProfileTimeStep=%i\n",&printTimeStep)<0)
                return -2;
        if(fscanf(pf,"PrintSensorTimeStep=%i\n",&printSensorStep)<0)
                return -2;
        if(fscanf(pf,"Rb=%lf\n",&R0)<0)
                return -2;
        if(fscanf(pf,"w=%lf\n",&width)<0)
                return -2;
        if(fscanf(pf,"d=%lf\n",&dmg)<0)
                return -2;
        if(fscanf(pf,"R3=%lf\n",&R3)<0)
                return -2;
        if(fscanf(pf,"depth=%lf\n",&depth)<0)
                return -2;
        if(fscanf(pf,"inserted=%lf\n",&Pz)<0)
                return -2;
        if(fscanf(pf,"length=%lf\n",&length)<0)
                return -2;
        if(fscanf(pf,"D=%lf\n",&D)<0)
                return -2;
        if(fscanf(pf,"Dp=%lf\n",&Dp)<0)
                return -2;
        if(fscanf(pf,"Lambda=%lf\n",&lambda)<0)
                return -2;
        if(fscanf(pf,"Mu=%lf\n",&mu)<0)
                return -2;
        if(fscanf(pf,"Vb=%lf\n",&Vb)<0)
                return -2;
        if(fscanf(pf,"Vt=%lf\n",&Vt)<0)
                return -2;
        if(fscanf(pf,"alphaB=%lf\n",&alphaB)<0)
                return -2;
        if(fscanf(pf,"alphaT=%lf\n",&alphaT)<0)
                return -2;

        /*grid sizes including fake points for boundary and continuity conditions */
        N = (int)ceil(R3/dx)+3;
        M = (int)ceil(depth/dz)+4;

        /*boundaries between regions*/
        R1=R0+width;
        R2=R1+dmg;
        Cz=Pz+length;
        Ez=Cz+width;
        Fz=Ez+dmg;
        fclose(pf);
```

readParameters

```
    return 0;

}
/*echo parameter values*/
int printParameters(FILE *fp)                                          printParameters
{
    fprintf(fp,"N=%i\n",N);
    fprintf(fp,"M=%i\n",M);
    fprintf(fp,"T=%lf\n",T);
    fprintf(fp,"dx=%le\n",dx);
    fprintf(fp,"dz=%le\n",dx);
    fprintf(fp,"dt=%le\n",dt);
    fprintf(fp,"PrintProfileTimeStep=%i\n",printTimeStep);
    fprintf(fp,"PrintSensorTimeStep=%i\n",printSensorStep);
    fprintf(fp,"Rb=%le\n",R0);
    fprintf(fp,"w=%le\n",width);
    fprintf(fp,"d=%le\n",dmg);
    fprintf(fp,"R3=%le\n",R3);
    fprintf(fp,"depth=%le\n",depth);
    fprintf(fp,"inserted=%le\n",Pz);
    fprintf(fp,"length=%le\n",length);
    fprintf(fp,"depth=%le\n",depth);
    fprintf(fp,"D=%le\n",D);
    fprintf(fp,"Dp=%le\n",Dp);
    fprintf(fp,"Lambda=%lf\n",lambda);
    fprintf(fp,"Mu=%lf\n",mu);
    fprintf(fp,"Vb=%lf\n",Vb);
    fprintf(fp,"Vt=%lf\n",Vt);
    fprintf(fp,"A*=%lf\n",A0);
    fprintf(fp,"alphaB=%lf\n",alphaB);
    fprintf(fp,"alphaT=%lf\n",alphaT);
    fflush(fp);
    return 0;
}

int main(int argc, char** argv)                                        main
{
  FILE *outProfile, *outSensor,*outFinal;
  int err;
  if(argc<4)
  {
       fprintf(stderr, "Insufficient arguments.\n REQUIRED:\t parameterFile, sensorOutput profilePrefix A0 \n");
    return -1;
  }
  err=readParameters(argv[1]);
  if(err==-1)
  {
    fprintf(stderr,"Failed to open file %s.\n",argv[1]);
    return -1;
  }
  else if(err==-2)
  {
    fprintf(stderr,"Failed to read a parameter from %s.\n",argv[1]);
    return -1;
  }

  if(D*dt/SQ(dx)>0.5 || D*dt/SQ(lambda*dx)>0.5 || MAX(D,Dp)*dt/SQ(mu*dx)>0.5)
  {
    fprintf(stderr,
    "Warning: Parameter give large CLT: \nD*dt/SQ(dx)>0.5\n(%le %le %le)\n",
    D*dt/SQ(dx), D*dt/SQ(lambda*dx),D*dt/SQ(lambda*dx));
  }
  outSensor = fopen(argv[2],"w");
  if(outSensor == NULL)
  {
    fprintf(stderr,"Failed to open file %s.\n",argv[3]);
    return -1;
  }
```

```
        A0=atof(argv[4]);
        printParameters(stderr);


1950    /*Call the actual method*/
        err = solver(outSensor,argv[3]);
        fprintf(stderr, "Function returned: %i\n",err);
        fflush(outSensor);
        fclose(outSensor);
1955    return 0;

    }
```

Bibliography

Abbott, N. J. (2004). Evidence for bulk flow of brain interstitial fluid: significance for physiology and pathology. *Neurochemistry international 45*(4), 545–552.

Agnati, L., D. Guidolin, M. Guescini, S. Genedani, and K. Fuxe (2010). Understanding wiring and volume transmission. *Brain research reviews 64*(1), 137–159.

Aitken, P., G. Breese, F. Dudek, F. Edwards, M. Espanol, P. Larkman, P. Lipton, G. Newman, T. Nowak Jr, K. Panizzon, et al. (1995). Preparative methods for brain slices: a discussion. *Journal of neuroscience methods 59*(1), 139–149.

Alanko, L., T. Porkka-Heiskanen, and S. Soinila (2006). Localization of equilibrative nucleoside transporters in the rat brain. *Journal of chemical neuroanatomy 31*(3), 162–168.

Anderson, C., S. Baldwin, J. Young, C. Cass, and F. Parkinson (1999). Distribution of mrna encoding a nitrobenzylthioinosine-insensitive nucleoside transporter (ent2) in rat brain. *Molecular brain research 70*(2), 293–297.

Anderson, C. M., W. Xiong, J. D. Young, C. E. Cass, and F. E. Parkinson (1996). Demonstration of the existence of mrnas encoding n1/cif and n2/cit sodium/nucleoside cotransporters in rat brain. *Molecular brain research 42*(2), 358–361.

Andrews, S. and D. Bray (2004). Stochastic simulation of chemical reactions with spatial resolution and single molecule detail. *Physical biology 1*, 137.

Araque, A., V. Parpura, R. P. Sanzgiri, and P. G. Haydon (1999). Tripartite synapses: glia, the unacknowledged partner. *Trends in neuro-*

sciences 22(5), 208–215.

Arch, J. and E. Newsholme (1978). Activities and some properties of 5'-nucleotidase, adenosine kinase and adenosine deaminase in tissues from vertebrates and invertebrates in relation to the control of the concentration and the physiological role of adenosine. *Biochemical Journal 174*(3), 965.

Attwell, D. and S. B. Laughlin (2001). An energy budget for signaling in the grey matter of the brain. *Journal of Cerebral Blood Flow & Metabolism 21*(10), 1133–1145.

Baldwin, S., P. Beal, S. Yao, A. King, C. Cass, and J. Young (2004). The equilibrative nucleoside transporter family, slc29. *Pflügers Archiv European Journal of Physiology 447*(5), 735–743.

Baronas, R., F. Ivanauskas, I. Kaunietis, and V. Laurinavicius (2006). Mathematical modeling of plate- gap biosensors with an outer porous membrane. *Sensors 6*(7), 727–745.

Baronas, R., F. Ivanauskas, I. I. Kulis, and J. Kulys (2009). *Mathematical modeling of biosensors: an introduction for chemists and mathematicians*, Volume 9. Springer.

Baronas, R., J. Kulys, A. Lančinskas, and A. Žilinskas (2014). Effect of diffusion limitations on multianalyte determination from biased biosensor response. *Sensors 14*(3), 4634–4656.

Bass, N., H. Hess, A. Pope, and C. Thalheimer (1971). Quantitative cytoarchitectonic distribution of neurons, glia, and DNA in rat cerebral cortex. *The Journal of comparative neurology 143*(4), 481–490.

Ben-Ari, Y., I. Khalilov, K. T. Kahle, and E. Cherubini (2012). The gaba excitatory/inhibitory shift in brain maturation and neurological disorders. *The Neuroscientist 18*(5), 467–486.

Bennett, M. (2011). The prefrontal–limbic network in depression: a core pathology of synapse regression. *Progress in neurobiology 93*(4), 457–467.

Berg, J. M., J. L. Tymoczko, and L. Stryer (2002). Biochemistry, ; w. h.

Betz, A. L. (1985). Identification of hypoxanthine transport and xanthine oxidase activity in brain capillaries. *Journal of neurochemistry 44*(2), 574–579.

Blasberg, R., C. Patlak, and J. Fenstermacher (1975). Intrathecal chemotherapy: brain tissue profiles after ventriculocisternal perfusion. *Journal of Pharmacology and Experimental Therapeutics 195*(1), 73–83.

Boison, D. (2006). Adenosine kinase, epilepsy and stroke: mechanisms and therapies. *Trends in pharmacological sciences 27*(12), 652–658.

Boison, D. (2008). The adenosine kinase hypothesis of epileptogenesis. *Progress in neurobiology 84*(3), 249–262.

Boison, D., P. Singer, H. Shen, J. Feldon, and B. Yee (2011). Adenosine hypothesis of schizophrenia-opportunities for pharmacotherapy. *Neuropharmacology*.

Bowen, W. J. and H. L. Martin (1964). The diffusion of adenosine triphosphate through aqueous solutions. *Archives of biochemistry and biophysics 107*(1), 30–36.

Brundege, J. and T. Dunwiddie (1996). Modulation of excitatory synaptic transmission by adenosine released from single hippocampal pyramidal neurons. *The Journal of neuroscience 16*(18), 5603–5612.

Bruno, J. P., C. Gash, B. Martin, A. Zmarowski, F. Pomerleau, J. Burmeister, P. Huettl, and G. A. Gerhardt (2006). Second-by-second measurement of acetylcholine release in prefrontal cortex. *European Journal of Neuroscience 24*(10), 2749–2757.

Bruns, R. F., G. H. Lu, and T. A. Pugsley (1986). Characterization of the a2 adenosine receptor labeled by [3h] neca in rat striatal membranes. *Molecular Pharmacology 29*(4), 331–346.

Burnstock, G. (1978). A basis for distinguishing two types of purinergic receptor. *Cell membrane receptors for drugs and hormones: a multidisciplinary approach*, 107–118.

Bush, T. G., T. C. Savidge, T. C. Freeman, H. J. Cox, E. A. Campbell, L. Mucke, M. H. Johnson, and M. V. Sofroniew (1998). Fulminant jejuno-ileitis following ablation of enteric glia in adult transgenic mice. *Cell 93*(2), 189–201.

Calker, D. v., M. Müller, and B. Hamprecht (1979). Adenosine regulates via two different types of receptors, the accumulation of cyclic AMp in cultured brain cells. *Journal of neurochemistry 33*(5), 999–1005.

Calverley, R., K. Bedi, and D. Jones (1988). Estimation of the numerical density of synapses in rat neocortex. comparison of the disectorwith an unfoldingmethod. *Journal of neuroscience methods 23*(3), 195–205.

Castellano, B., B. González, B. R. Finsen, and J. Zimmer (1990). Histochemical demonstration of purine nucleoside phosphorylase (PNpase) in microglial and astroglial cells of adult rat brain. *Journal of Histochemistry & Cytochemistry 38*(11), 1535–1539.

Cechova, S., A. Elsobky, and B. Venton (2010). A 1 receptors self-regulate adenosine release in the striatum: evidence of autoreceptor characteristics. *Neuroscience 171*(4), 1006–1015.

Chen, J.-F., H. K. Eltzschig, and B. B. Fredholm (2013). Adenosine receptors as drug targetswhat are the challenges? *Nature Reviews Drug Discovery 12*(4), 265–286.

Chen, Q., Y. Kobayashi, H. Takeshita, T. Hoshi, and J.-i. Anzai (1998). Avidin-biotin system-based enzyme multilayer membranes for biosensor applications: Optimization of loading of choline esterase and choline oxidase in the bienzyme membrane for acetylcholine biosensors. *Electroanalysis 10*(2), 94–97.

Chen, X., N. Matsumoto, Y. Hu, and G. S. Wilson (2002). Electrochemically mediated electrodeposition/electropolymerization to yield a glucose microbiosensor with improved characteristics. *Analytical chemistry 74*(2), 368–372.

Chih, C.-P. and E. L. Roberts (2003). Energy substrates for neurons during neural activity: a critical review of the astrocyte-neuron lactate shuttle hypothesis. *Journal of Cerebral Blood Flow & Metabolism 23*(11), 1263–1281.

Chin, J. (1989). Adenosine receptors in brain: neuromodulation and role in epilepsy. *Annals of neurology 26*(6), 695–698.

Chklovskii, D. B., T. Schikorski, and C. F. Stevens (2002). Wiring optimization in cortical circuits. *Neuron 34*(3), 341–347.

Choi, D.-S., M.-G. Cascini, W. Mailliard, H. Young, P. Paredes, T. McMahon, I. Diamond, A. Bonci, and R. O. Messing (2004). The type 1 equilibrative nucleoside transporter regulates ethanol intoxication and preference. *Nature neuroscience 7*(8), 855–861.

Chun, L. and P. H. Patterson (1977). Role of nerve growth factor in the development of rat sympathetic neurons in vitro. i. survival, growth, and differentiation of catecholamine production. *The Journal of cell biology 75*(3), 694–704.

Ciruela, F., C. Albergaria, A. Soriano, L. Cuffí, L. Carbonell, S. Sánchez, J. Gandía, and V. Fernández-Dueñas (2010). Adenosine receptors interacting proteins (arips): behind the biology of adenosine signaling. *Biochimica et Biophysica Acta (BBA)-Biomembranes 1798*(1), 9–20.

Clasadonte, J., S. R. McIver, L. I. Schmitt, M. M. Halassa, and P. G. Haydon (2014). Chronic sleep restriction disrupts sleep homeostasis and behavioral sensitivity to alcohol by reducing the extracellular accumulation of adenosine. *The Journal of Neuroscience 34*(5), 1879–1891.

Coche-Guerente, L., S. Cosnier, C. Innocent, and P. Mailley (1995). Development of amperometric biosensors based on the immobilization of enzymes in polymer films electrogenerated from a series of amphiphilic pyrrole derivatives. *Analytica Chimica Acta 311*(1), 23–30.

Dachir, S., D. Shabashov, V. Trembovler, A. G. Alexandrovich, L. I. Benowitz, and E. Shohami (2014). Inosine improves functional recovery after experimental traumatic brain injury. *Brain research 1555*, 78–88.

Dale, N. and B. G. Frenguelli (2009). Release of adenosine and atp during ischemia and epilepsy. *Current neuropharmacology 7*(3), 160.

Dale, N., S. Hatz, F. Tian, and E. Llaudet (2005). Listening to the brain: microelectrode biosensors for neurochemicals. *Trends in biotechnology 23*(8), 420–428.

Dar, M. S. and S. J. Mustafa (2002). Acute ethanol/cannabinoid-induced ataxia and its antagonism by oral/systemic/intracerebellar a 1 adenosine receptor antisense in mice. *Brain research 957*(1), 53–60.

Dash, M. B., M. Bellesi, G. Tononi, and C. Cirelli (2013). Sleep/wake dependent changes in cortical glucose concentrations. *Journal of neurochemistry 124*(1), 79–89.

De Jong, J. and C. Kalkman (1973). Myocardial adenosine kinase: activity and localization determined with rapid, radiometric assay. *Biochimica et Biophysica Acta (BBA)-General Subjects 320*(2), 388–396.

de Sa, V. C., R. Herna, J. Sua, S. Vidrio, M. Di, et al. (1993). Day-night variations of adenosine and its metabolizing enzymes in the brain cortex of the ratpossible physiological significance for the energetic homeostasis and the sleep-wake cycle. *Brain research 612*(1), 115–121.

Diamond, J. S. (2001). Neuronal glutamate transporters limit activation of nmda receptors by neurotransmitter spillover on ca1 pyramidal cells. *The Journal of Neuroscience 21*(21), 8328–8338.

Dunwiddie, T. and L. Diao (1994). Extracellular adenosine concentrations in hippocampal brain slices and the tonic inhibitory modulation of evoked excitatory responses. *Journal of Pharmacology and Experimental Therapeutics 268*(2), 537–545.

Dunwiddie, T. and S. Masino (2001). The role and regulation of adenosine in the central nervous system. *Annual review of neuroscience 24*(1), 31–55.

Endo, H., E. Takahashi, M. Murata, H. Ohnuki, H. Ren, W. Tsugawa, and K. Sode (2010). Wireless monitoring of blood glucose levels in flatfish with a needle biosensor. *Fisheries Science 76*(4), 687–694.

Etherington, L.-A. V., G. E. Patterson, L. Meechan, D. Boison, A. J. Irving, N. Dale, and B. G. Frenguelli (2009). Astrocytic adenosine kinase regulates basal synaptic adenosine levels and seizure activity but not activity-dependent adenosine release in the hippocampus. *Neuropharmacology 56*(2), 429–437.

Farzan, F. (2010). *Inhibition of Gamma Oscillations in Healthy Subjects and Patients with Schizophrenia*. Ph. D. thesis, University of Toronto.

Fedele, D. E., N. Gouder, M. Güttinger, L. Gabernet, L. Scheurer, T. Rülicke, F. Crestani, and D. Boison (2005). Astrogliosis in epilepsy leads to overexpression of adenosine kinase, resulting in seizure aggravation. *Brain 128*(10), 2383–2395.

Fowler, J. C. (1993). Purine release and inhibition of synaptic transmission during hypoxia and hypoglycemia in rat hippocampal slices. *Neuroscience letters 157*(1), 83–86.

Franco, R., V. Casadó, J. Mallol, C. Ferrada, S. Ferré, K. Fuxe, A. Cortés, F. Ciruela, C. Lluis, and E. I. Canela (2006). The two-state dimer

receptor model: a general model for receptor dimers. *Molecular pharmacology 69*(6), 1905–1912.

Fredholm, B., A. IJzerman, K. Jacobson, K. Klotz, and J. Linden (2001a). International union of pharmacology. xxv. nomenclature and classification of adenosine receptors. *Pharmacological reviews 53*(4), 527.

Fredholm, B. B., A. P. IJzerman, K. A. Jacobson, K.-N. Klotz, and J. Linden (2001b). International union of pharmacology. xxv. nomenclature and classification of adenosine receptors. *Pharmacological reviews 53*(4), 527–552.

Fredholm, B. B., A. P. IJzerman, K. A. Jacobson, J. Linden, and C. E. Müller (2011). International union of basic and clinical pharmacology. lxxxi. nomenclature and classification of adenosine receptorsan update. *Pharmacological reviews 63*(1), 1–34.

Frenguelli, B., E. Llaudet, and N. Dale (2003). High-resolution real-time recording with microelectrode biosensors reveals novel aspects of adenosine release during hypoxia in rat hippocampal slices. *Journal of neurochemistry 86*(6), 1506–1515.

Frenguelli, B., G. Wigmore, E. Llaudet, and N. Dale (2007). Temporal and mechanistic dissociation of ATP and adenosine release during ischaemia in the mammalian hippocampus. *Journal of neurochemistry 101*(5), 1400–1413.

Fujita, T., E. Williams, T. Jensen, N. Smith, T. Takano, K. Tieu, and M. Nedergaard (2011). Cultured astrocytes do not release adenosine during hypoxic conditions. *Journal of Cerebral Blood Flow & Metabolism 32*(1), e1–e2.

Fuxe, K., D. Marcellino, A. Woods, L. Giuseppina, T. Antonelli, L. Ferraro, S. Tanganelli, and L. Agnati (2009). Integrated signaling in heterodimers and receptor mosaics of different types of gpcrs of the forebrain: relevance for schizophrenia. *Journal of Neural Transmission 116*(8), 923–939.

Garcia-Belmonte, G. (2003). Effect of electrode morphology on the diffusion length of the doping process of electronically conducting polypyrrole films. *Electrochemistry communications 5*(3), 236–240.

Gavalas, V., N. Chaniotakis, and T. Gibson (1998). Improved operational

stability of biosensors based on enzyme-polyelectrolyte complex adsorbed into a porous carbon electrode. *Biosensors and Bioelectronics 13*(11), 1205–1211.

Geiger, J. D. and J. Nagy (1986). Distribution of adenosine deaminase activity in rat brain and spinal cord. *The Journal of neuroscience 6*(9), 2707–2714.

Gerwins, P., C. Nordstedt, and B. Fredholm (1990). Characterization of adenosine a1 receptors in intact ddt1 mf-2 smooth muscle cells. *Molecular pharmacology 38*(5), 660–666.

Gessi, S., S. Merighi, K. Varani, E. Leung, S. Mac Lennan, and P. Borea (2008). The a3 adenosine receptor: an enigmatic player in cell biology. *Pharmacology & therapeutics 117*(1), 123–140.

Gillespie, D. T. (1992). A rigorous derivation of the chemical master equation. *Physica A: Statistical Mechanics and its Applications 188*(1), 404–425.

Gillespie, D. T. (2000). The chemical langevin equation. *The Journal of Chemical Physics 113*(1), 297–306.

Gokel, G. W. (1997). *Advances in Supramolecular Chemistry*, Volume 4. Elsevier.

Gourine, A. V., E. Llaudet, N. Dale, and K. M. Spyer (2005). Release of ATP in the ventral medulla during hypoxia in rats: role in hypoxic ventilatory response. *The Journal of neuroscience 25*(5), 1211–1218.

Governo, R., J. Deuchars, S. Baldwin, and A. King (2005). Localization of the nbmpr-sensitive equilibrative nucleoside transporter, ent1, in the rat dorsal root ganglion and lumbar spinal cord. *Brain research 1059*(2), 129–138.

Gracia, E., A. Cortés, J. Meana, J. García-Sevilla, M. Herhsfield, E. Canela, J. Mallol, C. Lluís, R. Franco, and V. Casadó (2008). Human adenosine deaminase as an allosteric modulator of human a1 adenosine receptor: abolishment of negative cooperativity for [3h](r)-pia binding to the caudate nucleus. *Journal of neurochemistry 107*(1), 161–170.

Gray, J. H., R. P. Owen, and K. M. Giacomini (2004). The concentrative nucleoside transporter family, slc28. *Pflügers Archiv 447*(5), 728–734.

Greco, W. R., R. L. Priore, M. Sharma, and W. Korytnyk (1982). Rosfit: an enzyme kinetics nonlinear regression curve fitting package for a microcomputer. *Computers and Biomedical Research 15*(1), 39–45.

Guidolin, D., F. Ciruela, S. Genedani, M. Guescini, C. Tortorella, G. Albertin, K. Fuxe, and L. F. Agnati (2011). Bioinformatics and mathematical modelling in the study of receptor–receptor interactions and receptor oligomerization: Focus on adenosine receptors. *Biochimica et Biophysica Acta (BBA)-Biomembranes 1808*(5), 1267–1283.

Guillén-Gómez, E., M. Calbet, J. Casado, L. De Lecea, E. Soriano, M. Pastor-Anglada, and F. Burgaya (2004). Distribution of cnt2 and ent1 transcripts in rat brain: selective decrease of cnt2 mrna in the cerebral cortex of sleep-deprived rats. *Journal of neurochemistry 90*(4), 883–893.

Hallik, A., A. Alumaa, H. Kurig, A. Jänes, E. Lust, and J. Tamm (2007). On the porosity of polypyrrole films. *Synthetic Metals 157*(24), 1085–1090.

Hashimoto, S. (1974). A new spectrophotometric assay method of xanthine oxidase in crude tissue homogenate. *Analytical biochemistry 62*(2), 426–435.

Haskó, G., M. V. Sitkovsky, and C. Szabo (2004). Immunomodulatory and neuroprotective effects of inosine. *Trends in pharmacological sciences 25*(3), 152–157.

Hattne, J., D. Fange, and J. Elf (2005). Stochastic reaction-diffusion simulation with mesord. *Bioinformatics 21*(12), 2923.

Haynes, W. M. (2012). *CRC handbook of chemistry and physics*. CRC press.

Hertz, L., A. Schousboe, N. Boechler, S. Mukerji, and S. Fedoroff (1978). Kinetic characteristics of the glutamate uptake into normal astrocytes in cultures. *Neurochemical research 3*(1), 1–14.

Hodgkin, A. L. and A. F. Huxley (1952). A quantitative description of membrane current and its application to conduction and excitation in nerve. *The Journal of physiology 117*(4), 500–544.

Holst, S. C. and H.-P. Landolt (2015). Sleep homeostasis, metabolism, and adenosine. *Current Sleep Medicine Reports 1*(1), 27–37.

Honorat, J. A., M. Kinoshita, T. Okuno, K. Takata, T. Koda, S. Tada, T. Shirakura, H. Fujimura, H. Mochizuki, S. Sakoda, et al. (2013). Xanthine oxidase mediates axonal and myelin loss in a murine model of multiple sclerosis. *PloS one 8*(8), e71329.

Hrabe, J., S. Hrabtová, and K. Segeth (2004). A model of effective diffusion and tortuosity in the extracellular space of the brain. *Biophysical journal 87*(3), 1606–1617.

Hu, Y., K. M. Mitchell, F. N. Albahadily, E. K. Michaelis, and G. S. Wilson (1994). Direct measurement of glutamate release in the brain using a dual enzyme-based electrochemical sensor. *Brain research 659*(1), 117–125.

Huston, J., H. Haas, F. Boix, M. Pfister, U. Decking, J. Schrader, and R. Schwarting (1996). Extracellular adenosine levels in neostriatum and hippocampus during rest and activity periods of rats. *Neuroscience 73*(1), 99–107.

Iliff, J. J., M. Wang, Y. Liao, B. A. Plogg, W. Peng, G. A. Gundersen, H. Benveniste, G. E. Vates, R. Deane, S. A. Goldman, et al. (2012). A paravascular pathway facilitates csf flow through the brain parenchyma and the clearance of interstitial solutes, including amyloid β. *Science translational medicine 4*(147), 147ra111–147ra111.

Ivanauskas, F. and R. Baronas (2008). Numerical simulation of a plate-gap biosensor with an outer porous membrane. *Simulation modelling practice and theory 16*(8), 962–970.

Ivanauskas, F., I. Kaunietis, V. Laurinavičius, J. Razumienė, and R. Šimkus (2008). Apparent michaelis constant of the enzyme modified porous electrode. *Journal of mathematical chemistry 43*(4), 1516–1526.

Janssen, E., J. Kuiper, D. Hodgson, L. Zingman, A. Alekseev, A. Terzic, and B. Wieringa (2004). Two structurally distinct and spatially compartmentalized adenylate kinases are expressed from the ak1 gene in mouse brain. *Molecular and cellular biochemistry 256*(1), 59–72.

Jin, S., Z. Zador, and A. Verkman (2008). Random-walk model of diffusion in three dimensions in brain extracellular space: comparison with microfiberoptic photobleaching measurements. *Biophysical jour-*

nal 95(4), 1785–1794.

Kalinchuk, A., Y. Lu, D. Stenberg, P. Rosenberg, and T. Porkka-Heiskanen (2006). Nitric oxide production in the basal forebrain is required for recovery sleep. *Journal of neurochemistry 99*(2), 483–498.

Kampf, C., J. Linné, and A. Asplund (2009). The human protein atlas. *The Human Protein Atlas*, 20.

Kaster, M. P., J. Budni, M. Gazal, M. P. Cunha, A. R. Santos, and A. L. S. Rodrigues (2013). The antidepressant-like effect of inosine in the fst is associated with both adenosine a1 and a2a receptors. *Purinergic signalling 9*(3), 481–486.

Kerr, M. I., M. J. Wall, and M. J. Richardson (2013). Adenosine a1 receptor activation mediates the developmental shift at layer 5 pyramidal cell synapses and is a determinant of mature synaptic strength. *The Journal of physiology*.

Klyuch, B., M. Richardson, N. Dale, and M. Wall (2011). The dynamics of single spike-evoked adenosine release in the cerebellum. *The Journal of Physiology 589*(2), 283.

Klyuch, B. P., N. Dale, and M. J. Wall (2012a). Deletion of ecto-5-nucleotidase (CD73) reveals direct action potential-dependent adenosine release. *The Journal of Neuroscience 32*(11), 3842–3847.

Klyuch, B. P., N. Dale, and M. J. Wall (2012b). Receptor-mediated modulation of activity-dependent adenosine release in rat cerebellum. *Neuropharmacology 62*(2), 815–824.

Kobayashi, Y., T. Hoshi, and J.-i. Anzai (2001). Glucose and lactate biosensors prepared by a layer-by-layer deposition of concanavalin a and mannose-labeled enzymes: electrochemical response in the presence of electron mediators. *Chemical and pharmaceutical bulletin 49*(6), 755–757.

Kotanen, C. N., O. Karunwi, and A. Guiseppi-Elie (2014). Biofabrication using pyrrole electropolymerization for the immobilization of glucose oxidase and lactate oxidase on implanted microfabricated biotransducers. *Bioengineering 1*(1), 85–110.

Kovács, Z., G. Juhász, M. Palkovits, Á. Dobolyi, and K. A Kekesi (2011). Area, age and gender dependence of the nucleoside system in the

brain: a review of current literature. *Current topics in medicinal chemistry 11*(8), 1012–1033.

Krueger, J. M., Y. H. Huang, D. M. Rector, and D. J. Buysse (2013). Sleep: a synchrony of cell activity-driven small network states. *European Journal of Neuroscience 38*(2), 2199–2209.

Kuffler, S. W. and D. D. Potter (1964). Glia in the leech central nervous system: physiological properties and neuron-glia relationship. *Journal of Neurophysiology*.

Kurz, L. C., L. Moix, M. C. Riley, and C. Frieden (1992). The rate of formation of transition-state analogs in the active site of adenosine deaminase is encounter-controlled: implications for the mechanism. *Biochemistry 31*(1), 39–48.

Lalo, U., O. Palygin, S. Rasooli-Nejad, J. Andrew, P. G. Haydon, and Y. Pankratov (2014). Exocytosis of ATP from astrocytes modulates phasic and tonic inhibition in the neocortex. *PLoS biology 12*(1), e1001747.

Larkman, A. (2004). Dendritic morphology of pyramidal neurones of the visual cortex of the rat: Iii. spine distributions. *The Journal of comparative neurology 306*(2), 332–343.

Latini, S. and F. Pedata (2001). Adenosine in the central nervous system: release mechanisms and extracellular concentrations. *Journal of neurochemistry 79*(3), 463–484.

Laughton, C. (1984). Quantification of attached cells in microtiter plates based on coomassie brilliant blue g-250 staining of total cellular protein. *Analytical biochemistry 140*(2), 417–423.

Lee, M. R., C. L. Ruby, D. J. Hinton, S. Choi, C. A. Adams, N. Y. Kang, and D.-S. Choi (2012). Striatal adenosine signaling regulates eaat2 and astrocytic aqp4 expression and alcohol drinking in mice. *Neuropsychopharmacology*.

Lehmenkühler, A., E. Syková, J. Svoboda, K. Zilles, and C. Nicholson (1993). Extracellular space parameters in the rat neocortex and subcortical white matter during postnatal development determined by diffusion analysis. *Neuroscience 55*(2), 339–351.

Li, X.-H., Z.-H. Xie, H. Min, Y.-Z. Xian, and L.-T. Jin (2008). Amperometric biosensor for hypoxanthine based on immobilized xanthine oxidase on iron (iii) meso-tetraphenylporphyrin nanoparticles modified glassy carbon electrode. *Analytical Letters 41*(3), 456–468.

Ling, E. and C. Leblond (1973). Investigation of glial, this suggests around 51% of glia are astrocytes, however cells in semithin sections. ii. variation with age in the numbers of the various glial cell types in rat cortex and corpus callosum. *The Journal of comparative neurology 149*(1), 73–81.

Llaudet, E., N. P. Botting, J. A. Crayston, and N. Dale (2003). A three-enzyme microelectrode sensor for detecting purine release from central nervous system. *Biosensors and bioelectronics 18*(1), 43–52.

Llaudet, E., S. Hatz, M. Droniou, and N. Dale (2005). Microelectrode biosensor for real-time measurement of ATP in biological tissue. *Analytical chemistry 77*(10), 3267–3273.

Lohse, M., P. Hein, C. Hoffmann, V. Nikolaev, J.-P. Vilardaga, and M. Bünemann (2008). Kinetics of g-protein-coupled receptor signals in intact cells. *British journal of pharmacology 153*(S1), S125–S132.

Lohse, M. J., K.-N. Klotz, J. Lindenborn-Fotinos, M. Reddington, U. Schwabe, and R. A. Olsson (1987). 8-cyclopentyl-1, 3-dipropylxanthine (dpcpx)a selective high affinity antagonist radioligand for a1 adenosine receptors. *Naunyn-Schmiedeberg's archives of pharmacology 336*(2), 204–210.

Lopatář, J., N. Dale, and B. G. Frenguelli (2015). Pannexin-1-mediated ATP release from area ca3 drives mglu5-dependent neuronal oscillations. *Neuropharmacology 93*, 219–228.

Lovatt, D., Q. Xu, W. Liu, T. Takano, N. Smith, J. Schnermann, K. Tieu, and M. Nedergaard (2012). Neuronal adenosine release, and not astrocytic ATP release, mediates feedback inhibition of excitatory activity. *Proceedings of the National Academy of Sciences 109*(16), 6265–6270.

Marpegan, L., A. E. Swanstrom, K. Chung, T. Simon, P. G. Haydon, S. K. Khan, A. C. Liu, E. D. Herzog, and C. Beaulé (2011). Circadian regulation of atp release in astrocytes. *The Journal of Neuroscience 31*(23), 8342–8350.

Matz, H. and L. Hertz (1989). Adenosine metabolism in neurons and astrocytes in primary cultures. *Journal of neuroscience research 24*(2), 260–267.

May, L. T., T. J. Self, S. J. Briddon, and S. J. Hill (2010). The effect of allosteric modulators on the kinetics of agonist-g protein-coupled receptor interactions in single living cells. *Molecular pharmacology 78*(3), 511–523.

McKinney, J., K. Willoughby, S. Liang, and E. Ellis (1996). Stretch-induced injury of cultured neuronal, glial, and endothelial cells effect of polyethylene glycol–conjugated superoxide dismutase. *Stroke 27*(5), 934–940.

Mikeladze, E., A. Collins, M. Sukhacheva, A. Netrusov, and E. Csöregi (2002). Characterization of a glutamate biosensor based on a novel glutamate oxidase integrated into a redox hydrogel. *Electroanalysis 14*(15-16), 1052–1059.

Miller, M. W. and G. Potempa‘ (1990). Numbers of neurons and glia in mature rat somatosensory cortex: effects of prenatal exposure to ethanol. *Journal of Comparative Neurology 293*(1), 92–102.

Mishchenko, Y., T. Hu, J. Spacek, J. Mendenhall, K. M. Harris, and D. B. Chklovskii (2010). Ultrastructural analysis of hippocampal neuropil from the connectomics perspective. *Neuron 67*(6), 1009–1020.

Mondal, M. S. and S. Mitra (1994). Kinetics and thermodynamics of the molecular mechanism of the reductive half-reaction of xanthine oxidase. *Biochemistry 33*(34), 10305–10312.

Murillo-Rodriguez, E., C. Blanco-Centurion, D. Gerashchenko, R. Salin-Pascual, and P. Shiromani (2004). The diurnal rhythm of adenosine levels in the basal forebrain of young and old rats. *Neuroscience 123*(2), 361–370.

Muto, J., H. Lee, H. Lee, A. Uwaya, J. Park, S. Nakajima, K. Nagata, M. Ohno, I. Ohsawa, and T. Mikami (2014). Oral administration of inosine produces antidepressant-like effects in mice. *Scientific reports 4*.

Nagai, K., K. Nagasawa, and S. Fujimoto (2005). Transport mechanisms for adenosine and uridine in primary-cultured rat cortical neu-

rons and astrocytes. *Biochemical and biophysical research communications 334*(4), 1343–1350.

Nagy, J., J. Geiger, and P. Daddona (1985). Adenosine uptake sites in rat brain: identification using [3h] nitrobenzylthioinosine and colocalization with adenosine deaminase. *Neuroscience letters 55*(1), 47–53.

Nagy, J., L. LaBella, M. Buss, and P. Daddona (1984). Immunohistochemistry of adenosine deaminase: implications for adenosine neurotransmission. *Science 224*(4645), 166–168.

Nagy, J. I., F. E. Dudek, and J. E. Rash (2004). Update on connexins and gap junctions in neurons and glia in the mammalian nervous system. *Brain Research Reviews 47*(1), 191–215.

Nam, H. W., D. J. Hinton, N. Y. Kang, T. Kim, M. R. Lee, A. Oliveros, C. Adams, C. L. Ruby, and D.-S. Choi (2013). Adenosine transporter ent1 regulates the acquisition of goal-directed behavior and ethanol drinking through a2a receptor in the dorsomedial striatum. *The Journal of Neuroscience 33*(10), 4329–4338.

Nedergaard, M. (2013). Garbage truck of the brain. *Science (New York, NY) 340*(6140), 1529.

Nguyen, M. D., S. T. Lee, A. E. Ross, M. Ryals, V. I. Choudhry, and B. J. Venton (2014). Characterization of spontaneous, transient adenosine release in the caudate-putamen and prefrontal cortex. *PLOS ONE 9*(1), e87165.

Nicholson, C. (1995). Interaction between diffusion and michaelis-menten uptake of dopamine after iontophoresis in striatum. *Biophysical journal 68*(5), 1699–1715.

Nicholson, C. (2001). Diffusion and related transport mechanisms in brain tissue. *Reports on progress in Physics 64*, 815.

Nicholson, C. (2005). Factors governing diffusing molecular signals in brain extracellular space. *Journal of neural transmission 112*(1), 29–44.

Nicholson, C. and M. E. Rice (1987). Calcium diffusion in the brain cell microenvironment. *Canadian journal of physiology and pharmacology 65*(5), 1086–1091.

Noma, T. et al. (2005). Dynamics of nucleotide metabolism as a supporter of life phenomena. *J Med Invest 52*(3-4), 127–136.

Oldenziel, W., G. Dijkstra, T. Cremers, and B. Westerink (2006). In vivo monitoring of extracellular glutamate in the brain with a microsensor. *Brain research 1118*(1), 34–42.

Oldenziel, W. H. and B. H. Westerink (2005). Improving glutamate microsensors by optimizing the composition of the redox hydrogel. *Analytical chemistry 77*(17), 5520–5528.

Pajski, M. and B. Venton (2010). Adenosine release evoked by short electrical stimulations in striatal brain slices is primarily activity dependent. *ACS chemical neuroscience*.

Palanche, T., B. Ilien, S. Zoffmann, M.-P. Reck, B. Bucher, S. J. Edelstein, and J.-L. Galzi (2001). The neurokinin a receptor activates calcium and camp responses through distinct conformational states. *Journal of Biological Chemistry 276*(37), 34853–34861.

Parkinson, F. and W. Xiong (2004). Stimulus-and cell-type-specific release of purines in cultured rat forebrain astrocytes and neurons. *Journal of neurochemistry 88*(5), 1305–1312.

Patel, B. A., M. Rogers, T. Wieder, D. OHare, and M. G. Boutelle (2011). Atp microelectrode biosensor for stable long-term in vitro monitoring from gastrointestinal tissue. *Biosensors and Bioelectronics 26*(6), 2890–2896.

Paul, S., S. Khanapur, A. A. Rybczynska, C. Kwizera, J. W. Sijbesma, K. Ishiwata, A. T. Willemsen, P. H. Elsinga, R. A. Dierckx, and A. van Waarde (2011). Small-animal PET study of adenosine a1 receptors in rat brain: blocking receptors and raising extracellular adenosine. *Journal of Nuclear Medicine 52*(8), 1293–1300.

Pedata, F., S. Latini, A. M. Pugliese, and G. Pepeu (1993). Investigations into the adenosine outflow from hippocampal slices evoked by ischemia-like conditions. *Journal of neurochemistry 61*(1), 284–289.

Pérez-Pinzón, M., L. Tao, and C. Nicholson (1995). Extracellular potassium, volume fraction, and tortuosity in rat hippocampal ca1, ca3, and cortical slices during ischemia. *Journal of neurophysiology 74*, 565–565.

Perrella, F. W. (1988). Ez-fit: a practical curve-fitting microcomputer program for the analysis of enzyme kinetic data on ibm-pc compatible computers. *Analytical biochemistry 174*(2), 437–447.

Phillips, E. and E. Newsholme (1979). Maximum activities, properties and distribution of 5nucleotidase, adenosine kinase and adenosine deaminase in rat and human brain. *Journal of neurochemistry 33*(2), 553–558.

Phillis, J. W., G. A. Walter, M. H. O'Regan, and R. E. Stair (1987). Increases in cerebral cortical perfusate adenosine and inosine concentrations during hypoxia and ischemia. *Journal of Cerebral Blood Flow & Metabolism 7*(6), 679–686.

Pignataro, G., R. P. Simon, and D. Boison (2006). Transgenic overexpression of adenosine kinase aggravates cell death in ischemia. *Journal of Cerebral Blood Flow & Metabolism 27*(1), 1–5.

Pospischil, M., M. Toledo-Rodriguez, C. Monier, Z. Piwkowska, T. Bal, Y. Frégnac, H. Markram, and A. Destexhe (2008). Minimal hodgkin–huxley type models for different classes of cortical and thalamic neurons. *Biological cybernetics 99*(4-5), 427–441.

Rahman, A. (2009). The role of adenosine in alzheimers disease. *Current neuropharmacology 7*(3), 207.

Rang, H., M. M. Dale, J. Ritter, and P. Moore (2003). Pharmacology churchill livingstone. *New York*.

Razola, S. S., S. Pochet, K. Grosfils, and J. Kauffmann (2003). Amperometric determination of choline released from rat submandibular gland acinar cells using a choline oxidase biosensor. *Biosensors and Bioelectronics 18*(2), 185–191.

Ren, J., Y. Aika, C. Heizmann, and T. Kosaka (1992). Quantitative analysis of neurons and glial cells in the rat somatosensory cortex, with special reference to gabaergic neurons and parvalbumin-containing neurons. *Experimental brain research 92*(1), 1–14.

Ribeiro, J. and A. Sebastiao (1986). Adenosine receptors and calcium: Basis for proposing a third (a 3) adenosine receptor. *Progress in neurobiology 26*(3), 179–209.

Rice, M. and I. Russo-Menna (1997). Differential compartmentalization of brain ascorbate and glutathione between neurons and glia. *Neuroscience 82*(4), 1213–1223.

Rice, M. E. and C. Nicholson (1991). Diffusion characteristics and extracellular volume fraction during normoxia and hypoxia in slices of rat neostriatum. *Journal of neurophysiology 65*(2), 264–272.

Robinson, D. L., A. Hermans, A. T. Seipel, and R. M. Wightman (2008). Monitoring rapid chemical communication in the brain. *Chemical reviews 108*(7), 2554–2584.

Ross, A. E., M. D. Nguyen, E. Privman, and B. J. Venton (2014). Mechanical stimulation evokes rapid increases in extracellular adenosine concentration in the prefrontal cortex. *Journal of neurochemistry 130*(1), 50–60.

Saboury, A. A., A. A. M. Movahedi, and G. H. Hakimelahi (2002). Articles: A product inhibition study on adenosine deaminase by spectroscopy and calorimetry. *Biochemistry and Molecurar Biology Reports 35*(3), 302–305.

Sattin, A. and T. Rall (1970). The effect of adenosine and adenine nucleotides on the cyclic adenosine 3', 5'-phosphate content of guinea pig cerebral cortex slices. *Molecular pharmacology 6*(1), 13–23.

Schmitt, L. I., R. E. Sims, N. Dale, and P. G. Haydon (2012). Wakefulness affects synaptic and network activity by increasing extracellular astrocyte-derived adenosine. *The Journal of Neuroscience 32*(13), 4417–4425.

Schnell, S. and T. Turner (2004). Reaction kinetics in intracellular environments with macromolecular crowding: simulations and rate laws* 1. *Progress in Biophysics and Molecular Biology 85*(2-3), 235–260.

Schulmeister, T. (1990). Mathematical modelling of the dynamic behaviour of amperometric enzyme electrodes. *Selective electrode reviews 12*(2), 203–260.

Schultz, V. and J. Lowenstein (1978). The purine nucleotide cycle. studies of ammonia production and interconversions of adenine and hypoxanthine nucleotides and nucleosides by rat brain in situ. *Journal of Biological Chemistry 253*(6), 1938–1943.

Schwarzschild, M. A., L. Agnati, K. Fuxe, J.-F. Chen, and M. Morelli (2006). Targeting adenosine a 2a receptors in parkinson's disease. *Trends in neurosciences 29*(11), 647–654.

Sharma, R., P. Sahota, and M. M. Thakkar (2014). Role of adenosine and the orexinergic perifornical hypothalamus in sleep-promoting effects of ethanol. *Sleep 37*(3), 525.

Sharoyan, S., A. Antonyan, S. Mardanyan, G. Lupidi, and G. Cristalli (2006). Influence of dipeptidyl peptidase iv on enzymatic properties of adenosine deaminase. *ACTA BIOCHIMICA POLONICA-ENGLISH EDITION- 53*(3), 539.

Shigetomi, E., O. Jackson-Weaver, R. T. Huckstepp, T. J. O'Dell, and B. S. Khakh (2013). Trpa1 channels are regulators of astrocyte basal calcium levels and long-term potentiation via constitutive d-serine release. *The Journal of Neuroscience 33*(24), 10143–10153.

Silva, R. G., D. S. Santos, L. A. Basso, J. P. Oses, S. Wofchuk, L. V. C. Portela, and D. O. Souza (2004). Purine nucleoside phosphorylase activity in rat cerebrospinal fluid. *Neurochemical research 29*(10), 1831–1835.

Silver, R. A., J. Lübke, B. Sakmann, and D. Feldmeyer (2003). High-probability uniquantal transmission at excitatory synapses in barrel cortex. *Science 302*(5652), 1981–1984.

Šimelevičius, D. and R. Baronas (2010). Computational modelling of amperometric biosensors in the case of substrate and product inhibition. *Journal of mathematical chemistry 47*(1), 430–445.

Šimelevičius, D. and R. Baronas (2011). Mechanisms controlling the sensitivity of amperometric biosensors in the case of substrate and product inhibition. In *SIMUL 2011, The Third International Conference on Advances in System Simulation*, pp. 61–66.

Simelevicius, D., R. Baronas, and J. Kulys (2012). Modelling of amperometric biosensor used for synergistic substrates determination. *Sensors 12*(4), 4897–4917.

Sims, R. E. and N. Dale (2014). Activity-dependent adenosine release may be linked to activation of na+-k+ ATPase: an in vitro rat study. *PloS one 9*(1), e87481.

Sims, R. E., H. H. T. Wu, and N. Dale (2013). Sleep-wake sensitive mechanisms of adenosine release in the basal forebrain of rodents: an in vitro study. *PloS one 8*(1), e53814.

Singer, P., S. McGarrity, H.-Y. Shen, D. Boison, and B. Yee (2012). Working memory and the homeostatic control of brain adenosine by adenosine kinase. *Neuroscience 213*, 81–92.

Solaroli, N., C. Panayiotou, M. Johansson, and A. Karlsson (2009). Identification of two active functional domains of human adenylate kinase 5. *FEBS letters 583*(17), 2872–2876.

Štikonienė, O., F. Ivanauskas, and V. Laurinavicius (2010). The influence of external factors on the operational stability of the biosensor response. *Talanta 81*(4), 1245–1249.

Stutzmann, G., G. Marek, and G. Aghajanian (2001). Adenosine preferentially suppresses serotonin 2a receptor-enhanced excitatory postsynaptic currents in layer v neurons of the rat medial prefrontal cortex. *Neuroscience 105*(1), 55–69.

Subbalakshmi, G. and C. Murthy (1985). Isolation of astrocytes, neurons, and synaptosomes of rat brain cortex. *Neurochemical research 10*(2), 239–250.

Swamy, B. K. and B. J. Venton (2007). Subsecond detection of physiological adenosine concentrations using fast-scan cyclic voltammetry. *Analytical chemistry 79*(2), 744–750.

Syková, E. and C. Nicholson (2008). Diffusion in brain extracellular space. *Physiological reviews 88*(4), 1277–1340.

Syková, E., J. Svoboda, J. Polak, and A. Chvátal (1994). Extracellular volume fraction and diffusion characteristics during progressive ischemia and terminal anoxia in the spinal cord of the rat. *Journal of Cerebral Blood Flow & Metabolism 14*(2), 301–311.

Tao, L. and C. Nicholson (2004). Maximum geometrical hindrance to diffusion in brain extracellular space surrounding uniformly spaced convex cells. *Journal of theoretical biology 229*(1), 59–68.

Tian, F., A. V. Gourine, R. T. Huckstepp, and N. Dale (2009). A microelectrode biosensor for real time monitoring of l-glutamate release. *Analytica chimica acta 645*(1), 86–91.

Van Calker, D., M. Müller, and B. Hamprecht (1978). Adenosine inhibits the accumulation of cyclic AMp in cultured brain cells. *Nature 276*(5690), 839–841.

Van Gompel, J. J., M. R. Bower, G. A. Worrell, M. Stead, S.-Y. Chang, S. J. Goerss, I. Kim, K. E. Bennet, F. B. Meyer, W. R. Marsh, et al. (2014). Increased cortical extracellular adenosine correlates with seizure termination. *Epilepsia 55*(2), 233–244.

van Stroe-Biezen, S., F. Everaerts, L. Janssen, and R. Tacken (1993). Diffusion coefficients of oxygen, hydrogen peroxide and glucose in a hydrogel. *Analytica chimica acta 273*(1), 553–560.

Virus, R. M., M. Djuricic-Nedelson, M. Radulovacki, and R. Green (1983). The effects of adenosine and 2-deoxycoformycin on sleep and wakefulness in rats. *Neuropharmacology 22*(12), 1401–1404.

Voříšek, I., M. Hajek, J. Tintěra, K. Nicolay, and E. Sykova (2002). Water adc, extracellular space volume, and tortuosity in the rat cortex after traumatic injury. *Magnetic resonance in medicine 48*(6), 994–1003.

Waldhoer, M., A. Wise, G. Milligan, M. Freissmuth, and C. Nanoff (1999). Kinetics of ternary complex formation with fusion proteins composed of the a1-adenosine receptor and g protein α-subunits. *Journal of Biological Chemistry 274*(43), 30571–30579.

Wall, M. and N. Dale (2007). Auto-inhibition of rat parallel fibre–purkinje cell synapses by activity-dependent adenosine release. *The Journal of physiology 581*(2), 553–565.

Wall, M. and N. Dale (2008). Activity-dependent release of adenosine: a critical re-evaluation of mechanism. *Current neuropharmacology 6*(4), 329.

Wall, M. J., A. Atterbury, and N. Dale (2007). Control of basal extracellular adenosine concentration in rat cerebellum. *The Journal of physiology 582*(1), 137–151.

Wall, M. J. and N. Dale (2013). Neuronal transporter and astrocytic ATP exocytosis underlie activity-dependent adenosine release in the hippocampus. *The Journal of physiology 591*(16), 3853–3871.

Wall, M. J. and M. J. Richardson (2014). Localised adenosine signalling provides fine-tuned negative feedback over a wide dynamic range of

neocortical network activities. *Journal of neurophysiology*, jn–00620.

Walter, G. A., J. W. Phillis, and M. H. O'Reagan (1988). Determination of rat cerebrospinal fluid concentrations of adenosine, inosine, hypoxanthine, xanthine and uric acid by high performance liquid chromatography. *Journal of pharmacy and pharmacology 40*(2), 140–142.

Wang, Y., X. Liu, B. Schneider, E. A. Zverina, K. Russ, S. J. Wijeyesakere, C. A. Fierke, R. J. Richardson, and M. A. Philbert (2012). Mixed inhibition of adenosine deaminase activity by 1, 3-Dinitrobenzene: A model for understanding cell-selective neurotoxicity in chemically-induced energy deprivation syndromes in brain. *Toxicological Sciences 125*(2), 509–521.

Wells, J. A., I. N. Christie, P. S. Hosford, R. T. Huckstepp, P. R. Angelova, P. Vihko, S. C. Cork, A. Y. Abramov, A. G. Teschemacher, S. Kasparov, et al. (2015). A critical role for purinergic signalling in the mechanisms underlying generation of bold fmri responses. *The Journal of Neuroscience 35*(13), 5284–5292.

West, M. J., G. Danscher, and H. Gydesen (1978). A determination of the volumes of the layers of the rat hippocampal region. *Cell and tissue research 188*(3), 345–359.

Wetherington, J., G. Serrano, and R. Dingledine (2008). Astrocytes in the epileptic brain. *Neuron 58*(2), 168–178.

Winn, H., R. Rubio, and R. Berne (1979). Brain adenosine production in the rat during 60 seconds of ischemia. *Circulation research 45*(4), 486–492.

Wolak, D. J. and R. G. Thorne (2013). Diffusion of macromolecules in the brain: implications for drug delivery. *Molecular pharmaceutics 10*(5), 1492–1504.

Wu, P. and J. Phillis (1984). Uptake by central nervous tissues as a mechanism for the regulation of extracellular adenosine concentrations. *Neurochemistry international 6*(5), 613–632.

Xie, L., H. Kang, Q. Xu, M. J. Chen, Y. Liao, M. Thiyagarajan, J. ODonnell, D. J. Christensen, C. Nicholson, J. J. Iliff, et al. (2013). Sleep drives metabolite clearance from the adult brain. *science 342*(6156), 373–377.

Yamamoto, T., J. Geiger, P. Daddona, and J. Nagy (1987). Subcellular, regional and immunohistochemical localization of adenosine deaminase in various species. *Brain research bulletin 19*(4), 473–484.

Yamamoto, T., J. Ochi, P. Daddona, and J. Nagy (1990). Ultrastructural immunolocalization of adenosine deaminase in histaminergic neurons of the tuberomammillary nucleus of rat. *Brain Research 527*(2), 335–341.

Yao, S., A. Ng, W. Muzyka, M. Griffiths, C. Cass, S. Baldwin, and J. Young (1997). Molecular cloning and functional characterization of nitrobenzylthioinosine (nbmpr)-sensitive (es) and nbmpr-insensitive (ei) equilibrative nucleoside transporter proteins (rent1 and rent2) from rat tissues. *Journal of Biological Chemistry 272*(45), 28423–28430.

Zain, Z. M., R. D. ONeill, J. P. Lowry, K. W. Pierce, M. Tricklebank, A. Dewa, and S. Ab Ghani (2010). Development of an implantable d-serine biosensor for in vivo monitoring using mammalian d-amino acid oxidase on a poly (o-phenylenediamine) and nafion-modified platinum–iridium disk electrode. *Biosensors and Bioelectronics 25*(6), 1454–1459.

Zhang, H., S.-C. Lin, and M. A. Nicolelis (2010). Spatiotemporal coupling between hippocampal acetylcholine release and theta oscillations in vivo. *The Journal of Neuroscience 30*(40), 13431–13440.

Zhang, P., N. M. Bannon, V. Ilin, M. Volgushev, and M. Chistiakova (2015). Adenosine effects on inhibitory synaptic transmission and excitation–inhibition balance in the rat neocortex. *The Journal of physiology 593*(4), 825–841.

Zoref-Shani, E., Y. Bromberg, G. Lilling, I. Gozes, S. Brosh, Y. Sidi, and O. Sperling (1995). Developmental changes in purine nucleotide metabolism in cultured rat astroglia. *International journal of developmental neuroscience 13*(8), 887–896.